Efficient uncertainty propagation schemes for dynamical systems with stochastic finite element analysis.

Kundu, Abhishek

Efficient uncertainty propagation schemes for dynamical systems with Stochastic Finite Element Analysis

Swansea University
Prifysgol Abertawe

Abhishek Kundu

Submitted to Swansea University in fulfilment of the requirements
for the degree of Doctor of Philosophy

Swansea University
College of Engineering

June 2014

To you, Ma

Abstract

Efficient uncertainty propagation schemes for dynamical systems are investigated here within the framework of stochastic finite element analysis. Uncertainty in the mathematical models arises from the incomplete knowledge or inherent variability of the various parametric and geometric properties of the physical system. These input uncertainties necessitate the use of stochastic mathematical models to accurately capture their behavior. The resolution of such stochastic models is computationally quite expensive. This work is concerned with development of model order reduction techniques for obtaining the dynamical response statistics of stochastic finite element systems. Efficient numerical methods have been proposed to propagate the input uncertainty of dynamical systems to the response variables.

Response statistics of randomly parametrized structural dynamic systems have been investigated with a reduced spectral function approach. The frequency domain response and the transient evolution of the response of randomly parametrized structural dynamic systems have been studied with this approach. An efficient discrete representation of the input random field in a finite dimensional stochastic space is proposed here which has been integrated into the generic framework of the stochastic finite element weak formulation. This framework has been utilized to study the problem of random perturbation of the boundary surface of physical domains. Truncated reduced order representation of the complex mathematical quantities which are associated with the stochastic isoparametric mapping of the random domain to a deterministic master domain within the stochastic Galerkin framework have been provided. Lastly, an a-priori model reduction scheme for the resolution of the response statistics of stochastic dynamical systems has also been studied here which is based on the concept of balanced truncation. The performance and numerical accuracy of the methods proposed in this work have been exemplified with numerical simulations of stochastic dynamical systems and the convergence behavior of various error indicators.

Declaration

This work has not previously been accepted in substance for any degree and is not being concurrently submitted in candidature for any degree.

Signed .....(candidate)
Date .....06...JUNE....2014.....

STATEMENT 1

This thesis is the result of my own investigation, except where otherwise stated. Where correction services have been used, the extend and nature of the correction is clearly market in a footnote(s).

Other sources are acknowledged by footnotes giving explicit references. A bibliography is appended.

Signed .....(candidate)
Date .....06...JUNE...2014.....

STATEMENT 2

I hereby give consent for my thesis, if accepted, to be available for photocopying and for inter-library load, and for the title and summary to be made available to outsider organizations.

Signed .....(candidate)
Date .....06...JUNE...2014.....

Contents

Acknowledgements

I am very grateful to the College of Engineering, Swansea University for granting me the Zienkiewicz scholarship to support this work and providing an environment propitious for my research.

I would like to thank my supervisor Prof. Sondipon Adhikari for his guidance and encouragement throughout the period of my research work in Swansea. I would also like to thank Prof. Michael I. Friswell for his kind support and interest in my research.

I wish to thank my friends and colleagues in Civil and Computational Engineering, Swansea University for a friendly and congenial work atmosphere in the laboratory. Special thanks to Alejandro for the stimulating discussions we had over the course of this research.

Thanks to my parents for being a source of constant inspiration. And Amrita - her unconditional support and patience has made this work possible!

Swansea
June 2014

Abhishek Kundu

List of Figures

List of Tables

Nomenclature

Notations and Symbols

$\mathbb{C}$	Space of complex numbers
$\mathbb{R}$	Space of real numbers
$\mathrm{cov}(\bullet)$	Covariance of the field $(\bullet)$
$\det \lvert \bullet \rvert$	Determinant of $(\bullet)$
$\mathrm{vec}(\bullet)$	vectorization of matrix $(\bullet)$
$div(\bullet)$	divergence operator
$\mathrm{colsp}\,[\bullet]$	column space of $[\bullet]$
$\mathbf{A} : \mathbf{B}$	double dot product, inner product of second order tensors **A** and **B**
$\in$	Belongs to
$\forall$	For all
$\otimes$	tensor product
$\subset$	subset
$*$	convolution operation
$\langle \cdot, \cdot \rangle_{L^2}$	inner product in an L^2 space
$(\bullet)^T$	Matrix transpose of $(\bullet)$
$(\bullet)^{-1}$	Matrix inverse of $(\bullet)$
$(\bullet)^{-T}$	Inverse transpose of $(\bullet)$
$\dot{(\bullet)}$	Derivative of $(\bullet)$ with respect to t
$\lVert \cdot \rVert_{\mathrm{F}}$	Frobenius matrix norm of $(\bullet)$
$\lVert \bullet \rVert$	l_2 norm of $(\bullet)$
$\lvert \bullet \rvert$	Absolute value of $(\bullet)$

Abbreviations

PDE	Partial differential equation
SPDE	Stochastic partial differential equation
PDF	Probability density function
CDF	Cumulative distribution function
DOF	Degrees of freedom

FE(M)	Finite element method
SFEM	Stochastic Finite element method
MCS	Monte Carlo simulation
PC(E)	Polynomial Chaos (Expansion)
IID	Independent and identically distributed
ACF	Auto-correlation function
KL	Karhunen-Loève

Definitions

- **$(\Theta, \mathscr{F}, P)$ space:** The triple consists a measure space where Θ is a set and $\mathscr{F}$ is the σ-algebra over Θ. P is a function which is a non-negative measure associated with $\mathscr{F}$. This triplet is usually associated with a probability space where Θ is the set of possible outcomes, $\mathscr{F}$ is a set of events and P is the probability assigned to those events.

- **Continuous transformation:** A transformation R mapping a normed space X into another normed space Y is continuous if for every $\varepsilon > 0$ there is a $\delta > 0$ such that $\|x - x_0\| < \delta$ implies $\|R(x) - R(x_0)\| < \varepsilon$ at each point $x_0 \in X$.

- **Normed linear vector space:** A vector space X on which there is a real valued function ρ which maps each element $x \in X$ to a real number $\|x\|$ called the norm of x, i.e. $\rho : X \to \mathbb{R}$ is the norm on X. The space spanned by all vectors which have finite p-norm is termed as the L^p space of vectors.

- **Cauchy sequence:** A sequence x_n in a normed space is a Cauchy sequence if $\|x_n - x_m\| \to 0$ as $n, m \to \infty$. In a normed space every convergent sequence is a Cauchy sequence.

- **Completeness:** A normed linear vector space is complete if every Cauchy sequence from X has a limit in X.

- **Inner Product:** If two elements x_1 and x_2 belongs to a linear vector space X, then the inner product, denoted as $\langle x_1, x_2 \rangle$, is a map $X \times X \to \mathbb{R}$ where $\mathbb{R}$ is a field of scalars. In the Euclidean space, the inner product is usually referred to as 'dot product'. The inner product satisfies the axioms • $\langle x_1, x_2 \rangle = \langle x_2, x_1 \rangle$ • $\langle x_1 + x_3, x_2 \rangle = \langle x_1, x_2 \rangle + \langle x_3, x_2 \rangle$ • $\langle \alpha x_1, x_2 \rangle = \alpha \langle x_1, x_2 \rangle$ • $\langle x_1, x_1 \rangle \geq 0$

- **Hilbert Space:** A linear vector space equipped with an inner product defined on $H \times H$ and is complete in the norm is a Hilbert space.

- **Stochastic Hilbert space:** Stochastic Hilbert space is a Hilbert space of the random variables. If $\{\xi_1, \ldots, \xi_M\}$ is a finite collection of random variables and $P(\xi_1, \ldots, \xi_M)$ is their joint probability measure, then the stochastic Hilbert space consists of all such

functions of ξ_i where the inner product between two stochastic functions h_i and h_j is defined as $\langle h_i, h_j \rangle = \int_\Theta h_i, h_j dP$, and the space is complete in the norm.

- **Orthogonal basis:** A basis $\mathbf{x}$ is a subset of vector space X over field F which are linearly independent and spans X, i.e. any vector in X can be expressed as a linear combination the elements of $\mathbf{x}$. A linear vector space X equipped with an inner product $\langle \cdot, \cdot \rangle$ has a set of orthogonal basis $\mathbf{x}$ if the element of $\mathbf{x}$ are orthogonal to each other, i.e. $\langle x_i, x_j \rangle = 0$, for all $i \neq j$, $x_i, x_j \in \mathbf{x}$.

- **Bilinear form:** A bilinear form on a vector space X over field F is a function $\mathscr{B} : X \times X \to F$ which is linear in each argument separately. It satisfies the following axioms for all $u, v, w \in X$ • $\mathscr{B}(u+v, w) = \mathscr{B}(u, w) + \mathscr{B}(v, w)$ • $\mathscr{B}(u, v+w) = \mathscr{B}(u, v) + \mathscr{B}(u, w)$ • $\mathscr{B}(\alpha u, v) = \mathscr{B}(u, \alpha v) = \alpha \mathscr{B}(u, v)$.
  Bilinear forms are symmetric if $\mathscr{B}(u, v) = \mathscr{B}(v, u)$.
  For example, the inner product defined on a vector space X over real numbers $\mathbb{R}$ is a bilinear map $X \times X \to \mathbb{R}$ and its functional representation is a symmetric bilinear form.

- **Linear form:** A linear form $\mathscr{L}$ on a vector space X over field F is given as a function $\mathscr{L} : X \to F$ which is linear in X. For all $u, v \in X$ it satisfies • $\mathscr{L}(u+v) = \mathscr{L}(u) + \mathscr{L}(v)$ • $\mathscr{L}(\alpha u) = \alpha \mathscr{L}(u)$.

- **Krylov space:** In linear algebra, given a matrix $\mathbf{A} \in \mathbb{R}^{n \times n}$ and a vector $b \in \mathbb{R}^n$ a n-dimensional Krylov space (or subspace) $\mathscr{K}_n(\mathbf{A}, b)$ is given as the space spanned by the vectors $\{b, \mathbf{A}b, \mathbf{A}^2 b, \ldots, \mathbf{A}^{n-1} b\}$. Thus $\mathscr{K}_n(\mathbf{A}, b) = \text{span}\{b, \mathbf{A}b, \mathbf{A}^2 b, \ldots, \mathbf{A}^{n-1} b\}$.

Chapter 1

Introduction

1.1 Background

The mathematical models and the parameters used to model the physical system are idealizations of the physical process. They can not often be known for certainty and a degree of randomness is involved in these models. In fact, input uncertainty in the form of material parameters, geometrical configuration, boundary conditions are ubiquitous and intrinsic to the models being analyzed. For example the randomness of a gust of wind, the characterization of forces in boundary and initial conditions on mechanical systems, random micro-structural features of engineering materials, the random fluctuations in diffusion coefficient, convection coefficient, all make the characterizations provided by deterministic models of mechanics less satisfactory with respect to their predictive capabilities. Thus instead of a particular stable point of operation given by a numerical model or a deterministic estimation of the evolution of the system response, a statistical quantification of the variability of the input-output characteristics of the system becomes more pertinent. This randomness involved in the parametrization and modeling of complex engineering systems has been widely recognized by industry and researchers.

A few motivating examples are provided here to highlight the necessity of having the statistical summary of response quantities rather than just having deterministic point estimate. Corrugated skins, which exhibit a strong anisotropic behavior, are highly sensitivity to their geometrical and elastic properties. Hence optimal design of these components must be robust with respect to random fluctuations in their design parameters. And this can be ensured with a stochastic analysis of the system response subject to input variability. Also, many of the civil engineering problems are concerned with materials that are intrinsically random (such as concrete and soil) and using merely the average value of the material characterizations would not establish their behavior with desired confidence or reliability.

Fortunately, the entire subject of uncertainty can itself be addressed in a scientific and mathematically precise way and their random characteristics can be addressed by computa-

tional models. Computational models can make use a set of *basic input variables* for mathematical idealization of the complex mechanical systems. This would lead to the *response variables* such as displacement, stress, strain to be a stochastic quantities having statistical properties of their own and depending on the input variables. Hence this method involves dealing with differential equations with random coefficients and are collectively referred to as *stochastic partial differential equations.*

Hence future research in numerical methods, which aims to push the boundaries of computational mechanics by incorporating realistic models of complex engineering systems into their mathematical models, has to utilize the probabilistic description of the mechanical problem at hand. Including stochastic features into computational models will not only provide realistic simulations of physical events but will also provide the analyst with specific information on the probabilities that can be assigned to predictions. Thus, using probabilistic models of mechanics, the analyst may determine what the distribution of a response quantities in the space of possible event outcomes rather than just their bounds (upper or lower limit) which can be expected in view of the input uncertainty to the model. In particular, the probability of failure of the systems being studied can be known. Hence uncertainty quantification in computational mechanics and efficient estimation of the response statistics, probability distributions of the response quantities would be an important field of study.

1.2 Uncertainty quantification

Accounting for this uncertainty in the input parameters and/or the geometrical configurations of the physical systems has been reported in many recent articles. A few recent review papers by Nouy [2009], Charmpis *et al.* [2007], Stefanou [2009], Schuëller [2006] gives the justification of considering stochastic models into the framework of the established numerical techniques and investigations of efficient and novel solution techniques. It is worth mentioning here that the randomness in these input parameters of the mathematical model are different from the classical "stochastic differential equations". In the latter case, the random inputs are in the form of idealized processes (such as Wiener process, Poisson process, to name a few) and the stochastic calculus used for their study is a mature subject of active research [Karatzas and Shreve, 1988, Kloeden and Pearson, 1977]. The present work would consider the uncertain inputs to be in the form of multiplicative uncertainty associated with the input elastic or geometrical parameters of the governing partial differential equations [Matthies, 2007].

Uncertainties present in a system model due to incomplete knowledge of system parameters can be reduced by carrying out exhaustive experiments or using better measuring devices (which are often quite expensive and laborious exercises). These are classified as *epistemic uncertainty* and has been widely studied in literature [Jakeman *et al.*, 2010, Swiler *et al.*, 2009], sometimes employing interval arithmetic [Roy and Oberkampf, 2011]. On the other

hand, *aleatoric uncertainty* arises in situations where it is not possible to reduce the uncertainty in the parameters using additional experiments or better measuring device. In fact some of these may be abstract approximate mathematical quantities modeling a physical system such as the porosity of poroelastic materials, which while theoretically definable may not be measured directly. Most of the real-life practical engineering problems involve both types of uncertainties. Some researchers suggest that a clear distinction be made between the two types [Paté-Cornell, 1996]. However others suggest that it's often difficult to determine the category to which a particular uncertainty belongs [Kiureghian and Ditlevsen, 2009]. However, it has been recognized that uncertainty quantification (of both types) is essential for the analysis of realistic physical systems [Najm, 2009, Roy and Oberkampf, 2011, Cheng and Sandu, 2009]. It is a necessary step in assessing the reliability of computer simulations and, hence is a part of model validation and verification [Roache, 1998].

We briefly discuss here some of the principal methods employed for uncertainty quantification in practical engineering problems.

- **Worst-case-scenario:** The method is useful when having complete information about the probability distribution of the input data is difficult or quite expensive [Hlaváček, 2007]. For example, Babuška *et al.* [2005a] proposed a methodology which relies on a finite dimensional representation of the random data around the nominal values of the data while preserving minimal requirements (say the coerciveness) of the stochastic problem. The fundamental idea relies on the understanding that the stochastic function of interest can be represented by a linear functional in the admissible space solution space.

- **Probabilistic Estimation:** This method provides probabilistic description of the uncertainty associated with the input parameters of the mathematical model. The random parameter is described in a probability space of possible outcomes (called *events*). The characterization of this input uncertainty is made with covariance functions, nature of the associated probability distribution functions, variability of the field and such similar quantities. This concept has been widely studied in literature [Puig *et al.*, 2002, Ghanem and Spanos, 1991, Grigoriu, 2000, Sudret and Der-Kiureghian, 2000, Matthies, 2007].

- **Interval arithmetic:** There have been works based on interval modeling of the uncertainty in model inputs. Some of the methods belonging to this category have been studied by Chen and Rao [1997], Zalewski *et al.* [2009]. These methods rely on the interval concept to define the uncertain input parameters between deterministic upper and lower bounds. Based on these the *interval Finite Element* approach has been developed by Dimarogonas [1995]. However, they have been observed to give overestimation of the response quantities at each step of the interval algorithm. The deterministic bounds of the random parameter in the interval arithmetic may be subjected to uncertainties

and this has been studied in the fuzzy finite element approach proposed by Moens and Vandepitte [2002, 2005].

Apart from the above methods there are other approaches for approximation of the input uncertainty as model inputs such as evidence theory [Ferson *et al.*, 2003], Bayesian inference [Wang and Zabaras, 2005, Ching and Beck, 2004] and expert opinion to mention a few.

1.2.1 Probabilistic description of input uncertainty

We take a random field α defined on a compact region $\mathscr{D} \subseteq \mathbb{R}^d$ and a probability space $(\Theta, \mathscr{F}, P)$ such that the random field can be represented as a measurable mapping as $\alpha : \mathscr{D} \times \Theta \to \mathbb{R}$. Here $\theta \in \Theta$ is a point in the sampling space Θ, $\mathscr{F}$ is the complete Borel σ-algebra over the subsets of Θ and P is the non-negative probability measure. The random field at each point in the region has a certain degree of correlation with those at the other points characterized by a certain representative geometrical dimension, which provides the necessary spatial description of the uncertain parameter. The uncertainty characterization of the random field can be performed using 'Probabilistic Characterization' which defines indexed finite dimensional joint distribution functions as [Adler, 1981, Oksendal, 1995]

$$\begin{aligned} F_{r_1,\ldots,r_n}(\xi_1,\ldots,\xi_n) &= P\left\{\alpha(\mathbf{r}_i) \leq \xi_i,\ \forall i = 1,\ldots,n\right\}, \\ \text{where} \quad \mathbf{r}_i \in \mathscr{D}, &\quad \xi_i \in \mathbb{R} \quad \forall\, i = 1,\ldots,n \end{aligned} \tag{1.1}$$

such that the random field is defined as a set of random variables $\alpha(\mathbf{r}) := \alpha(\mathbf{r}, \cdot) : \Theta \to \mathbb{R}$ where Θ is characterized by $F_{r_1,\ldots,r_n}(\xi_1,\ldots,\xi_n)$. Θ can be constructed from the finite dimensional distribution functions under weak consistency conditions [Oksendal, 1995]. Alternatively, the random field is defined as a random variable whose elementary events θ in the region $\mathscr{D} \subseteq \mathbb{R}^d$ are realized as

$$\begin{aligned} \alpha(\cdot,\theta) : \mathscr{D} \to \mathbb{R} \quad \text{where} \quad \theta(\mathbf{r}) \equiv \alpha(\mathbf{r},\theta); \quad \mathbf{r} \in \mathscr{D}, \quad \theta \in \Theta \\ \text{such that} \quad \Theta \subset \{\theta | \theta : \mathscr{D} \to \mathbb{R}\} \end{aligned} \tag{1.2}$$

The above definition necessitates specifying a probability measure P_α on the function space Θ with a finite dimensional probability distribution. However, for most engineering applications, it is not practical to specify the random field with all its finite-dimensional distributions or with the measures on a probability space. Hence the introduction of random fluctuations in the parametric model may not lead to a physically meaningful description of the random field.

We briefly discuss here the methods of modeling Gaussian and non-Gaussian random fields where the random fields are modeled with a degenerate set of random variables. Gaussian models are frequently used in the modeling of random fields since the central limit theorem ensures their natural occurrence and they give the maximum entropy model if only

second-order information is available. Hence the Gaussian fields are completely defined by their second-order statistics, i.e. their mean $\mu_\alpha(\mathbf{r})$ and covariance function $C_\alpha(\mathbf{r}_1, \mathbf{r}_2)$ as

$$\mu_\alpha(\mathbf{r}) = \mathrm{E}\left[\alpha(\mathbf{r}, \theta)\right] \quad \text{and} \quad C_\alpha(\mathbf{r}_1, \mathbf{r}_2) = \mathrm{E}\left[\left(\alpha(\mathbf{r}_1, \theta) - \mu_\alpha(\mathbf{r}_1)\right)\left(\alpha(\mathbf{r}_2, \theta) - \mu_\alpha(\mathbf{r}_2)\right)\right]$$

Conversely, for any valid mean and covariance structure it is possible to find a Gaussian random field $\alpha(\mathbf{r}, \theta)$ which has these second-order statistics. The restrictions on the covariance kernel for which the above assumptions hold true are discussed later in this article.

For non-Gaussian random field models, we know that any random variable $\alpha(\theta)$ with a prescribed distribution function F_α can be non-linearly mapped onto a standard normal random variable $\xi \in \mathcal{N}(0,1)$ as $F_\alpha^{-1}(\mathrm{erf}(\mathcal{N}(0,1)))$ where 'erf' is the Gaussian distribution function. Hence a non-Gaussian random field $\alpha(\mathbf{r}, \theta)$ with a distribution function F_α can be defined with a non-linear transformation

$$\alpha(\mathbf{r}, \theta) = \eta(\mathbf{r}, \xi(\mathbf{r}, \theta)) := F^{-1}_{\alpha(\mathbf{r})} \circ \mathrm{erf}(\xi(\mathbf{r}, \theta)) \tag{1.3}$$

where $\alpha(\mathbf{r}, \theta)$ has a marginal distribution $F_\alpha(\mathbf{r})$ at any point $\mathbf{r} \in \mathscr{D}$. The higher order moments and covariance $C_\alpha(\mathbf{r}_1, \mathbf{r}_2)$ are obtained as

$$\begin{aligned} \mathrm{E}\left[\alpha(\mathbf{r}, \theta)^p\right] &= \int_\Theta \eta(\mathbf{r}, \xi)^p dF_\xi(\theta) \\ C_\alpha(\mathbf{r}_1, \mathbf{r}_2) &= \int_\Theta \int_\Theta \eta(\mathbf{r}_1, \theta_1)\eta(\mathbf{r}_2, \theta_2) dF_{\xi(\mathbf{r}_1),\xi(\mathbf{r}_2)}(\theta_1, \theta_2) - \mu_\alpha(\mathbf{r}_1)\mu_\alpha(\mathbf{r}_2) \end{aligned} \tag{1.4}$$

where $dF_{\xi(\mathbf{r}_1),\xi(\mathbf{r}_2)}(\theta_1, \theta_2)$ is the joint probability density of the Gaussian random variables $\xi(\mathbf{r}_1)$ and $\xi(\mathbf{r}_2)$. From the above equations it can be seen that given the second-order statistics of the non-Gaussian random field α, it is necessary to select η and the covariance of the normal random variables $C_\xi(\mathbf{r}_1, \mathbf{r}_2)$. This is often a non-trivial exercise and arbitrary choices of marginal distribution and/or the target covariance may lead to inconsistencies. Some analytical expressions for various marginal distributions can be found in Ogorodnikov and Prigarin [1996], Grigoriu [2000]. However, in general a finite dimensional representation of the random field is provided with a truncated series expansion. This would be discussed in detail later in the thesis in Sec. 2.2.1.

The input uncertainties considered in this work would be included in the mathematical model within the probabilistic framework, under the assumption that enough information is available for a complete statistical characterization of the physical system. The input data would be modeled with random fields with a given spatial correlation structure in a finite dimensional stochastic space. The stochastic model response and the other quantities of interest derived from it are sought in the function space of the input random field. Therefore, the goal of the mathematical and computational analysis is the prediction of statistical moments (mean

value, variance, covariance, etc.) or even the whole probability distribution of the quantities of physical interest, given an input distribution of the random data.

One of the significant issues involved in the numerical methods adopted to solve the problems driven by random inputs is the computational cost associated with them. The solution of the stochastic partial differential equations is significantly more expensive than the corresponding deterministic case. Hence the primary focus of this work would be on the development of efficient reduced order solution techniques which can produce reliable numerical approximations for a wide variety of applied stochastic mechanics problems. We briefly review the uncertainty propagation schemes in the following section.

1.3 Review of uncertainty propagation methods

The propagation of the input uncertainty to the system response of the randomly parametrized systems has been tackled with various methods ranging from the non-intrusive statistical simulation methods (such as the crude Monte Carlo simulation (MCS) and it's variants) to non-statistical analytical methods. Solution techniques based constructing the stochastic response surface from the evaluation of the system response at finite number of points in the stochastic space are regarded as non-intrusive scheme. This is because of the fact that it is not necessary to modify the simulator which gives the deterministic system solution for any value of the input parameters. The advantage of this is obvious when dealing with complicated and expensive solvers (such as in CFD applications) where the latter can be treated as a black-box with the stochastic routines wrapped around it. However, the imminent advantage is often offset by the computational cost as discussed later in this chapter. On the other hand, the analytical methods which aims to obtain a functional representation of the stochastic response (and which often turn out to be computationally advantageous) necessitates the modification of the deterministic solver which might involve changing/rewriting significant parts of the code. Hence it is often classified as an 'intrusive' method.

1.3.1 Stochastic sampling techniques

The stochastic sampling techniques employ Monte Carlo type simulation techniques (in conjunction with advanced sampling and/or interpolation schemes) which have been analyzed and used in the finite element analysis of random systems [Papadrakakis and Papadopoulos, 1996]. It has been used in context of structural dynamics problems by Pradlwarter and Schuëller [1997]. Non-intrusive techniques enable the use of the already existing deterministic codes to solve the stochastic problem at carefully chosen sample points. Hence, there is no necessity to modify the deterministic solvers and adapt them to the stochastic case, it only involves constructing some post-processing routines. Also, the deterministic solvers working independently of each other at various sample points are trivially parallelizable.

However, the convergence of the crude MCS is slow and the error converges as $\mathcal{O}(\frac{1}{\sqrt{N}})$ where N is the number of sample points in the stochastic space where the solution is needed. The computational efficacy of these sample-based techniques can be substantially improved by reducing the problem to important random variables using principal component analysis [Kreinin *et al.*, 1998] and various efficient variance reduction techniques such as importance sampling [Au and Beck, 1999], the multi-point estimate method, stratified sampling and Latin hypercube sampling [Stein, 1987, McKay *et al.*, 1979]. The quasi-Monte Carlo technique has received significant attention as an efficient sample-based solution technique where a grid of carefully chosen few sample points gives a good approximation of the stochastic system solution (see for example Sobol [1998], Caflisch [1998], Sloan *et al.* [2002], Graham *et al.* [2011], Kuo *et al.* [2012]). The limitations of these techniques are dictated by the input stochastic space dimension. On the other hand, while the convergence rate of the Monte Carlo methods is slow, its computational work grows only like a polynomial with respect to the number of random variables present in the problem. Hence the efficient sampling based methods are quite efficient and well-suited when the dimension of the input stochastic space is relatively small.

It is important to note that the brute force MCS solution is often treated as a benchmark solution in numerical simulations to test the approximation accuracy of the solution statistics, convergence rates and computational efficacy of the proposed stochastic solvers. This is quite common in the stochastic computational mechanics literature (see for example Lucor *et al.* [2004]). However, given the slow convergence of the MCS technique, it is essential to ensure that the MCS has converged before using it as the benchmark. In this work, MCS results have often been utilized as the benchmark to observe the convergence of second order statistics of the response. It has been verified that such second order statistics computed from the MCS solution scheme have converged with sufficient accuracy before using them to validate the results. However, it must be mentioned that for some measures such as the complete pdf, especially near their tails, it might be necessary to have very high sample size to get a good approximation. While this may be speeded up with selective sampling the target domain, these have not been considered in this study.

1.3.2 Approximate analytical solution schemes

The non-statistical methods provides an explicit functional relationship between the input random variables and hence allows the evaluation of the functional statistics/probabilities of the stochastic system response. There are a host of approximation schemes which aim to represent the stochastic solution with approximate lower order forms which can be a viable alternative to the expensive sampling based schemes detailed in Section 1.3.1. These approaches can be based on the following schemes

- **Perturbation Method:** This method gives the stochastic system solution as a low order expansion of the system solution about its deterministic response using the Taylor series expansion method [Kleiber and Hien, 1992, Yimin *et al.*, 1996, Lazarov *et al.*, 2012]. The approximate solution provided by this technique is valid only for low levels of input variability of the random quantity. Additionally, tracking the polynomial form of the solution beyond second order becomes a major difficulty.

- **Neumann Series:** This method relies on approximating the inverse of the stochastic matrix series in a Neumann type matrix series expansion about the baseline model [Yamazaki *et al.*, 1988, Lei and Qiu, 2000]. The stochastic system solution obtained using this series expansion and its approximation accuracy is a guided by the spectral radius of the deterministic part of the system matrix compared to the same for the stochastic parts [Ghanem and Spanos, 1991].

- **Response surface method:** This method aims to fit the random data of the stochastic quantities obtained at certain points in the stochastic space to a polynomial function of the input stochastic variables. The method utilizes a least square fit of the model data to give a response surface of the stochastic quantities. Non-intrusive projection schemes have been applied to evolute the coefficient associated with the least square fit [Chen *et al.*, 2004, Blatman and Sudret, 2010]. The number of random points required to have a good approximation of the stochastic system response increases rapidly with the degree and dimension associated with the input variability which limits its application in complex engineering problems.

All the above method basically attempts to obtain a good approximation of the stochastic system solution using lower order stochastic functions of input random variables. However, this method is often unsuitable for complex dynamical engineering problems in high dimensional stochastic space.

1.3.3 Stochastic spectral Galerkin method

One of the most generic frameworks for uncertainty propagation for randomly parametrized systems is the stochastic spectral Galerkin method [Ghanem and Spanos, 1991, Babuška *et al.*, 2004, 2005b]. Here the system solution is expressed with a set of a set of finite order stochastic polynomials spanning the stochastic Hilbert space of the input random variables. We discuss this method in some detail here.

We assume that the set of M iid input random vectors representing the input uncertainty to the system is denoted by the vector $\boldsymbol{\xi} = \{\xi_1, \ldots, \xi_M\}$. According to the *polynomial chaos* expansion scheme, the stochastic response $u_i(\theta)$ can be represented with a mean-square con-

vergent series as

$$
\begin{aligned}
u_i(\theta) =& u_{i_0}h_0 + \sum_{i_1=1}^{M} u_{i_1}h_1(\xi_{i_1}(\theta)) + \sum_{i_1=1}^{M}\sum_{i_2=1}^{i_1} u_{i_1 i_2}h_2(\xi_{i_1}(\theta),\xi_{i_2}(\theta)) \\
&+ \sum_{i_1=1}^{M}\sum_{i_2=1}^{i_1}\sum_{i_3=1}^{i_2} u_{i_1 i_2 i_3}h_3(\xi_{i_1}(\theta),\xi_{i_2}(\theta),\xi_{i_3}(\theta)) \\
&+ \sum_{i_1=1}^{M}\sum_{i_2=1}^{i_1}\sum_{i_3=1}^{i_2}\sum_{i_4=1}^{i_3} u_{i_1 i_2 i_3 i_4}\, h_4(\xi_{i_1}(\theta),\xi_{i_2}(\theta),\xi_{i_3}(\theta),\xi_{i_4}(\theta)) + \ldots
\end{aligned} \tag{1.5}
$$

where $u_{i_1 \ldots i_r}$ are deterministic constants to be evaluated and $h_r(\xi_{i_1}(\theta),\ldots,\xi_{i_r}(\theta))$ are the chaos terms. The solution is characterized by the maximum degree of polynomials used in the expansion and is generally termed as the order of polynomial chaos expansion. The approximation accuracy is controlled by this order of chaos. When $\boldsymbol{\xi}(\theta)$ are Gaussian random variables the associated stochastic polynomials are Hermite polynomials which are orthogonal with respect to the Gaussian joint distribution function.

The same idea can be extended to non-Gaussian random variables, provided more generalized functional bases are used [Xiu and Karniadakis, 2002, 2003b, Wan and Karniadakis, 2006] so that the orthonormality with respect to the probability density functions can be retained. Under such conditions, the type of independent random variables are chosen according to the type of random input distributions and according to Table 1.1. The Wiener-Hermite ex-

Table 1.1: Type of chaos expansion according to the type of input probability distribution [Xiu and Karniadakis, 2002].

Random Input	Chaos type	Support
Gaussian	Hermite-chaos	$(-\infty,\infty)$
Gamma	Laguerre-chaos	$[0,\infty)$
Beta	Jacobi-chaos	$[a,b]$
Uniform	Legendre-chaos	$[a,b]$

pansions in conjunction with the finite element (FE) methods have been widely applied to different problems such as fluid mechanics [Hou *et al.*, 2006, Knio and Maître, 2006, Najm, 2009], heat conductions [Xiu and Karniadakis, 2003a, Williams, 2010], dynamic systems [Pettit and Beran, 2006, Maute *et al.*, 2009] to mention a few.

The number of terms n_t in the polynomial chaos expansion depends on the dimension of the stochastic space (M) and the order of chaos (p) according to the relation

$$
n_t = \sum_{j=0}^{p} \frac{(M+j-1)!}{j!(M-1)!} = \binom{M+p}{p} \tag{1.6}
$$

It is obvious that the number of terms n_t increases significantly with the value of M and p and this is commonly referred to as the 'curse of dimensionality' in the literature. If we have

a finite element system with n degrees of freedom then the dimension of the linear system resulting from the spectral Galerkin approach becomes $n \times n_t$. As a result several methods have been developed including adaptive polynomial chaos (see for example Blatman and Sudret [2008, 2010]) aimed at reducing the computational cost.

Application of the spectral Galerkin approach to practical engineering problems may involve a fine discretization at the deterministic level (which involves a large resolution of the model at the deterministic level, i.e. large n) or a high dimensional representation at the stochastic level (large n_t). This results in the effective problem dimension to blow up rapidly leading to significant computational times and memory requirements. Hence the problem of model order reduction in the context of stochastic Galerkin methods is quite essential. This is discussed in more details in Sec. 1.4.

1.3.4 Stochastic collocation technique

The sparse-grid stochastic collocation methods are a computationally efficient alternative to direct Monte Carlo simulation technique. The collocation method relies on constructing the random solution using polynomial interpolation functions with a set of random responses evaluated at the zeros of these multidimensional stochastic interpolation functions [Nobile *et al.*, 2008b, Babuška *et al.*, 2010]. This requires resolution of the random system response at the sparse grid collocation points in a Monte Carlo sense and hence is non-intrusive and trivially parallelizable. For high-dimensional stochastic problems, adaptive sparse-grid collocation techniques have been proposed which aims to represent the problem with refinements (more grid points) along the important stochastic dimensions [Ma and Zabaras, 2009, Jakeman and Roberts, 2013, Nobile *et al.*, 2008a]. The computational evidence indicates the effectiveness of the sparse grid stochastic collocation method compared to full tensor and Monte Carlo approaches. Recently a multi-element probabilistic collocation method [Foo and Karniadakis, 2010] has also been used in this context which prescribe a collocation method on discretized elements of the parametric space. The collocation technique has been applied to various domains of applied computational mechanics problems such as natural convection [Ganapathysubramanian and Zabaras, 2007], computational fluid dynamics [Mathelin *et al.*, 2005], flow through porous medium [Li and Zhang, 2007] to name a few.

Various problems, which requires probabilistic models of the input random parameters, are often quite complicated to the extent that obtaining the system matrices with polynomials of the input random variables becomes a mathematically cumbersome exercise. Hence the spectral Galerkin methods is not the obvious first choice under such circumstances and the sparse grid collocation technique is often more readily applicable where the deterministic problem is solved at a set of quadrature points in the input stochastic space. Hence the solution can be reconstructed in the M-dimensional stochastic space with polynomial basis functions

of the random variables as

$$\mathscr{U}^{i_1} \otimes \ldots \otimes \mathscr{U}^{i_M} = \sum_{j_1=1}^{m_{i_1}} \cdots \sum_{j_M=1}^{m_{i_M}} f(x^{i_1}_{j_1=1}, \ldots, x^{i_M}_{j_M=1}) \cdot \left(a^{i_1}_{j_1} \otimes \ldots \otimes a^{i_M}_{j_M}\right) \tag{1.7}$$

$$\text{where} \quad \mathscr{U}^{i_k}(f) = \sum_{j=1}^{n_i} f(x^{i_k}_j) \cdot a^{i_k}_j$$

is the approximation of the random field along each stochastic dimension. The above tensor product formula requires evaluation of the stochastic objective function at $(m_{i_1} \ldots m_{i_M})$ grid points. For very high dimensional problems, i.e. large M, the above method becomes computationally intensive and a sparse grid technique is implemented using Smolyak's algorithm as [Barthelmann *et al.*, 2000]

$$\mathscr{A}(q, M) = \sum_{q-M+1 \leq |\mathbf{i}| \leq q} (-1)^{q-|\mathbf{i}|} \cdot \binom{M-1}{q-|\mathbf{i}|} \cdot \mathscr{U}^{i_1} \otimes \ldots \otimes \mathscr{U}^{i_M} \tag{1.8}$$

where $\mathscr{A}(q, M)$ are linear combinations of product formulas given in Eqn. (1.7), $q \geq M$ and $\mathbf{i} = (i_1, \ldots, i_M)$ with $|\mathbf{i}| = i_1 + \ldots + i_M$ which requires fewer realizations of the stochastic response in order to obtain the complete response statistics. Hence to compute $\mathscr{A}(q, M)$ the response has to be evaluated at the sparse grid points

$$\mathscr{X}(q, M) = \bigcup_{q-M+1 \leq |\mathbf{i}| \leq q} \left(X^{i_1} \times \ldots \times X^{i_M}\right) \tag{1.9}$$

with $X^{i_k} = \left\{x^{i_k}_1, \ldots, x^{i_k}_{m_i}\right\}$ denoting the set of points used by $\mathscr{U}^{i_k}$. Here we have used the Smolyak formulas that are based on polynomial interpolation at the extrema of the Chebyshev polynomials. This gives a nested set of nodes which can be used to approximate the stochastic quantity. However, when dealing with problems with high stochastic dimensions and input variability, the stochastic collocation often fails to provide substantial computational benefits over the direct Monte Carlo simulation method.

1.4 Review of stochastic model reduction techniques

The additional computational overhead associated with obtaining the response statistics of the randomly parametrized systems have motivated researchers to look into various model reduction techniques for the numerical solution of SPDE [Debusschere *et al.*, 2005]. A review of some of these techniques can be found in Keese [2003], Nouy [2009]. The computational overhead is reduced with careful choice of the stochastic space and the orthogonal chaos expansion spanning the space. Adapted basis functions has been used to approximate the stochastic functions based on piecewise polynomial basis on a partitioned stochastic space

[Maître *et al.*, 2004b, Wan and Karniadakis, 2005]. Another approach utilizes polynomial multi-wavelets basis for the stochastic space which allows for a multi-scale representation of the functions in the L^2 stochastic space [Maître *et al.*, 2004a]. A good approximation of the stochastic response function is guided by appropriate error estimators. This is especially suitable for adaptive basis building techniques.

A method belonging to this kind of model reduction approach is the Generalized Spectral Decomposition technique [Nouy, 2007, 2008]. It is an *a-priori* model reduction technique which gives an optimal decomposition of the solution of the stochastic problem by simultaneously satisfying a double Galerkin orthonormality criterion in a tensor product space. The method has been shown to be a natural extension of the Hilbert Karhunen-Loève decomposition and dedicated algorithms for the efficient resolution of the eigen problems associated with this method has been proposed.

The *a-priori* model reduction schemes in context of Galerkin spectral stochastic methods evaluate the stochastic basis functions for approximating the solution using well defined optimality criterion. On the other hand there are methods belonging to the class of *a-posteriori* model reduction where the optimal basis is calculated from a primary approximation of the statistics of the stochastic response. A method belonging to this later class attempts to perform a spectral (Hilbert Karhunen-Loève) decomposition of the stochastic solution to obtain the set of stochastic basis functions Doostan *et al.* [2007]. These are Proper Orthogonal Decomposition based methods where the approximation basis is constructed from several evaluations of deterministic problems in the stochastic sample space and then performing a singular value decomposition to evaluate the optimal orthogonal basis functions. Other such methods include a low-order Neumann expansion scheme to compute a estimation of the correlation structure of the response vector Matthies and Keese [2005]. Another similar a-posterior model reduction scheme is based on reusing the basis vectors spanning the dominant Krylov subspace of deterministic problems and using them to obtain a low order representation of the stochastic sample response of the subsequent problem sets Gosselet *et al.* [2003]. However, difficulty arises in the selection of pertinent subspaces for the subsequent resolutions, in order to avoid a significant increase in the dimension of the approximation space.

A 'reduced basis method' has been proposed by Boyaval *et al.* [2009] for the resolution of the stochastic elliptic symmetric problems with Monte Carlo method which is based on rigorous error estimation criterion. Another stochastic reduced basis method has been proposed for solving linear stochastic problems by Nair and Keane [2002], Sachdeva *et al.* [2006a] which relies on approximating the stochastic system response using projections of the solution on the preconditioned stochastic Krylov basis functions. This method however, is good for low order approximations of the stochastic response and becomes quite cumbersome for high order approximations. Moreover, it has been shown by Nouy [2009] that the successive stochastic basis functions are only the preconditioned basis functions of the classical spectral

Galerkin method for a particular choice of the preconditioner.

Recently a reduced spectral function approach has been proposed for the resolution of the stochastic system response static engineering systems by Adhikari [2011]. The method approximates the stochastic system solution using a truncated series representation of stochastic functions of input random variables termed as the spectral functions. Here a hybrid analytical and simulation based computational approach has been utilized to obtain the moments and probability density function of the solution.

Metamodeling strategies have also been utilized for having a computationally efficient scheme to evaluate the statistics of the stochastic systems. Such a metamodeling strategy, known as Gaussian process emulation [O'Hagan, 2006], is based on the analysis and design of computer experiments [Sacks *et al.*, 1989, Santner *et al.*, 2003] and on the concepts of Bayesian statistics. The non-expensive approximation of the output is made after evaluating a small number of points in the input space, hence reducing the required computer processing time. After conditioning on these training runs and updating a prior distribution, the mean of the resulting posterior distribution approximates the output of the simulator at any untried input, whereas it reproduces the known output at each design point. Gaussian process emulation has been implemented in various scientific fields with encouraging results. These fields include structural dynamics [DiazDelaO and Adhikari, 2010], multi-scale analysis [Flores *et al.*, 2012], stochastic finite elements [DiazDelaO and Adhikari, 2011], and domain decomposition [DiazDelaO and Adhikari, 2012] among many others.

1.5 Research objectives and scope

The research trend in the domain of computational mechanics clearly indicates the need for efficient numerical techniques to reduce the computational overhead associated with the evaluation of the system response of large-scale engineering problems [Nouy, 2009]. The incorporation of parametric/geometric uncertainty into the mathematical models results in a significant increase in the complexity of the solution methodology. This makes an optimal reduced order formulation for the resolution of stochastic systems highly desirable.

Although theoretical research in this domain has been encouraging and progress has been made in this field over the past decade, their widespread use is limited in the industry level engineering simulations and the wider engineering community on the whole. Additionally, their development within the computational mechanics community is very much ongoing. Generic stochastic solvers are not yet integrated with the most widely used industry standard commercial numerical analysis software packages. Stochastic simulation in industrial cases is often restricted to sample based techniques requiring solutions of large number of full system solutions. When using the probabilistic description of the input uncertainty, we identity a few important factors which needs further attention in this regard.

- A generic formulation for integrating the probabilistic description of the input uncertainty (parametric or geometric) with the classical finite element formulation is not well established.

- The added computational cost for obtaining the response statistics given an input uncertainty is computationally expensive. Model reduction techniques are important in this context to have a tractable computational overhead for an industry scale problem.

- Model reduction techniques for deterministic physical systems are often well established within the framework of the classical numerical algorithms adopted in their simulation studies. Integration of these model reduction schemes with the stochastic formulation has substantial scope of further improvement.

- The stochastic formulation for geometric uncertainty lacks adequate formal treatment within the stochastic finite element formulation both in terms of description of the input uncertainty and propagation of this uncertainty to the stochastic system response. This is largely due to the complicated mathematical nature of the expressions encountered in the problem.

The above points are identified as areas open to further research and has been considered in the present work. The objective of this work is to consider the state-of-the-art numerical algorithms in SFEM and provide novel improvements and generalization of the computational schemes to deal with the description and propagation of uncertainty in the mathematical models. The research broadly focuses on the development of efficient numerical methods which can give estimates of the response statistics of the physical system with probabilistic input uncertainty.

Discretization of a stochastic PDE in the spatial and stochastic dimensions within the SFEM framework results in a set of random algebraic equations. An approximation of the solution can be obtained with a low order approximation of the solution by retaining the dominant invariant properties of the system. The invariant subspace in which the solution is sought has to be chosen judiciously and has a significant impact on the accuracy and the computational efficacy of the numerical method. This would be the primary area of investigation in this work. The specific objectives of research are outlined as given in the following paragraphs.

1. **Reduced order spectral function approach in structural dynamics**
   A reduced order approach for a linear structural dynamic systems with stochastic coefficients would be investigated with a spectral function approach. The fundamental idea is to solve a discretized stochastic system in the frequency domain by projecting the solution on a reduced subspace of eigenvectors weighted by a set of rational stochastic coefficients termed as spectral functions. A Galerkin projection scheme would be used

to evaluate a set of unknown coefficients which can enhance the solution accuracy. The stochastic sampling necessary for the evaluation of the probability distributions of the response has been enhanced by hybridizing the spectral approach with a metamodeling technique.

2. **Stochastic Reduced order modeling of transient structural dynamic systems**
   The spectral function approach can be extended to study the transient dynamics of randomly parameterized structural dynamic systems. We would aim to use time adaptive stochastic spectral functions as weighting functions of the deterministic orthogonal basis onto which the solution is projected. The time integration required for the resolution of the transient stochastic response has been performed with the unconditionally stable single-step implicit Newmark scheme using a stochastic integration operator. The solution would also be investigated with finite order polynomial chaos expansion approach in terms of solution accuracy and computational time. The stochastic system response is expected to be accurately resolved even when using low order spectral functions which is computationally advantageous.

3. **A discretized spectral representation of the random field in SFEM**
   The problem of representing random fields describing the material and boundary properties of the physical system at discrete points of the spatial domain would be studied in the context of linear stochastic finite element method. A randomly parametrized diffusion system with a set of iid stochastic variables is considered. The discretized parametric fields would be incorporated into the weak isoparametric finite element formulation with multidimensional Lagrange polynomials. The treatment would potentially enable us to have a unified treatment of parametric uncertainty and random boundary fluctuations for dynamic systems. The convergence behavior of the proposed methodologies would be studied with numerical examples to establish the validity of the numerical scheme.

4. **Analysis of geometric uncertainty in SFEM**
   The proposed discretized random field representation would be utilized to express the random fluctuations of the domain boundary with nodal position coordinates and a set of random variables. The description of the boundary perturbation would be incorporated into the weak stochastic finite element formulation using a stochastic isoparametric mapping of the random domain to a deterministic master domain. A method for obtaining the linear system of equations under the proposed mapping using generic high order finite elements and the stochastic spectral Galerkin framework would be studied in detail.

5. **Reduced order modeling of the dynamic response of a stochastic linear time invariant state space system**

A model order reduction scheme of the transient response of large-scale randomly parametrized linear finite element system in state space form would be investigated. This would be an *a-priori* model reduction strategy based on the balanced truncation method would be utilized in conjunction with the stochastic spectral Galerkin finite element method. Approximation of the dominant modes of the controllable Gram matrix can be performed with iterative Arnoldi scheme applied to Lyapunov equations. The reduced order representation of the randomly parametrized dynamical system would be obtained with Arnoldi-Lyapunov vector basis using an implicit time stepping algorithm. The performance and the computational efficacy of the proposed scheme would be illustrated with numerical examples of randomly parametrized systems. The convergence of the proposed reduced order scheme would be investigated with a-posteriori error estimates.

1.6 Thesis layout

The thesis has been organized as follows:

Chapter 2 gives the theoretical development of a spectral function approach which has been applied to randomly parametrized structural dynamic systems which described with a probabilistic input uncertainty. This section contains a detailed description of the discretization of the random field to obtain a finite dimensional representation which can be used in the stochastic system matrix formulation. The deduced spectral function approach has been applied to typical structural systems with uncertain elastic properties and analyzed with respect to computational efficiency and accuracy with direct MCS and finite order chaos expansion techniques.

Chapter 3 gives the hybridization of the spectral function approach with a Gaussian process emulation to obtain a computationally efficient stochastic solution scheme. Analysis of the computational complexity of the hybrid method with other standalone techniques have been presented here. The proposed technique has been applied to a study the frequency response of a corrugated skin. The approximation accuracy of the proposed technique has been analyzed with respect to the benchmark MCS solutions.

Chapter 4 gives theoretical and numerical aspects of the extension of the spectral function approach to analyze the transient response statistics of randomly parametrized systems. The time evolution of this uncertainty propagation with different solution techniques is also considered herein. The objective here is to tackle the problem of the growing dimensionality of the classical spectral Galerkin approach for long time integration with an alternative formulation of the *spectral function* approach. The simulations have been performed for different degrees of variability of the input randomness and different dimensions of the input stochastic space and compared with the direct Monte Carlo simulations for accuracy and computational

efficiency.

Chapter 5 deals with the discrete representation of the input random field on arbitrary shaped physical domains. The approximated random field at finite number of points on the physical domain is incorporated into the stochastic weak formulation and the approximation accuracy is studied with respect to various error estimates. Using this description, the problem of obtaining the response statistics of systems on random topologies has been tackled. The computational cost and accuracies have been computed with respect to benchmark solutions.

Chapter 6 is concerned with reduced order realization of large stochastic dynamical systems based on the concept of balanced truncation. The theoretically overview of Lyapunov matrix equations for controllability Gramians have been presented and extended to the case of systems with random input parameters. The approximate method of evaluation the Arnoldi-Lyapunov basis spanning the dominant eigen space of the controllability Gramian has been detailed here. Numerical studied have been included to demonstrate the accuracy and computational efficacy of the proposed scheme.

Chapter 2

Frequency response of stochastic structural dynamic systems using spectral functions

2.1 Introduction

As has been noted in the previous chapter, the mathematical model of the physical system as well the accurate estimation of the input parameters are crucial in the numerical simulation of practical engineering systems. Since neither of the latter two may be exactly known, there has been increasing research activity to include probabilistic description of input parameters into the mathematical models. Thus stochastic models have been incorporated into the framework of the established numerical techniques and investigations of efficient and novel solution techniques [Charmpis *et al.*, 2007, Stefanou, 2009]. In this study we concentrate on the frequency domain response of damped structural dynamic systems with parametric uncertainty which is multiplicative in nature. Here we model the uncertainty with the probabilistic description, though other descriptions, like the concept of fuzzy random functions [Gersem *et al.*, 2005, Moens and Vandepitte, 2002], are also possible. There are two broad classifications of the solution strategies for the stochastic systems non-intrusive simulation techniques and intrusive spectral Galerkin methods.

Various Monte Carlo Simulation (MCS) techniques belong to the class of non-intrusive methods and have been widely used in context of the structural dynamics problems [Pradlwarter and Schuëller, 1997]. The advantage of these non-intrusive techniques, such as Monte-Carlo simulation, response surface method or projection methods, lies in the fact that they only require the use of a simple deterministic calculation code. As long as the associated deterministic code exists, the stochastic problems can be solved without any further developments. Also, they are naturally suited for parallelization. However, they require a huge number of deterministic calculations leading to high computational costs. In contrast to the full distribu-

tion function, some 'hybrid' approaches focus on the evaluation of lower-order moments of the response and efficient methods have been proposed to reduce the sample size with a view of reducing the computational burden in the stochastic space. While the convergence rate of the Monte Carlo methods is slow, its computational work grows only like a polynomial with respect to the number of random variables present in the problem. In particular cases their convergence can be accelerated by improved sampling techniques rather than random sampling. These include importance sampling, multi-point estimate method, stratified sampling, Latin hypercube sampling, orthogonal sampling, etc. which can be classified under the "variance reduction techniques" [Yamazaki and Shinozuka, 1988] and the response surface method or the experiment design method. The limitations of these techniques are dictated by the number of random variables required. Uncertain structural systems represented by few random variables subjected to deterministic loading can be well-suited to variance reduction procedures.

It is generally established that alternatives to Monte Carlo methods can provide us with an explicit functional relationship between the independent input random variables and hence can allow easy evaluation of functional statistics or probabilities. Non-statistical approaches are based on a perturbation method [Kleiber and Hien, 1992], or equivalently the lower-order Taylor approximation and the Neumann expansion method, [Yamazaki *et al.*, 1988, Zhu *et al.*, 1992] all of which comes down to the estimation of response surface in a parameter space. Through the estimated response surface, the response statistics can easily be evaluated. On the other hand the Galerkin-type methods [Deb *et al.*, 2001, Babuška *et al.*, 2005b, Matthies and Keese, 2005] developed with differing choice of the approximation space, systematically lead to a high precision solution allowing the response to be expressed explicitly in terms of the basic random variables describing the uncertainties. Their principle drawback lies in the fact that the dimensionality of the resulting system of linear equations is huge. In addition to these ad hoc Krylov-type iterative techniques have been proposed to make use of the sparsity of the system [Ghanem and Kruger, 1996, Keese and Matthies, 2005]. The difficulty to build efficient preconditioners and memory requirements induced by these techniques are still challenging and active areas of research. Ghanem and Spanos [Ghanem and Spanos, 1991] includes an example of a one-dimensional beam problem with a Karhunen-Loève (KL) discretization of the random reaction modulus of the supporting elastic foundation and the response is evaluated using orthogonal Hermite polynomials. Polynomial chaos expansion has also been successfully used in dynamic aerospace applications [Pettit and Beran, 2004, Pettit *et al.*, 2002]. A frequency dependent stochastic dynamic stiffness approach was developed in references [Manohar and Adhikari, 1998, Adhikari and Manohar, 2000] where axial and bending vibration of one-dimensional beam was considered.

Consider a bounded domain $\mathscr{D} \in \mathbb{R}^d$ with piecewise Lipschitz boundary $\partial\mathscr{D}$, where $d \leq 3$ is the spatial dimension and $t \in \mathbb{R}^+$ is the time. Further, consider that $(\Theta, \mathscr{F}, P)$ is a probabil-

ity space where $\theta \in \Theta$ is a sample point from the sampling space Θ, $\mathscr{F}$ is the complete Borel σ-algebra over the subsets of Θ and P is the probability measure. We consider here the linear stochastic partial differential equation (pde) along with the Dirichlet boundary conditions for an elastodynamic systems with parametric uncertainty

$$\begin{cases} \rho(\mathbf{r},\theta)\dfrac{\partial^2 u(\mathbf{r},t,\theta)}{\partial t^2} + \mathfrak{L}_{\mathbf{c}}\dfrac{\partial u(\mathbf{r},t,\theta)}{\partial t} + div\left(\sigma_\alpha(u(\mathbf{r},t,\theta))\right) = p(\mathbf{r},t); \\ \qquad\qquad \text{where} \quad \mathbf{r} \in \mathscr{D},\ t \in [0,T],\ \theta \in \Theta \\ \qquad \text{and} \quad u(\mathbf{r},t,\theta) = 0; \quad \mathbf{r} \text{ on } \partial\mathscr{D} \end{cases} \tag{2.1}$$

Here $\sigma_\alpha(u(\mathbf{r},t,\theta))$ denotes the stress tensor with the associated stiffness coefficient $\alpha(\mathbf{r},\theta)$ as a stationary, square integrable second order random field such that $\alpha : \mathbb{R}^d \times \Theta \to \mathbb{R}$. The operator $div(\sigma_\alpha)$ is taken to be a self-adjoint stochastic stiffness operator. $\mathfrak{L}_{\mathbf{c}}$ is the damping operator containing the stochastic coefficient vector $\mathbf{c}(\mathbf{r},\theta) : \mathbb{R}^d \times \Theta \to \mathbb{R}^\varsigma$, where ς denotes the number of damping coefficients used to represent the damping model. This form of the operator along with its coefficients can be utilized to represent various damping models like the strain rate dependent viscous damping or the velocity dependent viscous damping. $p(\mathbf{r},t)$ denotes the deterministic excitation field for which the solution $u(\mathbf{r},t,\theta)$ is sought. The present work is concentrated on the harmonic analysis, for which Eqn. (2.1) is transformed to the frequency domain as Eqn. (2.1) to obtain

$$-\omega^2\rho(\mathbf{r},\theta)\widetilde{u}(\mathbf{r},\omega,\theta) + i\omega\mathfrak{L}_{\mathbf{c}}\widetilde{u}(\mathbf{r},\omega,\theta) + div\left(\sigma_\alpha(\widetilde{u}(\mathbf{r},\omega,\theta))\right) = \widetilde{p}(\mathbf{r},\omega); \quad \omega \in \Omega \tag{2.2}$$

where Ω denotes the frequency space of the problem. Here the quantities $\widetilde{p}$ and $\widetilde{u}$ are used to represent the complex amplitudes of the harmonic input excitation and the system response respectively. The stress-strain relationship gives $\sigma_\alpha = \mathbf{E}(\alpha) : \varepsilon$ where $\mathbf{E}(\alpha)$ is the symemtric positive definite elasticity tensor depending on the scalar random parameter α and ε is the strain tensor expressed as $\varepsilon = \mathbf{D}\widetilde{\mathbf{u}}$, where $\mathbf{D}$ is the strain-displacement matrix. Well established techniques of variational formulation of the displacement-based deterministic finite-element methods [Ghanem and Spanos, 1991, Kleiber and Hien, 1992, Matthies *et al.*, 1997] gives the following bilinear form for the elastodynamic system

$$\begin{aligned} \mathscr{B}(\widetilde{\mathbf{v}},\widetilde{\mathbf{u}};\theta) &= -\omega^2\int_{\mathscr{D}} \widetilde{\mathbf{v}}\,\rho(\mathbf{r},\theta)\,\widetilde{\mathbf{u}}\,d\mathscr{D} + i\omega\int_{\mathscr{D}} \widetilde{\mathbf{v}}\,\mathfrak{L}_{\mathbf{c}}\,\widetilde{\mathbf{u}}\,d\mathscr{D} + \int_{\mathscr{D}} \{\mathbf{D}\widetilde{\mathbf{v}}\}^T\,\mathbf{E}(\alpha)\,\{\mathbf{D}\widetilde{\mathbf{u}}\}\,d\mathscr{D} \\ \mathscr{L}(\widetilde{\mathbf{v}};\theta) &= \int_{\mathscr{D}} \widetilde{\mathbf{v}}\widetilde{p}\,d\mathscr{D} \\ \text{so that,} \quad \mathscr{B}(\widetilde{\mathbf{v}},\widetilde{\mathbf{u}};\theta) &= \mathscr{L}(\widetilde{\mathbf{v}};\theta) \qquad \forall\ \widetilde{\mathbf{v}} \in \mathscr{E}[\mathscr{D}] \end{aligned} \tag{2.3}$$

where $\mathscr{E}[\mathscr{D}]$ is the space of admissible trial functions which have finite strain energy on the spatial domain and satisfying the prescribed boundary conditions. Eqn. (2.3) gives a set of

discretized linear algebraic equations in terms of the mass, damping and stiffness matrices. These can be expressed in a compact form as

$$\mathbf{A}(\omega,\theta)\widetilde{\mathbf{u}}(\omega,\theta) = \widetilde{\mathbf{p}}(\omega); \quad \forall\, \theta \in \Theta;\ \omega \in \Omega;\ \mathbf{A} \in \mathbb{C}^{n\times n};\ \widetilde{\mathbf{u}}, \widetilde{\mathbf{p}} \in \mathbb{C}^{n} \tag{2.4}$$

where $\mathbf{A}(\omega,\theta)$ is the complex frequency dependent coefficient matrix which inherits the uncertainty of the random parameters involved in the governing pde. There are a number of techniques to express the randomness of the uncertain system matrices with known covariance matrices which allows the decomposition of the $\mathbf{A}(\omega,\theta)$ into a standard mean stiffness matrix equivalent plus its deviatoric parts based on the expansion techniques of discretized random fields. The detailed description of these matrices arising for the case of structural dynamic systems is given in Sec. 2.3.1. It is to be noted that the stochastic linear algebraic set of equations, given in Eqn. (2.4), is commonly encountered for the stochastic FEA for structural dynamics and the primary focus of the present work is to study a Galerkin projection method to approximate the solution vector in a reduced space.

This chapter is organized as follows. In Sec. 2.2 an overview of the aspects of SFEM is given here. Discussion on the finite dimensional representation of the random field is given here. Section 2.3 gives a complete description of the spectral function approach proposed for the randomly parametrized structural dynamic system. In Sec. 2.4 a reduced Galerkin error minimization approach is proposed. The post processing of the results to obtain the response moments are discussed in Sec. 2.5. Based on the theoretical results, an example problem is shown in Sec. 2.6 where the proposed method of reduced spectral basis is applied to the stochastic dynamical system of an one-dimensional Euler-Bernoulli beam and a two-dimensional Kirchhoff-Love thin plate. A summary of the results and major conclusions arising from this study are given in Sec. 2.7.

2.2 Elements of the stochastic finite element method

2.2.1 Finite dimensional spectral representation of a random field

Most of the works in stochastic finite elements which are concerned with the solution of randomly parametrized systems generally assume a mathematically tractable model for the random field which might not always be experimentally justifiable. For these applications the random fields are chosen to obey certain physically meaningful regularity assumptions, such as mean-square continuity, homogeneity, isotropy, etc. [Kolovos *et al.*, 2004, Christakos, 1992].

To begin with, we take a stochastic parameter input to the mathematical model defined on a compact region $\mathscr{D} \subset \mathbb{R}^d$ and a probability space $(\Theta, \mathscr{F}, P)$ as $a(\mathbf{r},\theta) : \mathscr{D} \times \Theta \to \mathbb{R}$. This

parameter is written as a series expansion in a variable separable form as

$$a(\mathbf{r},\theta) = \sum_i \varphi_i(\mathbf{r})\kappa(\theta) = \boldsymbol{\varphi}(\mathbf{r})\mathscr{K}(\theta) \tag{2.5}$$

where the vector of random functions $\mathscr{K}(\theta) = \{\kappa_1(\theta),\ldots,\kappa_m(\theta)\}^T$ are weighted by the spatial shape functions $\boldsymbol{\varphi}(\mathbf{r}) = \{\varphi_1(\mathbf{r}),\ldots,\varphi_m(\mathbf{r})\}$. These shape functions can be chosen based on the type of series representation used to represent the random field. The different methods can be listed as **a)** the interpolation method [Liu *et al.*, 1986] where $\boldsymbol{\varphi}(\mathbf{r})$ are chosen as the finite element interpolation functions, **b)** the mid-point method [Li and Kiureghian, 1993] where the shape functions are piece-wise constants within an element (assuming at the mid-point), **c)** the Expansion Optimal Linear Estimation (EOLE) method [Li and Kiureghian, 1993] which seeks to obtain an optimal spectral decomposition (optimal in the sense of using minimum number of random variables used in the approximation) by minimizing the error variance between the continuous and approximated random fields, **d)** the spatial average method [Vanmarcke, 1983] which uses piecewise constant shape functions with the random functions being the spatial average of the random parameter over the discretized finite elements domains **e)** the orthogonal expansion method which emphasizes on using elements of $\boldsymbol{\varphi}(\mathbf{r})$ such that they are mutually orthogonal in $L^2(\mathscr{D})$ [Zhang and Ellingwood, 1994] and finally and perhaps most importantly **f)** the spectral decomposition of the stochastic process which relies on discretizing the latter with a finite number of spectral components of the covariance kernel associated with the random process. We discuss this last approach in some detail here.

The objective of the spectral decomposition method is to express the random parameter with a set of denumerable number of orthogonal random variables (spanning the stochastic Hilbert space) and the associated spatial eigen functions. Let $C_a : \mathscr{D}\times\mathscr{D} \to \mathbb{R}$ be a kernel function which admits to the following decomposition

$$\int_{\mathscr{D}} C_a(\mathbf{r}_1,\mathbf{r}_2)\varphi_j(\mathbf{r}_1)\mathrm{d}\mathbf{r}_1 = \nu_j\varphi_j(\mathbf{r}_2), \quad \forall\, j = 1,2,\ldots \tag{2.6}$$

The above is a homogeneous Fredholm integral equation of the second kind. Let us define the function $\mathscr{C}_a\varphi$ such that

$$(\mathscr{C}_a\varphi)(\mathbf{r}_1) = \int_{\mathscr{D}} C_a(\mathbf{r}_1,\mathbf{r}_2)\varphi(\mathbf{r}_2)d\mathbf{r}_2 \;\; \mathbf{r}_1,\mathbf{r}_2 \in \mathscr{D} \tag{2.7}$$

It can be easily verified that $\mathscr{C}_a : L^2(\mathscr{D}) \to L^2(\mathscr{D})$ is a linear operator on a vector space and hence Eqn. (2.6) can be expressed as

$$\mathscr{C}_a\varphi = \nu\varphi \tag{2.8}$$

Non-trivial solution to the above homogeneous equation exists only for those values of ν which makes $(I - \nu\mathscr{C}_a)$ non-invertible where I is the identity operator. The covariance functions C_a commonly encountered in the study of randomly parameterized engineering systems are bounded and symmetric, hence the associated linear operator $\mathscr{C}_a$ is compact and self-adjoint. Considering the fact that the solution of Eqn. (2.6) lies in some normed vector space, it is possible to represent the random parameter using a finite number of dominant components based on the eigen value problem in Eqn. (2.8).

The covariance functions C_a commonly encountered in the study of randomly parameterized engineering systems are bounded and symmetric when considered on a bounded domain $\mathscr{D} \subset \mathbb{R}^d$, hence the associated linear operator $\mathscr{C}_a$ is compact and self-adjoint. Hence the solution of the eigen-value problem in (2.8) yields ordered real eigenvalues $\nu = \{\nu_i : \nu_i \geq \nu_{i+1}\ \forall i$ and $\|C_a\|^2_{L^2(\mathscr{D}\times\mathscr{D})} = \sum_i \nu_i^2\}$ and mutually orthogonal eigenfunctions in $L^2(\mathscr{D})$. Thus the error in approximating the covariance function with a finite number (m) of eigenfunctions results in an error which can be expressed as

$$\text{error } \|C_a - C_{a_m}\|_{L^2(\mathscr{D}\times\mathscr{D})} = \sum_{i=m+1}^{\infty} \nu_i^2. \tag{2.9}$$

where C_{a_m} is the covariance function approximated with m eigenvalues. Thus it can be expressed as (from Mercer's theorem)

$$C_{a_m}(\mathbf{r}_1, \mathbf{r}_2) = \sum_{i=1}^{m} \nu_i \varphi_i(\mathbf{r}_1)\varphi_i(\mathbf{r}_2) \tag{2.10}$$

where C_{a_m} converges uniformly to C_a as $m \to \infty$.

The truncated Karhunen-Loève expansion of the stochastic process $a(\mathbf{r}, \theta)$ is thus expressed using these eigen-functions as

$$\hat{a}_m(\theta, \mathbf{r}) = E[a](\mathbf{r}) + \sum_{i=1}^{m} \sqrt{\nu_i}\varphi_i(\mathbf{r})\xi_i(\theta) \quad \forall m \in \mathbb{N}_+ \tag{2.11}$$

where $E[a](\mathbf{r})$ is the mean function, $\{\xi_i(\theta)\}_{i=1}^m$ are a set of mutually independent, uncorrelated standard Gaussian random variables with zero mean $(E(\xi_i) = 0)$ and unit variance $(E(\xi_i^2) = 1)$. The eigenfunctions $\varphi_i(\mathbf{r})$ can be assumed to have sufficient smoothness for smooth covariance functions, and if the eigenpairs are decaying according to at least $\sqrt{\nu_k}\,\|\varphi_k\|_{L^\infty(\mathscr{D})} = \mathcal{O}(\frac{1}{1+k^s})$ for some decay exponent $s > 1$, then $\|a - \hat{a}_m\|_{\tilde{L}^\infty(\mathscr{D})} \to 0$, [Babuška *et al.*, 2005b]. For practical engineering problems, the parametric randomness is modeled with a finite set of random variables $\boldsymbol{\xi} = (\xi_1, \xi_2, \ldots, \xi_m) : \Theta \to \mathbb{R}^m$, using first few largest eigenpairs in the reduced probability space $\left(\Theta^{(m)}, \mathscr{F}^{(m)}, P^{(m)}\right)$, where $\Theta^{(m)} = \text{Range}(\boldsymbol{\xi})$ is a subset of $\mathbb{R}^m$, $\mathscr{F}^{(m)}$ is the associated Borel σ-algebra and $P^{(m)}$ is the

image probability measure. This is facilitated by the fact that the non-negative eigenvalues satisfy the relation $\sum_{i=1}^{\infty_i} \lambda_i = \int_{\mathscr{D}} Var[a](\mathbf{r})d\mathbf{r}$ and decay in accordance with the aforementioned relation.

The model given in Eqn. (2.11) has been widely presented in literature (see for example [Deb *et al.*, 2001, Schuëller, 2006]). This form maybe used to represent the experimentally obtained data using a principal component analysis [Babuška *et al.*, 2003]. If dependent random variables are chosen, then the random field can be expressed as $\alpha(\mathbf{r}, \boldsymbol{\xi}) = \bar{\alpha}(\mathbf{r}) + \sum_{i=1}^{M} \varphi_i(\mathbf{r})\xi_i(\mathbf{r}_i, \theta)$ with $\xi_i(\mathbf{r}_i, \theta)$ being the experimental measurements of the random parametric field at positions $\mathbf{r}_i$ along with the weighting functions $\varphi_i(\mathbf{r})$. However, due to the absence of analytical information about the marginal distributions of the non-Gaussian $\alpha(\mathbf{r}, \boldsymbol{\xi})$, ad-hoc assumptions are made regarding the distribution of the ξ_i.

However, for arbitrary random field models, the random parameter can be expressed in a mean-square convergent series using the Wiener-Askey chaos expansion [Xiu and Karniadakis, 2002] where the stochastic process is discretized with a set of iid random variables $\hat{\xi}(\theta) = \{\hat{\xi}^{(1)}, \ldots, \hat{\xi}^{(n)}\}$ using a finite order chaos-expansion from the Askey scheme such that

$$a(\mathbf{r}, \theta) = \sum_{i=0}^{p} \mathscr{H}_i(\hat{\xi}(\theta))a_i(\mathbf{r}) \tag{2.12}$$

where $\mathscr{H}_i(\hat{\xi}(\theta))$ are the multivariate orthogonal stochastic polynomial functions depending on the joint probability density function of the stochastic Hilbert space. The undetermined coefficients $a_i(\mathbf{r})$ associated with the series expansion can be evaluated as

$$a_i(\mathbf{r}) = \frac{\left\langle a(\mathbf{r}, \theta), \mathscr{H}_i(\hat{\xi}(\theta)) \right\rangle_{L^2(\Theta)}}{\left\langle \mathscr{H}_i(\hat{\xi}(\theta)) \right\rangle_{L^2(\Theta)}} \tag{2.13}$$

The solution methodology presented here is applicable to this kind of general decomposition of the random field.

2.2.2 Spectral methods and other solution techniques for structural dynamics

The solution techniques of the stochastic linear systems consist of different methods which might involve the solution of the random eigenvalue problem [Scheidt and Purkert, 1983] using various approaches such as polynomial chaos [Pascual and Adhikari, 2012, Ghanem and Ghosh, 2007], and sensitivity based approaches [Eldred, 1992]. Now Eqn. (2.4) is a system of coupled, complex stochastic linear algebraic equations. For real valued systems, several methods have been proposed which include, low-order perturbation methods [Kleiber and Hien, 1992, Liu *et al.*, 1986], Neumann expansion method [Yamazaki *et al.*, 1988] and simulation

methods [Papadrakakis and Papadopoulos, 1996]. Reduced order methods [Adhikari, 2011] have been utilized to approximate the stochastic system response with finite order stochastic weighting functions called spectral functions. The stochastic spectral Galerkin methods (see [Nouy, 2009] for a recent review) is a class of intrusive uncertainty propagation method which expresses the system response with orthogonal family finite order stochastic polynomials. These include the polynomial chaos (PC) expansion [Ghanem and Spanos, 1991] and the Wiener–Askey chaos expansion [Xiu and Karniadakis, 2002]. For the calculation of frequency response function of dynamical systems, several approaches, such as meta-model based methods [Pichler *et al.*, 2009], interpolation based methods [Goller *et al.*, 2011], modal approaches [den Nieuwenhof and Coyette, 2003] and Approximate Principal Deformation Mode (APDM) approach [Falsone and Ferro, 2007] have been proposed.

It is known that the spatially discretized solution vector $\widetilde{\mathbf{u}}(\omega,\theta)$ lies in the tensor product space $\mathbb{C}^n \otimes \Upsilon$, where Υ is an ad-hoc function space for real-valued random variables [Nouy, 2009, Deb *et al.*, 2001]. Given that the stochastic system has been discretized and represented with a finite number of random variables $\hat{\xi}(\theta) = \{\hat{\xi}^{(1)}, \ldots, \hat{\xi}^{(p)}\}$ as in Sec. 2.2.1, the stochastic subspace reduces to Υ_p where $\Upsilon_p \subset \Upsilon$. When each random component $\hat{\xi}^{(i)}$ is independent, then Υ_p is a tensor product space $\Upsilon^1 \otimes \Upsilon^2 \otimes \ldots \otimes \Upsilon^p$. Now, according to the approximate basis building techniques that focus on expansion of the solution vector using some polynomial functions, the solution vector in Eqn. (2.4) can be expressed in the form

$$\widetilde{\mathbf{u}}(\omega,\theta) = \sum_{\alpha \in \mathscr{I}_p} \mathscr{H}_\alpha(\omega,\theta)\widetilde{u}_\alpha(\omega); \quad \widetilde{u}_\alpha(\omega) \in \mathbb{C}^n \tag{2.14}$$

where $\mathscr{H}_\alpha$ are the basis in Υ_p, $\widetilde{u}_\alpha(\omega)$ are the set of unknown coefficients to be evaluated and $\mathscr{I}_p$ is a subset of $\mathscr{I}$ with cardinal p. It is evident from the above steps that the approximate basis functions can be chosen to depend on frequency which can allow for the efficiency of the solution technique to be frequency adaptive and hence well suited for applications over a wide frequency range.

The form of the polynomial functions $\mathscr{H}_\alpha(\omega,\theta)$ used in Eqn. (2.14) varies according to the chosen solution approach. The spectral approaches (polynomial choas, generalized chaos) classically use orthogonal polynomial basis $\mathscr{H}_\alpha(\theta)$ to approximate the solution in stochastic space. Any random field can be spanned using the generalized functional basis from the Askey-chaos [Xiu and Karniadakis, 2002] so that the orthonormality with respect to the density functions can be retained. Thus the classical spectral Galerkin approximation techniques of solving the stochastic system using a finite number of stochastic basis can be posed as follows: it is necessary to find $\widetilde{u}_\alpha(\omega) \in \mathbb{C}^n \otimes \Upsilon_p$ such that

$$\sum_{\alpha \in \mathscr{I}_p} E(\mathbf{A}\mathscr{H}_\beta\mathscr{H}_\alpha)\widetilde{u}_\alpha = E(\mathscr{H}_\beta\widetilde{\mathbf{p}}) \quad \forall\, \beta \in \mathscr{I}_p \tag{2.15}$$

which leads to the set of linear algebraic equations for evaluating the unknown coefficients introduced in Eqn. (2.14). Frequency domain analysis of stochastic systems has been studied using this method by Sarkar and Ghanem [Sarkar and Ghanem, 2002] for the medium-frequency structural dynamic analysis. However, the computational cost associated with the inversion of the coefficient matrix in Eqn. (2.15) can become prohibitive for systems with large dimensions and near resonance frequencies even for moderate values of variability of the input random field. There are some Krylov-type solution techniques [Ghanem and Kruger, 1996, Keese and Matthies, 2005] have been established which takes advantage of the sparsity of the system and tries to employs a preconditioner to efficiently solve a given system. However, the availability of optimal pre-conditioners is limited to systems with low variance and hence for systems otherwise, the iterative technique results in drastic increase in computational costs.

2.3 Projection of stochastic dynamic response in the modal space

2.3.1 Stochastic FE modeling of structural dynamic systems

The random fields in Eqn. (2.1) can be discretized using the Karhunen-Loève expansion with a finite number of random variables based on the decaying eigen spectrum of the covariance kernel of the random fields. This has been illustrated in Sec. 2.2.1. Using the discretized random field model, the stochastic system matrices can be derived from Eqn. (2.1) using the well-established standard methods found in the stochastic FEM literature [Babuška *et al.*, 2004, 2005b, Ghanem and Spanos, 1991, Matthies and Keese, 2005]. Following those developments, the stochastic PDE along with the boundary conditions would result in a set of equations of the form

$$\mathbf{M}(\theta)\ddot{\mathbf{u}}(t,\theta) + \mathbf{C}(\theta)\dot{\mathbf{u}}(t,\theta) + \mathbf{K}(\theta)\mathbf{u}(t,\theta) = \mathbf{f}_0(t) \tag{2.16}$$

where $\mathbf{M}(\theta) = \mathbf{M}_0 + \sum_{i=1}^{p_1} \mu_i(\theta_i)\mathbf{M}_i \in \mathbb{R}^{n\times n}$ is the random mass matrix, $\mathbf{K}(\theta) = \mathbf{K}_0 + \sum_{i=1}^{p_2} \nu_i(\theta_i)\mathbf{K}_i \in \mathbb{R}^{n\times n}$ is the random stiffness matrix along with $\mathbf{C}(\theta) \in \mathbb{R}^{n\times n}$ the random damping matrix. Here the mass and stiffness matrices have been expressed in terms of their deterministic components ($\mathbf{M}_0$ and $\mathbf{K}_0$) along with their random contributions ($\mathbf{M}_i$ and $\mathbf{K}_i$), which have been obtained from discretizing the stochastic field with a finite number of random variables ($\mu_i(\theta_i)$ and $\nu_i(\theta_i)$) and their corresponding spatial basis functions. Hence the random mass and the stiffness matrices have been modeled with p_1 and p_2 random variables respectively. In the present work proportional damping is considered for which $\mathbf{C}(\theta) = \zeta_1\mathbf{M}(\theta) + \zeta_2\mathbf{K}(\theta)$, where ζ_1 and ζ_2 are deterministic scalars. For the harmonic analysis of the structural system considered in Eqn. (2.16), we represented it in the frequency domain

as

$$\left[-\omega^2\mathbf{M}(\theta) + i\omega\mathbf{C}(\theta) + \mathbf{K}(\theta)\right]\widetilde{\mathbf{u}}(\omega,\theta) = \widetilde{\mathbf{f}}_0(\omega) \tag{2.17}$$

where $\widetilde{\mathbf{u}}(\omega,\theta)$ is the complex frequency domain system response amplitude, $\widetilde{\mathbf{f}}_0(\omega)$ is the amplitude of the harmonic force and ω is the frequency.

Now, if the random variables associated with the mass and stiffness matrices are grouped as

$$\begin{aligned} &\xi_i(\theta) = \mu_i(\theta) \quad \text{for} \quad i = 1, 2, \ldots, p_1 \\ \text{and} \quad &\xi_j(\theta) = \nu_{j-p_1}(\theta) \quad \text{for} \quad j = p_1+1, p_1+2, \ldots, p_1+p_2 \end{aligned}$$

then it follows that the linear structural system in Eqn. (2.17) can be expressed as

$$\left(\mathbf{A}_0(\omega) + \sum_{i=1}^{M} \xi_i(\theta)\mathbf{A}_i(\omega)\right)\widetilde{\mathbf{u}}(\omega,\theta) = \widetilde{\mathbf{f}}_0(\omega) \tag{2.18}$$

where $\mathbf{A}_0 \in \mathbb{C}^{n\times n}$ and $\mathbf{A}_i \in \mathbb{C}^{n\times n}$ represent the complex deterministic and stochastic parts respectively of the mass, the stiffness and the damping matrices ensemble, and $M = p_1 + p_2$ is the total number of random variables used to represent the stochastic parameters in the spatial domain. The choice of M is based on the number of basis functions used to discretize the random parameter in the spatial domain following Eqn. (2.11). The expressions for $\mathbf{A}_0$ and $\mathbf{A}_i$ vary according to the damping model chosen for a particular application. For the case of proportional damping, the matrices $\mathbf{A}_0$ and $\mathbf{A}_i$ can be written as

$$\mathbf{A}_0(\omega) = \left[-\omega^2 + i\omega\zeta_1\right]\mathbf{M}_0 + \left[i\omega\zeta_2 + 1\right]\mathbf{K}_0 \tag{2.19}$$

$$\begin{aligned} \text{and,} \quad &\mathbf{A}_i(\omega) = \left[-\omega^2 + i\omega\zeta_1\right]\mathbf{M}_i \quad \text{for} \quad i = 1, 2, \ldots, p_1 \\ &\mathbf{A}_j(\omega) = \left[i\omega\zeta_2 + 1\right]\mathbf{K}_j \quad \text{for} \quad j = p_1+1, p_1+2, \ldots, p_1+p_2 \end{aligned} \tag{2.20}$$

Equation (2.18) together with the above two equations completely define the discretized system considered in this study.

In Eqn. (2.18), $\mathbf{A}_0(\omega)$ and $\mathbf{A}_i(\omega) \in \mathbb{C}^{n\times n}; i = 1, 2, \ldots, M$ are complex symmetric frequency dependent matrices, $\mathbf{u}(\omega,\theta) \in \mathbb{C}^n$ is the solution vector and $\widetilde{\mathbf{f}}_0(\omega) \in \mathbb{C}^n$ is the input vector. One of the main aims of a stochastic dynamic analysis is to obtain $\mathbf{u}(\omega,\theta)$ for $\theta \in \Theta$ and for all frequency ω from Eqn. (2.18) in an efficient manner. It is emphasized that the proposed solution technique is applicable for the case when $\xi_i(\theta)$ are in general non-Gaussian and correlated random variables.

2.3.2 Derivation of the frequency-dependent spectral functions

An approximation to the solution of Eqn. (2.18) can be construed as a linear combination of functions of random variables and deterministic vectors following the stochastic finite element method which has been studied previously in context of statical systems in [Adhikari, 2011]. The objective of an efficient scheme of resolution of the response statistics of the randomly parametrized system is to obtain a good approximation of it using a small number of basis functions. We utilize here a reduced order stochastic approximation in conjunction with a Galerkin approach which uses the generalized eigen modes of the baseline model to approximate the stochastic system response.

For the case of random system matrices, the deterministic eigen modes of the solution have to be weighed by some stochastic coefficients, which in turn can be approximated with non-linear functions of the input random variables. To begin with, the eigenvectors $\phi_k \in \mathbb{R}^n$ of the generalized eigenvalue problem are considered such that,

$$\mathbf{K}_0\phi_k = \lambda_k\mathbf{M}_0\phi_k; \quad k = 1, 2, \ldots n \tag{2.21}$$

Since the matrices $\mathbf{K}_0$ and $\mathbf{M}_0$ are symmetric and generally non-negative definite, the eigenvectors ϕ_k for $k = 1, 2, \ldots n$ form a complete basis. The matrices of the eigenvalues and eigenvectors from Eqn. (2.21) are $\boldsymbol{\lambda}_0 = \text{diag}\,[\lambda_1, \lambda_2, \ldots, \lambda_n] \in \mathbb{R}^{n\times n}$ and $\boldsymbol{\Phi} = [\phi_1, \phi_2, \ldots, \phi_n] \in \mathbb{R}^{n\times n}$. Eigenvalues are ordered in the ascending order so that $\lambda_1 < \lambda_2 < \ldots < \lambda_n$ with orthogonal eigenvectors $\boldsymbol{\Phi}$ which gives $\boldsymbol{\Phi}^T\mathbf{K}_0\boldsymbol{\Phi} = \boldsymbol{\lambda}_0$ and $\boldsymbol{\Phi}^T\mathbf{M}_0\boldsymbol{\Phi} = \mathbf{I}$. Since the undamped eigenvectors ϕ_k for $k = 1, 2, \ldots n$ form a complete basis, the solution of Eqn. (2.18), $\widetilde{\mathbf{u}}(\omega, \theta)$ can be projected to on this basis for a fixed value of ω.

The eigenvectors $\phi_k \in \mathbb{R}^n$ of the generalized eigenvalue problem of Eqn. (2.21) is considered here which gives from Eqn. (2.19)

$$\begin{aligned} & \boldsymbol{\Phi}^T\mathbf{A}_0\boldsymbol{\Phi} = \boldsymbol{\Phi}^T\left([-\omega^2 + i\omega\zeta_1]\mathbf{M}_0 + [i\omega\zeta_2 + 1]\mathbf{K}_0\right)\boldsymbol{\Phi} \\ \text{or,} \quad & \boldsymbol{\Phi}^T\mathbf{A}_0\boldsymbol{\Phi} = \left(-\omega^2 + i\omega\zeta_1\right)\mathbf{I} + \left(i\omega\zeta_2 + 1\right)\boldsymbol{\lambda}_0 \\ \text{from which,} \quad & \boldsymbol{\Phi}^T\mathbf{A}_0\boldsymbol{\Phi} = \boldsymbol{\Lambda}_0 \quad \text{and} \quad \mathbf{A}_0 = \boldsymbol{\Phi}^{-T}\boldsymbol{\Lambda}_0\boldsymbol{\Phi}^{-1} \end{aligned} \tag{2.22}$$

where $\boldsymbol{\Lambda}_0 = \left(-\omega^2 + i\omega\zeta_1\right)\mathbf{I} + \left(i\omega\zeta_2 + 1\right)\boldsymbol{\lambda}_0$ and $\mathbf{I}$ is the identity matrix. We also introduce the transformations

$$\widetilde{\mathbf{A}}_i = \boldsymbol{\Phi}^T\mathbf{A}_i\boldsymbol{\Phi} \quad \text{and} \quad \mathbf{A}_i = \boldsymbol{\Phi}^{-T}\widetilde{\mathbf{A}}_i\boldsymbol{\Phi}^{-1} \text{ where } \widetilde{\mathbf{A}}_\text{i}, \in \mathbb{C}^{n\times n};\ \mathbf{A}_\text{i} \in \mathbb{C}^{n\times n};\ \forall \text{i} = 1, 2, \ldots, \text{M} \tag{2.23}$$

Note that $\widetilde{\mathbf{A}}_0 = \boldsymbol{\Lambda}_0$ is a diagonal matrix. The solution of Eqn. (2.18) is given by

$$\widetilde{\mathbf{u}}(\omega, \theta) = \left[\mathbf{A}_0(\omega) + \sum_{i=1}^{M}\xi_i(\theta)\mathbf{A}_i(\omega)\right]^{-1}\widetilde{\mathbf{f}}_0(\omega) \tag{2.24}$$

Using Eqns. (2.22)–(2.23) one has

$$\widetilde{\mathbf{u}}(\omega,\theta)=\left[\mathbf{\Phi}^{-T}\mathbf{\Lambda}_0(\omega)\mathbf{\Phi}^{-1}+\sum_{i=1}^{M}\xi_i(\theta)\mathbf{\Phi}^{-T}\widetilde{\mathbf{A}}_i(\omega)\mathbf{\Phi}^{-1}\right]^{-1}\widetilde{\mathbf{f}}_0(\omega)=\mathbf{\Phi}\mathbf{\Psi}\left(\omega,\boldsymbol{\xi}(\theta)\right)\mathbf{\Phi}^T\widetilde{\mathbf{f}}_0(\omega) \tag{2.25}$$

where $\mathbf{\Psi}\left(\omega,\boldsymbol{\xi}(\theta)\right)=\left[\mathbf{\Lambda}_0(\omega)+\sum_{i=1}^{M}\xi_i(\theta)\widetilde{\mathbf{A}}_i(\omega)\right]^{-1}$ and the M-dimensional random vector

$$\boldsymbol{\xi}(\theta)=\{\xi_1(\theta),\xi_2(\theta),\ldots,\xi_M(\theta)\}^T \tag{2.26}$$

The matrix $\widetilde{\mathbf{A}}_i$ can be written in terms of it's diagonal and off-diagonal terms as $\widetilde{\mathbf{A}}_i=\mathbf{\Lambda}_i+\mathbf{\Delta}_i,\ i=1,2,\ldots,M$. Here the diagonal matrix is $\mathbf{\Lambda}_i=\text{diag}\left[\widetilde{\mathbf{A}}_i\right]=\text{diag}\left[\Lambda_{i_1},\Lambda_{i_2},\ldots,\Lambda_{i_n}\right]\in\mathbb{C}^{n\times n}$ and the matrix containing only the off-diagonal elements $\mathbf{\Delta}_i=\widetilde{\mathbf{A}}_i-\mathbf{\Lambda}_i$ is such that $\text{Trace}\left(\mathbf{\Delta}_i\right)=0$. Using these, from Eqn. (2.25) one has

$$\mathbf{\Psi}\left(\omega,\boldsymbol{\xi}(\theta)\right)=\left[\underbrace{\mathbf{\Lambda}_0(\omega)+\sum_{i=1}^{M}\xi_i(\theta)\mathbf{\Lambda}_i(\omega)}_{\mathbf{\Lambda}\left(\omega,\boldsymbol{\xi}(\theta)\right)}+\underbrace{\sum_{i=1}^{M}\xi_i(\theta)\mathbf{\Delta}_i(\omega)}_{\mathbf{\Delta}\left(\omega,\boldsymbol{\xi}(\theta)\right)}\right]^{-1} \tag{2.27}$$

where $\mathbf{\Lambda}\left(\omega,\boldsymbol{\xi}(\theta)\right)\in\mathbb{C}^{n\times n}$ is a diagonal matrix and $\mathbf{\Delta}\left(\omega,\boldsymbol{\xi}(\theta)\right)$ is an off-diagonal only matrix. Thus $\mathbf{\Psi}\left(\omega,\boldsymbol{\xi}(\theta)\right)=\left[\mathbf{\Lambda}\left(\omega,\boldsymbol{\xi}(\theta)\right)+\mathbf{\Delta}\left(\omega,\boldsymbol{\xi}(\theta)\right)\right]^{-1}$.

We introduce the transformation of the stochastic system response to the modal coordinates such that $\widetilde{\mathbf{u}}(\omega,\theta)=\sum_i\Phi_i c_i(\omega,\theta)=[\mathbf{\Phi}]\{\mathbf{c}_i(\omega,\theta)\}$, where $\mathbf{c}(\omega,\theta)\in\mathbb{C}^n$ is the complex, frequency dependent modal response vector and following from Eqns. (2.24)–(2.27) we have

$$\left[\mathbf{\Lambda}(\omega,\boldsymbol{\xi}(\theta))+\mathbf{\Delta}\left(\omega,\boldsymbol{\xi}(\theta)\right)\right]\mathbf{c}(\omega,\theta)=\mathbf{\Phi}^T\widetilde{\mathbf{f}}_0(\omega) \tag{2.28}$$

$$\text{such that,}\quad \mathbf{c}(\omega,\theta)=\left[\mathbf{\Lambda}\left(\omega,\boldsymbol{\xi}(\theta)\right)+\mathbf{\Delta}\left(\omega,\boldsymbol{\xi}(\theta)\right)\right]^{-1}\mathbf{\Phi}^T\widetilde{\mathbf{f}}_0(\omega)=\mathbf{\Psi}\left(\omega,\boldsymbol{\xi}(\theta)\right)\mathbf{\Phi}^T\widetilde{\mathbf{f}}_0(\omega)$$

From Eqns. (2.25)–(2.27), we have an m-th order Neumann matrix series representation of the modal response vector as

$$\mathbf{c}(\omega,\theta)=\mathbf{\Psi}^{(m)}\left(\omega,\boldsymbol{\xi}(\theta)\right)\mathbf{\Phi}^T\widetilde{\mathbf{f}}_0(\omega)=\mathbf{\Gamma}^{(m)}\left(\omega,\boldsymbol{\xi}(\theta)\right) \tag{2.29}$$

$$\text{where}\quad \mathbf{\Psi}^{(\mathrm{m})}\left(\omega,\boldsymbol{\xi}(\theta)\right)=\sum_{s=0}^{m-1}(-1)^s\left[\mathbf{\Lambda}^{-1}\left(\omega,\boldsymbol{\xi}(\theta)\right)\mathbf{\Delta}\left(\boldsymbol{\xi}(\theta)\right)\right]^s\mathbf{\Lambda}^{-1}\left(\omega,\boldsymbol{\xi}(\theta)\right) \tag{2.30}$$

where $\mathbf{\Gamma}^{(m)}(\omega,\boldsymbol{\xi}(\theta))=\left\{\Gamma_1^{(m)}(\omega,\boldsymbol{\xi}(\theta)),\ldots,\Gamma_n^{(m)}(\omega,\boldsymbol{\xi}(\theta))\right\}^T$ is the vector of complex frequency dependent stochastic coefficients obtained from the matrix series representation of

$\Psi^{(m)}(\omega, \boldsymbol{\xi}(\theta))$ in Eqn. (2.30). Hence the stochastic response vector $\widetilde{\mathbf{u}}(\theta)$ is given by

$$\widetilde{\mathbf{u}}^{(m)}(\omega, \theta) = \sum_{k=1}^{n} \Gamma_k^{(m)}(\omega, \boldsymbol{\xi}(\theta))\, \boldsymbol{\phi}_k \tag{2.31}$$

The solution vector $\widetilde{\mathbf{u}}(\theta)$ is projected in the space spanned by $\boldsymbol{\phi}_k$ and weighted by $\Gamma_k^{(m)}(\omega, \boldsymbol{\xi}(\theta))$ which are referred to as m-th order 'spectral functions' [Adhikari, 2011]. Since $\theta \in \Theta$ is arbitrary and the above development is not dependent on the choice of any particular joint distribution function of the random variables used to model the parametric uncertainty. Thus $\widetilde{\mathbf{u}}^{(m)}(\omega, \theta)$ is the solution of Eqn. (2.18) for a sufficiently large value of m. However, the computational efficiency demands the solution to be approximated to a sufficient degree of accuracy even with the lower order of spectral functions.

$\Gamma_k^{(m)}(\omega, \boldsymbol{\xi}(\theta)), k = 1, 2, \ldots n$ are termed as the *spectral functions* characterized by their order m and is expressed as a function of the spectral components of the mean system matrices. The spectral functions used in approximation of the stochastic system response are highly non-linear in $\boldsymbol{\xi}(\theta)$ indicating that the response vector is a non-linearly filtered version of the random variables used to model the parametric uncertainty. For structural mechanics problems, Eqn. (2.31) indicates that the response of a stochastic system is a linear combination of fundamental vibration modes weighted by the stochastic spectral functions Γ_k. It should be pointed out that the we denote the order m of the spectral functions as $m = s + 1$, where s is the order of expansion of the improved Neumann series.

The vector of spectral functions of order m can be obtained by retaining m terms in the series Eqn. (2.30) and can be expressed as

$$\boldsymbol{\Gamma}^{(m)}(\omega, \boldsymbol{\xi}(\theta)) = \left[\mathbf{I}_n - \mathbf{R}(\omega, \boldsymbol{\xi}(\theta)) + \mathbf{R}(\omega, \boldsymbol{\xi}(\theta))^2 - \mathbf{R}(\omega, \boldsymbol{\xi}(\theta))^3 \ldots m^{\text{th term}}\right] \boldsymbol{\Gamma}^{(1)}(\omega, \boldsymbol{\xi}(\theta)) \tag{2.32}$$

where $\mathbf{I}_n$ is the n-dimensional identity matrix and $\mathbf{R}$ is defined as

$$\mathbf{R}(\omega, \boldsymbol{\xi}(\theta)) = [\boldsymbol{\Lambda}^{-1}(\omega, \boldsymbol{\xi}(\theta))][\boldsymbol{\Delta}(\omega, \boldsymbol{\xi}(\theta))] \tag{2.33}$$

Here we present a theoretical analysis of the convergence of the solution with the order of approximation m as a function of the spectral radius of the $\mathbf{R}(\omega, \boldsymbol{\xi}(\theta))$ matrix.

Proposition 1. *If $\widetilde{\mathbf{u}}^m(\omega, \boldsymbol{\xi}(\theta))$ is the approximate solution constructed with m-th order spectral functions and $\widetilde{\mathbf{u}}(\omega, \boldsymbol{\xi}(\theta))$ is the exact solution of $\mathbf{A}\widetilde{\mathbf{u}} = \widetilde{\mathbf{f}}_0$, where $\mathbf{A} : \mathbb{R}^n \to \mathbb{R}^n$ is self-adjoint, then the error in the approximate solution for each random sample is bounded by*

$$\|\widetilde{\mathbf{u}} - \widetilde{\mathbf{u}}^m\| \leq c_\phi \sum_{k=m}^{\infty} \rho(\mathbf{R})^k \left\|\Lambda^{-1}\boldsymbol{\Phi}^T\widetilde{\mathbf{f}}_0\right\| \tag{2.34}$$

where $\mathbf{A} = \Lambda + \Delta$, $\rho(\mathbf{R})$ is the spectral radius of $\mathbf{R} = (\Lambda^{-1}\Delta)$, $\|\cdot\|$ denotes the 2-norm and

c_ϕ is a deterministic, frequency independent positive constant.

Proof. When the solution $\widetilde{\mathbf{u}}^m$, approximated with m-th order spectral functions $\Gamma^m(\omega, \boldsymbol{\xi}(\theta))$, is subtracted from $\widetilde{\mathbf{u}}$, we can write the difference as $\boldsymbol{\Phi}\left(\sum_{k=m}^{\infty}(-\mathbf{R})^k\Lambda^{-1}\boldsymbol{\Phi}^T\widetilde{\mathbf{f}}_0\right)$ from Eqns. (2.31) and (2.33). The notion of matrix norm is an extension of the vector norm. We denote $\|\cdot\|$ to be the Frobenius norm of a matrix and note that vector norm corresponding to this is actually the Euclidean norm. Also, the Frobenius norm is sub-multiplicative, i.e. $\|Ax\| \leq \|A\|\,\|x\|$ where A is any square matrix and $\|x\|$ is the Euclidean norm of vector x. Hence using the sub-multiplicative property and using the triangle inequality we have

$$\|\widetilde{\mathbf{u}} - \widetilde{\mathbf{u}}^m\| \leq \|\boldsymbol{\Phi}\| \left\|\sum_{k=m}^{\infty}(-\mathbf{R})^k\Lambda^{-1}\boldsymbol{\Phi}^T\widetilde{\mathbf{f}}_0\right\| \leq \sum_{k=m}^{\infty}\left\|\mathbf{R}^k\left(\Lambda^{-1}\boldsymbol{\Phi}^T\widetilde{\mathbf{f}}_0\right)\right\|\|\boldsymbol{\Phi}\|$$

We define $\rho(\mathbf{R}) = \max_j(|\lambda_{R_j}|)$ to be the spectral radius of $\mathbf{R}$, (λ_R being the eigenvalue of $\mathbf{R}$) and note that $\mathbf{R}$ is symmetric.We know from Gelfand's formula that $\lim_{k\to\infty}\left\|\mathbf{R}^k\right\|^{1/k} = \rho(\mathbf{R})$ and from [Kozyakin, 2009] it is seen that for any general matrix sets $\gamma^{(1+\ln k)/k}\left\|\mathbf{R}^k\right\|^{1/k} \leqslant \rho(\mathbf{R}) \leqslant \left\|\mathbf{R}^k\right\|^{1/k}$ where $\gamma \in (0,1)$. When using the 2-norm and as k increases, $\rho(\mathbf{R})$ approaches $\left\|\mathbf{R}^k\right\|^{1/k}$ such that we can approximate $\left\|\mathbf{R}^k\right\| = c_\rho\rho(\mathbf{R})^k$ where $c_\rho \to 1$. The norm of the orthonormalized matrix $\boldsymbol{\Phi}$ is $\sqrt{n}$ where n is the dimension of the linear system. We choose $c_\phi = \sqrt{n}c_\rho$ which is a deterministic, frequency independent positive constant. Hence, the above equation can be rewritten as

$$\|\widetilde{\mathbf{u}} - \widetilde{\mathbf{u}}^m\| \leq c_\phi\sum_{k=m}^{\infty}\rho(\mathbf{R})^k\left\|\Lambda^{-1}\boldsymbol{\Phi}^T\widetilde{\mathbf{f}}_0\right\| \tag{2.35}$$

Thus the approximation error for stochastic system solution approximated with m-th order spectral function converges with the m-th power of the spectral radius of $\mathbf{R}$. □

For $\rho(\mathbf{R}) << 1$ and square-integrable stochastic functions $\rho(\mathbf{R})^k$ and $\|\Lambda\|$ in the probability space $\left(\Theta^{(M)}, \mathscr{F}^{(M)}, P^{(M)}\right)$, with $\theta \in \Theta^{(M)}$, the expectation of the error norm can be written from Proposition 1 and using Hölder's inequality, as

$$\mathrm{E}\left[\|\widetilde{\mathbf{u}}^m - \widetilde{\mathbf{u}}\|\right] \leq \mathscr{O}(\langle\rho(\mathbf{R})^m\rangle_{L^2(\theta)})\,c(\omega) \tag{2.36}$$

where $c(\omega) = \left\langle c_\phi\left\|\Lambda^{-1}\boldsymbol{\Phi}^T\widetilde{\mathbf{f}}_0\right\|\right\rangle_{L^2(\theta)} \leq c_\phi\left\|\boldsymbol{\Phi}^T\widetilde{\mathbf{f}}_0\right\|\langle\|\Lambda^{-1}\|\rangle_{L^2(\theta)}$ is a constant that changes with the frequency step. Here $\langle\cdot\rangle_{L^2(\theta)}$ denotes the 2-norm in the probability space defined as $\left(\int_{\Theta^{(M)}}|\cdot|^2\,dP_\xi^{(M)}(\theta)\right)^{1/2}$ or $\mathrm{E}\left[|\cdot|^2\right]^{1/2}$. Thus the series converges rapidly as the order m of the spectral functions is increased.

The above development is not restricted to any specific choice of the joint distribution function of the input random variables. $\widetilde{\mathbf{u}}^{(m)}(\omega,\theta)$ is the solution of Eqn. (2.18) for a suffi-

ciently large value of m. The choice of the order of spectral functions m is guided by the desired accuracy of the solution and the consideration of computational efficacy. Hence, the series in Eqn. (2.31) approaches the exact solution of the discretized linear stochastic system for every $\theta \in \Theta$, $\omega \in \Omega$ as $m \to \infty$ as shown in Proposition 1.

2.3.3 Relationship between the spectral functions and the Krylov basis

A equivalence of the proposed approach with the idea of stochastic Krylov space is relevant in this context and which would help to establish the relationship between the complex frequency dependent rational stochastic functions $\mathbf{\Gamma}^{(m)}(\omega, \boldsymbol{\xi}(\theta))$ and the Krylov basis functions which are used to realize reduced order models of linear systems. Accurate approximation of the response vector in a reduced subspace alleviates much of the computational burden. This is the fundamental idea behind forming a reduced number of Krylov basis functions with which the solution is approximated. The dimension of this subspace is the degree of the minimal polynomial of the linear system $\mathbf{A}$ [Ipsen and Meyer, 1998].

A minimal polynomial F of $\mathbf{A}$ is a unique monic polynomial of minimal degree such that $F(\mathbf{A}) = 0$. This can be constructed with the distinct eigenvalues(λ_j) of $\mathbf{A}$ as

$$F(\mathbf{A}) = \prod_{j=1}^{d} (\mathbf{A} - \lambda_j \mathbf{I})^{m_j} \quad \text{and} \quad m \equiv \sum_{j=1}^{d} m_j \tag{2.37}$$

This idea can be used to construct the inverse of a non-singular matrix $\mathbf{A}$ in terms of the powers of $\mathbf{A}$ as

$$\mathbf{A}^{-1} = -\frac{1}{\alpha_0} \sum_{j=0}^{m-1} \alpha_{j+1} \mathbf{A}^j \tag{2.38}$$

where the coefficients α_i are evaluated from the minimal polynomial given in Eqn. (2.37). This can be immediately utilized to recognize that the solution vector $\mathbf{x}$ of the equation $\mathbf{Ax} = \mathbf{b}$ lies in the Krylov subspace of order m as

$$\mathscr{K}_m(\mathbf{A}, \mathbf{b}) = \text{span}\{\mathbf{b}, \mathbf{Ab}, \mathbf{A}^2\mathbf{b}, \ldots, \mathbf{A}^{m-1}\mathbf{b}\} \tag{2.39}$$

The Krylov subspace dimension is a key factor in terms of computational efficacy of a proposed approach.

It follows that the solution of the stochastic linear system (in Eqn. (2.18)), can be projected on to a finite number of basis spanning a *stochastic* Krylov space $\mathscr{K}_m \left[\mathbf{A}(\omega, \theta), \widetilde{\mathbf{f}}_0(\omega)\right]$ or in the modal space following Eqn. (2.28) as

$$\mathscr{K}_m \left[\{\mathbf{\Lambda}(\omega, \boldsymbol{\xi}(\theta)) + \mathbf{\Delta}(\omega, \boldsymbol{\xi}(\theta))\}, \mathbf{\Phi}^T \widetilde{\mathbf{f}}_0(\omega)\right] \tag{2.40}$$

Choice of the finite number of Krylov basis depends on the eigen-spectrum of the coefficient

of the system matrix $\mathbf{A}(\omega,\theta)$. A reduction in the dimension of the Krylov subspace can be achieved if we use a preconditioned stochastic Krylov space to arrive at a 'richer stochastic subspace'. The mean of the coefficient matrix $\langle \mathbf{A}(\omega,\theta)\rangle$ has been used as the preconditioner which helped in transforming $\mathbf{A}(\theta)$ such that the probability density functions of its eigenvalues show a high degree of overlap ([Nair and Keane, 2002]). It has also been shown that using the mean preconditioner is just equivalent to using a mean block-diagonal preconditioner of the linear system formed with stochastic Galerkin method using finite order chaos expansion [Nouy, 2009]. However, as the variability of the random field increases, it is desirable to incorporate 'some of the randomness' of the system matrices into the preconditioner such that order of the spectral basis functions can be kept low. This is the motivation for using a different preconditioner for the problem.

Now, referring back to Eqn. (4.26), we use the stochastic diagonal matrix $\mathbf{\Lambda}(\omega,\boldsymbol{\xi}(\theta))$ as the preconditioner of the stochastic Krylov space. The diagonal dominance of the matrices $\widetilde{\mathbf{A}}_i(\omega)$ is conducive to the approach being proposed here. Hence using $\mathbf{\Lambda}(\omega,\boldsymbol{\xi}(\theta))$ as the preconditioner we express the stochastic system response in the modal coordinates in the m dimensional Krylov space as

$$\begin{aligned}\mathbf{c}(\omega,\theta) &\in \mathscr{K}_m\left(\mathbf{\Lambda}^{-1}(\omega,\boldsymbol{\xi}(\theta))\left[\mathbf{\Lambda}(\omega,\boldsymbol{\xi}(\theta))+\mathbf{\Delta}(\omega,\boldsymbol{\xi}(\theta))\right],\mathbf{\Lambda}^{-1}(\omega,\boldsymbol{\xi}(\theta))\,\mathbf{\Phi}^T\widetilde{\mathbf{f}}_0(\omega)\right)\\ &\in \mathscr{K}_m\left(\left[I+\mathbf{\Lambda}^{-1}(\omega,\boldsymbol{\xi}(\theta))\,\mathbf{\Delta}(\omega,\boldsymbol{\xi}(\theta))\right],\mathbf{\Lambda}^{-1}(\omega,\boldsymbol{\xi}(\theta))\,\mathbf{\Phi}^T\widetilde{\mathbf{f}}_0(\omega)\right)\end{aligned} \tag{2.41}$$

Utilizing the property of the Krylov subspace shift invariance ([Grimme, 1997] which states that $\mathscr{K}_j(\alpha A+I,b)=\mathscr{K}_j(A,b)$ for any matrix A, vector b and nonzero scalar α we have from Eqn. (2.41)

$$\mathbf{c}(\omega,\theta) \in \mathscr{K}_m\left(\mathbf{\Lambda}^{-1}(\omega,\boldsymbol{\xi}(\theta))\,\mathbf{\Delta}(\omega,\boldsymbol{\xi}(\theta)),\mathbf{\Lambda}^{-1}(\omega,\boldsymbol{\xi}(\theta))\,\mathbf{\Phi}^T\widetilde{\mathbf{f}}_0\right) \tag{2.42}$$

which gives the Krylov subspace in which the stochastic system solution exists. The span of the Krylov space is then given by

$$\begin{aligned}\mathscr{K}_m(\mathbf{\Lambda}^{-1}\mathbf{\Delta},\mathbf{\Lambda}^{-1}\mathbf{\Phi}^T\widetilde{\mathbf{f}}_0) = \text{span}\{&\mathbf{\Lambda}^{-1}\mathbf{\Phi}^T\widetilde{\mathbf{f}}_0,(\mathbf{\Lambda}^{-1}\mathbf{\Delta})\mathbf{\Lambda}^{-1}\mathbf{\Phi}^T\widetilde{\mathbf{f}}_0,(\mathbf{\Lambda}^{-1}\mathbf{\Delta})^2\mathbf{\Lambda}^{-1}\mathbf{\Phi}^T\widetilde{\mathbf{f}}_0,\\ &\ldots,(\mathbf{\Lambda}^{-1}\mathbf{\Delta})^{m-1}\mathbf{\Lambda}^{-1}\mathbf{\Phi}^T\widetilde{\mathbf{f}}_0\}\end{aligned} \tag{2.43}$$

It is easily seen that the terms of this Krylov bases are equivalent to the terms in the matrix series expansion given in Eqns. (2.29)–(2.30). This preconditioning provides substantial advantage over the classical Neumann preconditioner with the deterministic part of the system matrices, especially near the resonance frequencies, where the radius of convergence of the preconditioned system becomes very small. This has been discussed in detail in the following section.

Thus the proposed computational scheme can be summarized in Algorithm 1 which is

applied at every $\omega \in \Omega$.

Algorithm 1 Stochastic FEM analysis using spectral functions

Input: $\omega \in \Omega$
Input: n design points : $\left\{\boldsymbol{\xi}^{(1)}, \ldots, \boldsymbol{\xi}^{(n)}\right\} \subset \Theta^{(M)}$.
Input: The KL modes $\varphi_i(\mathbf{r}_1)$ as $\varphi_i(\mathbf{r}_1) \mapsto \int_{\mathbb{R}^d} C_a(\mathbf{r}_1, \mathbf{r}_2)\varphi_i(\mathbf{r}_2)d\mathbf{r}_2$.
Input: Stochastic input parameter $a(\theta, \mathbf{r}) \in \mathbb{R} \times \Theta^{(M)}$.
Input: Compute system matrices $\widetilde{\mathbf{A}}_i \quad \forall i = 0, 1, 2, \ldots, M$ using the KL modes
Input: Solve the generalized eigenvalue problem, $\mathbf{K}_0\boldsymbol{\phi}_k = \lambda_k\mathbf{M}_0\boldsymbol{\phi}_k$ for first few eigenpairs.
Output: System response $\widetilde{\mathbf{u}}(\theta, \omega) \in \mathbb{R}^n \times \Theta$ in the output stochastic space.

```
for j = 1 to n do
    Evaluate the Krylov left-preconditioner Λ^{-1}(ω, ξ(θ)).
    Form the preconditioned linear system (Λ^{-1}Δ) and b = (Λ^{-1}Φ^T f̃_0)
    for r = 1 to m do
        Evaluate the successive powers of (Λ^{-1}Δ)^r.
        Construct the Krylov basis following Eqn. (2.43) using (Λ^{-1}Δ)^r and b.
    end for
    Create m^{th} order spectral functions {Γ^{(m)}(ω, ξ(θ))} from series expansion in
    Eqn. (2.29).
    Reconstruct the system response ũ(θ, ω) using Equation (2.31).
end for
globals n, {ξ^{(1)}, ..., ξ^{(n)}}, ũ(θ, ω)
```

2.3.4 Properties of the frequency-dependent spectral functions

The finite order spectral functions used to model the response of the randomly parameterized system are frequency dependent rational stochastic coefficients. The system response is given by a linear combination of the vibration modes the baseline model weighted by these spectral functions. In order to take a closer look at these spectral functions we write from the series expansion in Eqn. (2.30)

$$\begin{aligned}\boldsymbol{\Psi}\left(\omega, \boldsymbol{\xi}(\theta)\right) &= \boldsymbol{\Lambda}^{-1}\left(\omega, \boldsymbol{\xi}(\theta)\right) - \boldsymbol{\Lambda}^{-1}\left(\omega, \boldsymbol{\xi}(\theta)\right)\boldsymbol{\Delta}\left(\omega, \boldsymbol{\xi}(\theta)\right)\boldsymbol{\Lambda}^{-1}\left(\omega, \boldsymbol{\xi}(\theta)\right) \\ &\quad + \boldsymbol{\Lambda}^{-1}\left(\omega, \boldsymbol{\xi}(\theta)\right)\boldsymbol{\Delta}\left(\omega, \boldsymbol{\xi}(\theta)\right)\boldsymbol{\Lambda}^{-1}\left(\omega, \boldsymbol{\xi}(\theta)\right)\boldsymbol{\Delta}\left(\omega, \boldsymbol{\xi}(\theta)\right)\boldsymbol{\Lambda}^{-1}\left(\omega, \boldsymbol{\xi}(\theta)\right) + \ldots \quad (2.44)\end{aligned}$$

$\boldsymbol{\Lambda}^{-1}\left(\omega, \boldsymbol{\xi}(\theta)\right)$ is a diagonal matrix whose elements are stochastic in nature while $\boldsymbol{\Delta}\left(\omega, \boldsymbol{\xi}(\theta)\right)$ is a stochastic off-diagonal only matrix. The frequency dependence of these matrices ensures that the spectral radius is frequency adaptive in nature which is a significant advantage compared to the classical Neumann expansion technique. This will be demonstrated further in the discussions of these spectral functions and also in results of the statistical moments of the response vector. It is easily verified that the higher order terms in the series in Eqn. (2.44) are recursive in nature and hence computationally efficient. The different order so the spectral

functions are defined by the order of the truncated series in Eqn. (2.44).

In the spectral Galerkin approaches, the solution is projected onto *polynomial* basis functions spanning the stochastic subspace. The classical Neumann expansion technique [Ghanem and Spanos, 1991] expands the solution using an infinite series of polynomials of the random variables. In contrast, the series in Eqn. (2.30) is in terms of $[\mathbf{\Lambda}^{-1}(\omega, \boldsymbol{\xi}(\theta))][\mathbf{\Delta}(\omega, \boldsymbol{\xi}(\theta))]$, where both terms are random. The elements of this matrix series are not simple polynomials in $\xi_i(\theta)$, but are in terms of a ratio of polynomials as given in Eqn. (2.43). The convergence of this series depends of the spectral radius of $\mathbf{R}(\omega, \boldsymbol{\xi}(\theta))$. A generic term of this matrix can be obtained as

$$R_{rs} = \frac{\Delta_{rs}}{\Lambda_{rr}} = \frac{\sum_{i=1}^{M} \xi_i \Delta_{i_{rs}}}{\Lambda_{0_r} + \sum_{i=1}^{M} \xi_i \Lambda_{i_r}} = \frac{\sum_{i=1}^{M} \xi_i \widetilde{A}_{i_{rs}}}{\Lambda_{0_r} + \sum_{i=1}^{M} \xi_i \widetilde{A}_{i_{rr}}}; r \neq s \tag{2.45}$$

From Eqn. (2.45) it is seen that the spectral radius of $\mathbf{R}$ is controlled by the diagonal dominance of the $\widetilde{\mathbf{A}}_i$ matrices, i.e. if the diagonal terms are relatively larger than the off-diagonal terms, the series will converge faster even if the relative magnitude of Λ_{0_r} is not large. Especially near the resonance frequencies, where the radius of convergence of the system in classical Neumann expansion becomes quite small, the latter fails to converge. Hence the diagonal parts of the perturbation matrices has a significant role to play in this improved solution technique. This has been demonstrated later in the comparison of results with the classical Neumann expansion technique (refer to Fig. 2.11).

Recollecting the expression $\Lambda_{0_r}(\omega) = (-\omega^2 + i\omega\zeta_1) + (i\omega\zeta_2 + 1)\Lambda_r$, it can be seen that for those values of the ω where the denominator in Eqn. (2.45) becomes small (which is the case for resonance frequencies), the convergence of the spectral radius depends quite significantly on the diagonal elements of $\widetilde{\mathbf{A}}_i$ matrices. This indicates that even for low damping, the convergence of the mean response is ensured due to the presence of the diagonal terms of the perturbation matrices. In general the diagonal parts of the perturbation matrices, i.e. the terms $\Sigma_{i=1}^{M} \xi_i \Lambda_{i_r}$, would not have any zeros near the resonance frequencies. This is due to the fact that the perturbation matrices do not reduce to their principal components when treated with the eigen functions of the generalized eigenvalue problem of the deterministic system.

A one term approximation of the series comprising the n elements of $\mathbf{\Gamma}^{(m)}(\omega, \boldsymbol{\xi}(\theta))$ in Eqn. (2.31) such that $m = 1$ is termed as the first-order spectral functions. This gives from Eqn. (2.44) the first-order spectral functions as

$$\Gamma_k^{(1)}(\omega, \boldsymbol{\xi}(\theta)) = \frac{\boldsymbol{\phi}_k^T \widetilde{\mathbf{f}}_0(\omega)}{\Lambda_{0_k}(\omega) + \sum_{i=1}^{M} \xi_i(\theta) \Lambda_{i_k}(\omega)}; \quad k = 1, \ldots, n \tag{2.46}$$

Thus, $\Gamma_k^{(1)}(\omega, \boldsymbol{\xi}(\theta))$ are correlated and non-Gaussian random variables, which are rational function of the iid random variables $\xi_i(\theta)$. The response vector in terms of these spectral

functions can be simplified to

$$\widetilde{\mathbf{u}}^{(1)}(\omega,\theta) = \sum_{k=1}^{n} \underbrace{\left(\frac{1}{\Lambda_k}\left[\boldsymbol{\phi}_k^T \widetilde{\mathbf{f}}_0(\omega)\right]\right)}_{\Gamma_k^{(1)}(\omega,\boldsymbol{\xi}(\theta))} \boldsymbol{\phi}_k \tag{2.47}$$

The above equation shows that the response vector approximated with first order spectral functions does not involve the 'interaction' between different eigen modes, in other words, the response is expressed with the decoupled set of linear equations in modal coordinates which is normally obtained when a deterministic discretized linear FE system of equation is transformed to their modal coordinates using the eigen basis. However, here the modal coefficients (spectral functions in this case) are stochastic in nature. This is different from the classical Neumann expansion scheme in that, for this same order of expansion, the system response for the latter case is exactly equal to the deterministic case and hence fails to capture any effect of parametric uncertainty. It would be seen in subsequent discussions that the system response when captured with these first order spectral functions only and facilitated by the Galerkin method produces results which are agreeable with the direct MCS simulation.

A two term approximation of the series in Eqn. (2.44) gives the second-order spectral functions $\Gamma_k^{(2)}(\omega,\boldsymbol{\xi}(\theta))$ for $k = 1, 2, \ldots, n$. The second degree approximation of Eqn. (2.44) gives

$$\boldsymbol{\Psi}^{(2)}(\omega,\boldsymbol{\xi}(\theta)) = \boldsymbol{\Lambda}^{-1}(\omega,\boldsymbol{\xi}(\theta)) - \boldsymbol{\Lambda}^{-1}(\omega,\boldsymbol{\xi}(\theta))\,\boldsymbol{\Delta}(\omega,\boldsymbol{\xi}(\theta))\,\boldsymbol{\Lambda}^{-1}(\omega,\boldsymbol{\xi}(\theta)) \tag{2.48}$$

$$\text{or,}\quad \Psi_{kj}^{(2)}(\omega,\boldsymbol{\xi}(\theta)) = \frac{\delta_{kj}}{\Lambda_{0_k}(\omega) + \sum_{i=1}^{M}\xi_i(\theta)\Lambda_{i_k}(\omega)} - \frac{\sum_{i=1}^{M}\xi_i(\theta)\Delta_{i_{kj}}(\omega)}{\left(\Lambda_{0_k}(\omega) + \sum_{i=1}^{M}\xi_i(\theta)\Lambda_{i_k}(\omega)\right)\left(\Lambda_{0_j}(\omega) + \sum_{i=1}^{M}\xi_i(\theta)\Lambda_{i_j}(\omega)\right)} \tag{2.49}$$

Hence the second-order spectral functions can be written in explicitly as

$$\Gamma_k^{(2)}(\omega,\boldsymbol{\xi}(\theta)) = \frac{\boldsymbol{\phi}_k^T \widetilde{\mathbf{f}}_0(\omega)}{\Lambda_{0_k}(\omega) + \sum_{i=1}^{M}\xi_i(\theta)\Lambda_{i_k}(\omega)} - \sum_{\substack{j=1 \\ j\neq k}}^{n} \frac{\left(\boldsymbol{\phi}_j^T \widetilde{\mathbf{f}}_0(\omega)\right)\sum_{i=1}^{M}\xi_i(\theta)\Delta_{i_{kj}}(\omega)}{\left(\Lambda_{0_k}(\omega) + \sum_{i=1}^{M}\xi_i(\theta)\Lambda_{i_k}(\omega)\right)\left(\Lambda_{0_j}(\omega) + \sum_{i=1}^{M}\xi_i(\theta)\Lambda_{i_j}(\omega)\right)} \tag{2.50}$$

The second-order terms can be viewed as adding the modal coupling in the approximation of the system response when compared to Eqn. (2.46). The stochastic response vector can thus

be written as

$$\widetilde{\mathbf{u}}^{(2)}(\omega,\theta) = \widetilde{\mathbf{u}}^{(1)}(\omega,\theta) - \sum_i \left(\sum_j (1-\delta_{ij}) Q_{ij} (\boldsymbol{\phi}_j^T \widetilde{\mathbf{f}}_0(\omega)) \right) \boldsymbol{\phi}_i \tag{2.51}$$

where Q_{ij} is are the elements of the matrix $\mathbf{Q} = \boldsymbol{\Lambda}^{-1}(\omega, \boldsymbol{\xi}(\theta))\, \boldsymbol{\Delta}(\omega, \boldsymbol{\xi}(\theta))\, \boldsymbol{\Lambda}^{-1}(\omega, \boldsymbol{\xi}(\theta))$ which is the second term in Eqn. (2.48). The matrix $\mathbf{Q}$ is an off-diagonal only matrix and $(1-\delta_{ij})$ has been introduced to indicate this clearly. Hence from Eqn. (2.51) it is clear that the introduction of the second order terms helps to take into account the coupling of the deterministic eigen modes for the stochastic system response.

It can be noted that in general

$$\widetilde{\mathbf{u}}^{(m)}(\omega,\theta) = \widetilde{\mathbf{u}}^{(m-1)}(\omega,\theta) + (-1)^{m-1} \sum_i \left(\sum_j Q_{ij}^{(m)} (\boldsymbol{\phi}_j^T \widetilde{\mathbf{f}}_0(\omega)) \right) \boldsymbol{\phi}_i \quad \forall\, m > 2 \tag{2.52}$$

where $Q_{ij}^{(m)}$ are the elements of the matrix $\mathbf{Q}^{(m)} = \left(\boldsymbol{\Lambda}^{-1}(\omega, \boldsymbol{\xi}(\theta))\, \boldsymbol{\Delta}(\omega, \boldsymbol{\xi}(\theta)) \right)^{m-1} \boldsymbol{\Lambda}^{-1}(\omega, \boldsymbol{\xi}(\theta))$. The matrix $\mathbf{Q}^{(m)}$ is a full rank matrix and denotes the coupling of the eigen modes of the deterministic system to represent the solution of the stochastic system.

The essential features of the proposed approach for the resolution of the frequency domain response of randomly parameterized systems can be summarized as follows:

- The frequency domain response of the randomly parameterized vibrating system has been expressed with non-linear rational functions of the basic random variables, called spectral functions, and a set of reduced number of eigenvectors of the vibrating system.

- These spectral functions are frequency adaptive in nature and are rational functions of the input random variables. This is a key difference of the proposed approach with the exisiting stochastic Galerkin projection schemes which approximates the soution using stochastic polynomials.

- The stochastic preconditioner used in the proposed methodology depends on the input random variables and also on the value of the frequency. Hence the convergence radius of these spectral functions is frequency adaptive. This ensures rapid convergence of the solution even near the resonance frequencies of the vibrating system as can be seen from the comparison with the Neumman expansion and the 4^{th} order PC expansion in the numerical examples section.

- The spectral functions have been shown to comprise of linear combinations of the left-preconditioned Krylov basis functions. The use of the proposed stochastic preconditioner leads to the spectral functions being rational functions of the input random variables.

- The expression for the low-order spectral functions have been obtained explicitly in terms of the stochastic parameters and presented in Eqns. (2.46) and (2.50). These equations highlight the coupling of the eigenmodes and the associated random weighting coefficients in expressing the stochastic system solution.

The above points distinguish the proposed approach from the existing Galerkin projection schemes in terms of novelty and computational efficiency. Next we discuss the aspect of freqeuncy dependence of the spectral functions.

2.3.5 Frequency dependence of the spectral functions

From Eqn. (2.31), it can be observed that the spectral functions are not general stochastic basis functions, but are *specific* to the stochastic system being solved and depends on the forcing function. The frequency content, as well as the spatial location, of the applied force therefore has a significant influence on the spectral functions. Here we consider the applied force to be uniform in the frequency domain which helps in understanding the general nature of the frequency dependence of the spectral functions clearly.

Figure 2.1 shows the plot of the absolute values of the first seven complex spectral functions obtained for a particular random sample and for 4 values of standard deviation σ_a of the underlying random field. These spectral functions have been calculated for the example of the bending vibration of the Euler-Bernoulli cantilever beam presented later in Sec. 2.6.1. A unit harmonic force applied at the free edge of the cantilever beam is considered. The frequency response of each spectral function shows that their peaks correspond to the frequencies of the fundamental eigen modes with which they are associated. Also it is observed that for higher values of σ_a, the modal coupling increases, as is demonstrated by an increase in the spectral function amplitudes at other modal frequencies than those with which they are associated individually. This can be explained as follows: an increases in the variability of the random field results in a greater contribution of the deviatoric parts of the system matrices in Eqn. (2.18). It is naturally expected that this modification of the system matrices would be reflected in an enhanced interaction between the structural modes of the beam. Mathematically it can be seen from Eqn. (2.43) that the preconditioner chosen for the Krylov subspace method incorporates the diagonally dominant terms of the $\widetilde{\mathbf{A}}_i$ matrix along with the random variables used to discretize the stochastic field and this can be intuitively understood to contribute towards enhanced coupling between the individual modes for higher values of variability of the random field even for the lower order spectral functions.

Figure 2.2 shows the different orders (2, 3 and 4) of the spectral functions associated with the eigen modes i.e. $\Gamma_k^{(m)}(\omega, \boldsymbol{\xi}(\theta_j))$ for $m = 2, 3, 4$; $k = 2, 3, \ldots, 7$, θ_j being a particular random sample in the probability space. An increase in the order of spectral functions would improve the accuracy of the stochastic response vector.

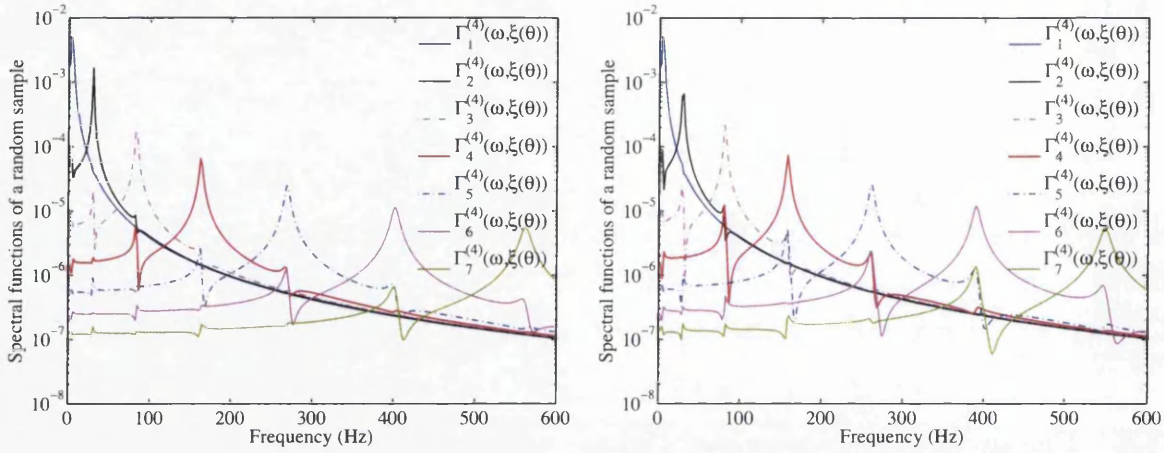

(a) Spectral functions for $\sigma_a = 0.05$.

(b) Spectral functions for $\sigma_a = 0.1$.

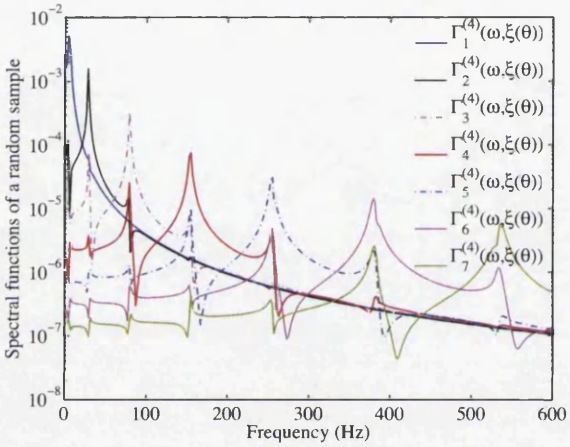

(c) Spectral functions for $\sigma_a = 0.15$.

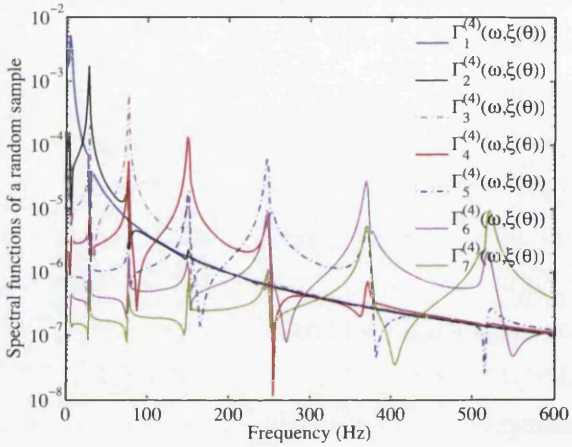

(d) Spectral functions for $\sigma_a = 0.2$.

Figure 2.1: The amplitude of first seven spectral functions of order 4 for a particular random sample under applied force. The spectral functions are obtained for four different standard deviation levels of the underlying random field: σ_a= {0.05, 0.10, 0.15, 0.20} .

The use of these kind of spectral functions results in capturing the frequency response of the system to a better extent compared to the spectral approaches which tend to formulate a stochastic basis using a general polynomial form of the random variables (for example, Hermite polynomials spanning the Hilbert space of random variables), in which case there is no frequency dependence of the basis functions. This may result in the requirement of a very high number of basis functions for the latter methods in order to satisfactorily capture the physics of the system response over a broad frequency spectrum. Especially the resonance frequencies can prove to be real obstacles to the success of those methods, which can be easily overcome using the methodology proposed in this work. It can be verified from a comparison of the results of the beam vibration problem with the frequency dependent spectral function approach and the polynomial chaos method which is presented later in Sec. 2.6.1. In addition to this, the proposed method has an advantage over the classical Neumann expansion technique in that the preconditioner for the linear system incorporates some of the randomness of

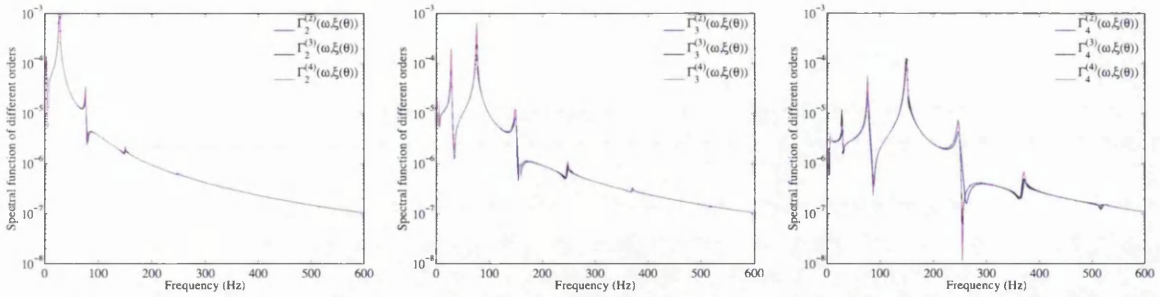

(a) Different orders of $\Gamma_2(\omega, \boldsymbol{\xi}(\theta))$. (b) Different orders of $\Gamma_3(\omega, \boldsymbol{\xi}(\theta))$. (c) Different orders of $\Gamma_4(\omega, \boldsymbol{\xi}(\theta))$.

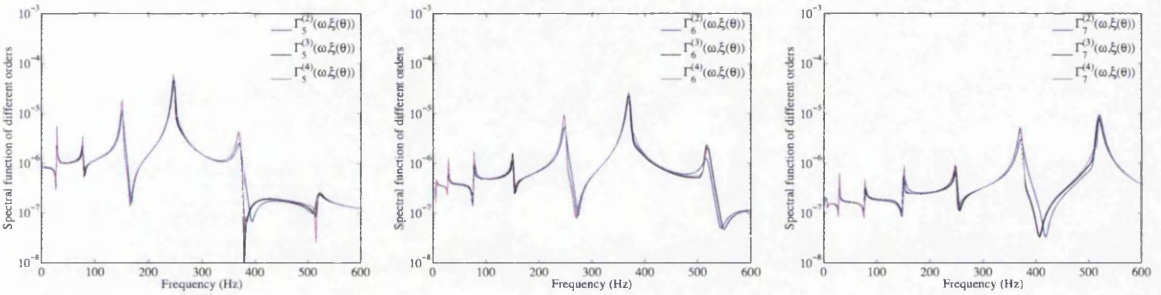

(d) Different orders of $\Gamma_5(\omega, \boldsymbol{\xi}(\theta))$. (e) Different orders of $\Gamma_6(\omega, \boldsymbol{\xi}(\theta))$. (f) Different orders of $\Gamma_7(\omega, \boldsymbol{\xi}(\theta))$.

Figure 2.2: The frequency domain spectral functions, $\Gamma_k^{(m)}(\omega, \boldsymbol{\xi}(\theta_j))$ of orders $m = 2, 3, 4$. The spectral functions are obtained for a particular random sample θ_j and for $\sigma_a = 0.20$.

the system which results in a better approximation with low order expansion of the Neumann series. This helps to reduces the computational cost of the method.

2.4 Model reduction and Galerkin error minimization technique

2.4.1 Model reduction

Model reduction for dynamic analysis of structural systems is achieved by using fewer number of eigenpairs of the generalized eigenvalue problem (usually those associated with the smallest eigenvalues). The cut-off frequency (Nyquist frequency) for dynamical analysis and hence the number of eigenpairs used to approximate the solution is guided by the fact that low to mid-frequency dynamical response can be captured using the first few eigenvectors and the higher modes can be neglected. The spatial resolution of the FE model must be able to represent the highest eigen mode with sufficient smoothness. Thus the system response is formulated with the n_r modal basis as

$$\frac{\omega}{\omega_j} << 1, \quad \text{for} \quad j > n_r \tag{2.53}$$

where ω_j is the natural frequency of the j^{th} mode and $\omega \in \Omega$ is the frequency domain. Thus, $n_r \leq n$ results in lower computational cost for resolving the system equations.

For the stochastic system, parametric uncertainty results in the distribution of the eigen modes around the deterministic natural frequencies in the sample space. The choice of the number of reduced basis in this case is based on an a priori understanding of the dependence of the solution on the eigen modes within the frequency range of interest. However, the spectral functions weighting the eigen basis is stochastic in nature and the contribution of the higher modes may become significant for certain samples. From the expression of the spectral functions

$$\Gamma_k^{(1)}(\omega, \boldsymbol{\xi}(\theta)) = \frac{\boldsymbol{\phi}_k^T \widetilde{\mathbf{f}}_0(\omega)}{\Lambda_{0_k}(\omega) + \sum_{i=1}^{M} \xi_i(\theta) \Lambda_{i_k}(\omega)} \tag{2.54}$$

it is observed that the stochastic weighting coefficients can modify the contribution of the individual vibration modes based on frequency and the nature of the elements perturbation matrices $\Lambda_{i_k}(\omega)$. For higher values of standard deviation, the effect becomes more significant.

Hence, it is suggested to go beyond the Nyquist criterion and increase the dimension of the modal subspace in approximating the stochastic system solution. This can help to avoid the errors which may arise from neglecting a significant contribution of the higher modes and their interactions in the response. A rigorous analysis of the spread of the stochastic natural frequencies of the vibrating system can definitively point to the number of essential eigen modes at each frequency. Also, posterior analysis of the variability of the spectral functions can further highlight this and can lead to the design of effective adaptive schemes to take care of the truncation error. However, this is beyond the scope of the present work.

Choosing a sufficient number of vibration modes, the solution can be projected onto those basis and the spectral functions associated with those modes can be calculated following the procedure detailed in previous sections. This model reduction technique can help to alleviate the computational cost of the problem significantly. Thus, following from Eqn. (2.31), the approximate solution can be represented in a reduced modal subspace of dimension (n_r) as

$$\widetilde{\mathbf{u}}(\omega, \theta) \approx \sum_{k=1}^{n_r} \widehat{\Gamma}_k^{(m)}(\omega, \boldsymbol{\xi}(\theta)) \boldsymbol{\phi}_k \tag{2.55}$$

where $\widehat{\Gamma}_k^{(m)}(\omega, \boldsymbol{\xi}(\theta))$ are m^{th} order stochastic spectral functions obtained with system matrices transformed to the reduced modal coordinates and $\boldsymbol{\phi}_k$ are the eigen vectors of the deterministic system respectively. The accuracy of this series in Eqn. (2.55) can be improved in two ways, (a) by increasing the dimension of the modal subspace (n_r), or (b) by increasing the order m of the spectral functions $\widehat{\Gamma}_k^{(m)}(\boldsymbol{\xi}(\omega, \theta))$.

This study has made use of the eigen modes that are within three-four times the frequency range of interest of the problem at hand. This helps in satisfactorily capturing the deformation shapes of the structural system at all frequencies. Reductions based on this kind of eigenso-

lution is of classical nature in various areas of structural mechanics and other engineering problems and extensive studies exist on this topic [Khalil *et al.*, 2007, Kerfriden *et al.*, 2011]. It should be noted, though, that the truncation of the series given in Eqn. (2.55) introduces approximation errors into the solution vector.

2.4.2 Galerkin type error minimization

In Sec. 2.3.2 we derived the spectral functions in terms of a convergent infinite series. These spectral functions are the coefficients of the orthonormal eigen modes which forms a complete basis of the solution space. The approximate solution so obtained is found to converge to the exact solution in probability 1 for each frequency value. First, second and higher order spectral functions obtained by truncating the infinite series have been derived. We have also showed that they capture the underlying physics of the frequency response of the system subjected to a given frequency dependent forcing. The well-established model reduction technique has been used to alleviate the computational burden by reducing the dimensionality of the linear stochastic system. However, the error introduced due to the finite order approximation of the spectral functions and the reduced dimension of the modal subspace induces error in the solution, and the idea here is to introduce a Galerkin-type orthogonalization of the residual to the modal basis with the aim of reducing this truncation error.

We express the solution vector by the series representation

$$\widetilde{\mathbf{u}}(\omega,\theta) = \sum_{k=1}^{n_r} c_k(\omega)\widehat{\Gamma}_k(\omega,\boldsymbol{\xi}(\theta))\boldsymbol{\phi}_k \tag{2.56}$$

where the functions $\widehat{\Gamma}_k$ are the spectral functions of finite order (as given in Eqn. (2.55)), $\boldsymbol{\phi}_k \in \mathbb{R}^n$ are the eigenvectors introduced earlier in Eqn. (2.21) and the constants $c_k(\omega) \in \mathbb{C}$ for a given value of the frequency has to be obtained using the Galerkin approach. Substituting the expansion of $\widetilde{\mathbf{u}}(\omega,\theta)$ in the governing equation Eqn. (2.18), the residual vector is given by

$$\boldsymbol{\varepsilon}(\omega,\theta) = \left(\sum_{i=0}^{M} \mathbf{A}_i(\omega)\xi_i(\theta)\right)\left(\sum_{k=1}^{n_r} c_k(\omega)\widehat{\Gamma}_k(\omega,\boldsymbol{\xi}(\theta))\boldsymbol{\phi}_k\right) - \widetilde{\mathbf{f}}_0(\omega) \in \mathbb{C}^n \tag{2.57}$$

where $\xi_0 = 1$ is used to simplify the first summation expression. The expression in Eqn. (2.56) can be viewed as a projection of the solution vector on to the deterministic modal basis weighed by the complex frequency dependent stochastic weighting functions $\widehat{\Gamma}_k(\omega,\boldsymbol{\xi}(\theta))$. Thus we wish to obtain the coefficients $c_k(\omega)$ using the Galerkin approach so that the residual is made orthogonal to the eigen basis in the mean sense at each frequency step, i.e. mathematically

$$\left\langle \boldsymbol{\phi}_j, \boldsymbol{\varepsilon}(\omega,\theta)\right\rangle = 0 \quad \forall\ j = 1,2,\ldots,n_r \tag{2.58}$$

Here $\langle \mathbf{u}(\theta), \mathbf{v}(\theta) \rangle = \int_\Theta \mathbf{u}(\theta)\mathbf{v}(\theta) P(\mathrm{d}\theta)$ defines the inner product norm. Imposing this condition and using the expression of $\boldsymbol{\varepsilon}(\omega, \theta)$ from Eqn. (2.57) one has

$$\mathrm{E}\left[\boldsymbol{\phi}_j^T \left(\sum_{i=0}^{M} \mathbf{A}_i(\omega)\xi_i(\theta)\right)\left(\sum_{k=1}^{n_r} c_k(\omega)\widehat{\Gamma}_k(\omega, \boldsymbol{\xi}(\theta))\boldsymbol{\phi}_k\right) - \boldsymbol{\phi}_j^T \widetilde{\mathbf{f}}_0(\omega)\right] = 0 \tag{2.59}$$

Interchanging the $\mathrm{E}[\bullet]$ and summation operations, this can be simplified to

$$\sum_{k=1}^{n_r}\left(\sum_{i=0}^{M}\left(\boldsymbol{\phi}_j^T \mathbf{A}_i(\omega)\boldsymbol{\phi}_k\right)\mathrm{E}\left[\xi_i(\omega,\theta)\widehat{\Gamma}_k(\omega, \boldsymbol{\xi}(\theta))\right]\right) c_k(\omega) = \left(\boldsymbol{\phi}_j^T \widetilde{\mathbf{f}}_0(\omega)\right) \tag{2.60}$$

$$\text{or} \quad \sum_{k=1}^{n_r}\left(\sum_{i=0}^{M} \widetilde{A}_{i_{jk}}(\omega) D_{ik}(\omega)\right) c_k(\omega) = b_j(\omega) \tag{2.61}$$

Defining the vector $\mathbf{c}(\omega) = \{c_1(\omega), c_2(\omega), \ldots, c_n(\omega)\}^T$, these equations can be expressed in a matrix form as

$$\mathbf{S}(\omega)\,\mathbf{c}(\omega) = \mathbf{b}(\omega) \tag{2.62}$$

with

$$S_{jk}(\omega) = \sum_{i=0}^{M} \widetilde{A}_{i_{jk}}(\omega) D_{ik}(\omega); \quad \forall\, j,k = 1,2,\ldots,n_r \tag{2.63}$$

where

$$\widetilde{A}_{i_{jk}}(\omega) = \boldsymbol{\phi}_j^T \mathbf{A}_i(\omega)\boldsymbol{\phi}_k \tag{2.64}$$

$$D_{ik}(\omega) = \mathrm{E}\left[\xi_i(\theta)\widehat{\Gamma}_k(\omega, \boldsymbol{\xi}(\theta))\right] \tag{2.65}$$

$$\text{and} \quad b_j(\omega) = \left(\boldsymbol{\phi}_j^T \widetilde{\mathbf{f}}_0(\omega)\right) \tag{2.66}$$

The number of equations to be solved for the unknown coefficients in Eqn. (2.62) is n_r which is the dimension of the reduced system in the modal coordinates represented by Eqn. (2.56). The complex coefficient matrix $\mathbf{S}(\omega)$ and the vector $\mathbf{b}(\omega)$ in Eqn. (2.62) should be obtained numerically using the Monte Carlo simulation or other numerical integration technique for every value of frequency. It can be observed that the matrix $\mathbf{S}(\omega)$ is symmetric. Therefore, one has to determine $n_r(n_r+1)/2$ elements of this matrix by numerical methods due to the necessity of evaluating the inner product of the functions in the probability space. It is possible to use any numerical integration scheme that is be applicable for the kind of joint probability density considered in the problem. For e.g. the Gauss-Hermite quadrature algorithm can be used effectively for the normally distributed random variables to evaluate the elements of $D_{ijk}(\omega)$ in Eqn. (2.64). In this work Monte Carlo simulation has been used. The samples of the spectral functions $\widehat{\Gamma}_k(\omega, \boldsymbol{\xi}(\theta))$ can be simulated from Eqns. (2.32), (2.46), (2.50) or depending on the order. The numerical method proposed here therefore can be considered as

a hybrid analytical-simulation approach.

2.5 Calculation of the dynamic response statistics

For practical application of the method developed here, the efficient computation of the response moments and pdf is important. A simulation based algorithm is proposed in this section. The coefficient vector $\mathbf{c} \in \mathbb{C}^{n_r}$ in Eqn. (2.56) can be calculated from a reduced set of equations given by Eqn. (2.62). Once these coefficients are calculated, the statistical moments of the solution can be obtained from using the Monte Carlo simulation as given below. The spectral functions used to obtain the vector $\mathbf{c}$ itself can to be reused to obtain the statistics and pdf of the solution. The mean vector can be obtained as

$$\bar{\mathbf{u}}(\omega) = \mathrm{E}\left[|\widetilde{\mathbf{u}}(\omega,\theta)|\right] = \sum_{k=1}^{n_r} |c_k| \mathrm{E}\left[\left|\widehat{\Gamma}_k(\omega,\boldsymbol{\xi}(\theta))\right|\right] \boldsymbol{\phi}_k \tag{2.67}$$

where $|\bullet|$ is the absolute value of the complex quantities. The covariance matrix of the solution vector is

$$\boldsymbol{\Sigma}_u(\omega) = \mathrm{E}\left[\left(|\widetilde{\mathbf{u}}(\omega,\theta)| - \bar{\mathbf{u}}(\omega)\right)\left(|\widetilde{\mathbf{u}}(\omega,\theta)| - \bar{\mathbf{u}}(\omega)\right)^T\right] = \sum_{k=1}^{n_r}\sum_{j=1}^{n_r} |c_k c_j| \, \Sigma_{\Gamma_{kj}}(\omega)\boldsymbol{\phi}_k\boldsymbol{\phi}_j^T \tag{2.68}$$

where the elements of the covariance matrix of the spectral functions are given by

$$\Sigma_{\Gamma_{kj}}(\omega) = \mathrm{E}\left[\left(\left|\widehat{\Gamma}_k(\omega,\boldsymbol{\xi}(\theta))\right| - \mathrm{E}\left[\left|\widehat{\Gamma}_k(\omega,\boldsymbol{\xi}(\theta))\right|\right]\right)\left(\left|\widehat{\Gamma}_j(\omega,\boldsymbol{\xi}(\theta))\right| - \mathrm{E}\left[\left|\widehat{\Gamma}_j(\omega,\boldsymbol{\xi}(\theta))\right|\right]\right)\right] \tag{2.69}$$

Considering the fact that the elements of the vector $\widetilde{\mathbf{u}}(\omega,\theta)$ are complex valued random processes, further statistical properties can also be obtained. For example one can calculate the two-point auto-correlation function of the absolute value as

$$\begin{aligned}\boldsymbol{\Sigma}_u(\omega_1,\omega_2) &= \mathrm{E}\left[\left(|\widetilde{\mathbf{u}}(\omega_1,\theta)| - \bar{\mathbf{u}}(\omega_1)\right)\left(|\widetilde{\mathbf{u}}(\omega_2,\theta)| - \bar{\mathbf{u}}(\omega_2)\right)^T\right] \\ &= \sum_{k=1}^{n_r}\sum_{j=1}^{n_r} |c_k c_j| \, \Sigma_{\Gamma_{kj}}(\omega_1,\omega_2)\boldsymbol{\phi}_k\boldsymbol{\phi}_j^T\end{aligned} \tag{2.70}$$

where the elements of the covariance matrix of the spectral functions are given by

$$\begin{aligned}\Sigma_{\Gamma_{kj}}(\omega_1,\omega_2) = \mathrm{E}\Big\{&\left(\left|\widehat{\Gamma}_k(\omega_1,\boldsymbol{\xi}(\theta))\right| - \mathrm{E}\left[\left|\widehat{\Gamma}_k(\omega_1,\boldsymbol{\xi}(\theta))\right|\right]\right)\left(\left|\widehat{\Gamma}_j(\omega_2,\boldsymbol{\xi}(\theta))\right| - \\ &\mathrm{E}\left[\left|\widehat{\Gamma}_j(\omega_2,\boldsymbol{\xi}(\theta))\right|\right]\right)\Big\}\end{aligned} \tag{2.71}$$

Based on the results derived in this work, a hybrid reduced simulation-analytical approach can thus be realized in practice. The method is applicable to general structural dynamics

problems with general non-Gaussian random fields. In the following section this approach has been applied to two physical problems.

2.6 Illustrative examples

In this section the problem of structural vibration of a one-dimensional Euler-Bernoulli cantilever beam and a two dimensional clamped plate are considered to demonstrate the effectiveness of the proposed spectral solution method for stochastic structural dynamic systems. The solution is obtained for a specified value of the correlation length of the parametric randomness and for different degrees of variability of the same. The spatially varying stochastic field has been discretized using a finite number of zero mean uncorrelated standard Gaussian variables using the Karhunen-Loève expansion theorem. For the beam problem we have chosen the elastic modulus EI as the the stochastic parameter while for the thin plate it is the bending stiffness D. The beam and plate problems have been solved for their dynamic steady state frequency domain vibration response. Direct Monte Carlo simulation (MCS) has been performed for these cases and is taken as the benchmark solution with respect to which the appropriateness of the different methods have been analyzed and the relative errors have been calculated. Also a comparison between the Polynomial Chaos method and the proposed spectral decomposition technique is presented for the beam problem. The plate problem however is solved only using the spectral reduced basis method and validated with the direct MCS results.

2.6.1 Case I: Euler-Bernoulli beam

In this section we apply the computational method to a cantilever beam clamped at one end (where the displacement and the rotational degree of freedom is set to zero). Figure 2.3(a) shows the configuration of the cantilever beam with a harmonic point load at its free end. We assume that the bending modulus (EI) is a stationary Gaussian random field of the form

$$EI(x,\theta) = EI_0(1 + a(x,\theta)) \tag{2.72}$$

where x is the coordinate along the length of the beam, EI_0 is the mean bending modulus, $a(x,\theta)$ is a zero mean stationary Gaussian random field. The covariance kernel of this random field is taken to be of the form

$$C_a(x_1,x_2) = \sigma_a^2 e^{-(|x_1-x_2|)/\mu_a} \tag{2.73}$$

where μ_a is the correlation length and σ_a is the standard deviation. The base-line parameters are chosen as $L = 1\text{m}$, cross-section $(b\times h)\,39\times 5.93\ \text{mm}^2$ and Young's modulus $E = 2\times 10^{11}$

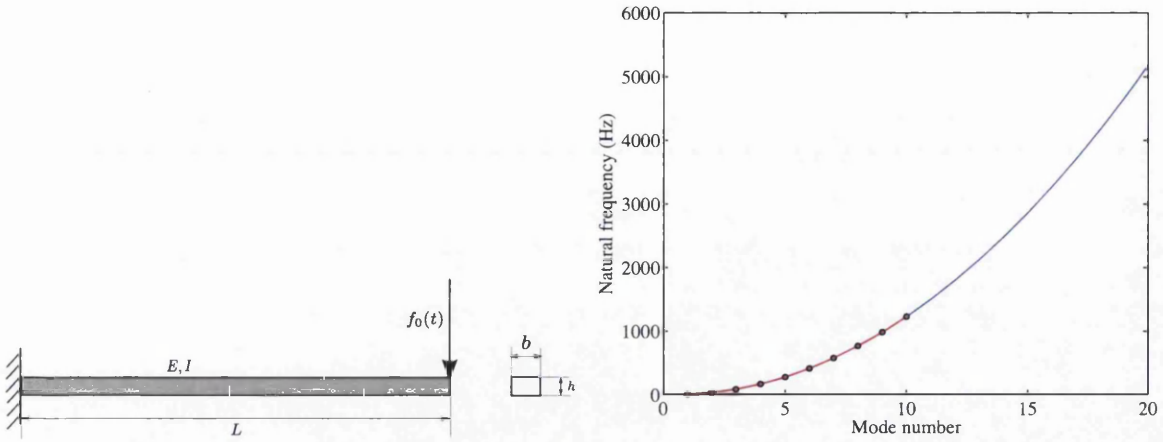

(a) Schematic diagram of the beam with a point load at the free end

(b) Natural frequency of the cantilever beam.

Figure 2.3: Schematic diagram of the cantilever beam with a harmonic point load at the free end along with its natural frequencies. The number of reduced eigenvectors chosen is $q = 10$ which covers upto twice (1200 Hz) the frequency range of interest (600 Hz).

Pa. In study we consider deflection of the tip of the beam under harmonic loads of amplitude $\tilde{f}_0 = 1.0N$. The correlation length considered in this numerical study is $\mu_a = L/2$. The number of terms used to represent the discretized random field in the spatial domain is chosen as $M = 2$. For the finite element discretization, the beam is divided into 100 elements. Standard four degrees of freedom Euler-Bernoulli beam model is used [Petyt, 1998]. After applying the fixed boundary condition at one edge, we obtain the number of degrees of freedom of the model to be $n = 200$. It has been verified that this spatial resolution is sufficient for the frequency of excitation considered in this study.

The dynamic analysis of the cantilever beam has been done for the case of unit amplitude harmonic point load acting on the free end of the beam over a frequency range of $0 - 600$ Hz at an interval of 2 Hz. The solution of the proposed reduced basis spectral method has been compared with the direct MCS results and the 4th order PC expansion. The simulations have been performed with $10,000$ MCS samples and for four different values of $\sigma_a = \{0.05, 0.10, 0.15, 0.20\}$, which is the standard deviation of the random bending stiffness of the beam, with the aim of simulating different levels of uncertainty.

Figure 2.3(b) presents the distribution of the natural frequencies of the cantilever beam, which are the square root of the eigenvalues λ_k of the generalized eigenvalues (Eqn. (2.21)) of the dynamic beam problem. The reduced basis of the problem should be chosen based on the frequency range of interest of this particular problem, i.e. all the eigen modes that covers up to 1200 Hz must be included in the formulation (given that the maximum frequency in the study is 600 Hz). However, based on the discussion given in Sec. 2.4.1, 10 eigen modes have been selected. We have applied a constant modal damping matrix with 1% damping factor for all the modes. Here the mass and damping matrices are assumed to be deterministic

in nature. However, the proposed theoretical approach is general and equally applicable for random mass, stiffness and damping matrices.

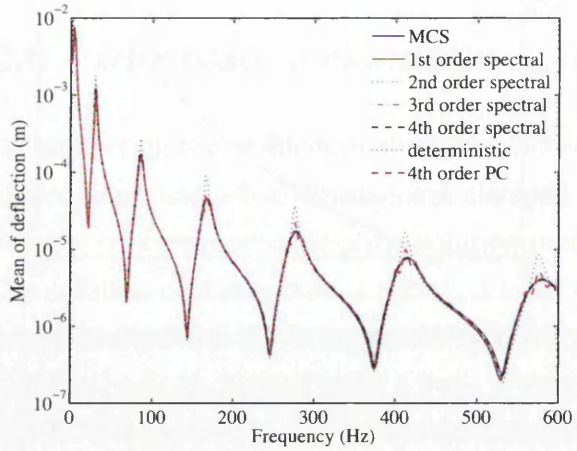

(a) Beam deflection for $\sigma_a = 0.05$.

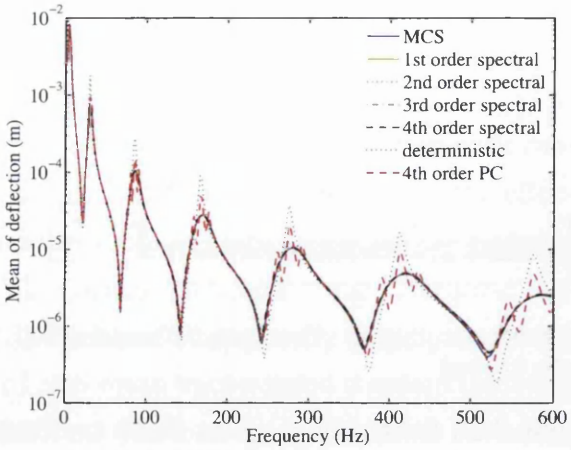

(b) Beam deflection for $\sigma_a = 0.1$.

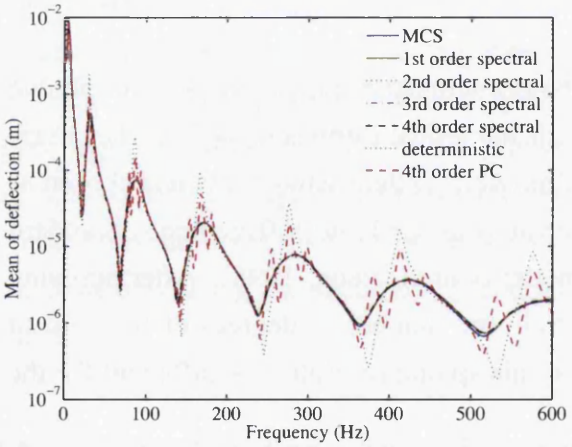

(c) Beam deflection for $\sigma_a = 0.15$.

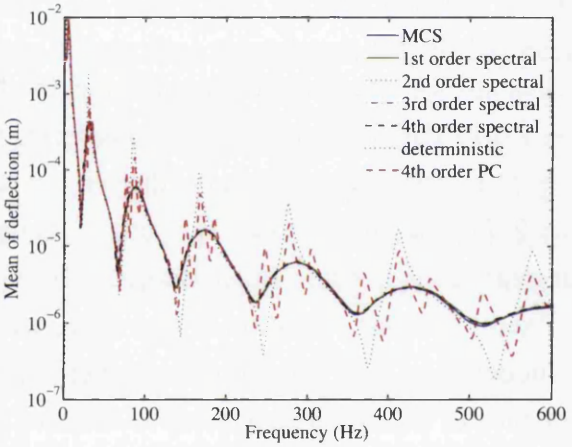

(d) Beam deflection for $\sigma_a = 0.2$.

Figure 2.4: The mean of the deflection amplitude of the tip of the Euler-Bernoulli beam under unit harmonic point load at the free end. The response is obtained with $10,000$ random samples and for $\sigma_a = \{0.05, 0.10, 0.15, 0.20\}$. The response for different order of spectral functions are shown. For this problem the degrees of freedom $n = 200$ and the number of random variables $M = 2$. The proposed Galerkin approach needs solution of a 10×10 linear system of equations only.

The frequency response of the mean deflection of the tip of the beam is shown in Fig. 2.4 for the four values of σ_a and for unit amplitude harmonic point load at the free end. The figures show a comparison of the reduced basis spectral method results with the direct MCS simulation and the 4th order polynomial chaos solution. A plot of the deterministic system response is also included for reference. The spectral solution has been obtained for different orders of the solution following Eqn. (2.30), where the orders $s = 2, 3, 4$. Since we consider the first 10 eigenmodes of the solution, the Galerkin method necessitates the solution of a 10×10 linear system of equations to obtain the undetermined coefficients associated with

the response, as given in Eqn. (2.62). In contrast, for the PC solution technique using 4^{th} order polynomial functions, it is essential to solve a 3000×3000 dimensional linear system of equations in order to obtain the undetermined coefficients associated with the Hermite polynomials at every frequency step.

A good agreement between the MCS simulation and the proposed spectral approach can be observed in Fig. 2.4. When compared with the deterministic system response, it shows that the uncertainty has an effect similar to that of damping at the resonance peaks. This can be explained by the fact that the parametric variation of the beam, results in its peak response for the different samples to get distributed around the resonance frequency zones instead of being concentrated at a particular frequency. As a results, when the subsequent averaging is applied, it smooths out the response peaks to a fair degree. The same explanation holds for the anti-resonance frequencies. It can also be observed that increased variability of the parametric uncertainties (as is represented by the increasing value of σ_a) results in an increase of this added 'damping kind of effect'. It should however be pointed out that this is not a phenomenon of physical damping and there might still be a high amplitude deflection obtained for a particular random sample in practical problems. The 4^{th} order PC solution shows an accurate mean response estimation at low frequencies for small variability (like for $\sigma_a = 0.05$) of the random field. However, the response tends to become inconsistent for higher values of variability, especially at the resonance frequencies. This can lead to serious practical problem as the response near the resonance frequency often the most crucial quantity of engineering interest.

As the response of the system is in terms of the spectral functions, it is now useful to understand the stochastic system response in terms of the statistical properties of these spectral functions. We show the plot of the first seven 4^{th} order mean spectral functions $E[\widehat{\Gamma}_k(\omega, \boldsymbol{\xi}(\theta))]$ in Fig. 2.5 as function of frequency for 4 different values of variability of the random field. We find that the resonance peak of each spectral function is obtained at the natural frequencies of the vibration modes with which they are associated and denotes mean of the stochastic modal amplitudes of the beam. Also, the amplitude of the functions at the resonance peaks are found to decrease for higher values of σ_a which is consistent with the observation in Fig. 2.4 that the effect of increased variability of the random field leads to an added damping kind of effect on the mean response. The ratio of the amplitudes of consecutive spectral functions at a resonance frequency increases with an increase in the value of σ_a. For e.g. the ratio of $E[\Gamma_6^4(\omega, \boldsymbol{\xi}(\theta))]/E[\Gamma_5^4(\omega, \boldsymbol{\xi}(\theta))]$ around 400 Hz is found to decrease with σ_a. This shows that the coupling of the vibration modes tend to increase with the increasing variability of the random field as has also been mentioned in discussion of spectral functions in Sec. 2.3.4.

Figure 2.6 shows the standard deviation of the frequency domain response of the tip deflection for different spectral orders of solution of the reduced basis approach and is compared with the direct MCS and 4^{th} order PC for different values of σ_a. We find that the standard de-

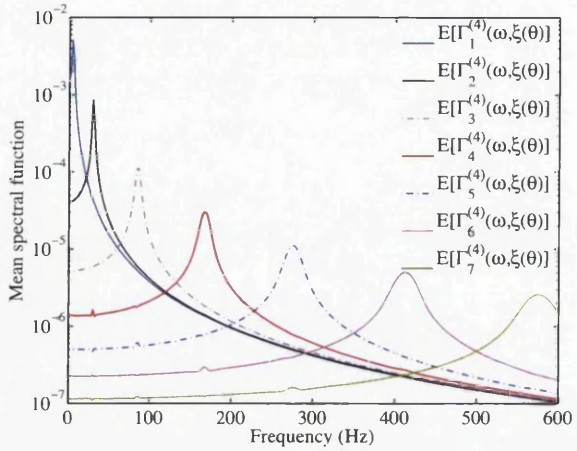

(a) Mean spectral functions for $\sigma_a = 0.05$.

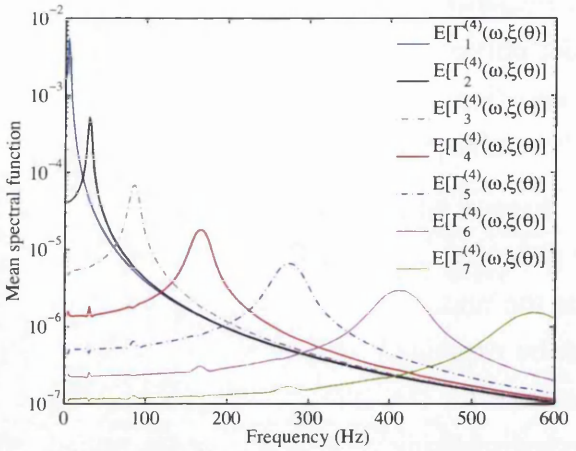

(b) Mean spectral functions for $\sigma_a = 0.1$.

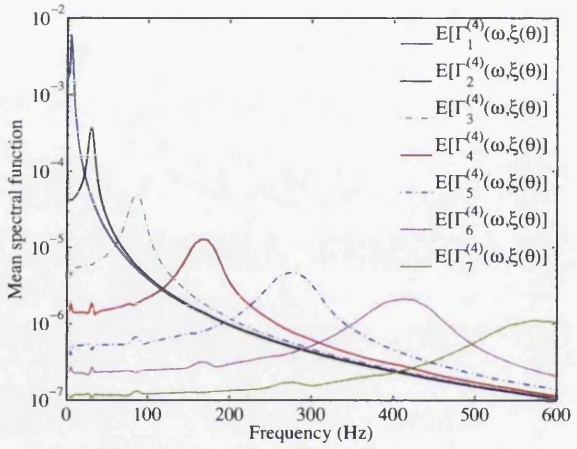

(c) Mean spectral functions for $\sigma_a = 0.15$.

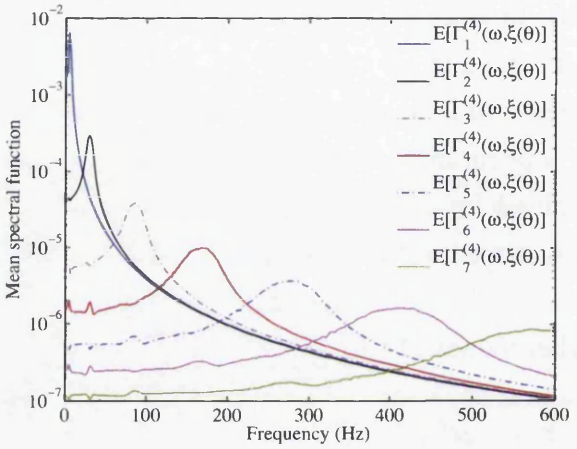

(d) Mean spectral functions for $\sigma_a = 0.2$.

Figure 2.5: The mean of the amplitude of the first seven spectral functions of order 4. The spectral functions are obtained for frequency up to 600 Hz with 10^4 sample MCS and for $\sigma_a = \{0.05, 0.10, 0.15, 0.20\}$.

viation is maximum at the resonance frequencies which is consistent with Fig. 2.4. It is again observed that the direct MCS solution and the reduced order approach give almost identical results, which demonstrate the effectiveness of the proposed approach. The 4^{th} order PC results however, show significant inconsistencies for higher values of σ_a and especially at high frequencies. Both these observations suggest that the PC expansion of a similar order to this proposed spectral function approach may not be well suited to handle the dynamic problem at high frequencies and for high degrees of variability of the random field involved.

It can also be considered that the system response constructed with the first order spectral functions corresponds to a zeroth order expansion in the classical Neumann scheme, if only the deterministic part of the system matrices are chosen as the pre-conditioners. Thus, it would correspond to the deterministic system response shown in Figs. 2.4. It can be seen that, the response with the first order spectral functions on the other hand gives a better ap-

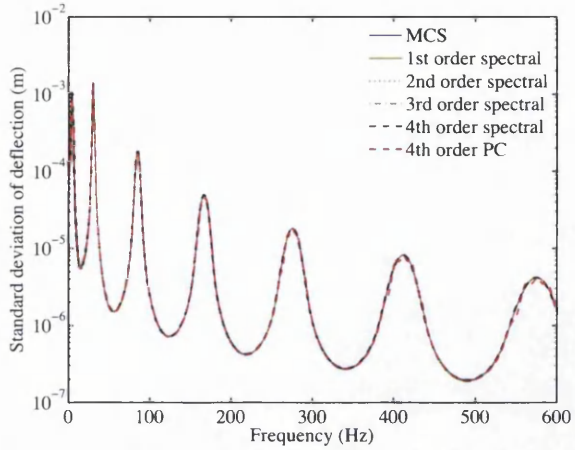

(a) Standard deviation of the response for $\sigma_a = 0.05$.

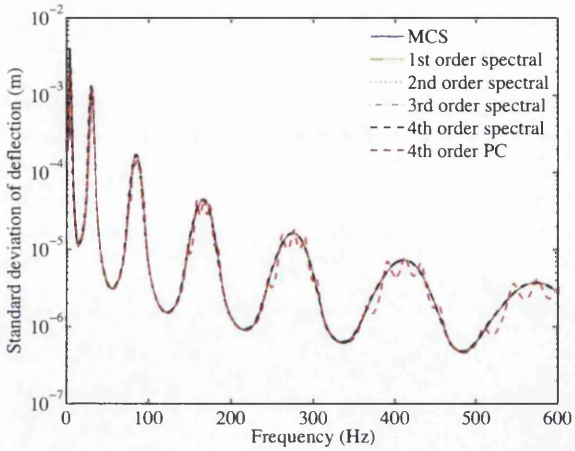

(b) Standard deviation of the response for $\sigma_a = 0.1$.

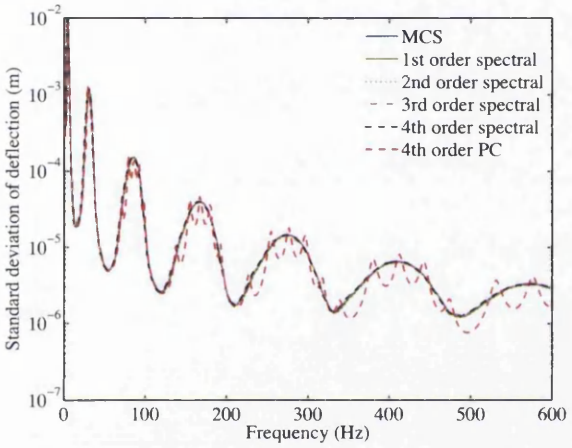

(c) Standard deviation of the response for $\sigma_a = 0.15$.

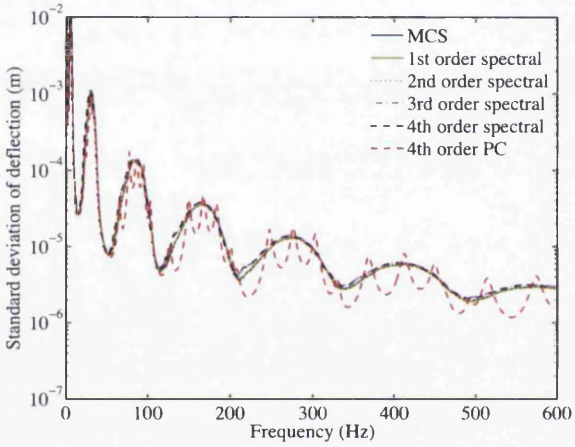

(d) Standard deviation of the response for $\sigma_a = 0.2$.

Figure 2.6: The standard deviation of the deflection amplitude of the tip of the Euler-Bernoulli beam under unit harmonic point load at the free end. The response is obtained with $10,000$ random samples and for $\sigma_a = \{0.05, 0.10, 0.15, 0.20\}$.

proximation of the solution even at high values of standard deviation of the random field. This is a significant advantage of the proposed method over the classical Neumann expansion technique, and the results obtained with the latter is given later in this section.

Figure 2.7 shows the standard deviation of the response of the beam at four different frequencies, 50 Hz, 168 Hz, 246 Hz and 418 Hz, as a function of the standard deviation of the random field. 168 Hz and 418 Hz correspond to the resonance frequencies of the cantilever beam, while 246 Hz corresponds to the anti-resonance frequency. The relative standard deviation values have been obtained for a set of 4 values of σ_a, which represents the different degrees of variability of the system parameters. The results obtained with the Galerkin approach for the different order of spectral functions have been compared with the direct MCS, and a good agreement is observed. However, the 4^{th} order PC result points to the fact that at high frequencies and for high values of the variance of the random field, the

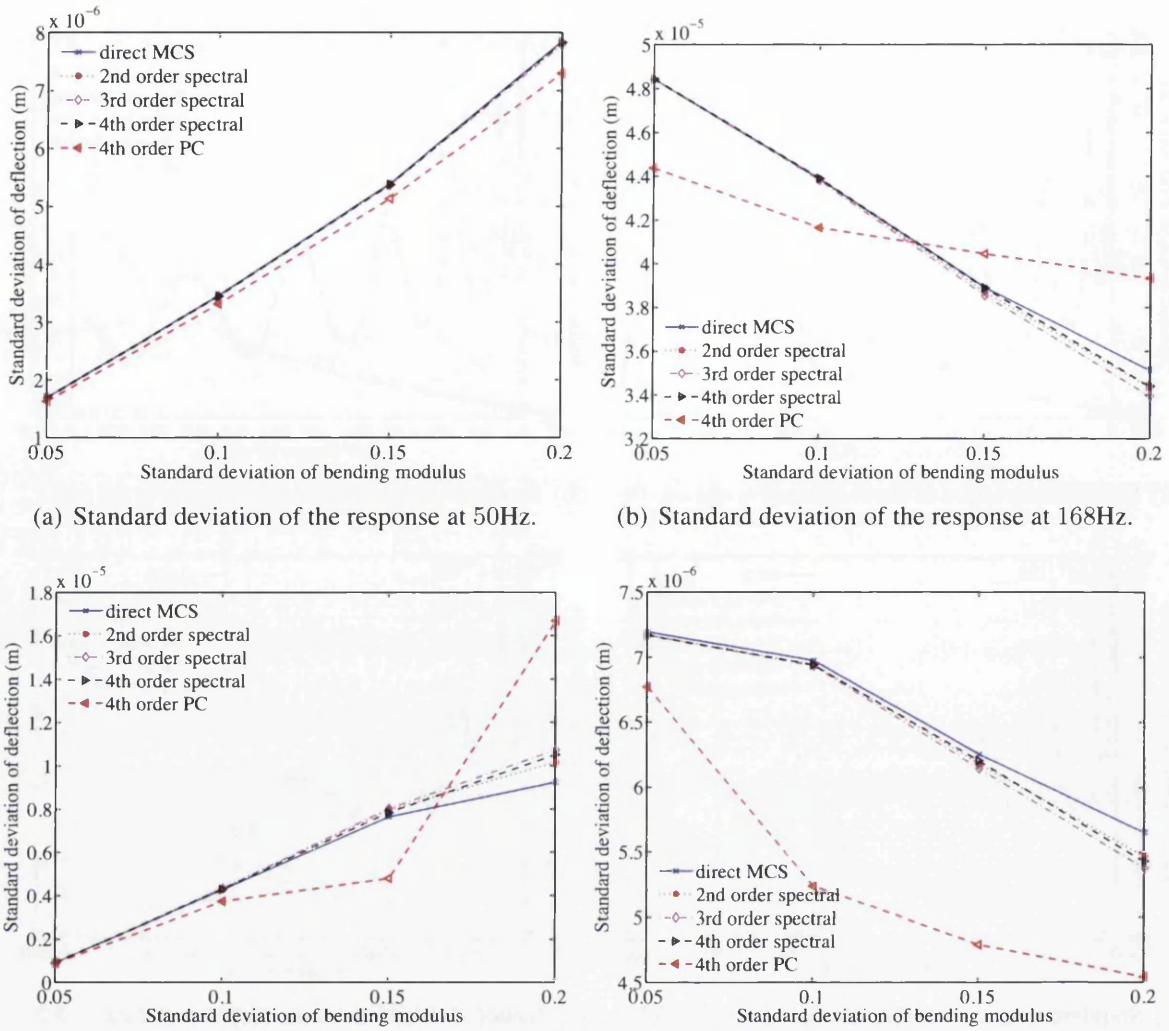

(a) Standard deviation of the response at 50Hz.

(b) Standard deviation of the response at 168Hz.

(c) Standard deviation of the response at 246Hz.

(d) Standard deviation of the response at 418Hz.

Figure 2.7: Standard deviation of the deflection amplitude of the tip of the Euler-Bernoulli beam for different degrees of parametric uncertainty represented by $\sigma_a = \{0.05, 0.10, 0.15, 0.20\}$ at 4 different frequencies and under unit harmonic point load at the free end. The response is obtained with $10,000$ random samples. Note that 168 and 418 Hz correspond to the resonance frequencies of the beam.

PC results provide a less accurate prediction of the solution moments for the same order of expansion of the polynomials of the random variables. It may be pointed out that the standard deviation decreases with the values of σ_a for the resonance frequency while it increases for the anti-resonance frequencies. This is once again consistent with the results shown in Fig. 2.4 which shows that an increased value of the variance of the random field has the effect of an enhanced system damping when plotting the mean value of the frequency response.

The probability density function of the deflection of the tip of the cantilever beam for different degrees of variability of the random field is shown in Fig. 2.8. The probability density functions have been calculated at the frequency of 418 Hz, which is a resonance frequency of the beam. A close match between the direct MCS and the reduced basis spectral solution is

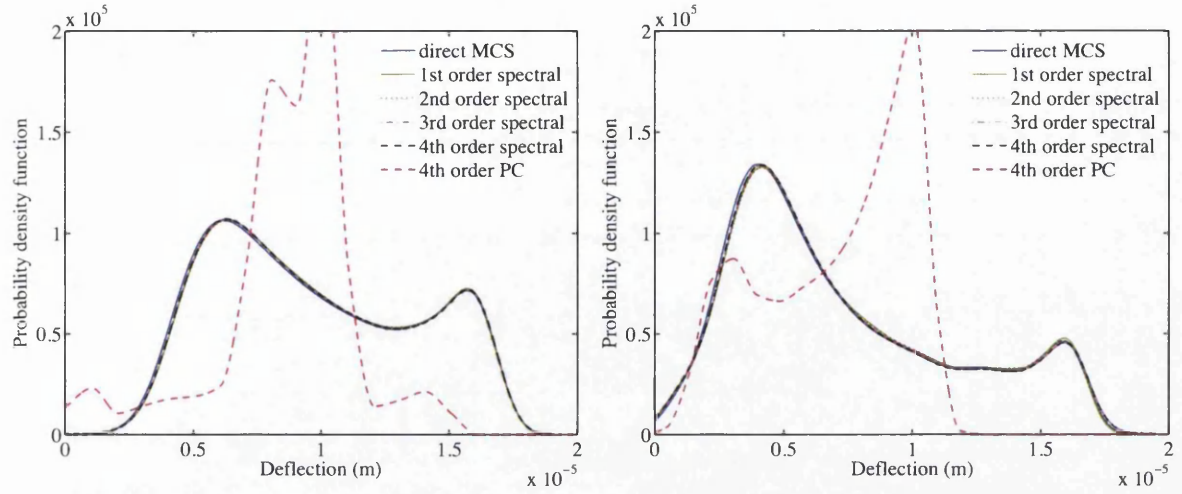

(a) Probability density function for $\sigma_a = 0.05$.

(b) Probability density function for $\sigma_a = 0.1$.

(c) Probability density function for $\sigma_a = 0.15$.

(d) Probability density function for $\sigma_a = 0.2$.

Figure 2.8: The probability density function of the deflection amplitude of the tip of the Euler-Bernoulli beam under a unit harmonic point load at the free end at 418 Hz. The correlation length of the random field describing the bending rigidity is taken to be $\mu_a = L/2$. The pdfs are obtained with $10,000$ random samples and for four values of σ_a.

obtained. However, the density functions obtained with 4^{th} order PC show inconsistencies, and the disparity increases with higher values of σ_a. These results establish the applicability of this spectral reduced basis method with Galerkin error minimization technique as a satisfactory working model for providing solution of the stochastic dynamical systems. The method is found to be consistent with the direct MCS approach, while being computationally efficient than either the direct MCS or PC approach. For a given order of expansion, the proposed method approximates the stochastic system response better than the classical Neumann expansion

It would now be interesting to highlight the behavior of an error norm of the system response obtained with this spectral function approach for different orders of the spectral

functions, the application of the Galerkin technique and for different degrees of variability of the parametric uncertainty. Hence we consider a L^2 relative error for the mean response of the cantilever beam. The L^2 relative error $\epsilon_{\boldsymbol{\mu}}^{(m)}(\omega)$ is defined at each frequency step ω for m^{th} order spectral functions as

$$\epsilon_{\boldsymbol{\mu}}^{(m)}(\omega) = \frac{\left\| \boldsymbol{\mu}_{SF}^{(m)}(\omega) - \boldsymbol{\mu}_{MCS}(\omega) \right\|_{L^2(\mathscr{D})}}{\|\boldsymbol{\mu}_{MCS}(\omega)\|_{L^2(\mathscr{D})}} \tag{2.74}$$

where $\boldsymbol{\mu}_{SF}^{(m)}(\omega)$ denotes the mean of the response vector obtained with the spectral weighting functions of order m and $\boldsymbol{\mu}_{MCS}(\omega)$ is the mean response vector calculated with the direct MCS simulation. Here we have studied the cases for which $m = 1, \ldots, 4$ and present the convergence of the L^2 relative error with increasing order of the spectral functions. Now, errors induced in the system due to the reduced number of basis functions and finite order of the spectral functions induces error in the computational scheme which has been minimized with the Galerkin-type error orthogonalization technique as presented in Sec. 2.4.2. Hence we present here the mean response calculated before and after the application of the Galerkin technique in order to demonstrate the effectiveness of the latter in approximating the solution for lower orders of the spectral functions and fewer modal basis vectors. Following from Eqn. (2.56), it can be seen that without the application of the Galerkin technique, the constants $c_k(\omega) = 1, \ \forall k = 1, \ldots, n_r; \ \ \omega \in \Omega$.

Figure 2.9(a) shows the behavior of the L^2 relative error as a function of frequency for the 2^{nd} order spectral functions with and without the application of the Galerkin type orthogonalization of the residual vector to the modal basis. It can be seen that for the Galerkin method consistently reduces the L^2 error at almost all frequencies, but performs better in the low frequency range. Also, the overall error tends to increase with frequency which is expected since the contribution of the higher order modes becomes significant at these frequencies and the truncation error grows. The standard deviation value has been chosen as $\sigma_a = 0.20$ which represents quite a high variability of the random field. Figure 2.9(b) shows a comparison of the L^2 error obtained with the 1^{st} and 4^{th} order spectral functions for $\sigma_a = 0.20$ and proves that increasing the spectral function order improves the results quite well at low frequencies. However, beyond 400 Hz, it is less effective, which can be explained as follows: at high frequencies, the overall error level increases (as is indicated by the increasing trend of the curve) which implies that the modal truncation, performed in obtaining the solution in the reduced space, results in the elimination of the contribution of some higher order modes which may be significant at these frequencies.

To study the convergence behavior of the response approximated with different orders of the spectral functions, we look at the mean squared error of the response at particular frequencies as a function of the spectral function order in Fig. 2.10 for different values of

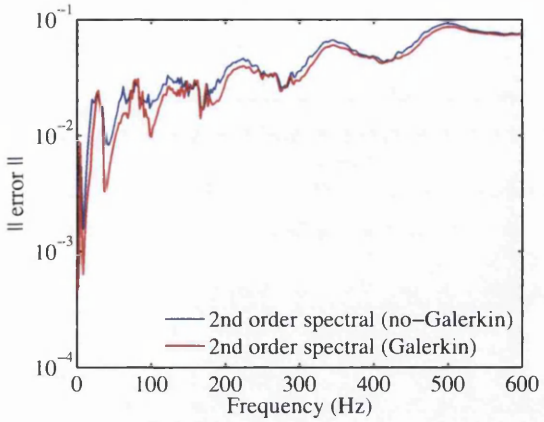

(a) L^2 error for 2^{nd} order spectral functions.

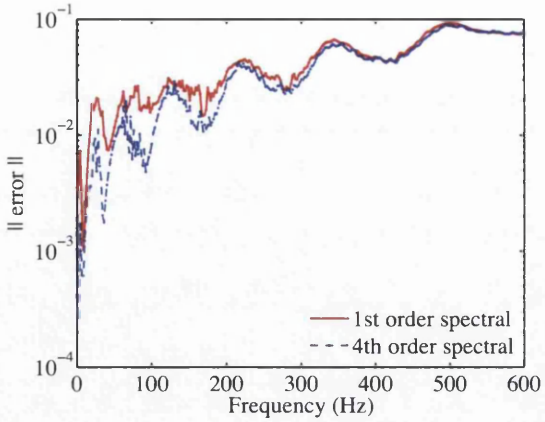

(b) Comparison ofL^2 error with 1^{st} and 4^{th} order spectral functions.

Figure 2.9: (a)The L^2 relative error of the response obtained with the 2^{nd} order spectral functions with and without the Galerkin type error minimization for the parametric standard deviation of $\sigma_a = 0.20$ (b) Comparison of the L^2 error of the response obtained using 1^{st} and 4^{th} order spectral functions in conjunction with the Galerkin type error minimization for the parametric standard deviation of $\sigma_a = 0.20$.

standard deviation of the underlying random parameter. It is found that the Galerkin error

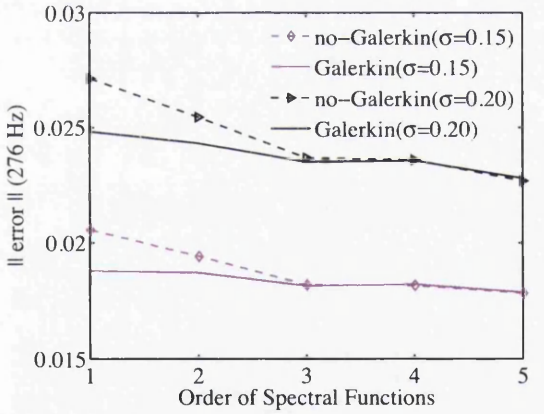

(a) L^2 error at 276 Hz.

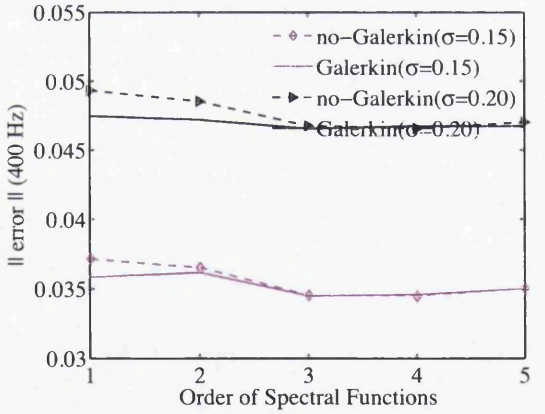

(b) L^2 error at 400 Hz.

Figure 2.10: Convergence of the L^2 error of the response vector at 276 Hz (resonance frequency) and 400 Hz with increasing order of spectral functions for the random parameter for two different values of standard deviation $\sigma_a = \{0.15, 0.20\}$.

reduction is quite effective for lower (1^{st} and 2^{nd}) order of spectral functions, however, for solutions approximated with higher order spectral functions, the application of the Galerkin scheme has no appreciable effect on the response.

The relative L^2 error for the mean response obtained with the spectral function approach decreases with an increase in the order of the spectral functions, which indicates that the spectral functions $\Gamma^{(m)}(\omega, \boldsymbol{\xi}(\theta))$ has converged satisfactorily, in the mean sense, in the probability

space with respect to the joint distribution function of the random variables. This shows that the response has been captured to high degree of accuracy even with the lower order spectral functions, such that an increase in the order does not bring about any significant improvement in terms of the solution accuracy. Also, the estimation of the higher order spectral functions is computationally more expensive and an optimal order can be chosen based on the convergence criterion required for the particular problem at hand. We demonstrate this aspect with another structural dynamic problem of plate bending with parametric uncertainty and observe the behavior of an identical L^2 relative error.

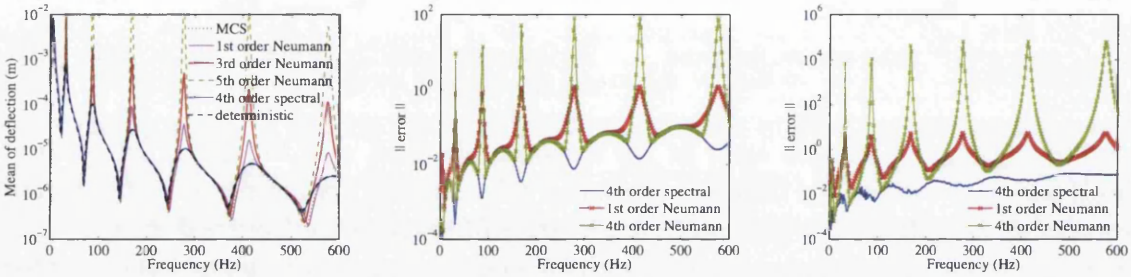

(a) Beam deflection for $\sigma_a = 0.10$. (b) L^2 error for $\sigma_a = 0.05$. (c) L^2 error for $\sigma_a = 0.20$.

Figure 2.11: (a) Stochastic system response calculated using different orders of Neumann expansion and compared to the direct MCS results for $\sigma_a = 0.10$. (b) Comparison of the L^2 relative error of the response vector obtained with the Neumann expansion and the spectral function approach for standard deviation $\sigma_a = 0.05$ (c) Comparison of the L^2 relative error of the response vector obtained with the Neumann expansion and the spectral function approach for standard deviation $\sigma_a = 0.20$.

Figure 2.11 shows the comparison of the results obtained with the spectral function approach with that of the classical Neumann expansion technique. It can be seen from Fig. 2.11(a) that near the resonance frequencies the Neumann expansion solution does not converge, since the contribution of the deterministic part of the system matrices decreases substantially and hence the norm of the preconditioned matrices goes beyond the radius of convergence. Figures 2.11(b) and 2.11(c) shows a comparison between the relative L^2 error of the system response obtained with the 4^{th} order spectral functions and different orders of expansion of the Neumann method for two different values of standard deviation of the parametric uncertainty, $\sigma_a = 0.05, 0.20$. It shows that while at non-resonance frequencies, the error values are identical to those predicted by the spectral function approach, they deteriorate significantly in the neighborhood of the resonance frequencies. The effect is more significant for high values of standard deviation, (like $\sigma_a = 0.20$), where the solution has been rendered meaningless over the entire frequency spectrum. It must be mentioned that the damping values chosen for the simulation has a significant impact on the Neumann expansion technique, and the radius of convergence increases for high damping.

Thus, the spectral function approach proposed here is found to provide accurate values of the system response at low computational cost (verified against the direct MCS results) over a

wide range of frequencies, and quite high values of standard deviation of the random parameter of the stochastic structural system. Even a comparison with the polynomial chaos method shows that the latter requires the use of higher order stochastic basis functions for providing a good approximation of the solution near the resonance frequencies and especially for high values of standard deviation of the random field σ_a. However, the added computational cost associated with this p-refinement is substantial. The spectral function approach proposed here uses a rational form of the polynomials of the random variables to approximate the solution in the stochastic space. This provides a better approximation of the system response even with lower order functions. The proposed method can be looked upon as an improved Neumann expansion technique where the stochastic linear system is treated with a stochastic preconditioner helping us to arrive at a 'richer' stochastic subspace, where a few number of basis functions is able to provide a good approximation of the solution for low values of order of the spectral functions and has a large radius of convergence compared to the classical Neumann expansion.

2.6.2 Case II: Kirchhoff-Love plate

In this section we apply the proposed spectral method to a Kirchhoff-Love plate clamped at one edge (where the displacement and the rotational degrees of freedom are set to zero). For the present case we have assumed the bending stiffness to be the stochastic parameter of the plate. The damping model chosen for this case is that of constant modal damping, with 1% damping factor for all the modes. Figure 2.12(a) shows the configuration of the rectangular

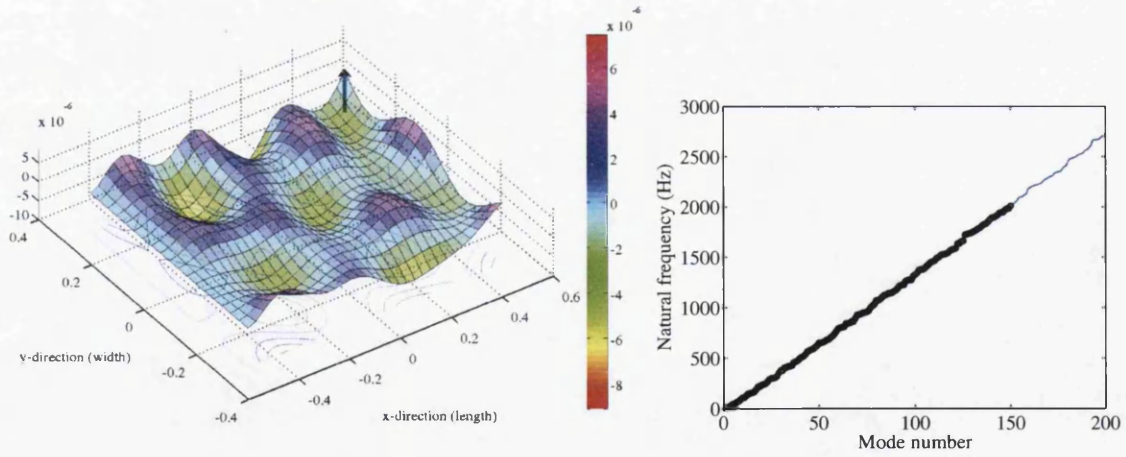

(a) Plate vibration shape at 300Hz.

(b) Natural frequency distribution.

Figure 2.12: (a) Dynamic plate vibration shape at 300 Hz with a harmonic point force at one of the free corners. The plate is clamped at one of its edges ($x = -0.5$). The plate is loaded at one of the free corners ($x = 0.5$, $y = 0.3$). (b) Natural frequency distribution of the vibrating plate highlighting the first 150 natural frequencies.

plate in a deformed configuration with a harmonic point load on one of its free corners. The

origin of the global coordinate system is assumed to be at the centre of the rectangular plate. We assume that the bending modulus is a stationary Gaussian random field of the form

$$D(x, y, \theta) = D_0(1 + \epsilon(x, y, \theta)) \tag{2.75}$$

where x and y are the coordinate direction along the length and width of the plate respectively, D_0 is the baseline modulus of elasticity, $\epsilon(x, y, \theta)$ is a zero mean stationary Gaussian random field. The autocorrelation function of this random field is assumed to be of the form

$$C_a(x_1, x_2; y_1, y_2) = \sigma_a^2 e^{-(|x_1 - x_2|)/\mu_x} e^{-(|y_1 - y_2|)/\mu_y} \tag{2.76}$$

where μ_x and μ_y are the correlation lengths along the x and y coordinate axes respectively, and σ_a is the standard deviation of the elastic modulus. We use the base-line parameters as the length $L_x = 1$m, width $L_y = 0.6$m, thickness $t = 3$mm, mass density $\rho = 7860$kg/m^3, Poisson ratio $\mu = 0.3$ and mean elastic modulus $D_0 = 2 \times 10^{11}$ Pa. For the finite element discretization, the beam is divided into 32 elements along its length (x direction) and 18 elements along its width (y direction). Standard 12 degree of freedom Kirchhoff plate elements [Petyt, 1998] are used for the finite element modeling. The total number of degrees of freedom of the plate system after the application of the boundary conditions come to $1,881$. The correlation length is taken as $1/5$th of the plate dimension along both the x and y directions, thus $\mu_x = L_x/5$ and $\mu_y = L_y/5$. The KL series expansion presented in Eqn. (2.11) is truncated at 4 terms along the orthogonal coordinate axes and using the tensor product of these eigen functions we have a total of 16 random variables to represent the discretized random elastic modulus in the spatial domain. Therefore, for this problem we have $n = 1881$ and $M = 16$. The vibration response have been obtained for two different values of the standard deviation of the random field, $\sigma_a = \{0.05, 0.15\}$. The external forcing vector is taken to be deterministic and having a unit norm.

The dynamic vibration response of the plate under the action of a point load acting at one of its free corners is now presented. The response is measured at the node under loading for four different values of the random field variability, σ_a. The frequency range of interest is $0 - 500$ Hz at an interval of 5 Hz. The reduced spectral method simulation and the reduced basis direct MCS simulation have been performed with $10,000$ random samples.

Figure 2.12(a) shows the mean deformation shape of the plate under a harmonic point load of unit amplitude (shown by the arrow) at one of its free ends at the frequency of 300 Hz. Figure 2.12(b) shows the distribution of the natural frequencies of the plate calculated with the deterministic system matrices. The chosen reduced number of eigenvectors (150) for the problem is marked in the figure, which approximately covers up to 2,000 Hz, which is about 4 times the maximum frequency of the problem (500 Hz). This choice is in line with the discussion give in Sec. 2.4.1. Thus the Galerkin method requires the solution of

a 150×150 system of linear equations in order to evaluate the constants associated with the stochastic basis. In contrast, for the PC solution technique using 4^{th} order polynomial functions, calculations reveal that it is necessary to solve a 9113445×9113445 dimensional linear system of equations in order to obtain the undetermined coefficients for every frequency point, which incurs a substantial computational cost. It must be noted though, that the linear system obtained after orthogonalizing the residual to the stochastic solution subspace is a large block sparse system and the solution can potentially be speeded up with iterative Krylov-based linear solvers and appropriate preconditioners [Saad, 2003]. If the PC expansion is applied to the dynamic system in its modal coordinates with the solution being projected on the first 150 eigenmodes, then it would be necessary to solve a block sparse linear system of dimension 726750×726750. However, now each 150×150 block of the 726750-dimensional sparse coefficient matrix would be a dense matrix.

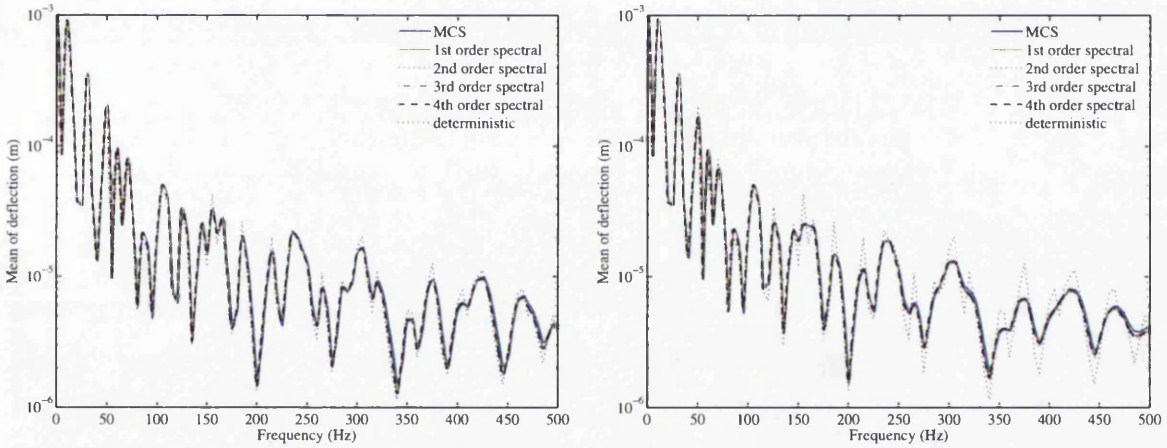

(a) Plate deflection for $\sigma_a = 0.05$.

(b) Plate deflection for $\sigma_a = 0.1$.

Figure 2.13: The mean of the deflection amplitude of a free corner of a Kirchhoff-Love thin plate under a unit harmonic point load. The response is obtained with $10,000$ random samples and for $\sigma_a = \{0.05, 0.10\}$. The response for different order of spectral functions are shown. For this problem the degrees of freedom $n = 1881$ and the number of random variables $M = 16$. The proposed Galerkin approach needs solution of a 150×150 linear system of equations.

Figure 2.13 shows the frequency domain response of the mean deflection of the Kirchhoff-Love plate obtained with different orders of spectral functions (1^{st}, 2^{nd}, 3^{rd} and 4^{th}) and has been compared with the direct MCS results and the deterministic system response. It is observed that the response obtained with the spectral method matches the direct MCS results quite closely. For higher values of σ_a we find the mean response to attenuate with frequency, which is similar to the case of beam bending problem in the previous section. This can be attributed to the fact that a high σ_a implies that the resonance modes are quite scattered around the neighborhood of a particular frequency and the expectation operation smooths out the curve. Hence at higher frequencies, some of the resonance modes which fall outside the

frequency range of interest otherwise, may have substantial contribution in the response, due to which significantly larger number of eigen modes have been chosen than that guided by the Nyquist frequency.

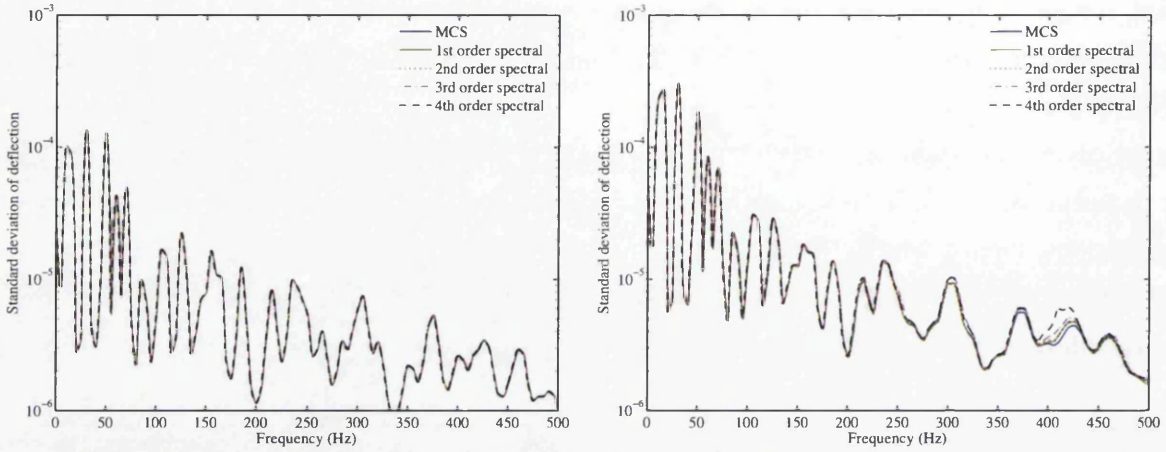

(a) Standard deviation of the response for $\sigma_a = 0.05$. (b) Standard deviation of the response for $\sigma_a = 0.1$.

Figure 2.14: The standard deviation of the deflection amplitude of a free corner of a Kirchhoff-Love thin plate under a unit harmonic point load. The response is obtained with $10,000$ random samples and for $\sigma_a = \{0.05, 0.10\}$.

The plots in Fig. 2.14 show the standard deviation of the stochastic system response over the frequency range. Once again, the spectral function approach produces agreeable results with the direct MCS simulation. The approximation of the different moments of the response with varying orders of the spectral functions is of particular interest to this study and has been studied with the L^2 relative error norm described in Eqn. (2.74). This is presented later in the section.

The results in Fig. 2.13 correspond to the mean of the direct receptance function of the vibrating system and shows that the response is a combination of a large number of vibration modes. We also present the cross-receptance results of the plate system here which is a physically significant quantity and indicates the drive point mobility of the plate. Figure 2.15 shows the frequency domain response of the amplitude of deflection of the center node of the plate under the point load at the free corner of the plate as shown in Fig. 2.12(a). It can be seen that the plots show a good agreement with the direct MCS results at all frequencies for both values of standard deviation of the random parameter σ_a. Figure 2.16 shows the plot of the standard deviation of the amplitude of the response, which is exactly similar to the direct MCS results. The above results show that the solutions obtained with the proposed reduced spectral basis is well-suited for obtaining the solution of these uncertain structural systems. Compared to the direct MCS solution or the PC technique (shown for the cantilever beam problem only) the computational cost is substantially lesser, since only a few number of basis functions are required to compute the solution vector. Thus the dimension of the

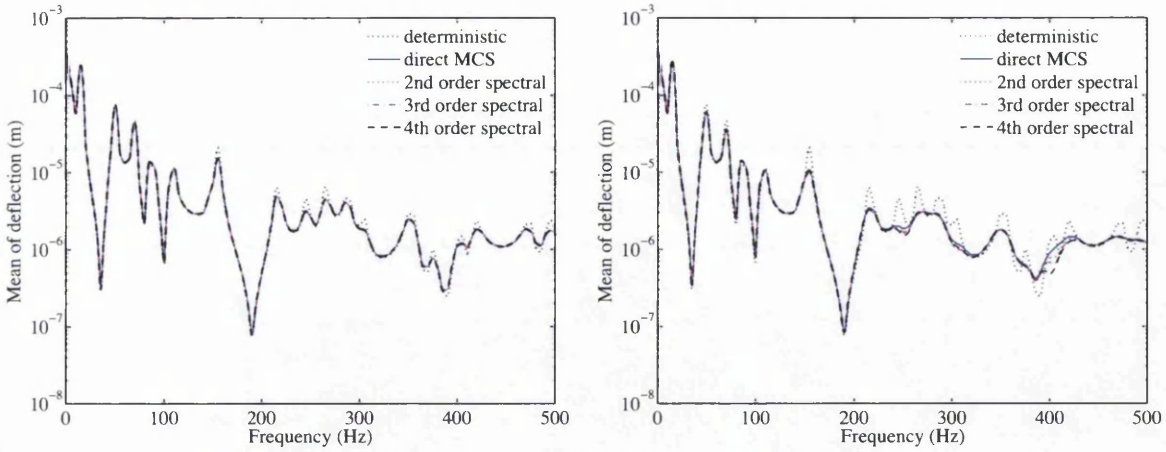

(a) Plate deflection for $\sigma_a = 0.05$. (b) Plate deflection for $\sigma_a = 0.1$.

Figure 2.15: The frequency domain response of deflection amplitude of the node at the center of the Kirchhoff-Love thin plate under a harmonic point load of unit amplitude at one of the free corners of the plate. The response is obtained with $10,000$ random samples and for $\sigma_a = \{0.05, 0.10\}$. The response for different order of spectral functions is shown.

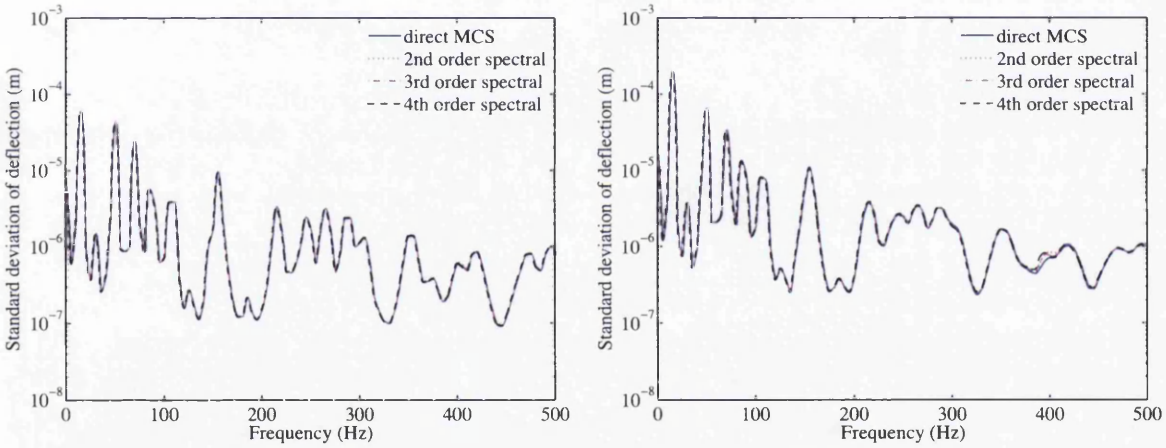

(a) Plate deflection for $\sigma_a = 0.05$. (b) Plate deflection for $\sigma_a = 0.1$.

Figure 2.16: The standard deviation of the deflection amplitude of the node at the center of the Kirchhoff-Love thin plate under a unit harmonic point load. The response is obtained with $10,000$ random samples and for $\sigma_a = \{0.05, 0.10\}$.

linear system for the Galerkin technique, which is used for the evaluation of the unknown deterministic coefficients, is also quite small. It is found that the estimated solution closely matches the direct MCS solution at all frequencies (including the resonance frequencies) for the considered values of variability σ_a of the system parameters. Hence the frequency adaptive nature of the spectral functions used to approximate the solution in this study is found to be quite useful for the systems studied in this work.

Figure 2.17 shows the probability density functions of the deflection of the plate node under loading at the frequency of 300 Hz, which is a resonance frequency. It is observed that

there is a consistent agreement with the direct MCS simulation results for all values of σ_a. It

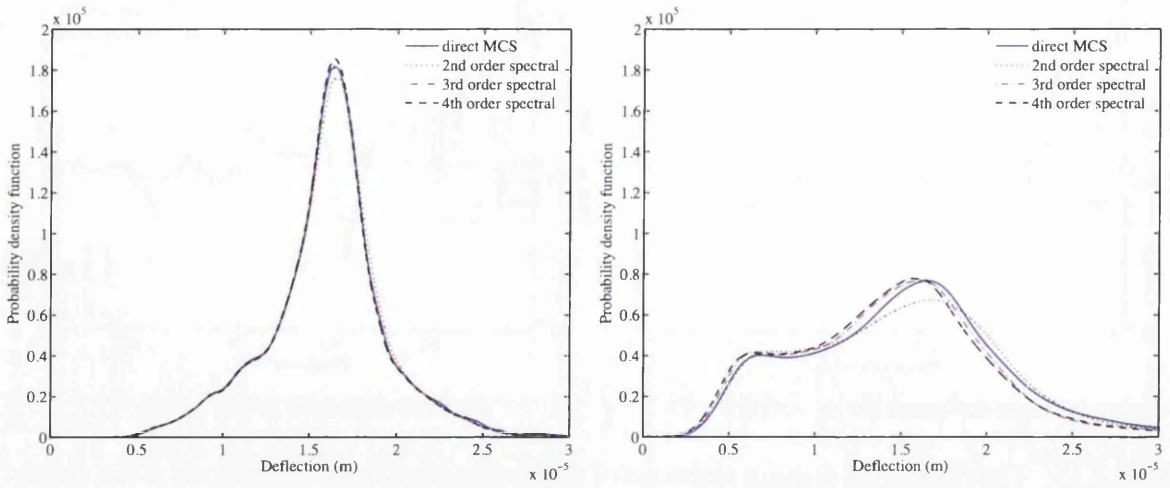

(a) Probability density function at $\sigma_a = 0.05$.

(b) Probability density function at $\sigma_a = 0.1$.

Figure 2.17: The probability density function (pdf) of the deflection amplitude of the point under harmonic loading at the frequency of 300Hz. The correlation length of the random field describing the bending rigidity is assumed to be $\mu_a = L/5$ along the orthogonal directions of length and breadth. The response is obtained using the Galerkin approach with $10,000$ random samples and for $\sigma_a = \{0.05, 0.10\}$.

can be seen that for $\sigma_a = 0.10$ the pdf is spread over a wider range of values of the deflection which indicates a high standard deviation of the system response.

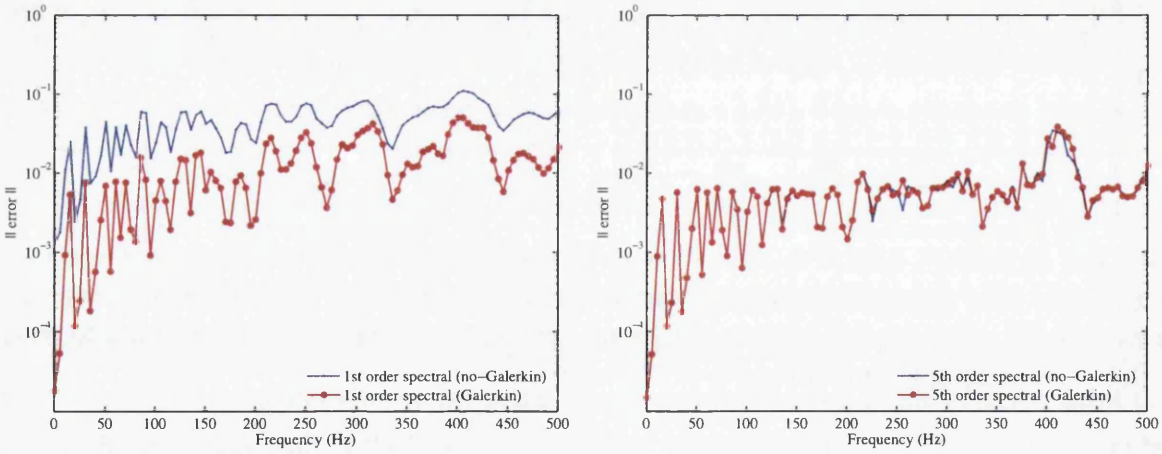

(a) L^2 error with 1^{st} order spectral functions.

(b) L^2 error with 5^{th} order spectral functions.

Figure 2.18: The relative L^2 error of the mean deflection of the Kirchhoff-Love thin plate under a unit harmonic point load. The response has been approximated with 1^{st} and 5^{th} order spectral functions and the error is studied before and after the application of the Galerkin scheme. Simulations have been performed with $10,000$ random samples and for standard deviation of $\sigma_a = 0.10$ of the random parameter.

Now we look into the relative L^2 error characteristics defined in Eqn. (2.74) to understand the advantages of using higher order spectral functions and the effect of Galerkin type error

minimization on the solution statistics. Figure 2.18 shows effectiveness of using the Galerkin technique in terms of improving the the relative L^2 error of the mean deflection calculated with the 1^{st} and 5^{th} order spectral functions. These calculations have been done for the higher value of standard deviation value $\sigma_a = 0.10$ of the parametric random field. It is seen that the Galerkin type error minimization has a significant effect on the solution approximated with the 1^{st} order spectral functions at almost all frequencies (Fig. 2.18(a)). The 1^{st} order spectral function approximates the response without having any modal coupling involved in it, in other words, the reduced system matrices in the generalized modal coordinates is only a diagonal matrix (see Eqn. (2.46) for more details). Thus, the Galerkin technique takes care of the coupling conditions by adjusting the values of the undetermined coefficients $c_k(\omega), k = 1, 2, \ldots, n_r$ where n_r is the dimension of the reduced system. However, the solution obtained with the 5^{th} order spectral functions, given in Fig. 2.18(b), shows little effect of the application of the Galerkin method. This indicates that the solutions have already been approximated to a sufficient degree of accuracy using the higher order terms in the spectral functions and the modal coupling of the vibrating system in approximating the response is already quite high. Hence the Galerkin error minimization has little effect in terms of improving the solution accuracy. Also, it can be seen that the overall relative error levels are reduced when we use the 5^{th} order spectral functions to approximate the solution, especially beyond the low frequency region (say 100 Hz).

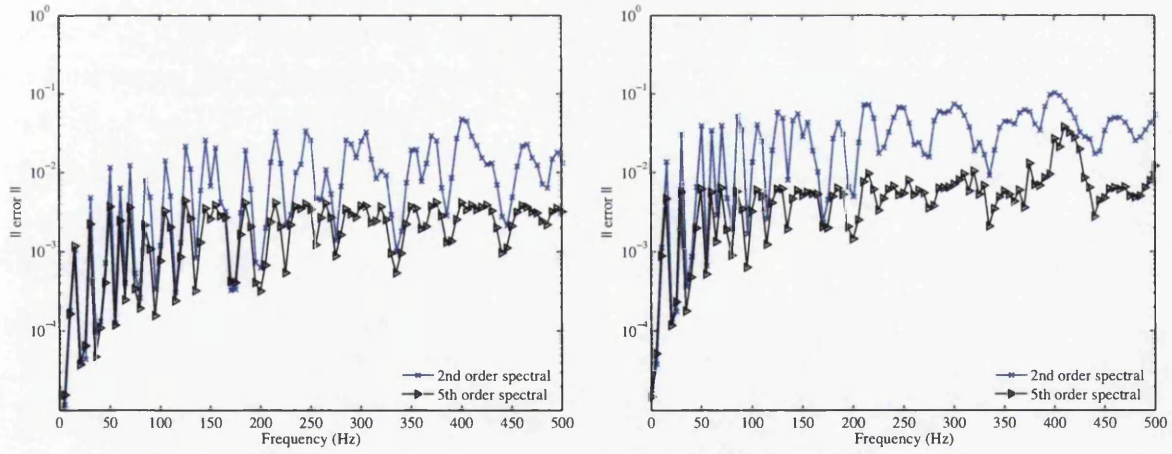

(a) L^2 error for $\sigma_a = 0.05$. (b) L^2 error for $\sigma_a = 0.10$.

Figure 2.19: The relative L^2 error of the mean deflection of the Kirchhoff-Love thin plate under a unit harmonic point load obtained with 2^{nd} and 5^{th} order spectral functions. Simulations have been performed with $5,000$ random samples and for standard deviation of $\sigma_a = 0.05$ and $\sigma_a = 0.10$ of the random parameter.

The improvement in the overall relative L^2 error at all frequencies is demonstrated in Fig. 2.19, which shows the error calculated with the mean deflection values obtained with 2^{nd} and 5^{th} order spectral functions in conjunction with the Galerkin method for different values of variability of the parametric randomness (indicated by σ_a). There is a good improvement

in the results with the 5^{th} order functions, except for the low frequency region (below 100 Hz) and for low value of σ_a. For a higher value of standard deviation of the random field ($\sigma_a = 0.10$), the improvement in results with the higher order spectral functions is more than that for $\sigma_a = 0.05$. Thus, implies that the higher order spectral functions are more useful for high values of standard deviation of the random field.

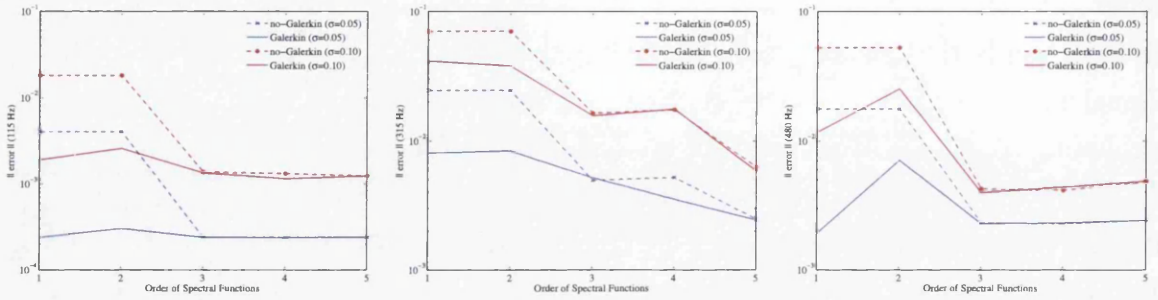

(a) L^2 error at 115 Hz. (b) L^2 error at 310 Hz. (c) L^2 error at 480 Hz.

Figure 2.20: The relative L^2 error of the mean deflection of the Kirchhoff-Love thin plate under a unit harmonic point load with increasing order of spectral functions at 110, 315 and 480 Hz. Simulations have been performed with $10,000$ random samples and for standard deviation of $\sigma_a = \{0.05, 0.10\}$ of the random parameter.

Finally, Fig. 2.20 demonstrates the effect of increasing the order of spectral functions on the L^2 relative error of the solution. The behavior is shown at particular values of frequencies, to clearly identify the solution traits. The frequencies are chosen such that the use of higher order functions improve the results significantly at those points. The curves show that the Galerkin method has a significant role in reducing the error of the solution obtained with 1^{st} and 2^{nd} order spectral functions, and little effect on those with higher orders. It is observed at all the frequencies that a significant improvement in the results is obtained as we move from the 2^{nd} to the 3^{rd} order values when the Galerkin technique is not being used. The application of the Galerkin error minimization technique brings down the error values close to those obtained normally (without the Galerkin) with the higher order (4 and 5) spectral functions. It can also be seen, especially in Fig. 2.20(c), that the Galerkin technique reduces the 1^{st} order error to a lower value than that with the second order spectral function. Also, while the higher order functions almost always provides a better solution accuracy yet, the higher order functions must be used prudently. An identifiable trend of the L^2 error with increasing spectral function order has not been observed in the results presented here, and hence the extent of this kind of 'p-refinement' (by increasing the order of spectral functions) may not be obvious. Investigation into some optimality criterion which can provide some adaptivity in terms of the optimum order of the spectral functions and the dimension of the reduced modal subsapce of the problem would be quite helpful to minimize the computational cost in these kind of problems.

2.7 Summary

We have considered the stochastic partial differential equation for structural dynamic systems with generally non-Gaussian random fields. The stochastic system response is resolved using a set of complex frequency-adaptive stochastic weighting functions, called the *spectral functions*. The spectral functions are rational functions of the input random variables and depends on the spectral properties of the mass and stiffness matrices. A Galerkin-type error minimization approach has been proposed which uses a set of frequency dependent undetermined coefficients to orthogonalize the residual to the reduced modal subspace. It has been shown that these unknown coefficients can be evaluated using a set of linear algebraic equations whose dimension is much smaller than that of the full finite element system. A hybrid analytical-simulation approach is proposed to obtain the statistical properties of the solution for different frequencies.

The proposed solution technique has been used to solve two example problems:

- An Euler-Bernoulli cantilever beam with random bending modulus subjected to a harmonic point force on its free end over the frequency range of $0 - 600$ Hz. The spatially varying random field has been discretized with two zero-mean uncorrelated standard Gaussian random variables. The results obtained with the spectral function approach is in good agreement with the direct MCS simulation at all frequencies and at all values of input standard deviation σ_a. However, the PC based solution approach, shows discrepancies near the resonance frequencies, even for moderate values of the σ_a, and deteriorates further as the latter increases. The solution obtained with the classical Neumann approach has also been presented for the sake of completeness, and it shows that near the resonance frequencies, the Neumann series diverges significantly.

- A Kirchhoff-Love thin plate, with random bending stiffness subjected to a harmonic point force loading over the frequency range of $0 - 500$ Hz. The random bending stiffness has been discretized with 16 random variables and the total number of degrees of freedom of the system is 1,881. Once again, the results obtained with the spectral function approach is in good agreement with the direct MCS simulation over the entire frequency range.

The good agreement between the direct MCS results and the proposed spectral function approach, even near the resonance frequencies and for high values of input standard deviation, indicates good convergence behavior of the spectral functions. An explanation of this fact has been provided in terms of the use of rational functions of the input random variables. Hence the response statistics approximated when using these are accurate even when lower-order spectral functions are used.

These results demonstrate the applicability and computational efficacy of the stochastic spectral function approach proposed in this work. The classical Neumann expansion is un-

suitable for this kind of frequency domain analysis of structural systems because the method relies on large convergence radius of the linear system preconditioned with the deterministic system matrices, which is not the case for (i) near-resonance frequencies, (ii) low values of damping, and (iii) a high standard deviation of the underlying input random field.

In the following chapter we address the issue of improving the computational efficacy of the spectral function approach further by hybridizing it with a Bayesian metamodeling technique. This can potentially offset the cost incurred when using higher order spectral functions to enhance the accuracy of the approximated stochastic response.

Chapter 3

Hybridization of the spectral function approach with metamodeling technique

3.1 Introduction

The spectral function approach presented in the previous chapter is found to perform well in terms of solution accuracy and computational efficacy with respect to the benchmark solutions provided by the MCS technique or the finite order chaos expansion methods. The stochastic system response was expressed as a series expansion using the basis functions of a left-preconditioned stochastic Krylov space. It gave an accurate prediction of the frequency response especially near resonance frequencies when compared to the PCE or the classical Neumann expansion technique. However, it is seen in Figs. 2.9–2.10 and Figs. 2.19–2.20, the approximation accuracy is enhanced with an increase in the order of spectral functions. However, this increased accuracy comes at a computational cost. We have adopted a Bayesian metamodeling approach to mitigate this cost.

This metamodeling strategy, known as Gaussian process emulation [O'Hagan, 2006], is based on the analysis and design of computer experiments [Sacks *et al.*, 1989, Santner *et al.*, 2003] and on the concepts of Bayesian statistics. The non-expensive approximation to the output is made after evaluating a small number of points in the input space, hence reducing the required computer processing time. After conditioning on these training runs and updating a prior distribution, the mean of the resulting posterior distribution approximates the output of the simulator at any untried input, whereas it reproduces the known output at each design point. Gaussian process emulation has been implemented in various scientific fields with encouraging results. These fields include structural dynamics [DiazDelaO and Adhikari, 2010], multi-scale analysis [Flores *et al.*, 2012], stochastic finite elements [DiazDelaO and

The work presented in this chapter has been done in collaboration with Dr F. A. Diaz Dela O.

Adhikari, 2011], and domain decomposition [DiazDelaO and Adhikari, 2012] among many others.

The corrugated skins are of particular importance in many aerospace applications (such as morphing aerospace structures) largely due to the high compliance it offers along the corrugation direction. For many aerospace applications, complicated structures such as these have inherent uncertainty in their parametric variables which can not be reduced despite repeated and strenuous measurements or expensive simulations. Hence it is required to incorporate these uncertainties into the mathematical model and treat them within the framework of stochastic finite element analysis.

In the present study we have considered the elastic parameters (such as the bending and elastic stiffness) of this panel as random fields. These form the stochastic input space of the mathematical model. The effect of this input uncertainty on the stochastic response statistics have been analyzed with the spectral function approach in conjunction with the Gaussian process emulation. The performance of the proposed hybridized spectral and metamodeling approach are compared with direct Monte Carlo simulations, which have been considered as the benchmark solution.

3.2 Metamodeling approach

In Eqn. (2.31), it was showed that the response vector $\widetilde{\mathbf{u}}^{(m)}$ at each frequency step ω is a approximated with a finite order rational function of the stochastic variables $\boldsymbol{\xi}(\theta)$. In this section, we briefly review a metamodeling strategy to cope with the computational cost of obtaining a statistical summary of the response. Let $\hat{u}_k^{(m)}(\boldsymbol{\xi}(\theta),\omega)$ be the k-th component of the response vector $\widetilde{\mathbf{u}}^{(m)}$ evaluated at the design point $\boldsymbol{\xi}(\theta)$. If the response vector $\widetilde{\mathbf{u}}^{(m)}$ is evaluated at n design points $\boldsymbol{\xi}^{(1)}(\theta),\ldots,\boldsymbol{\xi}^{(n)}(\theta)$, then a vector $\hat{\mathbf{u}}_k^{(m)} = \left(\hat{u}_k^{(m)}(\boldsymbol{\xi}^{(1)}(\theta),\omega),\ldots,\hat{u}_k^{(m)}(\boldsymbol{\xi}^{(n)}(\theta),\omega)\right)^{\mathsf{T}}$ is obtained. In order to simplify the notation, we make the dependence on θ and ω implicit and re-express $\hat{\mathbf{u}}_k^{(m)}$ as $\hat{\mathbf{u}}_k^{(m)} = \left(\hat{u}_k^{(m)}(\boldsymbol{\xi}^{(1)}),\ldots,\hat{u}_k^{(m)}(\boldsymbol{\xi}^{(n)})\right)^{\mathsf{T}} \in \mathbb{R}^n$.

3.2.1 Bayesian emulation

For an input $\boldsymbol{\xi} = (\xi_1,\ldots,\xi_p)^{\mathsf{T}}$, the k-th component of the global response calculated by Algorithm 1 is a scalar $\hat{u}_k^{(m)}(\boldsymbol{\xi})$. The cost of running the code makes it affordable to evaluate only a limited number of design points $\boldsymbol{\xi}^{(1)},\ldots,\boldsymbol{\xi}^{(n)}$ when using high order spectral functions. The uncertainty about the output that arises due to this cost can be modeled probabilistically. To that effect, let the vector $\widetilde{\mathbf{u}}^{(m)}$ of observed outputs be realizations of a Gaussian stochastic process. The model structure for a single component of the output vector is thus expressed as

$$\hat{u}_k^{(m)}(\boldsymbol{\xi}) = \mathbf{h}(\boldsymbol{\xi})^{\mathsf{T}}\boldsymbol{\beta} + Z(\boldsymbol{\xi}) \tag{3.1}$$

where $\mathbf{h}(\boldsymbol{\xi})$ is a vector of known functions and $\boldsymbol{\beta}$ is an unknown hyperparameter to be estimated from the data. The choice of $\mathbf{h}(\boldsymbol{\xi})$ is an active research area. Some authors such as Oakley and O'Hagan [2004], Vernon *et al.* [2010] point out that it should be chosen to reflect the available information about the functional form of the output, and that whenever possible, it is worth investing as much effort as possible modeling this mean function. In this work we choose a constant mean and delegate the responsibility of capturing complex relationships to the function $Z(\cdot)$. This function is a stochastic process with mean zero and covariance function

$$Cov\Big(Z(\boldsymbol{\xi}), Z(\boldsymbol{\xi}')\Big) = \sigma_z^2 C(\boldsymbol{\xi}, \boldsymbol{\xi}') \tag{3.2}$$

where $C(\boldsymbol{\xi}, \boldsymbol{\xi}')$ is a correlation function and σ_z^2 is the process variance, a hyperparameter that can also be estimated from the data. In order to choose a valid positive-definite correlation function, some authors [Sacks *et al.*, 1989] consider products of one-dimensional correlations, specifically functions of the form

$$C(\boldsymbol{\xi}, \boldsymbol{\xi}') = \prod_{i=1}^{n} \exp\Big\{ - b_i \Big(\xi_i - \xi_i'\Big)^2 \Big\} \tag{3.3}$$

where $b_i > 0$ for all i. This correlation function is infinitely differentiable, which is convenient to incorporate derivative information [O'Hagan, 1992]. The vector of smoothness hyperparameters $\mathbf{b} = \big(b_1, \ldots, b_n\big)^\intercal$ quantifies the rate at which the output varies as the input varies. Intuitively, the less smooth the output, the more strongly will it respond to small changes in the input. The above prior knowledge can be summarized in a prior probability distribution of the form

$$\hat{u}_k^{(m)}(\boldsymbol{\xi}) \big| \boldsymbol{\beta}, \sigma_z^2, \mathbf{b} \sim \mathcal{N}\Big(\mathbf{h}(\boldsymbol{\xi})^\intercal \boldsymbol{\beta}, \sigma_z^2 C(\boldsymbol{\xi}, \boldsymbol{\xi}')\Big) \tag{3.4}$$

Let $\mathcal{D} = \Big\{\big(\boldsymbol{\xi}^{(i)}, \hat{u}_k^{(m)}(\boldsymbol{\xi}^{(i)})\big) \big| i = 1, \ldots, n\Big\}$ be the set of training runs corresponding to the k-th component of the global finite element solution provided by Algorithm 1. Given this observed dataset, Bayes' theorem is used to estimate the hyperparameters [Haylock and O'Hagan, 1996, Oakley, 2002]. Once this is done, the prior distribution in Eqn. (3.4) is updated and the mean of the resulting posterior distribution approximates the output $\hat{u}_k^{(m)}(\boldsymbol{\xi}^*)$ at any untried input $\boldsymbol{\xi}^*$, whereas it interpolates the observed output at the design points $\boldsymbol{\xi}^{(1)}, \ldots, \boldsymbol{\xi}^{(n)}$. At the same time, the variance of the posterior distribution quantifies the uncertainty that arises from the limited availability of code evaluations [Rougier, 2007] due to computational cost. The resulting posterior distribution is of the form

$$\hat{u}_k^{(m)}(\boldsymbol{\xi}) \big| \hat{\mathbf{u}}_k^{(m)}, \boldsymbol{\beta}, \sigma_z^2 \sim \mathcal{N}\Big(m^*(\boldsymbol{\xi}), \sigma_z^2 C^*(\boldsymbol{\xi}, \boldsymbol{\xi}')\Big) \tag{3.5}$$

where the posterior mean and posterior variance are such that

$$m^*(\boldsymbol{\xi}) = \boldsymbol{\beta} + \mathbf{r}(\boldsymbol{\xi})^\intercal \mathbf{R}^{-1} (\hat{\mathbf{u}}_k^{(m)} - \mathbf{1}\boldsymbol{\beta}) \tag{3.6}$$

$$C^*(\boldsymbol{\xi}, \boldsymbol{\xi}') = C(\boldsymbol{\xi}, \boldsymbol{\xi}') - \mathbf{r}(\boldsymbol{\xi})^\intercal \mathbf{R}^{-1} \mathbf{r}(\boldsymbol{\xi}') \tag{3.7}$$

In the above expressions, $\mathbf{R} \in \mathbb{R}^{n \times n}$ with $[\mathbf{R}]_{ij} = C(\boldsymbol{\xi}^{(i)}, \boldsymbol{\xi}^{(j)})$; $\mathbf{r}(\boldsymbol{\xi}) \in \mathbb{R}^n$ such that $\mathbf{r}(\boldsymbol{\xi}) = \left(C(\boldsymbol{\xi}, \boldsymbol{\xi}^{(1)}), \ldots, C(\boldsymbol{\xi}, \boldsymbol{\xi}^{(n)})\right)^\intercal$; and $\mathbf{1} \in \mathbb{R}^n$ such that $\mathbf{1} = \left(1, \ldots, 1\right)^\intercal$. The posterior mean $m^*(\cdot)$ provides is a fast approximation of the output $\hat{u}_k^{(m)}(\boldsymbol{\xi})$ for any $\boldsymbol{\xi}$ in the input domain.

Since it could be difficult to specify $\boldsymbol{\beta}$ and σ_z^2, they can be integrated out in order to obtain the posterior distribution of $\hat{u}_k^{(m)}(\boldsymbol{\xi}) \big| \widetilde{\mathbf{u}}^{(m)}, \sigma_z^2$. That way, the posterior distribution becomes

$$\hat{u}_k^{(m)}(\boldsymbol{\xi}) \big| \hat{\mathbf{u}}_k^{(m)}, \sigma_z^2 \sim \mathcal{N}\left(m^{**}(\boldsymbol{\xi}), \sigma_z^2 C^{**}(\boldsymbol{\xi}, \boldsymbol{\xi}')\right) \tag{3.8}$$

with

$$m^{**}(\boldsymbol{\xi}) = \widehat{\boldsymbol{\beta}} + \mathbf{r}(\boldsymbol{\xi})^\intercal \mathbf{R}^{-1} (\hat{\mathbf{u}}_k^{(m)} - \mathbf{1}\widehat{\boldsymbol{\beta}}) \tag{3.9}$$

$$C^{**}(\boldsymbol{\xi}, \boldsymbol{\xi}') = C^*(\boldsymbol{\xi}, \boldsymbol{\xi}') + \left(1 - \mathbf{r}(\boldsymbol{\xi})^\intercal \mathbf{R}^{-1} \mathbf{1}\right) \left(\mathbf{1}^\intercal \mathbf{R}^{-1} \mathbf{1}\right)^{-1} \left(1 - \mathbf{r}(\boldsymbol{\xi}')^\intercal \mathbf{R}^{-1} \mathbf{1}\right)^\intercal \tag{3.10}$$

$$\widehat{\boldsymbol{\beta}} = (\mathbf{1}^\intercal \mathbf{R}^{-1} \mathbf{1})^{-1} \mathbf{1}^\intercal \mathbf{R}^{-1} \hat{\mathbf{u}}_k^{(m)} \tag{3.11}$$

Finally, σ_z^2 can also be integrated out in order to obtain

$$\frac{\hat{u}_k^{(m)}(\boldsymbol{\xi}) - m^{**}(\boldsymbol{\xi})}{\widehat{\sigma}_z \sqrt{C^{**}(\boldsymbol{\xi})}} \sim t_{n-1} \tag{3.12}$$

where

$$\widehat{\sigma}_z^2 = \frac{\hat{\mathbf{u}}_k^{(m)\intercal} \left(\mathbf{R}^{-1} - \mathbf{R}^{-1} \mathbf{1} (\mathbf{1}^\intercal \mathbf{R}^{-1} \mathbf{1}) \mathbf{1}^\intercal \mathbf{R}^{-1}\right) \hat{\mathbf{u}}_k^{(m)}}{n - 2} \tag{3.13}$$

which is a Student's t-distribution with $n - 1$ degrees of freedom.

Algorithm 2 Bayesian emulation

Input: Training runs $\mathcal{D} = \left\{\left(\boldsymbol{\xi}^{(i)}, \hat{u}_k^{(m)}(\boldsymbol{\xi}^{(i)})\right) \middle| i = 1, \ldots, n\right\}$ % {From Algorithm 1}

Output: Posterior mean $m^*(\boldsymbol{\xi})$ and posterior covariance $C^*(\boldsymbol{\xi}, \boldsymbol{\xi}')$

1: Obtain the hyperparameters' posterior distribution $\mathcal{P}(\beta, \sigma_z^2, \mathbf{b} \big| \mathcal{D}) = \frac{\mathcal{P}(\mathcal{D} \big| \beta, \sigma_z^2, \mathbf{b}) \mathcal{P}(\beta, \sigma_z^2, \mathbf{b})}{\mathcal{P}(\mathcal{D})}$

2: Update the prior in Eqn. (3.4) to obtain the posterior $\hat{u}_k^{(m)}(\boldsymbol{\xi}) \big| \hat{\mathbf{u}}_k^{(m)}, \sigma_z^2$ in Eqn. (3.8)

3: Compute $m^{**}(\boldsymbol{\xi})$ from Eqn. (3.9) and $C^{**}(\boldsymbol{\xi}, \boldsymbol{\xi}')$ from Eqn. (3.10) % {Pass to Algorithm 3}

3.2.2 Bayesian uncertainty analysis

A finite element code, such as the one considered here, is deterministic. This means that if it is run repeatedly at the same input $\boldsymbol{\xi}$, it will always return the same output $\hat{u}_k^{(m)}(\boldsymbol{\xi})$. However, the inputs we are interested in are physical parameters, the values of which are uncertain. The aim of uncertainty analysis is to propagate the uncertainty in the inputs through

the code in order to characterize the distribution of the output, which is itself a random variable $\mathbf{Y}$. The first stage of the uncertainty analysis is to quantify the uncertainty in the inputs by specifying a probability distribution $\mathcal{F}(\boldsymbol{\xi})$. If the code were not computationally expensive, the most straightforward uncertainty analysis would proceed by drawing a large sample $\left\{\boldsymbol{\xi}^{(1)}, \ldots, \boldsymbol{\xi}^{(N)}\right\}$ from the input distribution $\mathcal{F}(\boldsymbol{\xi})$ and then running the code at each realisation. This would result in an output sample from which any statistic or summary $\mathcal{S}(\mathbf{Y})$ can be estimated. $\mathcal{S}(\mathbf{Y})$ could be the mean, the variance, a particular percentile, or any other summary.

A simple way to carry out uncertainty analysis would be to directly replace the code with the emulator's posterior mean $m^{**}(\boldsymbol{\xi})$ in Eq. (3.8). Potentially, this predictive mean can be evaluated a large number of times at any untried input at very low cost. However, this approach would not incorporate the fact that $m^{**}(\boldsymbol{\xi})$ is itself an inexact approximation to the output and hence it introduces additional uncertainty. To circumvent this problem, an approach proposed in Oakley and O'Hagan [2002], Fricker *et al.* [2011] is employed and the strategy is detailed in Algorithm 3.

Algorithm 3 Uncertainty analysis using a GPE

Input: Posterior mean $m^{**}(\boldsymbol{\xi})$, and posterior covariance $C^{**}(\boldsymbol{\xi}, \boldsymbol{\xi}^{'})$ % {From Algorithm 2}
Input: Large sample $\left\{\boldsymbol{\xi}^{(1)}, \ldots, \boldsymbol{\xi}^{(N)}\right\}$ from the input distribution $\mathcal{F}(\boldsymbol{\xi})$,
Output: Summary $\mathcal{S}(\mathbf{Y})$ of the output distribution $\mathbf{Y}$

1: $\boldsymbol{\mathcal{S}} \leftarrow \varnothing$
2: Draw a large sample $\left\{\boldsymbol{\xi}^{(1)}, \ldots, \boldsymbol{\xi}^{(N)}\right\}$ from the distribution $\mathcal{F}(\boldsymbol{\xi})$
3: **for** j = 1 to K **do**
4: Draw a random function $y_{(j)}$ from the posterior distribution (3.8)
5: Evaluate $y_{(j)}(\boldsymbol{\xi}^{(1)}), \ldots, y_{(j)}(\boldsymbol{\xi}^{(N)})$
6: Obtain $\mathcal{S}_j(\mathbf{Y})$, the Monte Carlo estimate of $\mathcal{S}(\mathbf{Y})$
7: $\boldsymbol{\mathcal{S}} \leftarrow \boldsymbol{\mathcal{S}} \cup \mathcal{S}_j(\mathbf{Y})$
8: **end for**
9: Use $\boldsymbol{\mathcal{S}}$ to estimate any summary of the distribution of $\mathcal{S}(\mathbf{Y})$

For illustration of the complete process, Figure 3.1 shows ten iterations of Algorithm 3 for a toy model, with ξ uniformly distributed in the interval $[-5, 5]$. The training runs are generated by a simulator using Algorithm 1, then emulation is performed by Algorithm 2 to compute the posterior mean and variance, and finally the uncertainty distribution is generated by Algorithm 3.

3.3 Algorithmic complexity

The improvement in efficiency of the proposed hybrid spectral and metamodeling technique over the crude Monte Carlo simulation is presented here in light of the algorithmic complexity

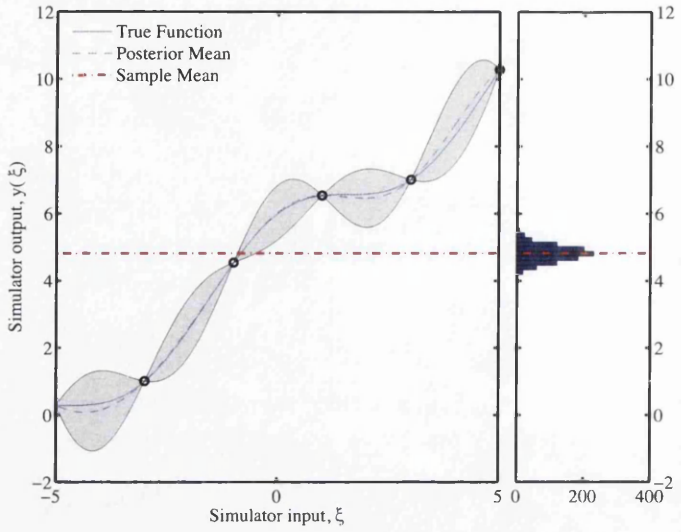

Figure 3.1: Illustration of the uncertainty analysis: The posterior mean (dotted curve) approximates the true output (solid curve) based on a few training runs (circles). The code inputs are random variables uniformly distributed as $\boldsymbol{\xi} \sim U(-5, 5)$. The 95% credible intervals are also shown (shaded areas). Note how the uncertainty in the training runs is zero, since the true output is known. The mean of each random function drawn from the posterior distribution results in a realisation of the sample mean, the distribution of which can be approximated (histogram) and a statistical summary estimated.

of the two methods. The improvement is due to the use of finite order spectral functions, a reduced number of orthogonal basis functions in constructing the stochastic system response and solving the random system at only a few design points in the stochastic input space.

Let n_{dof} be the dimension of the complete stochastic finite element linear system and let N_s be the number of Monte Carlo samples. Then, the total computational complexity at each frequency step is $N_s\mathcal{O}(n_{\text{dof}}^3)$. For the spectral method, the calculation of various orders of spectral functions requires the evaluation of $\boldsymbol{\Lambda}^{-1}(\omega, \boldsymbol{\xi}(\theta))\,\boldsymbol{\Delta}(\omega, \boldsymbol{\xi}(\theta))$ in Eqn. (2.42), whose complexity is $\mathcal{O}(n_{\text{dof}}^2)$. Hence, the p^{th} order spectral function has a complexity of $(p-1)\mathcal{O}(n_{\text{dof}}^2)$. Summing up all the computations required for calculating the mth order spectral functions (as shown in Eqn. (2.32)) or the m-dimensional stochastic Krylov basis functions as in Eqn. (2.43), and given that the successive basis can be obtained recursively from the previous basis, the computational complexity is $N_s m\mathcal{O}(n_{\text{dof}}^2)$ for the solution of system at all the N_s samples. We can see that the calculation of the finite order spectral functions is almost one order of magnitude less than that of the crude Monte Carlo. However, for most of the low to mid frequency structural dynamic problems, a good approximation of the vibration response is obtained by considering only the first few eigenpairs. If we adopt this reduced system, then the dimension of the linear system is reduced to n_r where $\boldsymbol{\lambda}_0 = \text{diag}\,[\lambda_1, \lambda_2, \ldots, \lambda_{n_r}]$ and $\boldsymbol{\Phi} = \left[\boldsymbol{\phi}_1, \boldsymbol{\phi}_2, \ldots, \boldsymbol{\phi}_{n_r}\right]$. The complexity involved in this case for the calculation of the p^{th} order spectral function would be $(p-1)\mathcal{O}(n_r^2)$. Hence, when

Method	Complexity	No. Samples
Crude Monte Carlo	$N_s\mathcal{O}(n_{\text{dof}}^3)$	N_s
Spectral Method	$N_s m\mathcal{O}(n_r^2)$	N_s
Spectral Method + Emulation	$nm\mathcal{O}(n_r^2) + \mathcal{O}(n^3)$	n

Table 3.1: Computational complexity of the proposed hybrid approach against crude Monte Carlo for each frequency level. The number of samples is such that $n << N_s$. The number of degrees of freedom is given by n_{dof}. The reduced number of modes is n_r. The order of the spectral functions, and hence the number of Krylov bases, is given by m.

constructing the system response using m-dimensional stochastic Krylov basis and a reduced number of orthogonal eigenmodes, the complexity is given by $N_s m\mathcal{O}(n_r^2)$, where $n_r << n_{\text{dof}}$. In the worst case scenario, if very high degrees of spectral functions are considered, such that $m \approx n_r$, the complexity becomes $N_s\mathcal{O}(n_r^3)$.

While the spectral approach is efficient in reducing the complexity of solving the linear system at the stochastic points, the metamodel is used to mitigate the cost of solving an $\mathcal{O}(n_r^3)$ complex system at each one of the N_s samples. Hence, n design points (with $n << N_s$) are chosen using a sampling plan (such as a Latin hypercube) and the stochastic system response is calculated to generate training runs. This results in the complexity being reduced further to $nm\mathcal{O}(n_r^2)$. Given these n training runs, the complexity of emulating the response is $\mathcal{O}(n^3)$. This is due to the linear system solved in Eqn. (3.9) and Eqn. (3.10), where $\mathbf{R} \in \mathbb{R}^{n\times n}$. Therefore, the complexity of the hybrid approach is the sum of the complexity associated with the generation of the training runs with the spectral method plus the complexity of the emulator. The above discussion is summarized in Table 3.1. The resolution of the eigenvalue problem required for the spectral method is done only once in the beginning and is stored and used in the subsequent steps of the algorithm. Iterative Krylov subspace methods (like the Arnoldi's method or Lanczos algorithm) are employed for this purpose since the system matrices in structural dynamic systems are sparse, symmetric and positive definite. The number of iterations required for the convergence of the required number of eigenpairs is driven by the condition number of the system [Saad, 2003]. Also, the determination of the first few eigenpairs of large sparse finite element systems is amenable to efficient parallelization and has been implemented in libraries such as ARPACK [Lehoucq *et al.*, 1998]. Hence the evaluation of the eigenpairs do not enhance the order of computational complexity associated with the Spectral method given in Table 3.1.

It is worth mentioning that the cost associated with the estimation of the hyperparameters can become prohibitive, especially for a large n. However, if the code that is emulated is very expensive, only a few training runs might be available. This might render the cost of estimating the hyperparameters relatively negligible [Kolachalama *et al.*, 2007]. Additionally, there are parallel methods available that deal with this problem [Choudhury *et al.*, 2002]. Naturally, the problem with having only few training runs undermines the predictive capabil-

ity of any metamodel. It is therefore the task of the investigator to keep a balance between computational cost and robustness of the metamodel. If the Bayesian metamodel presented here becomes non-robust, a possible alternative is the linear Bayes approach [Vernon *et al.*, 2010]. Rather than calculate a full posterior distribution for the model output, this approach assesses just the posterior mean and variance. Additionally, this approach can be combined with implausibility measures in order to rapidly exclude areas of the input domain in which fits are unlikely to be found.

We give here briefly an estimation of the computational times obtained with the proposed method and its comparison with the MCS method. We assume that the FE linear system is of dimension 6630 and that the solution with the spectral function approach has been approximated with 4th order spectral functions and 200 eigen modes of the baseline structural system. This choice is justified by the fact that the analysis is being carried out within the frequency bandwidth of 0-300 Hz and the chosen modes satisfactorily capture the deformation shapes within this frequency range. The average time taken for 10,000 sample direct MCS simulation at each frequency step using matrix factorization method is found to be $\approx 2.4 \times 10^4$s while the same for the 4th order spectral method is 374 s (assuming that the eigen modes have been precomputed). When the Biconjugate Gradient method is used to take advantage of the sparse FE system with an incomplete LU decomposition of the system matrix as the preconditioner the computational time for resolving 10000 sample solutions comes down to $\approx$ 5000s. It is to be mentioned that the Biconjugate Gradient solver is optimized to use the BLAS libraries for performing parallel matrix-vector operations on 8 computational cores of identical capability. On the other hand, when 125 samples are solved training runs are generated to be used as training runs for the emulation, the cost for the 4th order spectral method comes down to 6s and the cost of emulation is 50s. This shows that the computational efficacy of the proposed spectral function method with Bayesian metamodeling is significantly efficient when compared with brute force MCS technique with and without sparse solvers.

3.4 Application: Dynamic analysis of a corrugated panel

3.4.1 Stochastic modeling of corrugated panels

Corrugated laminates offer a plausible solution for morphing aircraft skins due to their extremely anisotropic behaviour. The corrugation direction (chordwise direction) offers compliance and the spanwise direction (transverse to corrugation) makes the structure much stiffer. This is particularly suitable for morphing applications which can do away with the need of having auxiliary components such as flaps and slats to attain necessary changes in geometry. The performance of this corrugated skins are studied here with respect to random fluctuations in their elastic properties.

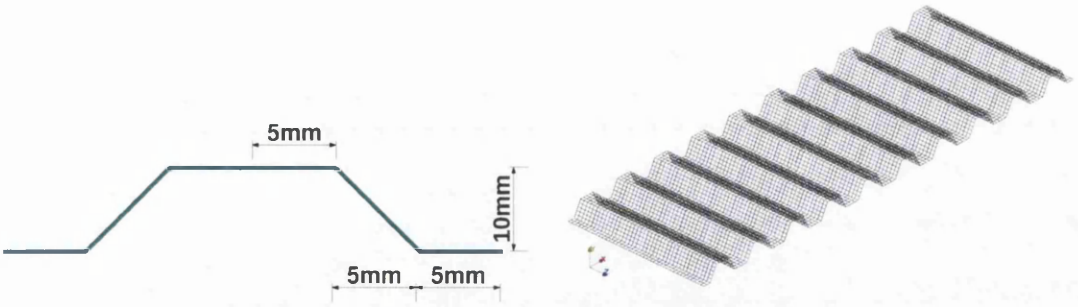

(a) Sketch of one corrugated unit (b) Meshed corrugated panel

Figure 3.2: Model of the corrugated panel employed in the analysis. (a) Unit cell; (b) Finite element model of the corrugated panel. The dimensions are: 300 mm in length, 75 mm in width, and 10 mm in height.

We consider the problem of structural vibration of a corrugated panel with random parameters. Corrugated panels are prone to geometric uncertainties (due to manufacturing) or material uncertainties, such as a random bending stiffness. We choose this last example to demonstrate the effectiveness of the hybrid spectral and metamodeling approach proposed. We analyze a composite corrugated panel similar to the one presented in [Dayyani *et al.*, 2012]. Figure 3.2(a) shows a sketch of the unit cell with the corresponding geometry. Figure 3.2(b) shows the meshed geometry of the corrugated panel that has been employed in the analysis. The panel's Young's modulus is taken as 16 GPa and its Poisson's ratio as 0.225. We applied the proposed computational approach to the corrugated panel, modeling it to be simply-supported at the ends (pinned at one end and a roller at the other). We have applied proportional Rayleigh damping for the present analysis. The frequency range of interest of the problem is $0-300$Hz. As mentioned above, we assumed the elastic parameters such as the bending stiffness and the axial stiffness of the plate to be random. We model these parameters as the stationary Gaussian random field

$$\alpha(\mathbf{r}, \xi(\theta)) = \alpha_0(1 + \epsilon(\mathbf{r}, \xi(\theta)) \tag{3.14}$$

where α is the random parameter of the corrugated panel, $\mathbf{r}$ is the length along the physical dimensions of the corrugated panel and $\epsilon(\mathbf{r}, \xi(\theta))$ is a zero mean stationary Gaussian random field. It might be mentioned that the Gaussian random field model, strictly speaking, might not be always physically meaningful since the elastic parameters being modeled are positive. However, if the number of KL expansion terms is chosen carefully then it is possible to show that the truncated statistical models are strictly positive [Powell and Elman, 2009]. We have chosen the baseline isotropic Young's modulus to be 16 GPa. The autocorrelation function of this random field has been assumed to be exponential. Thus if $\mathbf{r}_1 \neq \mathbf{r}_2$ then

$$C_\epsilon(\mathbf{r}_1, \mathbf{r}_2) = \sigma_\epsilon \exp\{-(|\mathbf{r}_1 - \mathbf{r}_2|)/\mu_\mathbf{r}\} \tag{3.15}$$

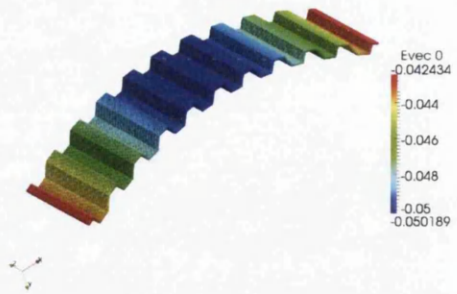

(a) 1^{st} KL eigenvector

(b) 3^{rd} KL eigenvector

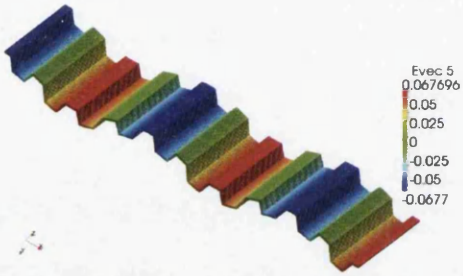

(c) 6^{th} KL eigenvector

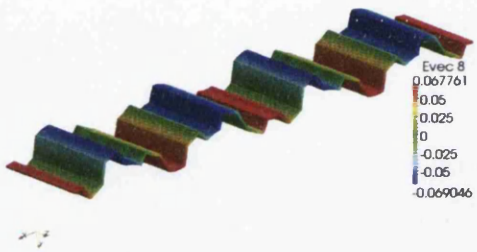

(d) 9^{th} KL eigenvector

Figure 3.3: Four different eigenvectors from the KL expansion of the random elastic parameter for the exponential covariance kernel with a correlation length of $L/2$, where L is the dimension of the physical domain. The eigenfunctions have been plotted as the out-of-plane displacements of the panel to graphically highlight their nature.

where $\mu_{\mathbf{r}}$ is the correlation length defined along the physical dimensions of the panel and σ_ϵ is the standard deviation associated with the random elastic parameters. For the finite element

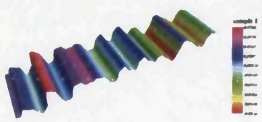

(a) Sample 1

(b) Sample 2

(c) Sample 3

(d) Sample 4

(e) Sample 5

(f) Sample 6

(g) Sample 7

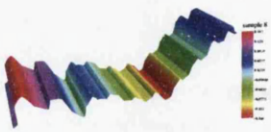

(h) Sample 8

Figure 3.4: Samples of the random elastic parameter plotted as the out-of-plane displacement of the corrugated panel to graphically highlight their nature. The correlation length has been chosen as $L/2$, where L is the dimension of the physical domain. The input standard deviation of the random field is 0.1

model, the panel has been modeled with plate elements allowing uniaxial bending deformation and in-plane stretching deformation. The corrugated panel has been meshed with a uniform mesh defined by a mesh parameter size of $h = 0.98$ mm. The correlation length

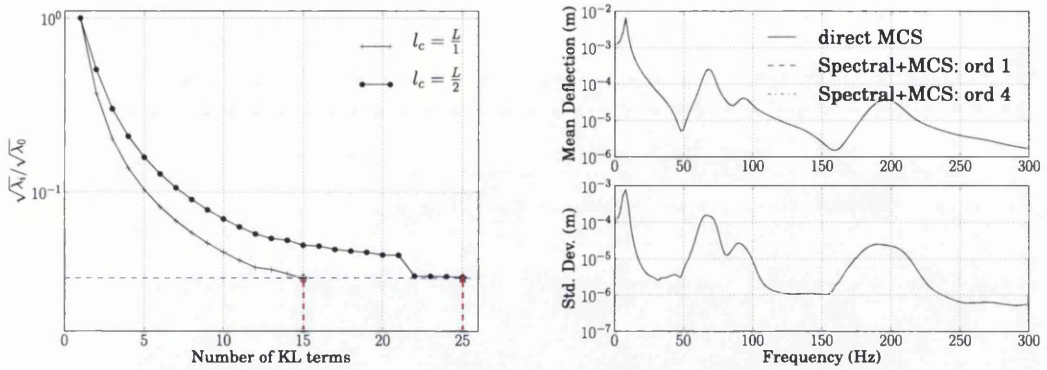

(a) The eigenvalue spectrum of the Covariance kernel

(b) The mean and standard deviation of the FRF of the plate

Figure 3.5: (a) The decay of the eigenvalue spectrum of the exponential covariance kernel of the corrugated plate for different correlation lengths defined as the L2 norm. (b) The mean and standard deviation of the FRF of the centre node of the plate calculated with the different orders of the spectral function approach with 10,000 stochastic sample simulations.

used in the autocorrelation model in Eqn. (3.15) has been chosen as half of the principal geometric length of the panel. Figure 3.3 shows a few chosen eigenvectors associated with the KL expansion of the covariance kernel. Note that the random elastic parameters and the KL eigenmodes are scalar quantities over the spatial domain. In order to facilitate better graphical representation of these quantities, they have been plotted as out-of-plane (y-direction) displacements of the panel. It shows that the higher modes are more complicated in shape which is similar to the behavior of higher structural vibrational modes. However, it must be noted that these KL modes are not the same as the vibrational modes of the structural finite element system.

Figure 3.4 presents the sample realization of the random field constructed with a finite dimensional expansion (25 terms in this case) of the covariance function with a set of independent identically distributed (iid) Gaussian random variables. The random variables have been sampled using a Latin-hypercube design from the input stochastic space of 25 random variables. The standard deviation of the random field is taken to be 0.1.

In order to decide the number of terms in the KL expansion, the eigenspectrum associated with the exponential covariance function is shown in Fig. 3.5(a) for two different correlation lengths $L/1$ and $L/2$ where L is the dimension of the physical domain of the problem. It is seen that the eigenvalues decay more rapidly for the larger correlation lengths indicating that fewer number of KL modes can capture most of the variability of the exponential kernel. For the stochastic vibration response analysis in the remainder of this work, we have chosen the correlation length to be $L/2$ and hence approximated the random field with the most dominant 25 modes of the expansion. This sets the dimension of the input stochastic space and 25 iid random variables were used to represent the discretized random elastic parameters

in the spatial domain. The standard deviation of the random field was assumed to be $\sigma_\epsilon = 0.1$.

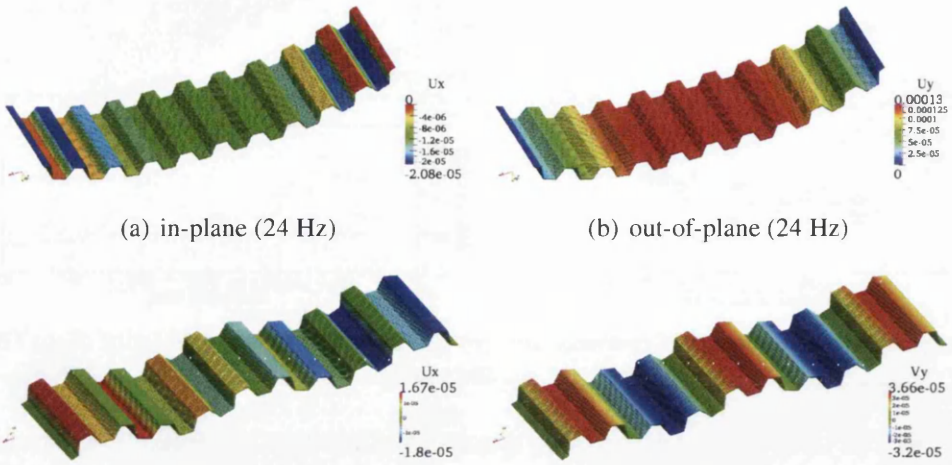

(a) in-plane (24 Hz)

(b) out-of-plane (24 Hz)

(c) in-plane (200 Hz)

(d) out-of-plane (200 Hz)

Figure 3.6: Mean deformation shape of the randomly parametrized corrugated panel at 24 Hz and 200 Hz. The colormap of the individual displacement components have been plotted on the deformed panel at that frequency.

Figure 3.5(b) shows the typical mean and standard deviation of the frequency response function of the center node of the corrugated panel subjected to unit amplitude harmonic out-of-plane force along the centerline of the plate over a frequency range of 0-300 Hz in steps of 2 Hz. The forcing vector is taken to be deterministic in nature. The plot presents a comparison of the second order statistics of the stochastic panel response calculated using the different orders (1 and 4) of spectral functions and with the direct MCS. A good agreement has been obtained. These response statistics have been obtained with a large sample size (10,000) and hence is computationally demanding. This cost would increase further if more accurate approximations of the solution are sought, and thus higher order spectral functions are considered. To alleviate the additional computational burden, we use a much smaller sample size and treat them as training runs upon which an emulator of the response is built.

Figure 3.6 gives the mean deformation shape of the corrugated panel at two different frequencies (24 Hz and 200 Hz) and plots the colormap of the individual displacement components on the deformed shape. The high frequency deformation shape shows the effect of increased contribution of the higher order structural modes in the response.

A rigorous convergence behavior of the response calculated with increasing order of spectral functions is demonstrated in Fig. 3.7 which shows the $L2$-relative error norm curves at different values of frequency. The L^2 relative error $\epsilon_{\boldsymbol{\mu}}^{(m)}(\omega)$ is defined at each frequency step ω for m^{th} order spectral functions as

$$\epsilon_{\boldsymbol{\mu}}^{(m)}(\omega) = \frac{\left\| \boldsymbol{\mu}_{SF}^{(m)}(\omega) - \boldsymbol{\mu}_{MCS}(\omega) \right\|_{L^2(\mathscr{D})}}{\left\| \boldsymbol{\mu}_{MCS}(\omega) \right\|_{L^2(\mathscr{D})}} \tag{3.16}$$

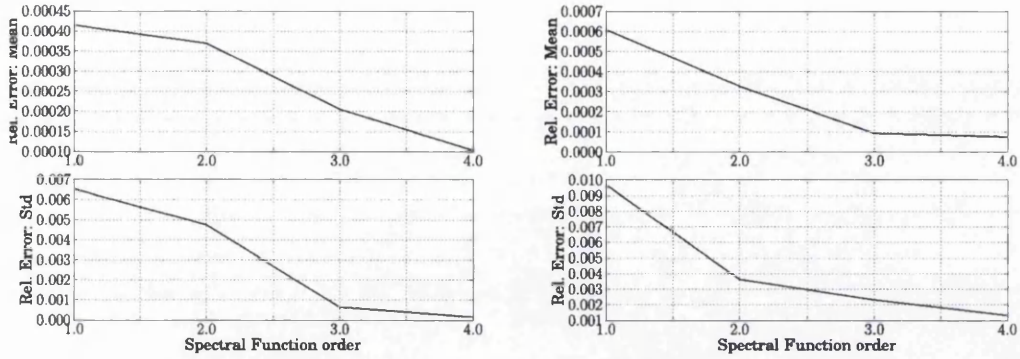

(a) Error at 98Hz

(b) Error at 138Hz

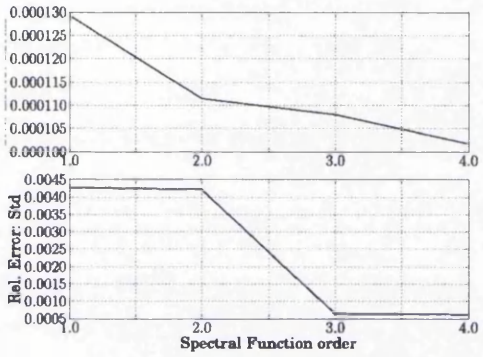

(c) Error at 214Hz

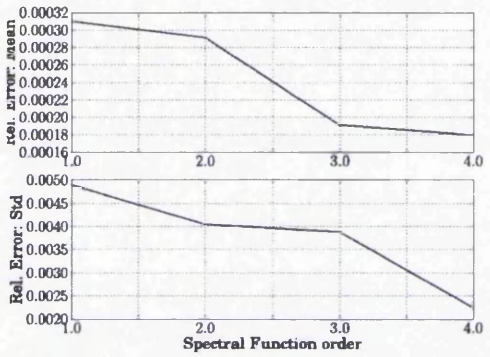

(d) Error at 272Hz

Figure 3.7: Convergence trend of the relative error defined with respect to the direct MCS calculations with increasing order of spectral functions at different frequency values.

where $\boldsymbol{\mu}_{SF}^{(m)}(\omega)$ denotes the mean or the standard deviation of the response vector obtained with the spectral weighting functions of order m and $\boldsymbol{\mu}_{MCS}(\omega)$ is the mean or standard deviation of the response vector calculated with direct MCS. We have studied the cases for which $m = 1, \ldots, 4$. Each of Fig. 3.7(a)–3.7(d) shows two sub-figures, top and bottom, which gives, respectively, the relative error for the calculated mean and standard deviation with the spectral function approach with respect to the direct MCS. It is observed that the solution computed with the higher order spectral function approach provides a better approximation of the direct MCS solution. However, the choice of the spectral function order is constrained by the consideration of the computational cost associated with it.

3.4.2 Metamodeling

As shown in Fig. 3.7, the higher the order of the spectral functions, the lower the relative error with respect to direct MCS. This, however, compromises the advantages of the spectral approach due to an increase in computational effort dictated by Eqn. (2.32) and as per the discussion presented in Sec. 2.3. In order to mitigate this increase in computation, we avoid

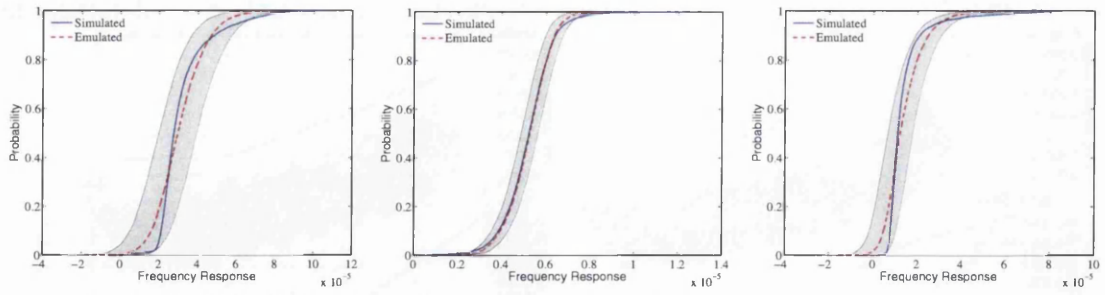

(a) Empirical cdf at 98Hz (b) Empirical cdf at 138Hz (c) Empirical cdf at 214Hz

Figure 3.8: Comparison between emulated and simulated cdfs for different frequency levels. 95% credible intervals (shaded areas) are shown for the cdfs.

running a complete MCS analysis and approximate the response $\widetilde{\mathbf{u}}(\theta, \omega)$ with the Bayesian metamodel introduced in Sec. 3.2. Given our choice of correlation length, we follow the suggestion in [Loeppky *et al.*, 2009] and generate a set of 250 training runs (corresponding to the 25 random variables in the KL expansion). In terms of Algorithm 1, for every frequency level ω, a sample of design points $\left\{\boldsymbol{\xi}^{(1)}, \ldots, \boldsymbol{\xi}^{(250)}\right\}$ is generated using a space-filling strategy, such as a Latin hypercube. Each design point is drawn from the input distribution $\mathcal{F}(\boldsymbol{\xi})$, a multivariate standard normal random variable in a 25-dimensional space. The design points are evaluated and the corresponding system response is reconstructed. The resulting training runs for each frequency level are of the form $\left(\boldsymbol{\xi}^{(i)}, \widetilde{\mathbf{u}}(\boldsymbol{\xi}^{(i)}, \omega)\right)$ for $i = 1, \ldots, 250$. Once the training runs are generated, they are passed to Algorithm 2, where the posterior mean and covariance are computed, and thus the posterior distribution in Eqn. (3.8) can be specified. As mentioned before, the posterior mean can be used as an approximation to the simulator's output. Figure 3.8 exemplifies the accuracy of such an approximation for some fixed frequency levels. In particular, it shows a comparison between the cumulative distribution functions (cdfs) generated with 10,000 Monte Carlo simulations and the cdfs obtained by emulation based on 250 training runs. The 95% credible intervals for emulated cdfs are also displayed. The advantages of Bayesian emulation become apparent: while every MCS run is independent, Bayesian emulation takes advantage of the information that each design point contains about the nearest design points. This information is contained in the covariance structure in Eqn. (3.2). It should be mentioned that the approximation of the cdf is not very accurate especially near the tails in Figs. 3.8(a) and 3.8(c) which corresponds to two resonance frequencies (as can be verified from Fig. 3.5(b)). While this approximates the second order response statistics at these frequencies with satisfactory accuracy (as seen later in Fig. 3.10) the prediction of higher order moments would be inaccurate. This indicates the lack of knowledge due to the limited number of training data and more data is needed to improve this approximation.

Once the posterior distribution has been computed using Algorithm 2, any statistical summary of the output distribution can be estimated by Algorithm 3. A large sample is drawn

from the input distributiion $\mathcal{F}(\boldsymbol{\xi})$ and samples generated from the posterior distribution are used to estimate the summary. The process is illustrated in Fig. 3.9, where samples of increasing size are drawn from the posterior distribution in order to estimate the mean of the output distribution. The prediction is contrasted with 10,000 Monte Carlo samples. It can be seen how the variance of the sample mean estimated via Bayesian emulation is reduced. Note however that this variance will always be greater than the Monte Carlo variance, since the emulator is built upon a finite number of training runs, and there will always be a lack of information due to this smaller set of simulator evaluations. It is therefore important to understand that our uncertainty about the mean is not due to Monte Carlo error, but due to lack of information due to the computational cost of the simulator.

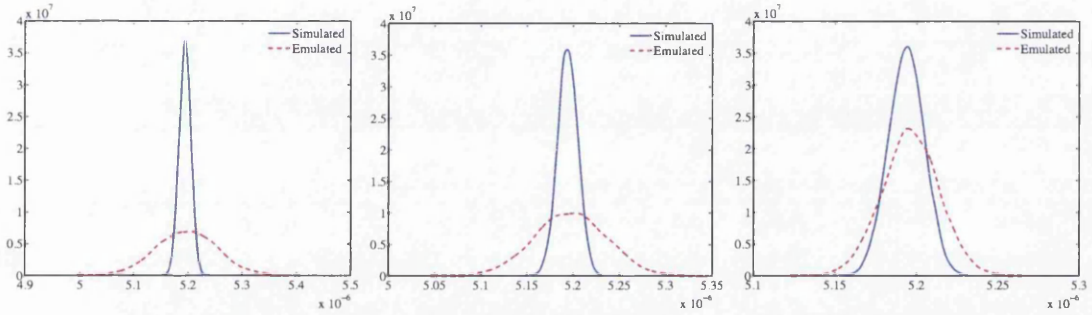

(a) $N = 1000$ (b) $N = 5000$ (c) $N = 10000$

Figure 3.9: Simulated vs emulated mean of the sample distribution. As the number of random functions generated with Algorithm 3 increases, the variance of the sample mean decreases. This means that uncertainty about the sample mean results from the lack of information due to the computational cost of the original simulator.

The analysis described above was repeated across the entire frequency range of 0-300Hz. For every frequency level ω, the Bayesian uncertainty analysis was performed and statistics of the FRF were obtained. Figure 3.10 shows the emulated mean and standard deviation of the FRF.

3.5 Summary

The hybridization of the spectral function approach with the Gaussian process emulation has been studied in this chapter. The stochastic system response has been evaluated with a hybrid spectral and metamodeling approach which provides a computationally efficient scheme of the evaluation of the probability distributions of the response variables. In the first step, the system response is resolved at random points in the stochastic input space using the spectral function approach which relies on projection of the solution onto a reduced space of structural modes of the vibrating system and a set of stochastic spectral weighting functions. Then the evaluated response at these random samples provide training runs which are used by a

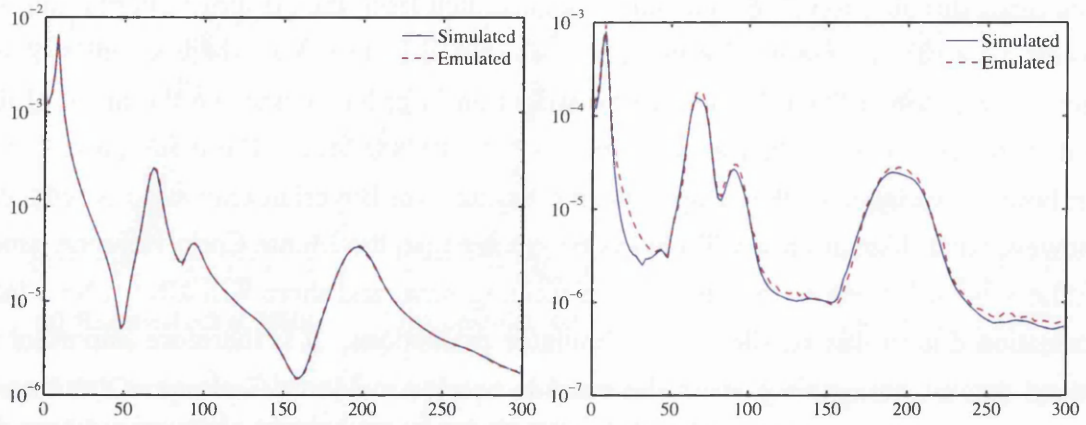

(a) Mean FRF (b) SD of the FRF

Figure 3.10: Emulation and simulation of the mean frequency response (a) and standard deviation of the frequency response (b). The simulation was performed for every frequency level in the input domain, based on 10,000 samples. Only 250 samples were necessary to emulate the statistics of the frequency response at a comparable accuracy.

Bayesian metamodel, which emulates the system response in order to estimate the uncertainty distribution and derive response statistics across the frequency range. The principal contributions of the work presented here can be summarized as follows:

- The spectral functions hybridized with a Bayesian metamodeling scheme gives a more efficient solution algorithm compared to the crude Monte Carlo simulation.
- A Bayesian emulator has be used to reduce the cost associated with an increasing order of spectral functions which produces a better approximation of the solution. Samples drawn from the posterior distribution has been used to perform uncertainty analysis of the response.
- A corrugated panel with random elastic parameters has been analyzed with the proposed approach. This might contribute to the understanding of the dynamic behavior of this type of structure and their use in future applications of morphing aircraft.
- The second order statistics of the frequency response functions obtained with the hybrid spectral function and metamodeling approach is in good agreement with the direct MCS solutions even near the resonance frequencies.

These results demonstrate the applicability and computational efficacy attained with the hybrid spectral function approach in conjunction with the Bayesian emulation and has been demonstrated with numerical examples. This approach is found to be especially suitable when higher order spectral functions are used to approximate the stochastic response quantities.

Until here, we have dealt with approximating the frequency domain response of the stochastic structural dynamic systems using reduced order uncertainty propagation methods.

In the following chapter we extend the concept of the spectral functions to study the transient response of stochastic structural dynamic systems under impulse loading. The time domain response of this structural system has also been compared to the polynomial chaos approach used in conjunction with an implicit time integration technique.

Chapter 4

Transient response of stochastic structural dynamic systems

4.1 Introduction

The previous chapters were devoted to the frequency response of randomly parametrized structural dynamic systems under the action of harmonic external loads. In the present chapter we concentrate on obtaining the transient or unsteady response of such randomly parametrized systems. The concept of stochastic spectral functions developed in the previous chapters is extended to the case of resolution of transient response of stochastic structural dynamic systems under the action of time varying forcing function. The solution is approximated in a stochastic subspace using *spectral functions* of different orders which are highly non-linear functions of the input random variables. The statistical properties of the response quantities changes with time and we investigate the time evolution of this uncertainty propagation with different solution techniques considered herein. The objective here is to tackle the problem of the growing dimensionality of the classical spectral Galerkin approach for long time integration with an alternative formulation of the *spectral function* approach.

The time integration required for the resolution of the transient stochastic response has been performed with the unconditionally stable single-step implicit Newmark scheme using a stochastic integration operator. A semi-statistical hybrid analytical and simulation based computational approach has been utilized to obtain the moments and probability density functions of the solution. The simulations have been performed for different degrees of variability of the input randomness and different dimensions of the input stochastic space and compared with the direct Monte Carlo simulations for accuracy and computational efficiency.

We begin by considering a damped structural dynamic system with stochastic parameters, defined on domain $\mathscr{D}$, subjected to an externally applied force excitation p varying with time t. The force equilibrium condition gives the following stochastic partial differential equation

(SPDE)

$$\rho\frac{\partial^2 u}{\partial t^2} + \mathfrak{L}_\eta\frac{\partial u}{\partial t} + div(\sigma_\alpha(u)) = p \quad \text{on } \mathscr{D}. \tag{4.1}$$

with the associated Dirichlet boundary condition

$$u = 0; \quad \text{on } \partial\mathscr{D}. \tag{4.2}$$

where $\sigma_\alpha(u)$ is the stress related to the displacement field $u = \{u : u(\mathbf{r}, t; \theta) \in \mathscr{D} \times T \times \Theta\}$, ρ is the mass density, and p is the external volume force density varying with time $t \in T \to \mathbb{R}$. $\mathfrak{L}_\eta$ is the damping operator, with η as the damping parameter, and it can be used to represent different damping models such as the strain rate dependent viscous damping or the velocity dependent viscous damping. Also $\mathscr{D} \in \mathbb{R}^d$ is a bounded domain with piecewise Lipschitz boundary $\partial\mathscr{D}$, where $d \leq 3$ is the spatial dimension and $T \in \mathbb{R}^+$ is the time. $(\Theta, \mathscr{F}, P)$ is the probability space where $\theta \in \Theta$ is a sample point from the sampling space Θ, $\mathscr{F}$ is the associated Borel σ-algebra and P is the image probability measure. The constitutive equations relating the stress field to the displacement u is given as

$$\sigma_\alpha(u) = \alpha(\mathbf{r}, \theta) : \varepsilon(u)$$

where α is the Hooke's elasticity tensor and is a second order, stationary, square integrable random field such that $\alpha : \mathbb{R}^d \times \Theta \to \mathbb{R}$. Depending on the physical problem the random field $\alpha(\mathbf{r}, \theta)$ can be used to model different physical systems. Here p denotes the time dependent deterministic excitation field for which the solution u is sought in the time domain.

This chapter is organized as follows: The next section gives the details of the FE treatment of the SPDE in time domain with a brief description of the stochastic system matrices. Following this the details of the solution techniques of the discretized stochastic FE system using the spectral function method in the stochastic subspace is given. In the section following it the numerical implementation of the proposed solution technique for the case of a cantilever Euler-Bernoulli beam under an impulse load is discussed. This section includes a comparison of the time domain response of the beam using different solution techniques such as the direct MCS, the proposed spectral function approach and the 4^{th} order polynomial chaos (PC) approach, which demonstrates the accuracy and computational efficacy of the proposed methodology. A detailed discussion of *a-posteriori* error analysis and the behavior of the autocorrelation function has also been included. Section 4.5 lists the significant conclusions which can be reached from this study.

4.2 Brief overview of SFEM for transient structural dynamic systems

The parametric uncertainty is modeled as a random field based on the input probability distribution function and a covariance function describing the variation of the random field in the spatial domain. A truncated representation of the random field in a finite dimensional stochastic space is utilized in the mathematical models. The random field is modeled with a finite number of random variables along the dominant spectral components of the covariance function as given in Sec. 2.2.1. We briefly recount that the random parameter $a(\mathbf{r},\theta) : \mathscr{D} \times \Theta$ in the truncated spectral representation takes the form of

$$a(\mathbf{r},\theta) = a_0(\mathbf{r}) + \sum_{i=1}^{m} \sqrt{\nu_i}\xi_i(\theta)\varphi_i(\mathbf{r}), \tag{4.3}$$

where $a_0(\mathbf{r}) = \mathbb{E}\left[a(\mathbf{r},\theta)\right]$ is the mean of the stochastic parameter and $\xi_i(\theta)$ are mutually uncorrelated random variables with zero mean ($\mathbb{E}\left[\xi_i(\theta)\right] = 0$) and unit variance ($\mathbb{E}\left[\xi_i(\theta)^2\right] = 1$). In addition, ν_i and $\varphi_i(\mathbf{r})$ are eigenvalues and eigenfunctions satisfying the integral equation in (2.6). For Gaussian random fields, the $\xi_i(\theta)$ are uncorrelated Gaussian random variables by virtue of the property of Gaussian variables.

Alternatively, when $a(\mathbf{r},\theta)$ is a non-Gaussian random field, it can be expressed in a mean-square convergent series using the Wiener-Askey chaos expansion scheme [Xiu and Karniadakis, 2002, 2003b]. The formulation presented here is applicable to this kind of general decomposition of the random field. For the numerical implementation of the above method, the probabilistic content of the problem is represented using a finite set of random variables $\boldsymbol{\xi} = (\xi_1, \xi_2, \ldots, \xi_m) : \Theta \to \mathbb{R}^m$. Thus the stochastic problem can be equivalently formulated on the finite dimensional probability space $\left(\Theta^{(m)}, \mathscr{F}^{(m)}, P^{(m)}\right)$ where $\Theta^{(m)} = \text{Range}(\boldsymbol{\xi})$ is a subset of $\mathbb{R}^m$, $\mathscr{F}^{(m)}$ is the associated Borel σ-algebra and $P^{(m)}$ is the image probability measure.

4.2.1 Finite elements for the transient response of uncertain structures

The FE treatment of the governing SPDE involves spatial discretization of the continuum $\mathscr{D} \in \mathbb{R}^d$ into domains with polygonal boundaries $\mathscr{D}^h$ where h is the mesh space parameter. Also, it's known from the Doob-Dynkin lemma [Bobrowski, 2005] that for the parametrized equation in Eqn. (4.1) where the input randomness is expressed in terms of a finite dimensional vector $\boldsymbol{\xi}(\theta)$ (as in (4.3)), the solution can be expressed entirely in terms of the same random variables. Thus the solution of the discretized FE system lies in the Hilbert space $\mathscr{H}(\mathscr{D}^h \times T \times \Theta)$. This space can be expressed in a separable form with the Hilbert spaces $\mathscr{H}_1$ and $\mathscr{H}_2$ such that $\mathscr{H} \simeq \mathscr{H}_1 \otimes \mathscr{H}_2$. Now, $\mathscr{H}_1$ and $\mathscr{H}_2$ can be chosen to have different

forms and the solution separable spaces vary accordingly. We take the FE shape functions to lie in $L^2(\mathscr{D}^h)$ space. Strictly speaking, the space of these ansatz functions are governed by the continuity requirement of the field over the element domain; for e.g. if symmetric bilinear forms are obtained from applying the variational principle to elliptic differential operators of order $2k$ (and with Dirichlet boundary conditions), then these trial functions lie in the Hilbert space $H_0^k \subset L^2(\mathscr{D}^h)$ and are C^k-continuous within the element domain. The principle of virtual work is utilized to arrive at the discretized set of linear algebraic equations from Eqn. (4.1). For the virtual displacements, we choose a set of stochastic kinematically admissible displacement functions $v(\cdot;\theta)$ satisfying the boundary condition $v(\cdot;\theta)|_{\partial\mathscr{D}} = 0$ and which have finite strain energy on the spatial domain lying in $E(\mathscr{D}) \subset L^2(\mathscr{D})$. Thus, denoting the set of all such functions by $\overset{o}{E}(\mathscr{D})$ we have

$$\overset{o}{E}(\mathscr{D}) = \{v(\cdot;\theta) : v(\cdot;\theta) \in E(\mathscr{D}), \quad \text{and} \quad v(\cdot;\theta)|_{\partial\mathscr{D}} = 0\}. \tag{4.4}$$

Thus, from the principle of virtual work

$$\int_{\mathscr{D}} v : \left\{ \rho \frac{\partial^2 u}{\partial t^2} + \mathfrak{L}_\eta \frac{\partial u}{\partial t} + div(\sigma_a(u)) \right\} d\mathbf{r} \qquad \forall v \in \overset{o}{E}(\mathscr{D}). \tag{4.5}$$

We apply the Green-Gauss theorem to the above equation and noting that the initial strain and that the boundary integral terms are set to zero we can define the bilinear form $\mathscr{B}(u, v; \theta)$ and the linear form $\mathscr{F}(v, \theta)$ such that

$$\mathscr{B}(u, v; \theta) \overset{\text{def}}{=} \int_{\mathscr{D}} \varepsilon(v) : a(\mathbf{r}, \theta) : \varepsilon(u) d\mathbf{r} + \int_{\mathscr{D}} \rho(\mathbf{r}, \theta) v \cdot \frac{\partial^2 u}{\partial t^2} d\mathbf{r} + \int_{\mathscr{D}} v \cdot \mathfrak{L}_{\eta(\mathbf{r},\theta)} \frac{\partial u}{\partial t} d\mathbf{r} \tag{4.6}$$

$$\mathscr{L}(v; \theta) \overset{\text{def}}{=} \int_{\mathscr{D}} v \cdot p \, d\mathbf{r} \tag{4.7}$$

The FE approximation of the admissible function space $\overset{o}{E}(\mathscr{D})$ can be written as $\overset{o}{E}(\mathscr{D})_n \subset \overset{o}{E}(\mathscr{D})$ such that $u^n = \sum_i^n \psi(\mathbf{r}) u_i(t;\theta)$, $u_i \in \mathbb{R}$. Hence using this discrete form of $u^n \in \overset{o}{E}(\mathscr{D})_n$ in Eqns. (4.6) and (4.7) we have

$$\mathscr{B}(u^n, v^n; \theta) = \mathscr{L}(v^n; \theta) \quad \forall \; v^n \in \overset{o}{E}(\mathscr{D})_n. \tag{4.8}$$

Denoting the nodal components of the displacement field as $\mathbf{u}(t;\theta) = [u_1(t;\theta), \ldots, u_n(t;\theta)]^T \in \mathbb{R}^n$, we have the FE system of equations from Eqn. (4.8) as

$$\mathbf{v}^T \left(\sum_{i=0}^{2} \mathbf{A}_i(\theta) \mathbf{u}_{,i}(t;\theta) \right) = \mathbf{v}^T \mathbf{p}(t), \quad \forall \mathbf{v} \in \mathbb{R}^n \tag{4.9}$$

where the $\mathbf{A}_i(\theta)$ denote the system matrices (stiffness, damping, mass for i=0,1,2 respectively) and $\mathbf{u}_{,i}(t;\theta)$ denote the i^{th} time derivative of the displacement field. The system matrices inherit the randomness of the input stochastic parameters and hence the stochastic linear system for structural dynamics takes the form of

$$\mathbf{M}(\theta)\ddot{\mathbf{u}}(t;\theta) + \mathbf{C}(\theta)\dot{\mathbf{u}}(t;\theta) + \mathbf{K}(\theta)\mathbf{u}(t;\theta) = \mathbf{p}(t) \tag{4.10}$$

where $\mathbf{M}(\theta)$, $\mathbf{C}(\theta)$ and $\mathbf{K}(\theta)$ are the random mass, damping and stiffness matrices respectively, $\mathbf{u}(t;\theta)$ and its dotted variants are the system response vector and its time derivatives respectively, and $\mathbf{p}(t)$ is the deterministic forcing vector. Following from the discretized spectral representation of the random field in Eqn. (4.3) and the bilinear form in Eqn. (4.6), the system matrices can be expanded in terms of the functions of the input random variables as

$$\mathbf{M}(\theta) = \mathbf{M}_0 + \sum_{i=1}^{p_1} \mu_i(\theta_i)\mathbf{M}_i \in \mathbb{R}^{n\times n} \quad \text{and} \quad \mathbf{K}(\theta) = \mathbf{K}_0 + \sum_{i=1}^{p_2} \nu_i(\theta_i)\mathbf{K}_i \in \mathbb{R}^{n\times n} \tag{4.11}$$

Here the mass and stiffness matrices have been expressed in terms of their deterministic components ($\mathbf{M}_0$ and $\mathbf{K}_0$) and the corresponding random contributions ($\mathbf{M}_i$ and $\mathbf{K}_i$) obtained from discretizing the mass and stiffness parameters with finite number of random variables ($\mu_i(\theta)$ and $\nu_i(\theta)$). The total number of random variables utilized to represent the stochastic system matrices is $M = p_1 + p_2$. For most cases the damping parameter is expressed as linear combination of the mass matrix and the system stiffness matrix which is the 'proportional damping model' and this has been adopted in the present work.

4.3 Solution technique

The solution of the stochastic system response $\ddot{\mathbf{u}}(t;\theta)$ in Eqn. (4.10) is sought in the space $L^2(\Theta; T \times \mathbb{R}^n)$, which is the space of real-valued square integrable functions defined on the probability space $(\Theta, \mathscr{F}, P)$. The nature and characteristics of this function space will be explored later in more detail in Sec. 4.3.2. A direct time integration scheme is introduced at first to transform the Eqn. (4.10) to a set of linear algebraic equations which is to be solved at each time step. The solution of this system can then be written to exist in $L^2(\Theta; \mathbb{R}^n \times t)$ where $t \in \mathbb{R}^+$ denotes the dependence of the FE solution vector on the time t.

4.3.1 Time integration technique

The time-domain response of the stochastic linear system in Eqn. (4.10) necessitates a time integration scheme. This is achieved using different time-stepping techniques which may be implicit or explicit in nature (based on how the response quantities depend on those obtained

at the previous steps). Here we employ an implicit direct integration operator and describe the solution methodology for the linear stochastic systems obtained with such an approach.

Let us introduce the direct integration operators $\bar{\mathbf{A}}_1$ and $\bar{\mathbf{A}}_0$ which depend on the system matrices but independent of the response quantities. The system equation can be generally written in terms of this operator as

$$\bar{\mathbf{A}}_1 \bar{\mathbf{u}}(t_{s+1}) = \bar{\mathbf{p}}(t_{s+1}) + \bar{\mathbf{A}}_0 \bar{\mathbf{u}}(t_s, t_{s-1}, \ldots) \tag{4.12}$$

where the integration operators transform the system response at the earlier time steps $t_s, t_{s-1}, \ldots$ to the response at t_{s+1}. The quantities $\bar{\mathbf{u}}(t_{s+1})$ and $\bar{\mathbf{u}}(t_s, t_{s-1}, \ldots)$ are defined as follows:

$$\begin{aligned} \bar{\mathbf{u}}(t_{s+1}) &= \langle \mathbf{u}(t_{s+1}); \dot{\mathbf{u}}(t_{s+1}); \ddot{\mathbf{u}}(t_{s+1}) \rangle \\ \bar{\mathbf{u}}(t_s, t_{s-1}, \ldots) &= \langle \{\mathbf{u}(t_s); \dot{\mathbf{u}}(t_s); \ddot{\mathbf{u}}(t_s)\}; \{\mathbf{u}(t_{s-1}); \dot{\mathbf{u}}(t_{s-1}); \ddot{\mathbf{u}}(t_{s-1})\}; \ldots \rangle \,. \end{aligned} \tag{4.13}$$

For single-step schemes, the response at t_{s+1} depends only on the previous time step t_s. When the operators $\bar{\mathbf{A}}_1$ and $\bar{\mathbf{A}}_0$ can be written in upper or lower triangular form (in the block sense), it becomes an explicit time-integration scheme. The stability and convergence behavior of the time-integration scheme is discussed later in this section.

For the case of stochastic linear systems, the system matrices inherit the parametric randomness and hence themselves are random in nature. This leads to the integration operators $\bar{\mathbf{A}}_1$ and $\bar{\mathbf{A}}_0$ in to being random in nature. The integration operators are linear combinations of the system matrices and hence can be expressed as the polynomial series of random variables as in Eqns. (4.8) and (4.9) such that the series expansion takes the form of $\bar{\mathbf{A}}_1(\theta) = \mathbb{E}\left[\bar{\mathbf{A}}_1(\theta)\right] + \sum_i \varphi_j(\chi_i)(\bar{\mathbf{A}}_1)_i$ where $(\bar{\mathbf{A}}_1)_i$ denotes the perturbation components of the integration operator associated with the random variables $\varphi_j(\chi_i)$ (see Eqn. (2.12)) which inherits the input randomness.

For the present case we have used the Newmark generalized acceleration operator [Bathe, 1996, Hahn, 1991] which gives an unconditionally stable time integration scheme. Other such methods include the Wilson Averaging operator and the Houbolt operator [Nickel, 1971], both of which offers unconditional stability. The integration operators for the stochastic dynamic case for the Newmark method are of the following form

$$\begin{bmatrix} a_0\mathbf{M}(\theta) + a_1\mathbf{C}(\theta) + \mathbf{K}(\theta) & 0 & 0 \\ 0 & 1 & -a_7 \\ -a_0 & 0 & 1 \end{bmatrix} \begin{Bmatrix} \mathbf{u}_{t+\Delta t} \\ \dot{\mathbf{u}}_{t+\Delta t} \\ \ddot{\mathbf{u}}_{t+\Delta t} \end{Bmatrix} = \begin{bmatrix} \mathbf{p}_{t+\Delta t} \\ 0 \\ 0 \end{bmatrix} + \begin{bmatrix} a_0\mathbf{M}(\theta) + a_1\mathbf{C}(\theta) & a_2\mathbf{M}(\theta) + a_4\mathbf{C}(\theta) & a_3\mathbf{M}(\theta) + a_5\mathbf{C}(\theta) \\ -a_0 & -a_2 & -a_3 \\ 0 & 1 & a_6 \end{bmatrix} \begin{Bmatrix} \mathbf{u}_t \\ \dot{\mathbf{u}}_t \\ \ddot{\mathbf{u}}_t \end{Bmatrix} \tag{4.14}$$

where the integration constants $a_i,\ i = 1, 2, \ldots, 7$ are given by

$$a_0 = \frac{1}{\alpha \Delta t^2}; \qquad a_1 = \frac{\gamma}{\alpha \Delta t}; \qquad a_2 = \frac{1}{\alpha \Delta t}; \qquad a_3 = \frac{1}{2\alpha} - 1; \tag{4.15}$$
$$a_4 = \frac{\gamma}{\alpha} - 1; \qquad a_5 = \frac{\Delta t}{2}\left(\frac{\gamma}{\alpha} - 2\right); \qquad a_6 = \Delta t(1-\gamma); \qquad a_7 = \gamma \Delta t$$

The parameters α and γ which has to be chosen is guided by the consideration of *unconditional stability* which is ensured using the following two criterion [Bathe, 1996]: $\gamma \geq 0.50$ and $\alpha \geq 0.25(0.5 + \gamma)^2$. While the implicit Newmark's method provide unconditional stability under the above mentioned criterion, it is conditionally convergent [Hahn, 1991]. The convergence is guided by the condition [Newmark, 1959]

$$\frac{\Delta t}{T} < \frac{1}{2\pi}\left(\frac{1}{\alpha}\right)^{1/2} \quad \text{for} \quad \alpha > 0 \tag{4.16}$$

where T is the natural time period of vibration of a single degree-of-freedom (d.o.f.) system. For multiple d.o.f. systems it is required that the T be interpreted as the time period of the highest vibration mode of the system. This results in the choice of time step to be guided by the dimension of the linear system being solved i.e. higher the dimension of the linear system, lower is the value of T (associated with the highest vibration mode) and hence smaller is the upper bound on the time step size Δt. This can have a huge adverse effect for the spectral Galerkin solution technique, since the dimension of the linear system increases exponentially with the order of the stochastic polynomials used in the solution basis. Thus the PC method would typically require a significantly lower value of the time step size Δt to produce the time integration results of identical numerical accuracy compared to other techniques such as direct MCS which deals with the dimension of the original discretized FE system.

We rewrite Eqn. (4.14) in a more compact form following Eqn. (4.12) as

$$\bar{\mathbf{A}}_1(\theta)\bar{\mathbf{u}}_{t+\Delta t}(\theta) = \bar{\mathbf{p}}_{t+\Delta t} + \bar{\mathbf{A}}_0(\theta)\bar{\mathbf{u}}_t(\theta) \tag{4.17}$$

where $\bar{\mathbf{u}}_{t+\Delta t} \in \mathbb{R}^N \times \Theta$ is the ensemble of the stochastic displacement, velocity and acceleration vector of dimension $N = 3n$ (n is the dimension of the discretized FE system), the integration operators $\bar{\mathbf{A}}_1(\theta) \in \mathbb{R}^{N\times N}$, $\bar{\mathbf{A}}_0(\theta) \in \mathbb{R}^{N\times N}$ are as defined in Eqn. (4.14). We utilize this form in the subsequent sections to formulate a solution methodology using the different solution methodologies associated with stochastic dynamical systems. Following from the Newmark operator given in Eqn. (4.14) we can represent the equation for the displacement field in Eqn. (4.10) to be solved at each time step as

$$\left[a_0\mathbf{M}(\theta) + a_1\mathbf{C}(\theta) + \mathbf{K}(\theta)\right]\mathbf{u}_{t+\Delta t}(\theta) = \mathbf{p}^{eqv}_{t+\Delta t}(\theta) \tag{4.18}$$

where $\mathbf{p}^{eqv}_{t+\Delta t}(\theta)$ is the equivalent force at time $t + \Delta t$ which consists of contributions of the

system response (displacement, velocity and acceleration fields) at the previous time step. The 'equivalent force' at each time step hence becomes a stochastic quantity due to the presence of the stochastic system matrices on the right hand side and also the system response at previous time steps which themselves are random quantities.

Following from the discussion of the expansion of the system matrices in Eqn. (4.10) in terms of their mean and perturbation components, and expressing the structural damping in proportional form, $\mathbf{C}(\theta) = \zeta_1\mathbf{M}(\theta) + \zeta_2\mathbf{K}(\theta)$, we define the matrices $\mathbf{A}_0 \in \mathbb{R}^{n\times n}$ and $\mathbf{A}_i \in \mathbb{R}^{n\times n}; i = 1, 2, \ldots, M$ as

$$\mathbf{A}_0 = a_0\mathbf{M}_0 + a_1\mathbf{C}_0 + \mathbf{K}_0 = (a_0 + a_1\zeta_1)\mathbf{M}_0 + (a_1\zeta_2 + 1)\mathbf{K}_0 \tag{4.19a}$$

$$\mathbf{A}_i = \begin{cases} (a_0 + a_1\zeta_1)\mathbf{M}_i & \text{for} \quad i = 1, 2, \ldots, p_1 \\ (1 + a_1\zeta_2)\mathbf{K}_{i-p_1} & \text{for} \quad i = p_1 + 1, p_1 + 2, \ldots, p_1 + p_2 \end{cases} \tag{4.19b}$$

Hence the linear structural system in Eqn. (4.18) can be expressed as

$$\underbrace{\left[\mathbf{A}_0 + \sum_{i=1}^{M} \xi_i(\theta)\mathbf{A}_i\right]}_{\mathbf{A}(\theta)} \mathbf{u}_{t+\Delta t}(\theta) = \mathbf{p}^{equ}_{t+\Delta t}(\boldsymbol{\xi}(\theta)). \tag{4.20}$$

Here $\mathbf{A}_0$ and $\mathbf{A}_i$ represent the deterministic and stochastic parts of the system matrices respectively. $\mathbf{A}_0$ and $\mathbf{A}_i \in \mathbb{R}^{n\times n}; i = 1, 2, \ldots, M$ are symmetric matrices, $\mathbf{u}_{t+\Delta t}(\theta) \in \mathbb{R}^n$ is the solution vector and $\mathbf{p}^{equ}_{t+\Delta t}(\boldsymbol{\xi}(\theta)) \in \mathbb{R}^n$ is the forcing vector which comprises of the deterministic forcing function at each time step plus the stochastic system response at earlier time steps. Hence they have a non-linear functional dependence on the random variables which have been used to model the parametric uncertainty. The number of terms M in Eqn. (4.20) can be selected based on the accuracy desired for the representation of the underlying random field. This is the specific form of the system matrices under the Newmark time stepping scheme. However, the general scheme of the solution technique remains the same for this class of implicit time-tepping techniques. The expressions for $\mathbf{A}_0$ and $\mathbf{A}_i$ vary according to the damping model chosen for a particular application. One of the main aims of stochastic dynamic analysis is to obtain $\mathbf{u}_{t+\Delta t}(\theta)$ for $\theta \in \Theta$ and for all time steps $t \in [0, T]$ in an efficient manner, which is the primary motivation for this work.

4.3.2 Overview of the spectral Galerkin approach for structural dynamics

Several methods have been utilized to resolve the time-domain response of stochastic systems. These include the direct MCS [Shinozuka, 1972], perturbation based stochastic FEM method [Wall and Bucher, 1987] and Neumann expansion method [Lei and Qiu, 2000], for exam-

ple. However, the spectral Galerkin methods have been studied with particular enthusiasm over the past two decades. Spectral Galerkin methods are used in conjunction with various time integration techniques to evaluate the time-domain response. The long time integration scheme has been used with Generalized Polynomial Chaos in [Gerritsma *et al.*, 2010] which shows a growth of error with time. Lucor et al. [Lucor *et al.*, 2004] implemented the temporal discretization of a single degree of freedom linear oscillator with the implicit Newmark method which shows that high polynomial degree is essential for accuracy of the computed results. Xiu et al considered the generalized chaos for transient response of FE thermal systems [Xiu and Karniadakis, 2003a] with random heat conductivity and capacity. However, the use of implicit time integration schemes for stochastic FE structural dynamic systems with Galerkin projection schemes remains a sparsely studied area of research. The novelty of the approach described here lies in the formulation of the stochastic time integration operator in conjunction with the spectral Galerkin approach and we present the linear algebraic system that results from the implementation.

Here we present the solution of the assembled system of stochastic linear algebraic equations as given Eqn. (4.17). From Eqn. (4.20) we can identify the appropriate function space in which the solution of the stochastic problem exists. The random matrices $\mathbf{A}_i \in \mathbb{R}^{n\times n}$ inherits the continuity and coercivity properties from the governing SPDE through the weak formulation. The forcing vector $\mathbf{p}^{eqv}_{t+\Delta t}$ depends on the system response at earlier time steps, which in turn can be assumed to be continuous. The spatially discretized solution vector $\mathbf{u}_{t+\Delta t}$, at each time step, lies in the tensor product space $\mathbb{R}^n \otimes \Upsilon$, where Υ is the space of real-valued random variables. Given that the stochastic system has been discretized and represented with a finite number of random variables $\boldsymbol{\xi}(\theta) = \{\xi_1, \ldots, \xi_M\}$ (as for instance in Eqn. (4.20)), the stochastic subspace reduces to Υ_M where $\Upsilon_M \subset \Upsilon$. When each random component ξ_i is independent, then Υ_M is a tensor product space $\Upsilon^{(1)} \otimes \Upsilon^{(2)} \otimes \ldots \otimes \Upsilon^{(M)}$. According to the approximate basis building techniques that focus on expansion of the solution vector using some polynomial functions, the solution vector can be expressed in the form

$$\mathbf{u}_t = \sum_{a\in\mathscr{J}_M} \mathscr{H}_\alpha(\boldsymbol{\xi}(\theta))\tilde{\mathbf{u}}_{t,\alpha}; \quad \tilde{\mathbf{u}}_{t,\alpha} \in \mathbb{R}^n, \tag{4.21}$$

where $\mathscr{H}_\alpha(\boldsymbol{\xi}(\theta))$ are the basis in Υ_M, $\tilde{\mathbf{u}}_{t,\alpha}$ are the set of unknown coefficients to be evaluated and $\mathscr{J}_M$ is a subset of $\mathscr{J}$ with cardinal M. The form of the polynomial functions $\mathscr{H}_\alpha(\boldsymbol{\xi}(\theta))$ used in Eqn. (4.21) varies according to the chosen solution approach, and the well-known spectral approaches such as PC, gPC use orthogonal polynomial basis from the Wiener-Askey scheme. When $\boldsymbol{\xi}(\theta)$ is a vector of independent identically distributed Gaussian random variables, the functions $\mathscr{H}_\alpha$ are finite order Hermite polynomials which are orthonormal with respect to the joint probability density function of the input vector $\boldsymbol{\xi}(\theta)$. The same idea can be extended to non-Gaussian random variables, provided more generalized functional bases

are used so that the orthonormality with respect to the probability density functions can be retained. Suppose the series in Eqn. (4.21) is truncated after P terms. The value of P depends on the number of basic random variables M and the desired order of the PC expansion. Hence there are P number of unknown vectors of dimension n. The successive time derivatives of the displacement field can be expressed as

$$\frac{\partial^i \mathbf{u}_t}{\partial t^i} = \sum_{a \in \mathscr{I}_M} \mathscr{H}_\alpha(\boldsymbol{\xi}(\theta)) \frac{\partial^i \widetilde{\mathbf{u}}_{t,\alpha}}{\partial t^i} \quad i = 1, 2 \tag{4.22}$$

such that the same stochastic basis is used to formulate the time derivatives of the response at all time steps. We introduce the inner product in $\Upsilon_M \times \mathbb{R}^N$ (where N is the dimension of is the dimension of the ensemble of the displacement, velocity and acceleration vector in Eqn. (4.17)) as

$$\langle \mathbf{v}, \mathbf{u} \rangle \stackrel{\text{def}}{=} \int_\Theta \mathbf{v}^T(\boldsymbol{\xi}(\theta)) \mathbf{u}(\boldsymbol{\xi}(\theta))\, dP_\xi = \mathbb{E}\left[\mathbf{v}^T(\boldsymbol{\xi}(\theta)) \mathbf{u}(\boldsymbol{\xi}(\theta))\right] \tag{4.23}$$

where $\mathbb{E}[\bullet]$ is the expectation operator. Thus the Galerkin formulation of Eqn. (4.17) for the single-step time integration scheme is

$$\left\langle \bar{\mathbf{v}}^T_{t+\Delta t}, \bar{\mathbf{A}}_1 \bar{\mathbf{u}}_{t+\Delta t} \right\rangle = \left\langle \bar{\mathbf{v}}^T_{t+\Delta t}, \bar{\mathbf{p}}_{t+\Delta t} \right\rangle + \left\langle \bar{\mathbf{v}}^T_{t+\Delta t}, \bar{\mathbf{A}}_0 \bar{\mathbf{u}}_t \right\rangle \quad \forall\, \bar{\mathbf{v}}_{t+\Delta t} \in \Upsilon_M \times \mathbb{R}^N \tag{4.24}$$

where the Galerkin projection is implemented at each time step $t + \Delta t$. The vector $\bar{\mathbf{u}}_t$ is as defined in Eqn. (4.13) which is of the form $\bar{\mathbf{u}}_t = \langle \mathbf{u}_t; \dot{\mathbf{u}}_t; \ddot{\mathbf{u}}_t \rangle$.

Following this, the mean-square error minimization is applied and the unknown vectors are solved from the resulting linear algebraic system. The linear system is given as

$$\begin{bmatrix} \bar{\mathbf{A}}_{1_{(0,0)}} & \bar{\mathbf{A}}_{1_{(0,1)}} & \cdots & \bar{\mathbf{A}}_{1_{(0,P)}} \\ \bar{\mathbf{A}}_{1_{(1,0)}} & \bar{\mathbf{A}}_{1_{(1,1)}} & & \bar{\mathbf{A}}_{1_{(1,P)}} \\ \vdots & & \ddots & \vdots \\ \bar{\mathbf{A}}_{1_{(P,0)}} & \bar{\mathbf{A}}_{1_{(P,1)}} & \cdots & \bar{\mathbf{A}}_{1_{(P,P)}} \end{bmatrix} \begin{bmatrix} \bar{\mathbf{u}}_{t+\Delta t,(1)} \\ \bar{\mathbf{u}}_{t+\Delta t,(2)} \\ \vdots \\ \bar{\mathbf{u}}_{t+\Delta t,(P)} \end{bmatrix} = \begin{bmatrix} \bar{\mathbf{p}}_{t+\Delta t,(1)} \\ \bar{\mathbf{p}}_{t+\Delta t,(2)} \\ \vdots \\ \bar{\mathbf{p}}_{t+\Delta t,(P)} \end{bmatrix} + \begin{bmatrix} \bar{\mathbf{A}}_{0_{(0,0)}} & \bar{\mathbf{A}}_{0_{(0,1)}} & \cdots & \bar{\mathbf{A}}_{0_{(0,P)}} \\ \bar{\mathbf{A}}_{0_{(1,0)}} & \bar{\mathbf{A}}_{0_{(1,1)}} & & \bar{\mathbf{A}}_{0_{(1,P)}} \\ \vdots & & \ddots & \vdots \\ \bar{\mathbf{A}}_{0_{(P,0)}} & \bar{\mathbf{A}}_{0_{(P,1)}} & \cdots & \bar{\mathbf{A}}_{0_{(P,P)}} \end{bmatrix} \begin{bmatrix} \bar{\mathbf{u}}_{t,(1)} \\ \bar{\mathbf{u}}_{t,(2)} \\ \vdots \\ \bar{\mathbf{u}}_{t,(P)} \end{bmatrix} \tag{4.25}$$

where $\bar{\mathbf{A}}_{1_{(i,j)}}$ is the $N \times N$ blocks coefficient matrix of the linear system of dimension $NP \times NP$ and $\bar{\mathbf{u}}_{t+\Delta t,(i)}$ and $\bar{\mathbf{u}}_{t,(i)}$ are the i^{th} components of the system response at time $t + \Delta t$ and t respectively. It must be noted that the coefficient matrices of the linear system in Eqn. (4.25) are block sparse matrices and symmetric in nature. This structure is conducive to the numerical Krylov based iterative techniques like the Bi-conjugate gradient stabilized

(BiCGStab) algorithm which has been employed in this work to solve the linear systems resulting from the spectral Galerkin method. It should be noted that the Krylov iterative techniques can exploit the multicore architecture of modern day computational platforms for performing the large matrix-vector operations. The performance improvement obtained with this technique is illustrated later in this work while comparing the computation cost of the different methods.

However, P increases exponentially with the order of chaos and the number of input random variables M, so the dimension NP of the linear system obtained from Eqn. (4.24) becomes very high. As a result several methods have been developed (see for example [Sachdeva *et al.*, 2006b, Blatman and Sudret, 2010]) to reduce the computational cost. In the PC based solution approach, the *only* information used to construct the basis is the probability density function of the random variables. In context of the discretized Eqn. (4.20), more information such as the matrices $\mathbf{A}_i, i = 0, 1, 2 \ldots M$ are available. Equation (4.21) also shows that the stochastic basis is independent of the time step and hence lacks any adaptive properties which would result in errors growing with the time. This becomes a significant problem for long time integration. This is because the non-linear effect of the input random variables on the stochastic system response is compounded with each time step. It may be possible to construct alternative stochastic basis using the invariant properties of the linear system and the time-step. Here we investigate such an approach, where the solution is projected on to a reduced eigenspace obtained from the underlying deterministic system, weighted by a set of highly non-linear stochastic weighting functions termed as 'spectral functions'.

4.3.3 Transient response with spectral functions

Following the spectral stochastic FE method, an approximation to the solution of Eqn. (4.20) can be expressed as a linear combination of functions of random variables and deterministic vectors. The aim is to use small number of terms to reduce the computation without losing the accuracy. Here we adopt the approach of the spectral functions presented in Chapter 2 for the case of frequency response of the structural dynamic systems and extend it to the case of using stochastic long time integration for the evaluation of the unsteady response statistics of the randomly parametrized system.

The stochastic linear set of equations presented in Eqn. (4.20), for which a solution of the response vector $\mathbf{u}_{t+\Delta t}(\theta)$ is sought, it follows directly from the above discussion that the solution at each time step $t + \Delta t$ can be projected on to a finite number of bases spanning a

stochastic Krylov space which can be defined at that time step as

$$\mathscr{K}_m \left[\underbrace{\left(\mathbf{A}_0 + \sum_{i=1}^{M} \xi_i(\theta_i)\mathbf{A}_i \right)}_{\mathbf{A}(\theta)}, \mathbf{p}^{eqv}_{t+\Delta t}\left(\boldsymbol{\xi}(\theta)\right) \right]. \tag{4.26}$$

where $\boldsymbol{\xi}(\theta)$ is the M-dimensional random vector $\boldsymbol{\xi}(\theta) = \{\xi_1(\theta), \xi_2(\theta), \ldots, \xi_M(\theta)\}^T$. A choice of a finite number of Krylov bases depends on the eigen-spectrum of the coefficient of the system matrix $\mathbf{A}(\theta)$. Since the eigenvalues of the coefficient matrix $\mathbf{A}(\theta)$ are distributed over a long interval on the real axis, the required number of basis functions (m) on which the solution would be projected would become close to the number of degrees of freedom (n) of the system. This increases the computational cost substantially and hence, highly undesirable.

Thus we describe the derivation of the spectral functions for the resolution of the stochastic response at each step of the time stepping algorithm. The derivation is follows from the analysis presented in Sec. 2.3.2 for the frequency response of stochastic structural systems. To begin with, we again consider the eigenvectors $\phi_k \in \mathbb{R}^n$ of the generalized eigenvalue problem

$$\mathbf{K}_0\phi_k = \lambda_k\mathbf{M}_0\phi_k; \quad k = 1, 2, \ldots n. \tag{4.27}$$

Since the matrices $\mathbf{K}_0$ and $\mathbf{M}_0$ are symmetric and generally non-negative definite, the eigenvectors ϕ_k for $k = 1, 2, \ldots n$ form a complete basis. Note that in principle any complete basis can be used. This choice is selected due to the analytical simplicity as will be seen later. For notational convenience, the matrices of eigenvalues and eigenvectors are defined as $\boldsymbol{\lambda}_0 = \text{diag}\,[\lambda_1, \lambda_2, \ldots, \lambda_n] \in \mathbb{R}^{n\times n}$ and $\boldsymbol{\Phi} = [\phi_1, \phi_2, \ldots, \phi_n] \in \mathbb{R}^{n\times n}$. The eigenvalues of structural dynamic systems can be ordered in the ascending order so that $\lambda_1 < \lambda_2 < \ldots < \lambda_n$. The orthogonality property of the modal matrix $\boldsymbol{\Phi}$ can be used to write $\boldsymbol{\Phi}^T\mathbf{K}_0\boldsymbol{\Phi} = \boldsymbol{\lambda}_0$ and $\boldsymbol{\Phi}^T\mathbf{M}_0\boldsymbol{\Phi} = \mathbf{I}$. Since the damping matrix is assumed to be proportional, the deterministic coefficient matrix as given in Eqns. (4.19)–(4.20) is reduced to the diagonal form if the modal coordinate transformation is applied. We introduce the following transformations

$$\left.\begin{aligned} &\boldsymbol{\Phi}^T\mathbf{A}_0\boldsymbol{\Phi} = \boldsymbol{\Lambda}_0; \\ \text{so that,}\quad &\mathbf{A}_0 = \boldsymbol{\Phi}^{-T}\boldsymbol{\Lambda}_0\boldsymbol{\Phi}^{-1} \end{aligned}\right\} \quad \text{and} \quad \widetilde{\mathbf{A}}_i = \boldsymbol{\Phi}^T\mathbf{A}_i\boldsymbol{\Phi} \in \mathbb{R}^{n\times n};\ i = 0, 1, 2, \ldots, M \tag{4.28}$$

Hence, it can be said that each diagonal component of $\boldsymbol{\Lambda}_0 = \text{diag}\,[\Lambda_{0_1}, \Lambda_{0_2}, \ldots, \Lambda_{0_n}] \in \mathbb{R}^{n\times n}$, i.e. Λ_{0_i} can also be expressed as a linear function of the eigenvalue λ_i obtained in Eqn. (4.27). Suppose the solution of Eqn. (4.20) is given by $\mathbf{u}_{t+\Delta t}(\theta) = \left[\mathbf{A}_0 + \sum_{i=1}^{M} \xi_i(\theta)\mathbf{A}_i\right]^{-1} \mathbf{p}^{eqv}_{t+\Delta t}\left(\boldsymbol{\xi}(\theta)\right)$.

Using the above discussions and the introduced transformations in Eqn. (4.28) we have

$$\begin{aligned}\mathbf{u}_{t+\Delta t}(\theta) &= \left[\boldsymbol{\Phi}^{-T}\boldsymbol{\Lambda}_0\boldsymbol{\Phi}^{-1} + \sum_{i=1}^{M}\xi_i(\theta)\boldsymbol{\Phi}^{-T}\widetilde{\mathbf{A}}_i\boldsymbol{\Phi}^{-1}\right]^{-1}\mathbf{p}^{eqv}_{t+\Delta t}\left(\boldsymbol{\xi}(\theta)\right)\\ &= \boldsymbol{\Phi}\boldsymbol{\Psi}\left(\boldsymbol{\xi}(\theta)\right)\boldsymbol{\Phi}^{T}\mathbf{p}^{eqv}_{t+\Delta t}\left(\boldsymbol{\xi}(\theta)\right)\end{aligned} \tag{4.29}$$

where $\boldsymbol{\Psi}\left(\boldsymbol{\xi}(\theta)\right) = \left[\boldsymbol{\Lambda}_0 + \sum_{i=1}^{M}\xi_i(\theta)\widetilde{\mathbf{A}}_i\right]^{-1}$ Separating the diagonal and off-diagonal terms of the $\widetilde{\mathbf{A}}_i$ matrices as $\widetilde{\mathbf{A}}_i = \boldsymbol{\Lambda}_i + \boldsymbol{\Delta}_i, \quad i = 1, 2, \ldots, M$ where the diagonal matrix is given as $\boldsymbol{\Lambda}_i = \text{diag}\left[\widetilde{\mathbf{A}}_i\right] = \text{diag}\left[\Lambda_{i_1}, \Lambda_{i_2}, \ldots, \Lambda_{i_n}\right] \in \mathbb{R}^{n\times n}$ and the matrix containing only the off-diagonal elements $\boldsymbol{\Delta}_i = \widetilde{\mathbf{A}}_i - \boldsymbol{\Lambda}_i$ is such that $\text{Trace}\left(\boldsymbol{\Delta}_i\right) = 0$. Using these, we can write

$$\boldsymbol{\Psi}\left(\boldsymbol{\xi}(\theta)\right) = \left[\underbrace{\boldsymbol{\Lambda}_0 + \sum_{i=1}^{M}\xi_i(\theta)\boldsymbol{\Lambda}_i}_{\boldsymbol{\Lambda}(\boldsymbol{\xi}(\theta))} + \underbrace{\sum_{i=1}^{M}\xi_i(\theta)\boldsymbol{\Delta}_i}_{\boldsymbol{\Delta}(\boldsymbol{\xi}(\theta))}\right]^{-1} \tag{4.30}$$

where $\boldsymbol{\Lambda}\left(\boldsymbol{\xi}(\theta)\right) \in \mathbb{R}^{n\times n}$ is a diagonal matrix and $\boldsymbol{\Delta}\left(\boldsymbol{\xi}(\theta)\right) \in \mathbb{R}^{n\times n}$) is an off-diagonal only matrix.

This diagonal matrix $\boldsymbol{\Lambda}\left(\boldsymbol{\xi}(\theta)\right)$ is treated as the preconditioner to the stochastic Krylov space given in Eqn. (4.26), such that the solution can be projected onto a very few basis functions and yet it would be possible to predict an accurate solution of the response vector using this left preconditioned stochastic Krylov subspace. As mentioned before, the diagonal dominance of the matrices $\widetilde{\mathbf{A}}_i$ is conducive to the approach being proposed here. Thus we can write

$$\begin{aligned}\mathscr{K}_m(\boldsymbol{\Lambda}^{-1}\boldsymbol{\Psi}, \boldsymbol{\Lambda}^{-1}\mathbf{p}^{eqv}_{t+\Delta t}) = \text{span}\{&\boldsymbol{\Phi}^{T}\boldsymbol{\Lambda}^{-1}\boldsymbol{\Phi}\mathbf{p}^{eqv}_{t+\Delta t}, \boldsymbol{\Phi}^{T}\mathbf{R}\left(\boldsymbol{\xi}(\theta)\right)\boldsymbol{\Lambda}^{-1}\boldsymbol{\Phi}\mathbf{p}^{eqv}_{t+\Delta t},\\ &\boldsymbol{\Phi}^{T}\mathbf{R}\left(\boldsymbol{\xi}(\theta)\right)^{2}\boldsymbol{\Lambda}^{-1}\boldsymbol{\Phi}\mathbf{p}^{eqv}_{t+\Delta t}, \ldots, \boldsymbol{\Phi}^{T}\mathbf{R}\left(\boldsymbol{\xi}(\theta)\right)^{m-1}\boldsymbol{\Lambda}^{-1}\boldsymbol{\Phi}\mathbf{p}^{eqv}_{t+\Delta t}\}\end{aligned} \tag{4.31}$$

$$\text{where,} \quad \mathbf{R}\left(\boldsymbol{\xi}(\theta)\right) = \left(\boldsymbol{\Lambda}^{-1}(\boldsymbol{\xi}(\theta))\boldsymbol{\Delta}(\boldsymbol{\xi}(\theta))\right) \tag{4.32}$$

Equation (4.31) shows that the Krylov bases are temporally adaptive stochastic basis functions due to the equivalent forcing term $\mathbf{p}^{eqv}_{t+\Delta t}$ which inherit the response characteristics from the previous time step. The equivalent infinite Neumann series representation of the above equation is

$$\boldsymbol{\Psi}\left(\boldsymbol{\xi}(\theta)\right) = \sum_{s=0}^{\infty}(-1)^{s}\left[\mathbf{R}\left(\boldsymbol{\xi}(\theta)\right)\right]^{s}\boldsymbol{\Lambda}^{-1}\left(\boldsymbol{\xi}(\theta)\right) \tag{4.33}$$

Taking an arbitrary r-th element of $\mathbf{u}(t,\theta)$, Eqn. (4.29) can be rearranged to have

$$u^r_{t+\Delta t}(\theta) = \sum_{k=1}^{n} \Phi_{rk} \left(\sum_{j=1}^{n} \Psi_{kj} \left(\boldsymbol{\xi}(\theta) \right) \left(\boldsymbol{\phi}_j^T \mathbf{p}^{eqv}_{t+\Delta t} \left(\boldsymbol{\xi}(\theta) \right) \right) \right). \tag{4.34}$$

We define a vector $\boldsymbol{\Gamma}_{t+\Delta t}\left(\boldsymbol{\xi}(\theta)\right)$ of dimension $n \times 1$ as

$$\boldsymbol{\Gamma}_{t+\Delta t}\left(\boldsymbol{\xi}(\theta)\right) = \boldsymbol{\Psi}\left(\boldsymbol{\xi}(\theta)\right) \left(\boldsymbol{\Phi}^T \mathbf{p}^{eqv}_{t+\Delta t}\left(\boldsymbol{\xi}(\theta)\right) \right) \tag{4.35}$$

where $\boldsymbol{\Gamma}_{t+\Delta t}\left(\boldsymbol{\xi}(\theta)\right)$ is the vector of highly non-linear functions of the random variables $\{\xi_i(\theta) : i = 1, \ldots, M\}$ and expressed in terms of the spectral properties of the system matrices. Combining Eqns. (4.34) and (4.35) we have

$$\mathbf{u}_{t+\Delta t}(\theta) = \sum_{k=1}^{n} \Gamma^k_{t+\Delta t}\left(\boldsymbol{\xi}(\theta)\right) \boldsymbol{\phi}_k \tag{4.36}$$

where $\Gamma^k_{t+\Delta t}\left(\boldsymbol{\xi}(\theta)\right)$ is the k^{th} element of the vector of stochastic functions contained in $\boldsymbol{\Gamma}_{t+\Delta t}\left(\boldsymbol{\xi}(\theta)\right)$ and $\boldsymbol{\phi}_k$ is the k^{th} eigen mode of the deterministic structural system. Thus the time domain response of the structural system is projected on to the deterministic eigen modes of the structural system and weighted by a set of 'spectral functions' $\Gamma^k_{t+\Delta t}\left(\boldsymbol{\xi}(\theta)\right)$.

We assume that the series in Eqn. (4.33) is truncated after m terms. This is equivalent to taking m terms of the minimal polynomial of the left-preconditioned stochastic Krylov space. The truncated function can then be expressed as
$\boldsymbol{\Psi}^{(m)}\left(\boldsymbol{\xi}(\theta)\right) = \sum_{s=0}^{m}(-1)^s \left[\boldsymbol{\Lambda}^{-1}\left(\boldsymbol{\xi}(\theta)\right)\boldsymbol{\Delta}\left(\boldsymbol{\xi}(\theta)\right)\right]^s \boldsymbol{\Lambda}^{-1}\left(\boldsymbol{\xi}(\theta)\right)$. From this, one can obtain a sequence for different values of m as

$$\mathbf{u}^{(m)}_{t+\Delta t}(\theta) = \sum_{k=1}^{n} \Gamma^{k,(m)}_{t+\Delta t}\left(\boldsymbol{\xi}(\theta)\right) \boldsymbol{\phi}_k; \quad m = 1, 2, 3, \ldots \tag{4.37}$$

Since $\theta \in \Theta$ is arbitrary, comparing Eqn. (4.20) and Eqn. (4.29) we observe that $\mathbf{u}^{(m)}_{t+\Delta t}(\theta)$ is the solution of Eqn. (4.20) for every θ as $m \to \infty$. It is to be noted that the proposed solution technique is not limited to any particular choice of the probability measure of the input parametric randomness and hence is applicable to almost all random fields as long as the solution exists.

It is seen as before that the series in Eqn. (4.33) is in terms of $[\boldsymbol{\Lambda}^{-1}\left(\boldsymbol{\xi}(\theta)\right)][\boldsymbol{\Delta}\left(\boldsymbol{\xi}(\theta)\right)]$, where both terms are random and hence the elements of this matrix series are *not simple polynomials* in $\xi_i(\theta)$, but are in terms of a *ratio of polynomials* as seen in the following equations. The convergence of this series depends of the spectral radius of $\mathbf{R}\left(\boldsymbol{\xi}(\theta)\right)$ in Eqn. (4.32). Note that $\boldsymbol{\Lambda}\left(\boldsymbol{\xi}(\theta)\right)$ is a diagonal matrix, its inverse is also a diagonal matrix. Also recall that the diagonal of $\boldsymbol{\Delta}\left(\boldsymbol{\xi}(\theta)\right)$ contains only zeros. Hence a generic term of this matrix can be obtained

as

$$R_{rs} = \frac{\Delta_{rs}(1-\delta_{rs})}{\Lambda_{rr}} = \frac{\sum_{i=1}^{M}\xi_i\Delta_{i_rs}(1-\delta_{rs})}{\Lambda_{0_r}+\sum_{i=1}^{M}\xi_i\Lambda_{i_r}} = \frac{\sum_{i=1}^{M}\xi_i\widetilde{A}_{i_rs}(1-\delta_{rs})}{\Lambda_{0_r}+\sum_{i=1}^{M}\xi_i\widetilde{A}_{i_rr}}$$
$$= \frac{\sum_{i=1}^{M}\xi_i\widetilde{A}_{i_rs}(1-\delta_{rs})}{(a_0+a_1\zeta_1)\lambda_r+(a_1\zeta_2+1)+\sum_{i=1}^{M}\xi_i\widetilde{A}_{i_rr}} \tag{4.38}$$

where λ_r is the r^{th} eigenvalue of the deterministic system as per Eqn. (4.27) and δ_{rs} is the Kronecker delta. It can be seen from Eqn. (4.38) that the spectral radius of $\mathbf{R}$ is also controlled by the diagonal dominance of the $\widetilde{\mathbf{A}}_i$ matrices.

It was seen in Sec. 2.3.4 that the spectral radius of the matrix $\mathbf{R}$ is a function of the frequency step being considered. In contrast to that, Eqn. (4.38) shows that the spectral radius depends on the implicit time integration parameters (α and γ) and the time-step size, Δt. When Eqn. (4.38) is expressed explicitly in terms of these parameters we have after some simplifications

$$R_{rs} = \frac{\alpha\Delta t^2\left(\sum_{i=1}^{M}\xi_i\widetilde{A}_{i_rs}(1-\delta_{rs})\right)}{\lambda_r+(\lambda_r\zeta_1+\gamma\zeta_2)\Delta t+\left(\sum_{i=1}^{M}\xi_i\widetilde{A}_{i_rr}\right)\alpha\Delta t^2} \tag{4.39}$$

We analyze the above equation for the effect of time step size on $\mathbf{R}$ for a given fixed structural system. Since the constants α and γ are positive quantities and assuming that the time step size chosen is generally quite small, we can write

$$R_{rs} = O(\Delta t^2) \quad \text{for} \quad 0 < \Delta t << 1 \tag{4.40}$$

This indicates that a smaller time-step size improves the convergence behavior of the spectral functions. However, smaller time steps incur higher computational cost.

The functions $\Gamma^k_{t+\Delta t}\left(\boldsymbol{\xi}(\theta)\right), k = 1, 2, \ldots n$ are the time adaptive stochastic spectral functions which are rational functions of the input random variables. They are expressed in terms of the spectral properties of the coefficient matrix of the discretized system equation. They depend on the parameters of the time integration and the time step size. These are the time domain counterparts of frequency dependent spectral functions considered in context of the frequency response of stochastic structural dynamic systems.

Truncating the series in Eqn. (4.33) up to different terms, we obtain the spectral functions of different order. Using the expression in Eqn. (4.35), the first-order spectral functions at each time-step can be explicitly obtained as

$$\Gamma^{k,(1)}_{t+\Delta t}\left(\boldsymbol{\xi}(\theta)\right) = \sum_{j=1}^{n}\Psi^{(1)}_{kj}\left(\boldsymbol{\xi}(\theta)\right)\left(\boldsymbol{\phi}_j^T\mathbf{p}^{eqv}_{t+\Delta t}\left(\boldsymbol{\xi}(\theta)\right)\right)$$
$$= \frac{\boldsymbol{\phi}_k^T\mathbf{p}^{eqv}_{t+\Delta t}\left(\boldsymbol{\xi}(\theta)\right)}{(a_0+a_1\zeta_1)\lambda_r+(a_1\zeta_2+1)+\sum_{i=1}^{M}\xi_i(\theta)\Lambda_{i_k}} \tag{4.41}$$

Here the spectral functions are rational functions of the basic random variables and change at each time step due to the associated forcing function $\mathbf{p}^{equ}_{t+\Delta t}(\boldsymbol{\xi}(\theta))$. The vector of spectral functions of order m is given as

$$\boldsymbol{\Gamma}^{(m)}_{t+\Delta t}(\boldsymbol{\xi}(\theta)) = \left[\mathbf{I}_n - \mathbf{R}(\boldsymbol{\xi}(\theta)) + \mathbf{R}(\boldsymbol{\xi}(\theta))^2 - \mathbf{R}(\boldsymbol{\xi}(\theta))^3 \ldots m^{\text{th term}}\right] \boldsymbol{\Gamma}^{(1)}_{t+\Delta t}(\boldsymbol{\xi}(\theta)) \qquad (4.42)$$

where $\mathbf{I}_n$ is the n-dimensional identity matrix and $\mathbf{R}$ is defined in Eqn. (4.32). The availability of the recursive formula, makes the calculation of the higher-order spectral functions are expected to be less involved.

The computational complexity involved in calculating the proposed spectral function is presented here. If the stochastic FE system solution is projected on to its modal coordinates with the first n_r modes (from Eqn. (4.27)) and N_s is the number of stochastic samples points where the system is solved in the direct MCS approach then the total computational complexity is $\frac{T}{\Delta t} N_s \mathscr{O}(n_r^3)$ where T is the total time for which the system response is evaluated and Δt is the time-step size. For the spectral method, the calculation of the various orders of the spectral functions requires the evaluation of the quantity $\boldsymbol{\Lambda}^{-1}(\boldsymbol{\xi}(\theta))\,\boldsymbol{\Delta}(\boldsymbol{\xi}(\theta))$ in Eqn. (4.32), whose complexity is given as $\mathscr{O}(n_r^2)$. Hence the complete system response resolution using the m^{th} order spectral functions is $\frac{T}{\Delta t} N_s (m-1) N_t \mathscr{O}(n_r^2)$. Thus the computational complexity of the spectral function approach is found to be growing as a cube of the dimension of the reduced eigenspace which is approximately one order more efficient than the direct MCS calculations.

Statistical moments of the response vector

Given that the stochastic displacement vector is a function of the sequence of the input random variables, we can construct, at each time step t, the mean and the higher-order statistical moments of the solution $\mathbf{u}^{(m)}_t : \mathbb{R}^n \times \Theta \rightarrow \mathbb{R}^n$ about a given point $\boldsymbol{\xi}_0$ in the stochastic space using the relation

$$\boldsymbol{\Sigma}^{(m)}_{p,t} = \int_\theta \left(\mathbf{u}^{(m)}_t(\boldsymbol{\xi}(\Theta)) - \mathbf{u}(\boldsymbol{\xi}_0)\right)^p dP(\boldsymbol{\xi}(\theta)) \quad p = 1, 2, 3, \ldots \qquad (4.43)$$

where $\boldsymbol{\Sigma}^{(m)}_{p,t} \in \mathbb{R}^{n \times n}$ denotes the p^{th} order statistical moment of the solution about $\mathbf{u}(\boldsymbol{\xi}_0) \in \mathbb{R}^n$ calculated with the m^{th} order spectral function at time step t and P denotes the joint density function of the input random variables. From the above the expressions for mean ($p = 1$, $\mathbf{u}(\boldsymbol{\xi}_0) = 0$) and variance ($p = 2$, $\mathbf{u}(\boldsymbol{\xi}_0) = \boldsymbol{\Sigma}^{(m)}_{1,t}$) of the stochastic solution vector

can be written as:

$$\Sigma_{1,t}^{(m)} = \sum_{k=1}^{n} \mathbb{E}\left[\Gamma_t^{k,(m)}\left(\boldsymbol{\xi}(\theta)\right)\right] \boldsymbol{\phi}_k \tag{4.44}$$

$$\begin{aligned}\Sigma_{2,t}^{(m)} &= \mathbb{E}\left[\left(\sum_{k=1}^{n} \Gamma_t^{k,(m)}\left(\boldsymbol{\xi}(\theta)\right) - \mathbb{E}\left[\Gamma_t^{k,(m)}\left(\boldsymbol{\xi}(\theta)\right)\right]\right)\boldsymbol{\phi}_k\right] \\ &= \boldsymbol{\Phi}\Xi_t\boldsymbol{\Phi}^T\end{aligned} \tag{4.45}$$

where $\boldsymbol{\Phi}$ is the matrix of eigen vectors, Ξ_t is the temporal variance-covariance matrix at time t of the vector $\boldsymbol{\Gamma}_t^{(m)} = \left[\Gamma_t^{1,(m)}, \Gamma_t^{2,(m)}, \ldots, \Gamma_t^{n,(m)}\right]$ such that $\Xi_{t,ij} = \mathbb{E}\left[\Gamma_t^{i,(m)}\Gamma_t^{j,(m)}\right]$ and $\mathbb{E}\left[\bullet\right]$ is the expectation operator associated with the stochastic space. If the components of the random vector $\boldsymbol{\Gamma}_t^{(m)}$ are uncorrelated then Ξ_t becomes a diagonal matrix. However, since the spectral functions considered here are correlated random variables, we obtain a fully populated Ξ_t matrix at every time step. Hence for this correlated nature of the spectral functions, integration in the stochastic space defined in Eqn. (4.43) calls for efficient sampling techniques or metamodeling strategies which can be used in conjunction with the solution methodology proposed here.

In the following section we provide some numerical examples to highlight the performance and computational accuracy of the spectral Galerkin approaches and the proposed spectral function approach with the implicit time integration scheme. The direct MCS results have also been obtained which serve as the benchmark solution. The appropriate error estimates, convergence behavior and the simulation times of the solution are presented for effective comparison of the different solution methodologies.

Here we present Algorithm 4 which summarizes the proposed spectral function approach used to resolve the stochastic system response using an implicit time integration technique.

4.4 Illustrative example: Transient dynamic analysis of an Euler-Bernoulli beam

To demonstrate the applicability of the methods detailed in the previous sections, we consider here a prototype problem of the dynamic uni-planar flexural vibration of a one dimensional Euler-Bernoulli cantilever beam. This application is used to demonstrate the effectiveness of the proposed spectral solution method to this class of SPDE. The solution is obtained for a specified value of the correlation length and for different degrees of variability of the input random field. The spatially varying stochastic field has been discretized using a finite number of zero mean uncorrelated standard Gaussian variables using the KL expansion theorem. For the beam problem we have chosen the elastic modulus EI_z as the stochastic parameter. The beam problem has been solved for its transient response in the time-domain under the

Algorithm 4 Transient Stochastic FEM with spectral functions

Input: Choose time-step size (Δt) and discretize time axis T into N_t points, $N_t = T/\Delta t$.
Input: Stochastic input parameter $\boldsymbol{\alpha}(\theta, \mathbf{r}) \in \mathbb{R} \times \Theta^{(M)}$ using KL modes from (4.3).
Input: Calculate the system matrices from $\mathscr{B}(u^n, v^n; \theta) = \mathscr{L}(v^n; \theta)$ using Eqns. (4.5)–(4.10).
Input: Choose parameters α and β, evaluate integration constants from Eqn. (4.14).
Output: System response $\mathbf{u}_{t+\Delta t}(\theta), \dot{\mathbf{u}}_{t+\Delta t}(\theta), \ddot{\mathbf{u}}_{t+\Delta t}(\theta) \in \mathbb{R}^n \times \Theta$ at each $t \in [0, T]$.

1: Evaluate the first n_r eigenpairs $[\boldsymbol{\lambda}_0, \boldsymbol{\Phi}]$ from Eqn. (4.27).
2: Construct $\mathbf{R}(\boldsymbol{\xi}(\theta))$ and its successive powers $\mathbf{R}^k(\boldsymbol{\xi}(\theta))$ for $k = 1, \ldots, m$ using Eqn. (4.32).
3: Initialize $\mathbf{u}_0(\theta)$, $\dot{\mathbf{u}}_0(\theta)$, $\ddot{\mathbf{u}}_0(\theta)$.
4: **for** j = 1 to N_t **do**
5: Calculate $\mathbf{p}^{eqv}_{t+\Delta t}$ with $\mathbf{u}_t(\theta), \dot{\mathbf{u}}_t(\theta), \ddot{\mathbf{u}}_t(\theta)$ following Eqns. (4.14) and (4.18).
6: **for** r = 1 to m **do**
7: Construct the Krylov basis following Eqn. (4.31) using $\mathbf{R}^r(\boldsymbol{\xi}(\theta))$, $\boldsymbol{\Phi}$ and $\mathbf{p}^{eqv}_{t+\Delta t}$.
8: Create the m^{th} order spectral function vector $\boldsymbol{\Gamma}^{(m)}_{t+\Delta t}(\boldsymbol{\xi}(\theta))$ from Eqn. (4.35).
9: **end for**
10: Project the system response $\mathbf{u}_{t+\Delta t}(\theta)$ in the eigenspace using $\boldsymbol{\Gamma}^{(m)}_{t+\Delta t}(\boldsymbol{\xi}(\theta))$ from Eqn. (4.36).
11: Evaluate $\dot{\mathbf{u}}_{t+\Delta t}(\theta), \ddot{\mathbf{u}}_{t+\Delta t}(\theta)$ at $t = j\Delta_t$ from Eqn. (4.14).
12: Evaluate the moments of the response using Eqns. (4.44)–(4.45).
13: Make $\mathbf{u}_t(\theta), \dot{\mathbf{u}}_t(\theta), \ddot{\mathbf{u}}_t(\theta)$ equal to $\mathbf{u}_{t+\Delta t}(\theta), \dot{\mathbf{u}}_{t+\Delta t}(\theta), \ddot{\mathbf{u}}_{t+\Delta t}(\theta)$ respectively.
14: **end for**

action of an impulse loading. Direct MCS has been performed for these cases and is taken as the benchmark solution with respect to which the appropriateness of the different methods have been analyzed. A comparison between the PC method and the proposed spectral decomposition technique is presented for the beam problem.

The cantilever beam is taken to be clamped at one end (where the displacement and the rotational degree of freedom is both taken to be zero). Figure 4.1(a) shows the configuration of the cantilever beam with an impulse load at its free end in the z-direction. The beam bending occurs in the $x - z$ plane. We assume that the bending modulus (EI_y) is a stationary Gaussian random field of the form

$$EI_y(x, \theta) = EI_0(1 + a(x, \theta)) \tag{4.46}$$

where x is the coordinate along the length of the beam, EI_0 is the mean bending modulus, $a(x, \theta)$ is a zero mean stationary Gaussian random field. It must be mentioned that though the Gaussian random field model is not physically meaningful in strict sense, since the physical quantities being model are strictly positive, yet the model has been used extensively in the existing stochastic FE literatures [Ghanem and Spanos, 1991, Sarkar and Ghanem, 2003]. However, it has been shown that when the number of KL expansion terms is chosen carefully, the truncated statistical models are strictly positive [Powell and Elman, 2009].

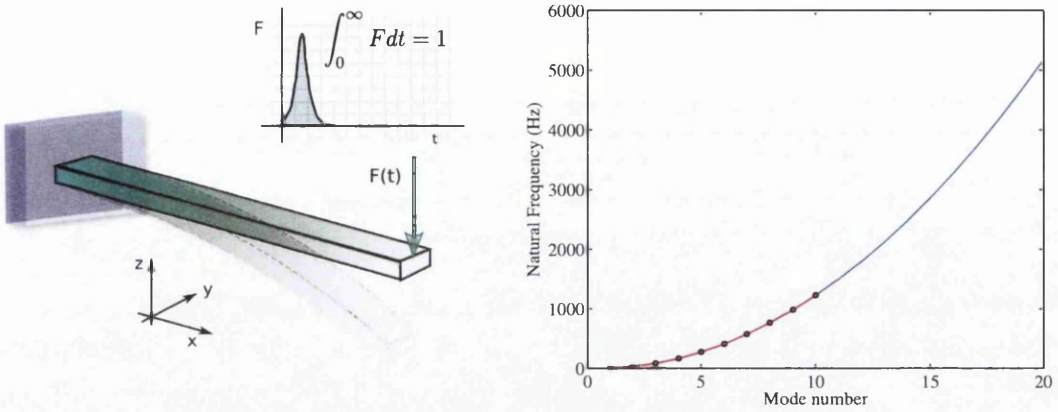

(a) Schematic diagram of the beam with a point load at the free end

(b) Natural frequency of the cantilever beam.

Figure 4.1: Schematic diagram of the cantilever beam with a point load at the free end along with its natural frequencies. The number of reduced eigenvectors chosen is $q = 10$ which covers the frequency of up to 1200 Hz. The fundamental frequency is found to be 4.85 Hz

The autocovariance function of this random field is assumed to be

$$C_a(x_1, x_2) = \sigma_a^2 e^{-(|x_1 - x_2|)/\mu_a} \tag{4.47}$$

where μ_a is the correlation length and σ_a is the standard deviation. We use the base-line parameters as the length $L = 1$m, cross-section $(b \times h)$ 39×5.93 mm^2 and Young's modulus $E = 2 \times 10^{11}$ Pa. In this study we consider deflection of the tip of the beam under an impulse load of $\mathbf{I}_{F(t)} = 1.0$N-s at $t = 0$. Here the forcing is assumed to be deterministic in nature. The case when the forcing is random has been treated extensively in literature within the scope of 'Random Vibration' [Lin, 1967]. For example, if the forcing function is independent of the parametric uncertainty, the proposed spectral function approach could be applied at chosen points in the stochastic space associated with the excitation and the second order response statistics can be constructed from it. The correlation length considered in the numerical study for comparison with the PC expansion method is $\mu_a = L/2$ and for this case the number of terms retained (M) in the KL expansion Eqn. (4.3) is two. Thus the input stochastic space is two dimensional in this case. For the FE discretization, the beam is divided into 100 elements. Standard four degrees of freedom Euler-Bernoulli beam model is used. After applying the fixed boundary condition at one edge, we obtain the number of degrees of freedom of the model to be $n = 200$. It has been verified that this spatial resolution is sufficient to capture the excitation response of the system completely.

The solution obtained with the proposed reduced basis spectral function has been compared with the direct MCS results and the 4^{th} order PC expansion. The MCS in the stochastic space is performed with $10,000$ samples. The calculations have been performed for four values of input standard deviation, $\sigma_a = \{0.05, 0.10, 0.15, 0.20\}$, which simulates increasing

input uncertainty.

Figure 4.1(b) presents the distribution of the natural frequencies of the cantilever beam from the generalized eigenvalue problem given in Eqn. (4.27). The reduced basis of the problem has been chosen based on the time-step size or the sampling frequency of the problem, i.e. all the eigen modes that cover up to 1200 Hz have been chosen. The time step size for the numerical integration scheme has been chosen as $1/800$ seconds. We have applied a constant modal damping with 1% damping factor for all the modes.

Figure 4.2 shows the time-domain response of the deflection of the tip of the cantilever beam under the action of an unit impulse around time $t = 0$ for the different input standard deviation values. The proposed spectral method and the direct MCS results shows good

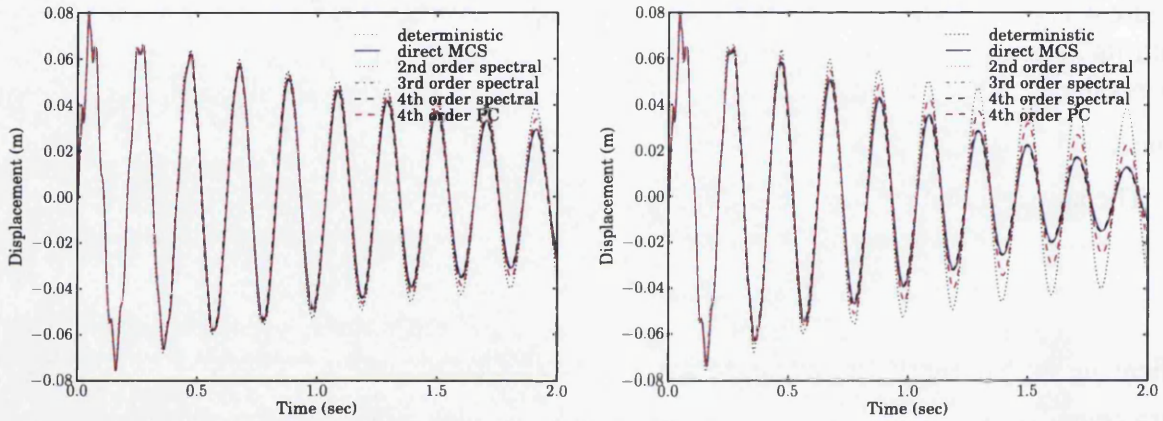

(a) Mean deflection, $\sigma_a = 0.05$.

(b) Mean deflection, $\sigma_a = 0.1$.

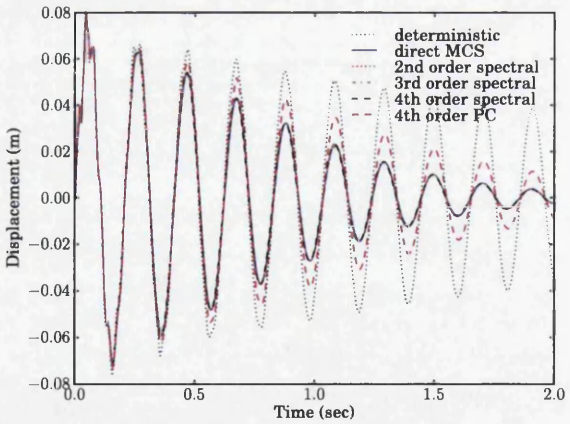

(c) Mean deflection, $\sigma_a = 0.15$.

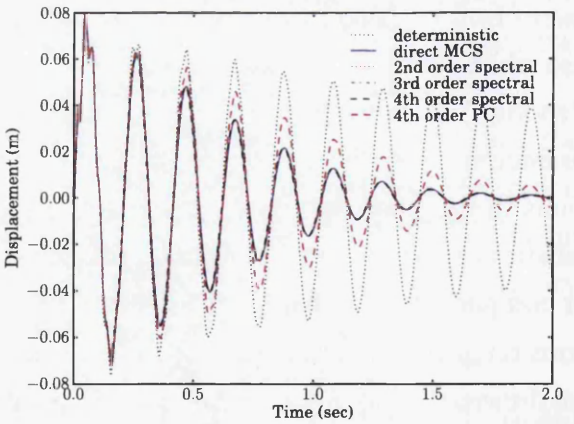

(d) Mean deflection, $\sigma_a = 0.2$.

Figure 4.2: The mean deflection of the free end of the cantilever beam under an unit impulse load at time $t = 0$ for the duration of $1/800$ seconds. The response of the reduced order spectral function method is obtained with $10,000$ samples and for $\sigma_a = \{0.05, 0.10, 0.15, 0.20\}$.

agreement at all time steps. However the solution generated by PC method, while closely approximating the MCS solution at earlier times, diverges for higher values of t. For high input standard deviation (σ_a), this discrepancy sets in even earlier.

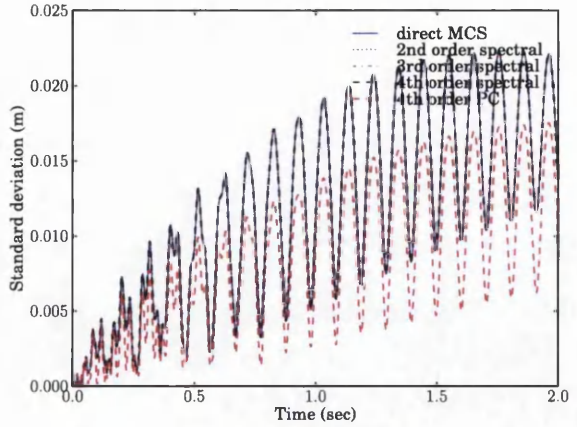

(a) Standard deviation of deflection, $\sigma_a = 0.05$.

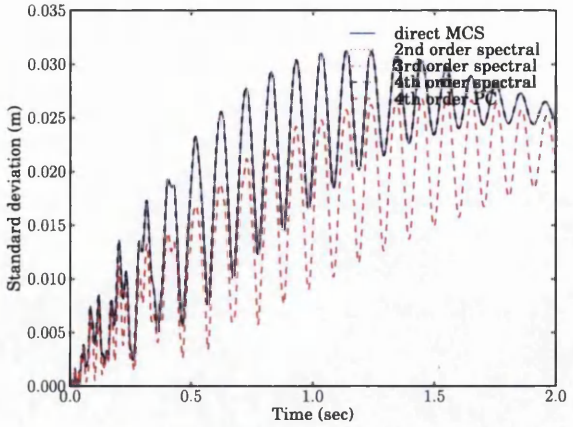

(b) Standard deviation of deflection, $\sigma_a = 0.1$.

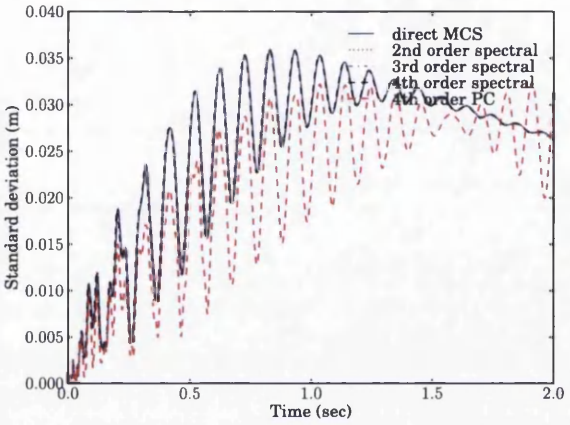

(c) Standard deviation of deflection, $\sigma_a = 0.15$.

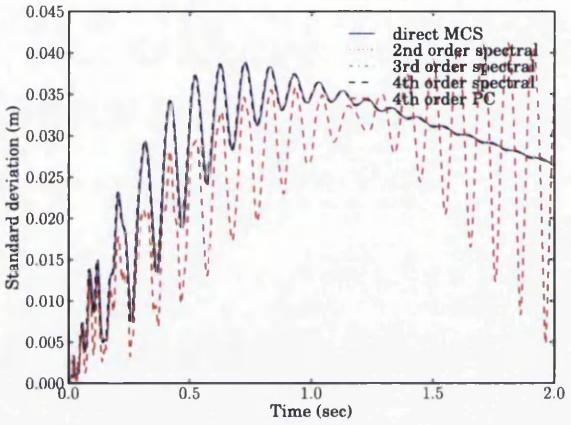

(d) Standard deviation of deflection, $\sigma_a = 0.2$.

Figure 4.3: The standard deviation of the deflection of the free end of the cantilever beam under unit impulse load at time $t = 0$ for the duration of $1/800$ seconds. The response of the reduced order spectral function method is obtained with $10,000$ samples and for $\sigma_a = \{0.05, 0.10, 0.15, 0.20\}$.

Similar behavior is seen in Fig. 4.3 in the plot for standard deviation of the deflection of the free end of the beam. The values predicted by the proposed spectral function method is in good agreement with the direct MCS simulation results, while the 4^{th} order PC results show inconsistencies, especially for longer values of t. The accurate prediction of higher order moments using the spectral Galerkin approaches requires a high order of the chaos to be used with the solution. Hence it is expected that the higher moments of the response would tend to deviate significantly.

It can also be noted from Fig. 4.2 that higher values of input standard deviation produces an effect equivalent to that of damping on the mean deflection values. This is because the randomness in the system parameters tend to distribute the peak response around a neighborhood of the resonance frequency of the deterministic system, and the subsequent averaging smooths out or damps the response at those frequencies. The response is largely comprised of

the fundamental frequency (4.85 Hz) of vibration of the beam, since the higher order modes decay out rapidly. While the mean response for higher values of σ_a shows an added damping-kind-behavior, in reality any random sample would still produce high levels of vibration in the response.

The fact that the higher order moments are not properly reproduced by the 4^{th} order PC method is also verified from the plots of the probability density function of the deflection of the free end of the beam at $t = 0.119$s and $t = 0.134$s as shown in Fig. 4.4. It shows that while the mean value is closely approximated by the PC solution, the values of the higher order moments are significantly different from those obtained with the MCS and the spectral methods. We find a very good agreement of the density functions given by the latter two methods. The error in the density function produced using the 4^{th} order PC is much larger

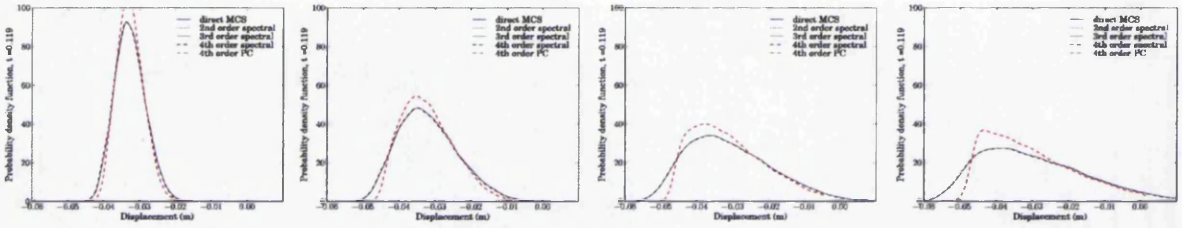

(a) PDF of deflection at $t = 0.119$s. The 4 sub-figures correspond to $\sigma_a = \{0.05, 0.10, 0.15, 0.20\}$.

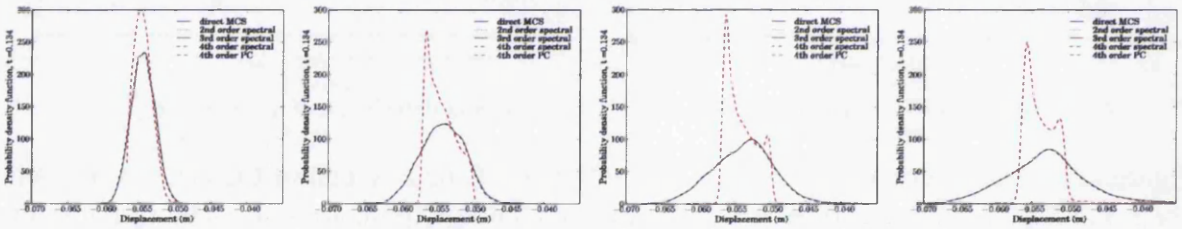

(b) PDF of deflection at $t = 0.134$s. The 4 sub-figures correspond to $\sigma_a = \{0.05, 0.10, 0.15, 0.20\}$.

Figure 4.4: The probability density function of the deflection of the free end of the cantilever beam at $t = 0.119$s and $t = 0.134$s under a unit impulse load at time $t = 0$ for a duration of $1/800$s. The response of the reduced order spectral function method is obtained with $10,000$ samples and for input standard deviation of $\sigma_a = \{0.05, 0.10, 0.15, 0.20\}$ of the parametric random field.

(compared to the direct MCS solution) at $t = 0.134$s in Fig. 4.4(b) than at $t = 0.119$s in Fig. 4.4(a). This indicates that as the time integration proceeds, the polynomial order of the solution needs to be enhanced to account for the compounded stochastic non-linearity of the transient system. Similar observations have been reported in the literatures [Najm, 2009, Gerritsma *et al.*, 2010] for long time integration which tend to generate unacceptable error levels if higher order chaos functions are not used to for projection of the solution in the stochastic subspace. This however, has detrimental effects in terms of the computational efficacy of the solution. Hence it might be desirable to have some 'time-adaptivity' characteristics in the stochastic basis functions. The accurate estimation of the density curve using different order

of spectral functions is found to be highly conducive to this effect since the stochastic spectral functions change with each time step.

Table 4.1: Comparison of calculation time (in seconds) of the proposed reduced order spectral function approach with direct MCS simulation and 4^{th} order PC. All calculations were performed using a single processor core. The last entry '4^{th} order PC (parallel BiCGStab)', indicates the block sparse linear system solved solved with parallelized Bi-conjugate gradient stabilized algorithm on 8 computational cores.

Methodology	Avg Time(s)	Min Time(s)	Max Time(s)
Direct MCS	13.589	13.506	13.798
2nd order spectral	1.375	1.345	1.396
3rd order spectral	1.445	1.414	1.465
4th order spectral	1.500	1.481	1.523
4th order PC	5.117	4.975	5.327
4th order PC (parallel BiCGStab)	1.329	1.201	1.477

Table 5.2 presents a comparison of the calculation time of the different methods used in this study to demonstrate the relative computational efficacy of the proposed method. The calculation times are shown for a single time step, performed on a single core of a computational platform. The last entry '4^{th} order PC (parallel BiCGStab)', denotes the time taken in solving the linear block-sparse system obtained from the spectral Galerkin approach using a parallel implementation of the Bi-conjugate gradient stabilized algorithm on 8 computational cores where each core is identical to the single core used in solving the other linear systems mentioned in the table. It can be seen from the table that the 2^{nd} order spectral function approach is on an average 10 times more efficient than the direct MCS simulation and about $3.5 - 4$ times more efficient than the 4^{th} order PC method. When we implement the PC with parallel BiCGStab, we find that the speed obtained is around that of the 2^{nd} order method. It is also seen that as the order of the spectral function is increased, the computational time increases with it. It must be mentioned that the performance of the spectral function method can potentially be enhanced significantly using the efficient sampling techniques. The choice of the 4^{th} order PC to compare the accuracy of the results is justified from this comparison of computational efficacy.

The autocorrelation function (ACF), which is useful for identifying the relation between time signals separated by a finite space in time τ is defined as

$$ACF(t,\tau) = \frac{E\left[(u_t - \mu_t)(u_{t+\tau} - \mu_{t+\tau})\right]}{\sigma_t \, \sigma_{t+\tau}} \tag{4.48}$$

where u_t is the system response at time t, σ_t denotes the standard deviation of the response at time t and $\mathbb{E}\left[\bullet\right]$ is the expectation operator defined over the sample space. The ACF gives important information about the harmonic components contained in the signal and also the stationarity of the signals. Figure 4.5 shows the autocorrelation surface of the transient re-

ponse of the free end of the cantilever beam under the unit impulse load for two different values of standard deviation of the input randomness, $\sigma_a = 0.15$ in Fig. 4.5(a) and $\sigma_a = 0.20$ in Fig. 4.5(b). The ACF surface is plotted against the time t and the parameter τ for the length of the time domain reponse, $0.0 - 2.0$ seconds as shown in Figs. 4.2 and 4.3. Hence the ACF surface is triangular in shape, i.e. the time t and the parameter τ varies between $0.0 - 2.0$ seconds. The definition of the ACF in Eqn. (4.48) ensures that the ACF reponse surface remains

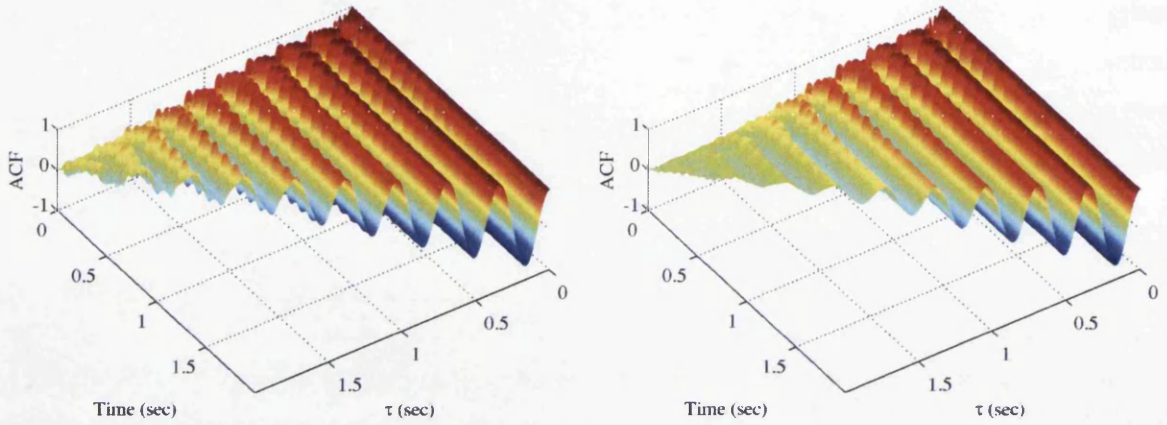

(a) ACF, $\sigma_a = 0.15$.

(b) ACF, $\sigma_a = 0.20$.

Figure 4.5: The autocorrelation function of the beam response under a unit impulse load at time $t = 0$ as a function of the τ and t as given in Eqn. (4.48). The ACF surface has been obtained with direct MCS simulation and is very closely approximated by the results obtained with the spectral function approach.

between -1 and $+1$, due to normalization with the standard deviation of the response. For very small values of τ, the correlation between the signals for all values of t is almost perfect, which leads to ACF being close to 1 along $\tau \approx 0$. The correlation attenuates with increase in τ, and it can be seen that the attenuation is more rapid for the case of higher variability of input randomness, i.e. for $\sigma_a = 0.20$. This is expected as a higher input randomness results in the less correlated response with time. This also explains the rapid attenuation of the mean response for higher degree of variability of the input randomness (say for $\sigma_a = 0.20$) as was observed in Fig. 4.2.

Figure 4.6 shows the ACF for specific values of time t and the parameter τ and for the random field variability of $\sigma_a = 0.20$ which corresponds to the response on specific planes placed perpendicular to the t-axis and the τ-axis in Fig. 4.5(b). Figure 4.6(a) shows that, the autocorrelation attenuates with τ for all values of t and this attenuation is more rapid for higher parametric uncertainties (as established in Fig. 4.5). It is also seen that the ACF obtained with different orders of spectral functions are in very good agreement with the direct MCS results. The 4^{th} order PC produces slower attenuation of the ACF with increasing τ as can be seen in Fig. 4.6(a) (which is consistent with the 4^{th} order PC results seen in Fig. 4.2). Also, from Fig. 4.6(b) it is found that for very small values of τ, the correlation is quite high and the time

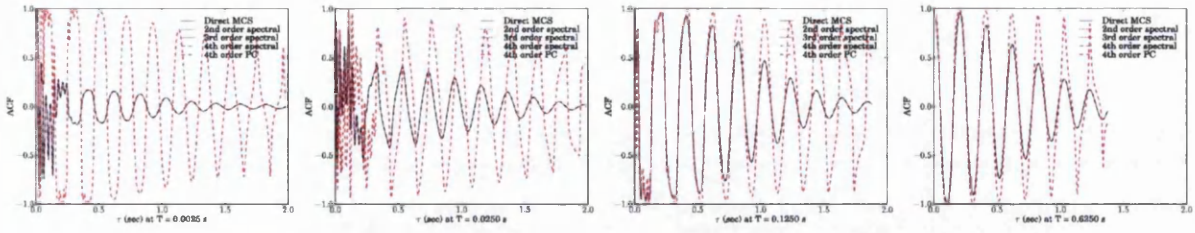

(a) ACF as a function of τ at specific time steps $t = 0.0025, 0.025, 0.125, 0.625$ for $\sigma_a = 0.20$.

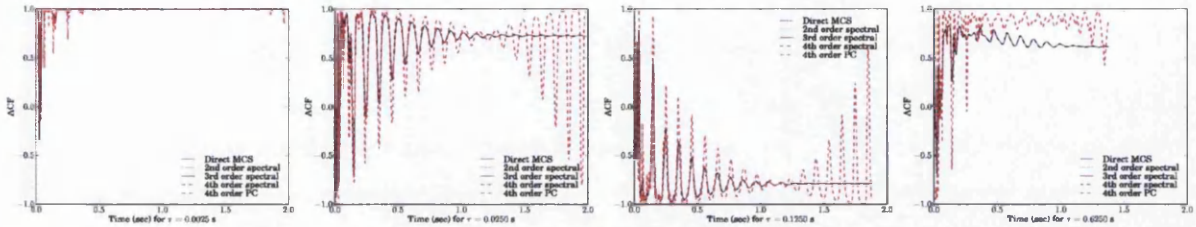

(b) ACF as a function of time t at specific values of the parameter $\tau = 0.0025, 0.025, 0.125, 0.625$ for $\sigma_a = 0.20$.

Figure 4.6: The autocorrelation function of the cantilever beam response a unit impulse load at time $t = 0$ for input parametric randomness of $\sigma_a = 0.20$.

response becomes almost stationary as the value of t increases, which indicates the transition of the transient response towards steady state. In other words, the ACF becomes a function of the parameter τ only for sufficiently large values of t. The 4^{th} order PC however, do not produce this tendency towards stationarity which is contrary to the physics of the structural dynamic system. This discrepancy can be attributed to the growing error associated with the time integration scheme and would have to be addressed with enhanced order of the PC expansion.

The Galerkin method involved in approximating the solution with the 4^{th} order Hermite polynomials requires the solution of a linear system of equation of size 3000×3000 at each time step (compared to the original discretized FE system of 200 d.o.f.). This can impose a stringent condition on the upper bound of the time step size Δt and, as explained in context of Eqn. (4.16), can result in a growth of the error associated with the time integration scheme. This can lead to a growth of the error associated with spectral Galerkin methods faster than that associated with other sampling based techniques where the dimension of the linear system to be solved remains the same as the original deterministic system. Similar behavior is also observed in the standard deviation results shown in Fig. 4.3 where we find that for higher values of variability of the input randomness (indicated by large σ_a) there is a 'tipping point' beyond which the discrepancy of the 4^{th} order PC result grows and this point arrives earlier for higher values of input variability. This can be tackled with increased order PC expansion, however, the high dimension of the resulting linear system can significantly increase the computational cost of the time integration scheme due to the enhanced limitation on the maximum time step size.

The convergence behavior of the proposed spectral function approach with order of ex-

pansion of the spectral functions can be studied with an error indicator. We define a relative L^2 error for the system response $\epsilon^{(m)}_{\boldsymbol{\Sigma}_j}(t)$, at each time step t for m^{th} order spectral function as

$$\epsilon^{(m)}_{\boldsymbol{\Sigma}_j}(t) = \frac{\left\| \boldsymbol{\Sigma}^{(m)}_{jSF}(t) - \boldsymbol{\Sigma}_{jMCS}(t) \right\|_{L^2(\mathscr{D})}}{\left\| \boldsymbol{\Sigma}_{jMCS}(t) \right\|_{L^2(\mathscr{D})}} \quad \text{for} \quad j = 1, 2 \tag{4.49}$$

where $\boldsymbol{\Sigma}^{(m)}_{jSF}(t)$ is the mean ($j = 1$) or the standard deviation ($j = 2$) of the system response vector, and $\boldsymbol{\Sigma}_{jMCS}(t)$ is the same calculated with the direct MCS simulation result. The norm $L^2(\mathscr{D})$ covers the discretized FE spatial domain $\mathscr{D}$. Here we have studied the cases for which the spectral function order varies as $m = 1, \ldots, 8$ and present the convergence of the L^2 relative error as functions of the spectral function order.

For the sake of rigor, here we study a beam vibration problem where a shorter correlation length of the input random parameter (bending modulus) has been assumed. This results in an increase in dimension of the input stochastic space such that for the same approximation error we need to have a higher value of m while choosing a finite spectrum from the KL expansion in Eqn. (4.3). In the present case, the correlation length is taken to be $\mu_a = L/5$ in Eqn. (4.47) and for this, the random bending modulus EI_y is approximated with 20 random variables using the KL expansion. Figure 4.7 shows the L^2 error calculated with the mean

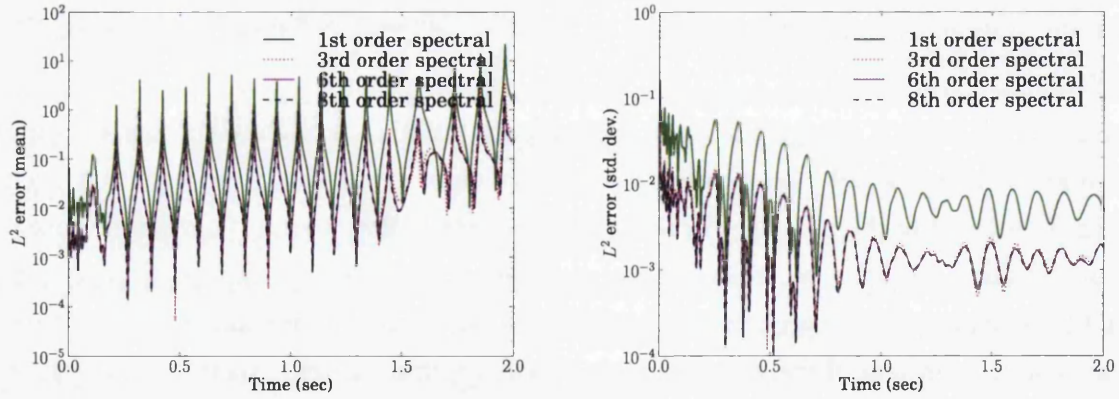

(a) L^2 mean error.

(b) L^2 standard deviation error.

Figure 4.7: L^2 relative error calculated with the mean (a) and standard deviation (b) of the cantilever beam response for different orders of expansion of the spectral functions for an input random field variability of $\sigma_a = 0.20$.

and standard deviation of the response for different orders of the spectral functions with time t for the highest value of the input randomness considered in this study ($\sigma_a = 0.20$). It can be seen that the higher order spectral functions definitely provide a better approximation of the results. The same behavior is highlighted at certain time steps, $t = 1.375$s and $t = 2.000$s, in Fig. 4.8 for different degrees of variability of input randomness $\sigma_a = \{0.05, 0.10, 0.15, 0.20\}$.

However, the higher order spectral functions have enhanced computational cost associated with them and hence has to be chosen prudently. The error norm can be used to determine a desired order of expansion for approximating the solution of the system at each time step.

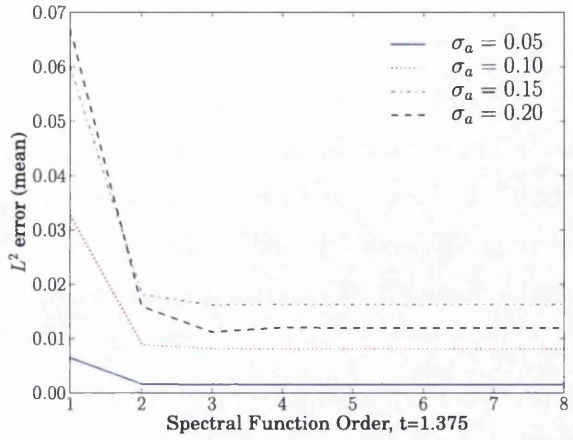

(a) L^2 error (mean).

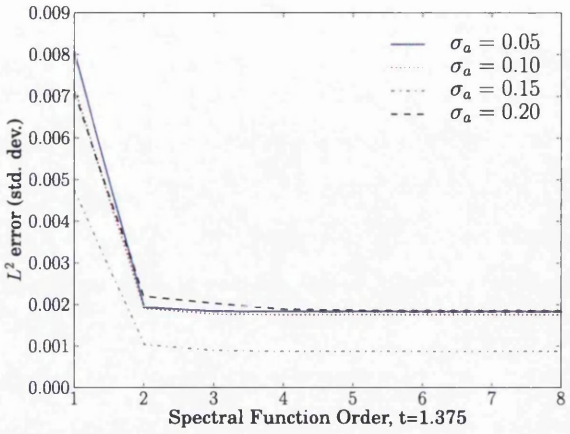

(b) L^2 error (standard deviation).

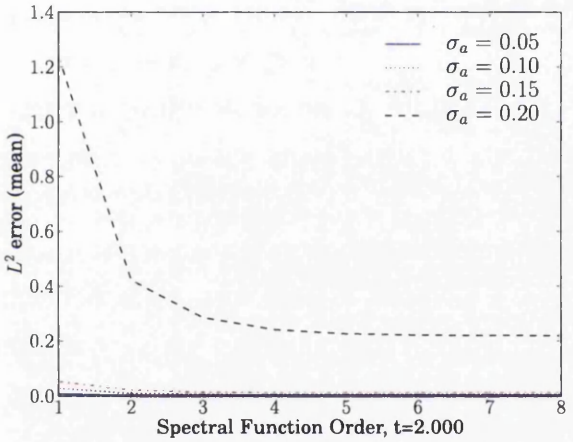

(c) L^2 error (mean).

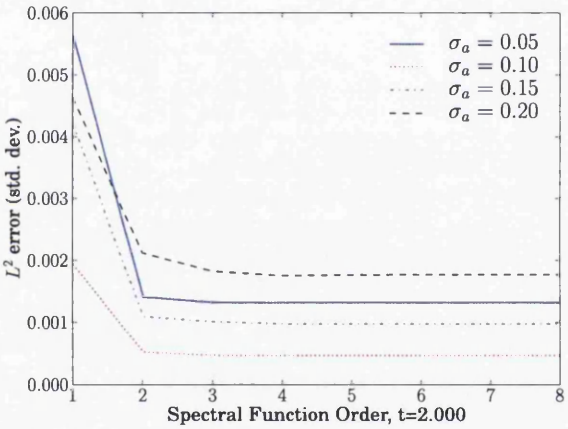

(d) L^2 error (standard deviation).

Figure 4.8: L^2 relative error calculated with the mean ((a) and (c)) and standard deviation ((b) and (d)) of the cantilever beam response at $t = 1.375$s and $t = 2.000$s for different orders of expansion of the spectral functions.

The above results show that the solution obtained using the spectral functions and a set of orthonormal vector basis functions is well-suited for obtaining the unsteady dynamic response of random structural systems, both in terms of accuracy and computational efficiency. Compared to the direct MCS solution method or the spectral Galerkin techniques, the computational cost is favorable due to the reduced order of the system and finite order approximation of the solution in the stochastic space. It is found that the estimated solution closely matches the direct MCS solution at all time steps for all values of variability of the system parameters. For the PC method, the growth in the errors on time integration has to be eliminated with enhanced order expansion of the stochastic basis which incurs a heavy computational cost. The possibility of using the parallel implementations of the iterative linear system solvers to

address the issue of computational cost is highly promising.

4.5 Summary

Two distinct solution strategies for the resolution of the transient response of stochastic dynamic systems have been proposed. In the classical spectral stochastic finite element approach, the solution is projected on to a finite set of orthonormal basis functions spanning a reduced stochastic space using a finite order of the chaos functions from the Wiener-Askey scheme. Secondly, we have proposed an efficient reduced order left-preconditioned Krylov subspace projection of the stochastic solution on to a finite set of deterministic eigen basis which are weighted by dynamic stochastic coefficient functions known as spectral functions. A single-step implicit unconditionally-stable time integration scheme has been utilized here with the integration operators being stochastic in nature. Hence the approach utilizes stochastic temporally adaptive Krylov bases.

The results obtained with the spectral function approach demonstrate good agreement with the direct MCS at all time steps and for different values of input standard deviation σ_a. The 4^{th} order PC, on the other hand, shows a rapid growth of error for long time integration and for higher order moments of the solution, which has to be addressed with higher order chaos expansions which incurs higher computational cost (as found in Table 5.2). Also, the high dimension of the linear algebraic system encountered in the PC expansion restricts the time-step size Δt of the time-integration scheme which further enhances the associated computational cost. This demonstrates the applicability and computational efficacy of the spectral function approach proposed in this work in context of unsteady dynamical response of stochastic structural systems.

The following chapter is devoted to the development of a generic stochastic finite element framework within which we can provide the description of the input random field on arbitrary shaped physical domains for any given correlation description and facilitate its easy integration with the isoparametric finite element weak formulation. This framework would be utilized to study the problem of random fluctuations of the boundary of the physical domain or the geometric uncertainties associated with it.

Chapter 5

Parametric and boundary uncertainty in diffusion systems

The preceding chapters of the thesis were devoted to the discussion of the propagation of parametric uncertainty in structural dynamic systems using a reduced spectral function approach. The input uncertainty in these structural systems was modeled with the established numerical techniques available for spectral decomposition of random fields. The physical domains in these problems were discretized with regular finite element mesh. However, many practical engineering problems are described on complicated geometries which require the use of unstructured mesh. Under this condition, a generic framework for representing the random field at discrete points in the arbitrarily shaped domains has been considered here. Moreover the integration of this discrete random field description into the weak formulation of the stochastic finite elements is addressed in this chapter.

Next, the above discretized random field representation would be utilized to express the random fluctuations of the domain boundary with nodal position coordinates and a set of random variables. The description of the boundary perturbation would be incorporated into the weak stochastic finite element formulation using a stochastic isoparametric mapping of the random domain to a deterministic master domain. A method for obtaining the linear system of equations under the proposed mapping using generic finite element weak formulation and the stochastic spectral Galerkin framework would be studied here.

5.1 Introduction

Accounting for surface roughness in the mathematical models is an important consideration for systems where random perturbations of domain topologies can have considerable impact on the accuracy of the numerical results. This phenomenon can be widely observed in nano-scale designs, high-speed flow problems, aerodynamic systems, thermal systems with boundary flux, corrosion, to mention a few. The uncertainty stems from the inability to control the

geometrical profiles of the individual components in large engineering designs or not having a accurate measurement (which might not be feasible physically/economically or due to errors) or, they can be aleatoric or epistemic in nature. Hence the problem can be conceived to be defined on a domain which has random boundaries. The boundary fluctuations have been tackled with a number of methods ranging from parametrization of surface inhomogeneities to using fractals. In the present study we resort to the probabilistic description to account for the random perturbations in the topology of the boundary surface. The framework for the solution of problems on random domains and their error bounds has been presented for Neumann [Babuška and Chleboun, 2002] and Dirichlet [Babuška and Chleboun, 2003] boundary value problems. Natural convection with sparse-grid collocation technique [Ganapathysubramanian and Zabaras, 2007], transport in rough walled tubes [Tartakovsky and Xiu, 2006], acoustic scattering from rough surfaces [Xiu *et al.*, 2007] inspired from the transformation to obtain boundary perturbations [Nicholls and Shen, 2006]. Also, random domains have been represented with fractals and studied with the MCS technique [Blyth and Pozrikidis, 2003] which turned out to be computationally expensive.

A novel framework for tackling the random boundary problems with stochastic mapping has been studied in [Xiu and Tartakovsky, 2006], where the concept of boundary conforming coordinate system [Thompson *et al.*, 1985] has been used to represent a parametrized boundary fluctuation. The approach relies on Laplace equation to represent the stochastic mapping from a baseline deterministic model (which maybe the mean model or the upper/lower bounds) to the random domain. The solution of these Laplace equations would consist of harmonic functions with a stochastic component. In contrast to this, the present work utilizes the idea of stochastic mapping onto a deterministic domain but utilizes a discrete stochastic isoparametric mapping to transform the variational weak form of the equation on the random domain onto a deterministic master domain. The method relies on mapping the perturbed realizations of the random boundary surface (or a volume adjacent to the boundary) using a finite set of iid random variables to a master element using the concept of isoparametric mapping. Thus the proposed method can be regarded as a stochastic isoparametric mapping of the perturbed elemental domains on to deterministic parent domains using a tensor product of the piecewise Lagrange polynomial functions as the spatial FE shape functions and a set of orthogonal stochastic functions. The details of the implementation and a discussion about the comparison of proposed method with that of [Xiu and Tartakovsky, 2006] has been discussed later in the manuscript.

The focus of the current work is the consideration of parametric and geometrical uncertainties in computational mechanics within the framework of the stochastic finite element method. The first part is concerned with the stochastic discretization of the random field with a finite set of random variables. The random field model is characterized by a covariance function which describes the statistical dependence of the random field across the spatial do-

main. The Karhunen-Loève (KL) expansion of the covariance function is performed using numerical methods applicable for the resolution of Fredholm integral equations of the second kind. These methods include analytical solution of the covariance function to using Galerkin type orthogonalization schemes of the error to the test function space in each element of the finite element mesh of the spatial domain [Ghanem and Spanos, 1991]. An alternative discrete KL expansion is investigated in this study where the principal spectral components of the covariance kernel is obtained by solving a simple eigenvalue problem of the covariance matrix constructed at the discrete set of points on the spatial domain. The resulting discrete formulation is interpolated inside the element domain at the quadrature integration points using finite element shape functions. The error analysis shows satisfactory convergence behavior for varying mesh sizes and correlation lengths of the random field.

The chapter is organized as follows. In Sec. 5.2 we discuss the random field model used to describe the uncertain parameter along with the methods of expressing the random field using various series expansion techniques with a set of random variables. Following this we present the motivation and the methodology to use numerical methods for the resolution of the covariance function in Sec. 5.3. Subsequently we present a discussion of the Galerkin type spectral decomposition technique of the covariance function using the finite element shape functions. This is followed by a small discussion on discretizing the lognormal field with closed form expressions of the coefficients of the stochastic terms. Section 5.4 gives the method to incorporate the discrete representation of the random field into the weak form of the SPDE for a steady state diffusion problem and the stochastic spectral Galerkin method of solving the system. Section 5.5 presents the description of the boundary roughness and the stochastic isoparametric mapping of the weak formulation from the random domain to the deterministic parent domain. Following this the solution methodology is discussed. Section 6.4 demonstrates the proposed techniques for the spectral decomposition of the random field with numerical examples and error analysis. This is followed by the numerical examples to demonstrate the random boundary problem for transient stochastic systems. Section 5.8 lists the principal conclusions that can be drawn from this work and the direction of future research.

5.2 Finite dimensional random field representation

The probabilistic description of the random field has been discussed in detail in Sec. 1.2.1 and the methods used for a finite dimensional representation of this random field is given in Sec. 2.2.1. In the following section we discuss the numerical methods employed to represent the random field on the finite element mesh in a generic manner on arbitrary shaped spatial domains.

5.3 Numerical methods for spectral decomposition of the covariance function

The KL expansion presented in Eqn. (2.11) represents the random parameter with a finite number of random variables weighted by the spatial eigen-basis which are evaluated from the decomposition of the covariance kernel. However, exact solutions of the Fredholm integral equations of the second type, Eqn. (2.6), are available for a few specific types of covariance kernels and a few special geometries. A number of solutions of the decomposition of the covariance kernel for one-dimensional domains have been given in [Ghanem, 1989]. However, analytical methods of decomposition of the kernel function is not available for complicated generalized spatial domains and numerical methods have to be employed to tackle such problems. Hence we present here a solution technique which solves the spectral decomposition of the covariance kernel at discrete set of points on the physical domain.

5.3.1 Discrete Karhunen-Loève expansion

If we consider the various geometrical configurations shown in Fig. 5.1, we see that there are a number of possible definitions of the correlation length associated with the covariance kernel description. For example the 'red' colored lines denote the L^2 length between points P_1 and P_2 while the 'blue' lines denote a length defined along the geometry which would be considered as an L^1 norm. The resolution of the KL expansion for such varied kinds of geometry might result in discontinuous eigenfunctions which cannot be described with closed form analytical functions. Additionally, we should also take into account the discrete index based correlation of the various parameters (such as angles, widths and heights of corrugation in Fig. 5.1(c) across the length of the panel) and include them within the covariance description of the random field.

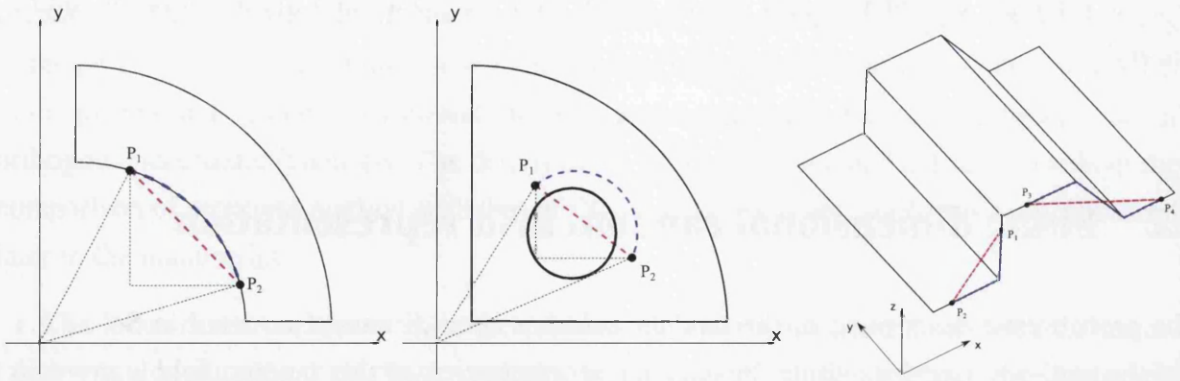

(a) Configuration 1 (b) Configuration 2 (c) Configuration 3

Figure 5.1: Different geometrical configurations highlighting the various possible definitions of the correlation length of the random field.

Recalling the discussion presented in Sec. 2.2.1, the covariance function defined as $\mathscr{C}_a\varphi = (\mathscr{C}_a\varphi)(\mathbf{r}_1) = \int_{\mathscr{D}} C_a(\mathbf{r}_1, \mathbf{r}_2)\varphi(\mathbf{r}_2)d\mathbf{r}_2 \quad \mathbf{r}_1, \mathbf{r}_2 \in \mathscr{D}$ is seen to be linear operator $\mathscr{C}_a : L^2(\mathscr{D}) \rightarrow L^2(\mathscr{D})$ on a vector space. Hence the integral equation in Eqn. (2.6) can be written as

$$\mathscr{C}_a\varphi = \nu\varphi \tag{5.1}$$

Non-trivial solutions of the above homogeneous equation exists only for those values of ν which makes $(I - \nu\mathscr{C}_a)$ non-invertible, I being the identity operator. It is possible to represent the random field using a finite number of dominant components based on the eigen spectrum of the kernel in Eqn. (5.1).

Here we start by discretizing the spatial domain on which the solution of the integral equation is sought. Commonly, the spatial domain is discretized with the finite element nodes and hence the random parameter can be expressed on them with the vector $\mathbf{a}(\theta) : \mathscr{D} \times \Theta \rightarrow \mathbb{R}^n$ where n is the number of FE nodes. The covariance matrix is hence defined as

$$C_{\mathbf{a}} = \mathbb{E}\left[(\mathbf{a}(\theta) - \bar{\mathbf{a}}_0)(\mathbf{a}(\theta) - \bar{\mathbf{a}}_0)^T\right] \quad \text{where} \quad C_{\mathbf{a}} \in \mathbb{R}^{n \times n} \tag{5.2}$$

Here $C_{\mathbf{a}}$ is a Hermitian matrix with identical diagonal terms.

For stationary random fields and a *uniformly spaced finite element mesh* over a one dimensional spatial domain, it is easy to see that the discrete covariance matrix $C_{\mathbf{a}}$ is a *Toeplitz matrix* where the entries are constant along the diagonals parallel to the main diagonal. This property can be used efficiently to improve the memory requirement to store a dense covariance matrix, where the entire covariance matrix can be stored with as few as $2n + 1$ elements (compared to the $n(n + 1)/2$ elements required for just symmetric matrices) and a set of 'forward shift' and 'backward shift' matrices which are matrices with all elements of the super-diagonal and sub-diagonal set to 1 respectively and zeros everywhere else. The case of evaluating the spectral components of a 2D discrete covariance matrix has been investigated in [Graham *et al.*, 2011] where lexicographic ordering of points has been used in the 2D case and an FFT method is utilized to obtain the eigen components.

However, the spatial domains $\mathscr{D} \in \mathbb{R}^n$, where $n \geq 1$, with a non-uniform mesh would not lead to a Toeplitz matrix of spatially discretized covariance matrices. Hence the eigenvalue problem in Eqn. (5.1) becomes more expensive. We apply Lanczos iterative techniques to solve for the largest eigenvalues, and write the expression for the rank-m approximation of the covariance operator as

$$\mathscr{C}_a^{(m)} = \Phi\Lambda\Phi^T \quad \text{where} \quad \Phi \in \mathbb{R}^{n \times m} \quad \text{and} \quad \Lambda = \text{diag}\,[\lambda_1, \ldots, \lambda_m] \tag{5.3}$$

where Φ is the matrix of eigenvectors and Λ is the diagonal matrix of eigenvalues. The above equation holds true for any positive continuous semidefinite kernel on a finite interval

due to Mercer's theorem. Only the first few largest eigen components are utilized in (5.3), where $\lambda_1 \geq \ldots \geq \lambda_m$. This suggests that the covariance kernel is approximated with the desired accuracy using the eigen functions obtained from Eqn. (5.3). When the correlation length of the random field on the spatial domain is small, higher eigen modes have to be incorporated into the random field approximation. These modes have complex shapes which implies the necessity of higher mesh resolution to capture their behavior. Also, Kolmogorov's theorem [Adler, 1981] implies that the realizations of the random fields $a(\mathbf{r}, \theta)$ are Holder continuous with respect to $\mathbf{r}$ (with Hölder exponent $\alpha < 1/2$) with probability 1. Hence the random vectors can be quite irregular. The choice of the discrete points in the spatial domain is crucial in this discussion, since the computational cost of resolving the eigenvalue problem of Eqn. (5.1) directly depends on the size of the covariance matrix while the accuracy requirements may necessitate a high mesh resolution. When the finite element nodes are chosen as the discrete points in space, the random field is obtained as $\mathbf{a}(\theta) \in \mathbb{R}^{n_h}$ where n_h is the dimension of the linear system based on the finite element mesh parameter size h. The random parameter vector at discrete points in the spatial domain is thus represented as

$$\mathbf{a}(\theta) = \mathbf{a}_0 + \sum_{i=0}^{M} \phi_i \sqrt{\lambda} \xi_i(\theta) \tag{5.4}$$

where $\mathbf{a}_0$ is the vector of the deterministic parametric field over the spatial domain while $\mathrm{diag}(\xi(\theta))$ is a diagonal matrix of independent random variables $\xi = \{\xi_1, \ldots, \xi_M\}$. It might be mentioned that the covariance matrix may be chosen to be on the quadrature integration points in the spatial domain which are employed in the weak formulation. This will be discussed in more detail in the next section.

5.3.2 Spectral decomposition of the covariance kernel with Galerkin formulation

In this section, we present the solution methodology of the Fredholm integral equation of the second type with a Galerkin error orthogonalization technique. The solution methodology presented in Sec. 5.3.1 is quite efficient and straight forward in terms of the numerical implementation. The resulting coefficient matrix is a fully populated symmetric matrix. However, if higher order isoparametric elements are used on a coarse finite element mesh, the error accumulated in the formation of the discrete KL eigenvectors might increase. This might be undesirable in applications which require highly accurate models of the random system matrices. Hence we discuss here an alternative, where the spatial interpolation functions in the element geometry are utilized to solve the KL expansion and which was forwarded in [Ghanem and Spanos, 1991]. We point out though, that while the method results in an enhanced accuracy of the approximate solution at the cost of additional numerical complexity

to form the linear systems required for the eigenvalue problem, it offers no benefits in terms of the memory requirement or using an efficient algorithm to resolve the dominant eigen modes of the covariance functions. This would be obvious in the discussions presented in the subsequent paragraphs.

The objective here is to obtain the solution of the Fredholm integral equation using the finite element mesh as well as the spatial interpolation functions employed to construct the system matrices. If we define the collection of the set of elements as $\mathscr{E} = \{\Delta(\mathscr{D})_h : h \text{ is the mesh parameter size}\}$ then the integral equation in Eqn. (2.6) can be rewritten as

$$\sum_{k\in\mathscr{E}_m} \int_{\Omega_k^e} C_a(\mathbf{r}_{1_k}, \mathbf{r}_2)\phi_j(\mathbf{r}_{1_k})d\mathbf{r}_{1_k} = \nu_j\phi_j(\mathbf{r}_2); \quad \mathbf{r}_{1_k} \in \Omega_k^e, \quad \mathbf{r}_2 \in \mathscr{D} \quad \forall\, j = 1, 2, \ldots \tag{5.5}$$

where the integration has been split up into integrations over each elemental domain Ω_k^e and $\mathscr{E}_m$ is the cardinality of the set $\mathscr{E}$. Here each of the integrations can be carried out separately and finally the system can be assembled to obtain the realization of $\phi(\mathbf{r})$ over the entire domain. This is the general framework within which the FE system is resolved to obtain the solution vector at the nodal points. We approximate the eigenfunctions $\phi(\mathbf{r})$ in each element domain as $\phi(\mathbf{r}) = \sum_i \mathscr{N}_i(\mathbf{r})\widetilde{\phi}_i = [\mathscr{N}(\mathbf{r})]^T\{\widetilde{\phi}\}$ where $[\mathscr{N}(\mathbf{r})]$ is the vector of the FE shape functions of a chosen degree based on the order of the elements and $\{\widetilde{\phi}\}$ is a vector of the functional values of ϕ at the discrete finite element node points.

Thus Eqn. (5.5) can be rewritten in terms of the residual ε as

$$\varepsilon(\mathbf{r}_2) = \sum_{k\in\mathscr{E}_m} \int_{\Omega_k^e} C_a(\mathbf{r}_{1_k}, \mathbf{r}_2)[\mathscr{N}(\mathbf{r}_{1_k})]^T\{\widetilde{\phi}\}_k d\mathbf{r}_{1_k} - \nu_j\phi_j(\mathbf{r}_2) \tag{5.6}$$

A Galerkin error orthogonalization is hence applied where the residual in the above equation is made orthogonal to the interpolation/shape functions $[\mathscr{N}]$ i.e. $\varepsilon \perp \mathscr{N}_i, \quad \forall\ i$ on every element $\Delta(\mathscr{D})_h$. This gives,

$$\sum_{k\in\mathscr{E}_m} \int_{\Omega_p^e}\int_{\Omega_k^e} [\mathscr{N}(\mathbf{r}_{2_p})]C_a(\mathbf{r}_{1_k}, \mathbf{r}_{2_p})[\mathscr{N}(\mathbf{r}_{1_k})]^T\{\widetilde{\phi}\}_k d\mathbf{r}_{1_k}d\mathbf{r}_{2_p} =$$

$$\nu_j \int_{\Omega_p^e} [\mathscr{N}(\mathbf{r}_{2_p})][\mathscr{N}(\mathbf{r}_{2_p})]^T\{\widetilde{\phi}\}_p d\mathbf{r}_{2_p} \quad \forall p \in \mathscr{E}_m \tag{5.7}$$

The above integral equation would gives a linear system from which the principal eigen modes of the covariance function can be determined. A closer look reveals that in contrast to the finite element system assembly, this method produces element matrices which, during the assembly process, occupy square sub-blocks along a particular row block of the FE linear system. For example, for a given value of p in the above equation, if we look at the element matrix $\mathbf{a}^e$ for the element k which has n_e nodes, then the linear system $\mathbf{A}$ is assembled as

such that, $\mathbf{A}[\text{ix\_}(n_{pk}, n_{pk})] \leftarrow \mathbf{a}^e_{pk}$

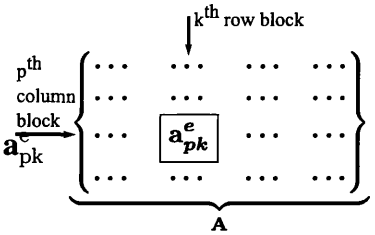

The above graphical representation of course assumes that the nodes of the k-th element are numbered consecutively. It has been used to highlight the assembling procedure where the individual element level matrices obtained from successive calculations for a particular value of p using Eqn. (5.7) are placed across the columns of the p^{th} row sub-block. Thus we have a fully populated coefficient matrix. Thus there is no benefit in terms of the memory requirement associated with this method when compared to the discrete KL expansion presented in Sec. 5.3.1.

Another method to evaluate the above integral may be to approximate the covariance kernel inside the element domain with the spatial shape functions. Let $C^e_{a_{pk}} \in \mathbb{R}^{n_e \times n_e}$ be the covariance function constructed between the elements p and k. The approximation of this function within these elemental domains is given as

$$C_e^{a_{pk}}(\mathbf{r}_{1_k}, \mathbf{r}_{2_p}) = [\mathcal{N}(\mathbf{r}_{1_k}) \otimes \mathcal{N}(\mathbf{r}_{2_p})] : \mathcal{C}^e(r_i, r_j) = [\mathcal{N}(\mathbf{r}_{2_p})]^T \mathcal{C}^e(r_{i_k}, r_{j_p})[\mathcal{N}(\mathbf{r}_{1_k})] \quad (5.8)$$

where $\mathcal{C}(r_i, r_j)$ is the discrete covariance matrix of the random parameter constructed at the nodal points. The above equation can be incorporated into the Galerkin framework from which we would obtain the nature of the element level sub-blocks as

$$\begin{aligned}\mathbf{a}^e_{pk} &= \int_{\Omega^e_p}\int_{\Omega^e_k} [\mathcal{N}(\mathbf{r}_{2_p})][\mathcal{N}(\mathbf{r}_{2_p})]^T \mathcal{C}^e(r_{i_k}, r_{j_p})[\mathcal{N}(\mathbf{r}_{1_k})][\mathcal{N}(\mathbf{r}_{1_k})]^T d\mathbf{r}_{1_k} d\mathbf{r}_{2_p} \\ &= \underbrace{\left(\int_{\Omega^e_p} [\mathcal{N}(\mathbf{r}_{2_p})][\mathcal{N}(\mathbf{r}_{2_p})]^T d\mathbf{r}_{2_p}\right)}_{\mathbf{M}^e_p} \mathcal{C}^e(r_{i_k}, r_{j_p}) \underbrace{\left(\int_{\Omega^e_k} [\mathcal{N}(\mathbf{r}_{1_k})][\mathcal{N}(\mathbf{r}_{1_k})]^T d\mathbf{r}_{1_k}\right)}_{\mathbf{M}^e_k} \end{aligned} \quad (5.9)$$

where the integration of the shape functions with the above form leads to element mass matrices (with unit mass density). Hence the element matrix can be written as

$$\mathbf{a}^e_{pk} = \mathbf{M}^e_p \mathcal{C}^e(r_{i_k}, r_{j_p}) \mathbf{M}^e_k \quad (5.10)$$

Thus the global system matrix can be constructed with the elements of the mass matrix. It is to be noted however that the global stiffness operator is not of the simple form $\mathbf{A} = \mathbf{M}\underline{\underline{\mathcal{C}}}\,\mathbf{M}$, rather it is a 'dyadic' combination of the 'vector' of block element mass matrices like $\mathbf{M}_v = [\mathbf{M}^e_1, \mathbf{M}^e_2, \ldots, \mathbf{M}^e_{n_m}]^T$ where n_m is the number of elements in the mesh. The global linear system is a fully populated symmetric matrix, as is the case with the method proposed in Sec. 5.3.1.

The right side of Eqn. (5.7) is however just the mass matrix $\mathbf{M}$ which is sparse and symmetric in nature. Taking these expressions together we have the linear system of the form

$$\mathbf{A}\phi = \nu\mathbf{M}\phi \tag{5.11}$$

which is a generalized eigenvalue problem and would give a set of n eigen pairs where n is the total number of degrees of freedom of the system. The rate of decay of the eigenvalues depends on the chosen correlation length of the random field and the description of the random field which is studied in detail in the subsequent sections. Since the formation of the element level matrices requires the evaluation of the elemental mass matrices, all of the classical FE formulation (such as the isoparametric formulation for arbitrary element shape and geometry) are applicable here. The eigenvalue problem in Eqn. (5.11) involves a dense matrix $\mathbf{A}$ which maybe quite expensive for large systems. Lanczos type iterative techniques can be applied here to evaluate the largest eigen modes of the system quite similar to the one discussed in context of the discrete KL expansion in Sec. 5.3.1.

Discrete representation of the lognormal field model

The Gaussian random field models, while offering an easier scheme for computational implementation, is often unsuitable for modeling the uncertainty for those physical systems where the parametric variation has to be considered strictly positive to make any practical sense. Under such circumstances, the lognormal field is generally the favored distribution and has been adopted in the present work. The discrete KL expansion framework laid out in the previous sections can easily be extended to incorporate this kind of random field distributions. A lognormal field of the discretized random field $\mathbf{a}_l(\theta) \in \mathbb{R}^n \times \Theta^{(M)}$ is expressed as the exponential of the corresponding Gaussian field model $\mathbf{a}(\theta)$. Following from the discretized KL expansion in Eqn. (5.4)

$$\mathbf{a}_l(\theta) = \exp\left(\bar{\mathbf{a}}_0 + \sum_{i=1}^{M} \xi_i(\theta)\widetilde{\mathbf{a}}_i\right) \tag{5.12}$$

where $\xi = \{\xi_1, \ldots, \xi_M\}$ is the vector of iid Gaussian random variables. To make the above expression computationally favorable, the lognormal field is often expressed as a finite order multivariate expansion of the basic iid random variables from the Wiener-Askey scheme. When the basic iid random fields are Gaussian in nature, the polynomial expansion of the lognormal field is

$$\mathbf{a}_l = \sum_{i=0}^{m} \mathbf{a}_i^l \mathscr{H}_i(\boldsymbol{\xi}(\boldsymbol{\theta})) \quad \text{where} \quad \mathbf{a}_i^l = \frac{\langle \mathbf{a}_l(\boldsymbol{\theta}), \mathscr{H}_i(\boldsymbol{\xi}(\boldsymbol{\theta}))\rangle_{L^2(\Theta^{(M)}, dP_\xi)}}{\langle \mathscr{H}_i(\boldsymbol{\xi}(\boldsymbol{\theta}))\rangle^2_{L^2(\Theta^{(M)}, dP_\xi)}} \tag{5.13}$$

where $\mathscr{H}_i(\xi(\theta))$ are the multivariate Hermite polynomials spanning the stochastic space $\theta \in \Theta^{(M)}$ and $\langle \cdot, \cdot \rangle_{L^2(\Theta^{(M)}, dP_\xi)}$ denotes the inner product in the same space. The value of m is

guided by the dimension of the input polynomial space M and the chosen order of expansion p as $m = \binom{M+p}{p}$. The L^2 norm of the Hermite polynomials are easily available generally pre-computed and fed into the solver. The inner products essential for the evaluation of the numerator in Eqn. (5.13) can be computed using the analytical expression applicable for Gaussian fields as

$$\mathbf{a}_i^l = \exp\left(\bar{\mathbf{a}}_0\right) \prod_{i=1}^{M} \exp\left(\widetilde{\mathbf{a}}_i^2\right) \frac{\mathscr{H}_i^{hd}\left(\widetilde{\mathbf{a}}_1, \ldots, \widetilde{\mathbf{a}}_M\right)}{\left\langle \mathscr{H}_i(\xi(\theta)) \right\rangle^2_{L^2(\Theta^{(M)}, dP_\xi)}} \tag{5.14}$$

where $\mathscr{H}_i^{hd}\left(\mathbf{a}_1, \ldots, \mathbf{a}_M\right)$ denotes the highest order term associated with the i^{th} Hermite polynomial and the arguments are replaced by the coefficients of the random variables (which are the eigen modes obtained from the discretized KL expansion) instead of the random vector $\xi = \{\xi_1, \ldots, \xi_M\}$ itself. The proof of this has been provided in Appendix A.1. This provides an efficient analytical way to compute the undetermined coefficients associated with the log-normal random field given in Eqn. (5.13) instead of a multi-dimensional integration in the stochastic subspace for each coefficient.

5.4 Stochastic weak formulation with discrete random parameter

Here we consider the finite element spaces associated with the spatial and stochastic dimensions of the randomly parametrized system laid out in the previous sections. The spatial set $\mathscr{D} \in \mathbb{R}^d$ and the set of random outcomes modeled in the finite dimensional stochastic space $\Theta^{(M)} \subset \Theta$ will be used to define the tensor product space $\mathscr{D} \times \Theta^{(M)}$ where the solution to the stochastic weak formulation is sought.

5.4.1 Finite element spaces

The spaces involved in the construction of the stochastic finite element method (SFEM) for the stochastic weak formulation is presented in [Babuška *et al.*, 2005b] which gives two paradigms in which the solution of the above problem is sought: a) the $k \times h$-SFEM version and the b) the $p \times h$-SFEM version. We consider these in detail here: let the spatial domain $\mathscr{D}$ be meshed as $\Delta(\mathscr{D})$ such that mesh parameter size is given by $h(\Delta(\mathscr{D}))$. The finite dimensional stochastic domain may be partitioned with a finite number of disjoint boxes having finite intervals along each dimension and we denote this rectangular mesh as $\Delta(\Theta^{(M)}) = \Delta(\Theta_1) \times \ldots \times \Delta(\Theta_M)$ with the mesh parameter size k defined as the maximum interval size along a stochastic dimension. Thus the mesh on the tensor product space is denoted as $\Delta(\mathscr{D}, \Theta^{(M)})$ and the elements as $\tau(\Delta(\mathscr{D}, \Theta^{(M)})) = \tau(\Delta(\mathscr{D})) \times \tau(\Delta(\Theta^{(M)}))$. The

approximating functions on this tensor product space is given by the set

$$S^{p,q}(\mathscr{D},\Theta^{(M)}) = \Big\{ v(\mathbf{r},\xi) \in W | v(\mathbf{r},\xi)|_{\tau(\Delta(\mathscr{D},\Theta^{(M)}))} \text{ is a polynomial of degree } p \text{ in } \mathbf{r}, \\ \forall\, \xi \in \theta \text{ and of degree q in } \xi, \forall \mathbf{r} \in \mathscr{D} \Big\}, \tag{5.15}$$

$$\text{where} \quad W|v(\mathbf{r},\xi)|_{\mathscr{D},\Theta^{(M)}} = \Big\{ v(\mathbf{r},\theta) : \int_{\Theta^{(M)}} \|v(\mathbf{r},\xi)\|_{L^2(\mathscr{D})}\, dP_\xi(\theta) \leq \infty, \\ \theta \in \Theta^{(M)} \text{ and } v(\mathbf{r},\xi) = 0 \text{ on } \partial\mathscr{D},\ \forall \xi \in \theta \Big\} \tag{5.16}$$

is the space of polynomials which converge in the $L^2\left(\Theta^{(M)}, dP_\xi; \mathscr{D}\right)$ sense. The definition of the L^2 norm depends on the physical problem at hand (for example, when we have an elliptic stochastic differential operator, $\|v(\mathbf{r},\xi)\|_{L^2(\mathscr{D})} = \int_{\Delta(\mathscr{D})} a(\mathbf{r},\theta)\, |\nabla_{\mathbf{r}} v(\mathbf{r},\xi)|^2\, d\mathbf{r}$). The assumptions on the chosen random parameter $a(\mathbf{r},\theta)$ and its joint probability distribution renders W a Hilbert space. For the standard deterministic finite elements, the weak form of the governing partial differential equations is stated as: $b(u(\mathbf{r}), v(\mathbf{r})) = l(v(\mathbf{r}))\ \forall v \in L^2(\mathscr{D})$ where u is the solution that is sought, v consists of the test functions in the admissible L^2 space and b and l are the continuous bilinear and linear forms respectively on the spatial domain $\mathbf{r} \in \mathscr{D}$. Thus the bilinear and linear forms associated with the weak stochastic FE formulation is written as

$$\begin{aligned} \mathscr{B}(u,v) &= \int_{\Theta^{(M)}} b(u(\mathbf{r},\theta), v(\mathbf{r},\theta);\theta) dP_\xi(\theta); \\ \mathscr{L}(v) &= \int_{\Theta^{(M)}} l(v(\mathbf{r},\theta);\theta) dP_\xi(\theta) \\ \text{so that,} \quad \mathscr{B}(u,v) &= \mathscr{L}(v) \end{aligned} \tag{5.17}$$

The basic finite element theory ensures the existence and uniqueness of the solution $u_{S^{p,q}} \in S^{p,q}(\mathscr{D},\Theta^{(M)})$ and the convergence to the actual solution as

$$\begin{aligned} & \|u - u_{S^{p,q}}\|_{W(\mathscr{D},\Theta^{(M)})} \to 0 \ \text{ as } \ h(\Delta(\mathscr{D}))\ ,\ k(\Delta(\Theta^{(M)})) \to 0 \\ \text{and} \quad & \|u - u_{S^{p,q}}\|_{W(\mathscr{D},\Theta^{(M)})} \to 0 \ \text{ as } \ p,q \to \infty \end{aligned}$$

The above equations stand for the convergence of the h-version and the p-version of the SFEM respectively. The $p \times h$-SFEM seeks the solution in tensor product space $\Theta^{(M),q} \otimes \Delta(\mathscr{D}_h)$ and produces exponential convergence of the solution with p [Babuška *et al.*, 2004]. We consider here this latter version of the weak formulation where the input stochastic space has been discretized with a finite set of independent identically distributed random variables and the solution at the nodal points in the discretized spatial domain is expressed with a finite p-th order polynomial function of the random variables.

5.4.2 Description of the stochastic steady-state diffusion problem

Let us consider here steady-state diffusion problem on an arbitrary-shaped domain in the three dimensional space and the diffusion coefficient K is assumed to be uncertain. If we consider the heat transport problem then K becomes the thermal diffusivity. The governing partial differential equation of the steady state diffusion problem along with the Dirichlet boundary conditions may be written as

$$\nabla\left(K(\mathbf{r};\theta)\nabla u\right) = Q(\mathbf{r}) \quad \text{and} \quad u = 0 \ \text{ on } \ \partial\mathscr{D} \tag{5.18}$$

where Q is the source/sink term in the domain. When formulating the weak form of the above system at a particular point in the stochastic sample space θ, we have

$$\begin{aligned} b(u,v;\theta) &= l(v;\theta) \quad \text{where} \\ b(u,v;\theta) = \int_{\mathscr{D}} K(\mathbf{r};\theta)(\nabla v)\cdot(\nabla u)d\mathscr{D}; &\quad \text{and} \quad l(v;\theta) = \int_{\mathscr{D}} vQd\mathscr{D} \end{aligned} \tag{5.19}$$

Here $K(\mathbf{r},\theta)$ is modeled with a finite set of random variables following the discrete KL-expansion (detailed in section 5.3.1) of the covariance kernel associated with the random field on the domain such that

$$\boldsymbol{K(\theta)} = \overline{K}_0 + \sum_{j=1}^{m} \mathscr{H}_j(\boldsymbol{\xi(\theta)})\boldsymbol{K_j}; \quad \boldsymbol{\overline{K}_0, K_j} \in \mathbb{R}^{n\times n} \tag{5.20}$$

is expressed by its mean $\overline{K}_0$ and perturbation components K_j in the series expansion form. The spatial discretization of the random parameter may be performed using the same mesh that is used for the resolution of the response of the finite element system, i.e. $\Delta(\mathscr{D})$, and the vector $K(\theta)$ are the parameter values at the finite element nodes. Here we introduce the following finite element discretization spaces: i) $\bar{X}^q(\Theta^{(M)}) \subset L^2(\Theta^{(M)})$ such that $\bar{X}^q(\theta_i) \subset L^2(\theta_i)$ consists of up to q-th order polynomials in $L^2(\theta_i)$ and $\bar{X}^q(\Theta^{(M)}) = \bigotimes_{i=1}^{M} \bar{X}^2(\theta_i)$ where $\bar{X}^2(\theta_i)$ consists of all square integrable functions in θ_i with $\Theta^{(M)} = \prod_{i=1}^{M}\theta_i \subset \mathbb{R}^M$ and the probability density support $P(\xi) = \prod_{i=1}^{M} P(\xi_i)$ $\xi_i \in \theta_i$ $\forall i$ and ii) $H_0^1(\Delta(\mathscr{D}_h))$ consists of all functions which vanishes on the boundary with the norm $\|v\| = \left\{\int_{\Delta(\mathscr{D})} |\nabla v|^2 \, d\mathbf{r}\right\}^{1/2}$. Thus the approximation space of the test functions v_e in $\Theta^{(M),q} \times \Delta(\mathscr{D}_h)$, which is meshless in $\Theta^{(M)}$, for the weak form is given as

$$\begin{aligned} \bar{X}^q(\Theta^{(M)}) \otimes H_0^1(\Delta(\mathscr{D}_h)) = \big\{ v_e = v_e(\mathbf{r},\xi) \in L^2(\Theta^{(M)} \times \Delta(\mathscr{D}_h)) : \\ v_e \in \text{span}\left(\mathscr{N}(\mathbf{r}_h)\mathscr{H}(\xi(\theta)) : \mathscr{N} \in H_0^1, \mathscr{H} \in \bar{X}^q\right)\big\} \end{aligned} \tag{5.21}$$

where $\Delta(\mathscr{D}_h)$ denotes the mesh with the mesh parameter size h. This corresponds to the

$p \times h$-SFEM version. We expand the solution in each discretized element $\Theta^{(M),q} \otimes \Delta(\mathscr{D}_h)$ as

$$u_e(\mathbf{r}_h, \theta) = \sum_{i=1}^{n_e} u_i^{q,M}(\theta) \mathcal{N}_i^p(\mathbf{r}_h); \quad \mathbf{r}_h \in \tau(\Delta(\mathscr{D})), \quad \theta \in \Theta^{(M),q} \tag{5.22}$$

where p and q denote the order of the polynomials of the spatial and stochastic basis functions respectively, M is the dimension of the input stochastic space, h is the mesh size parameter and $\mathcal{N}_i^p(\mathbf{r}_h)$ are the multidimensional Lagrange basis functions of order p on $\mathbf{r}_h$. For the $p \times h$-SFEM we have the vector of random coefficients $\mathbf{u}_e^{q,M}(\theta) = \{u_1^{q,M}, \ldots, u_{n_e}^{q,M}\}$ expressed with polynomial functions $\mathscr{H}(\xi(\theta))$ of the input iid random variables. Here $\mathbf{u}_e^{q,M} \in \mathbb{R}^{n_e}$ where n_e is the number of nodes associated with each element of the FE mesh.

The vector of the random parameter values at the nodal points is interpolated inside the spatial domain of the elements using the deterministic finite element shape functions which are the basis functions for the expansion of the stochastic system response in the spatial domain i.e. $\mathcal{N}_i^p(\mathbf{r}_h)$. The random parameter has already been expressed in the stochastic domain with the global stochastic polynomial basis as per Eqn. (5.4). Then the stochastic bilinear operator associated with the weak form on each individual spatial element of the finite element mesh $\Delta(\mathscr{D})$ and the global stochastic function space $\Theta^{(M)}$ may be written as (following from Eqns. (5.17) and (5.19))

$$\mathscr{B}_{\Theta^{(M),q} \otimes \Delta(\mathscr{D}_h)}(u_e, v_e) = \int_{\Theta^{(M)}} \int_{\Delta(\mathscr{D}_h)} [\mathcal{N}^p(\mathbf{r}_h)]^T [K_e(\theta)] (\nabla v_e) \cdot (\nabla u_e) d\mathscr{D} dP_\xi(\theta) \tag{5.23}$$

where $[\mathcal{N}^p] = \{\mathcal{N}_1^p, \ldots, \mathcal{N}_P^p\}$ is the vector of the spatial basis functions (of order p) and $[K_e(\theta)]$ is the vector of the random parameter at the nodal points belonging to the element $\tau(\Delta(\mathscr{D}_h))$. The linear form accordingly becomes

$$\mathscr{L}_{\Theta^{(M),q} \otimes \Delta(\mathscr{D}_h)}(v_e) = \int_{\Theta^{(M)}} \int_{\Delta(\mathscr{D}_h)} v_e Q(\mathbf{r}_h) d\mathscr{D} dP_\xi(\theta) \tag{5.24}$$

The element level equations take the following form

$$\mathscr{B}_{\Theta^{(M),q} \otimes \Delta(\mathscr{D}_h)}(u_e, v_e) = \mathscr{L}_{\Theta^{(M),q} \otimes \Delta(\mathscr{D}_h)}(v_e) \tag{5.25}$$

The perturbation matrices of the finite element system are then given as

$$\mathbf{A}_i^{(e)} = \sum_{i=1}^{d} \int_{\Delta(\mathscr{D}_h)} [\mathcal{N}^p(\mathbf{r}_h)]^T [K_{e,i}] \left[\frac{\partial \mathcal{N}^p(\mathbf{r}_h)}{\partial \eta_i}\right] \left[\frac{\partial \mathcal{N}^p(\mathbf{r}_h)}{\partial \eta_i}\right]^T d\mathscr{D} \tag{5.26}$$

where d denotes the dimension of the Euclidean space in which the physical domain of the problem exists, i.e. $\mathscr{D} \subset \mathbb{R}^d$, η_i is the i^{th} coordinate axes in the same Euclidean space, and $K_{e,i}$ is the i^{th} term in the series expansion of the random parameter following Eqn. (5.4).

Equation (5.26) can be extended to include the linear or isoparametric mapping for a spatial domain meshed with non-uniform elements. For example, if we consider the mapping of the Cartesian coordinate axes η_i to the parameter space, we have

$$\eta_i = Q_i\left(\widetilde{\eta}_1, \ldots, \widetilde{\eta}_d\right) \quad \forall i = 1, \ldots, d; \quad \text{and} \quad \Delta(\mathscr{D}_h) = \bar{\mathbf{Q}}\left(\Delta(\mathbf{D})\right) \tag{5.27}$$

where $\widetilde{\eta} = \{\widetilde{\eta}_1, \ldots, \widetilde{\eta}_d\}$ are the set of parent axes with $\Delta(\mathbf{D})$ being the parent hypercube onto which the elements $\Delta(\mathscr{D}_h)$ are mapped using the transformation $\bar{\mathbf{Q}}$. The system matrices can then be written in terms of the isoparametric integration as

$$\mathbf{A}_i^{(e)} = \sum_{i=1}^{d} \int_{\Delta(\mathbf{D})} [\mathcal{N}^p(\widetilde{\eta})]^T [K_{e,i}] \left[\frac{\partial \mathcal{N}^p(\widetilde{\eta})}{\partial \eta_i}\right] \left[\frac{\partial \mathcal{N}^p(\widetilde{\eta})}{\partial \eta_i}\right]^T |\mathbf{J}(\widetilde{\eta})| \, d\mathbf{D} \tag{5.28}$$

$$\text{where} \quad J_{ij}(\widetilde{\eta}) \stackrel{\text{def}}{=} \frac{\partial \eta_i}{\partial \widetilde{\eta}_j} \quad \forall i, j \in [1, \ldots, d]$$

i.e. $|\mathbf{J}(\widetilde{\eta})|$ is the determinant of the Jacobian matrix and $d\mathbf{D} = d\widetilde{\eta}_1 \ldots d\widetilde{\eta}_d$. The above integral is usually evaluated with a finite order Gauss-Legendre quadrature. The order is guided by the degree of polynomial involved in the integration. When the integration is performed with n points, Gauss-Legendre quadrature produces exact integrals for all polynomials of order up to $2n - 1$. The interpolating shape functions used to express the KL eigenmodes within the element domain increases the polynomial order, and hence more Gauss points are necessary to compute the perturbation parts of the diffusion matrix, compared to its deterministic counterpart $\mathbf{A}_0^{(e)}$. Let us denote the grid of n^d Gauss points $\mathscr{G}_{\hat{\eta}}$ and weights $\mathscr{G}_{\widetilde{W}}$ in the parent hypercube in as

$$\mathscr{G}_{\hat{\eta}} = \left\{\hat{\eta}_m : \hat{\eta}_m = x_{j_1 \ldots j_d} \;\; \forall j_1, \ldots, j_d \in \{1, \ldots, n\} \text{ and } m = 1, \ldots, n^d\right\}$$
$$\mathscr{G}_{\widetilde{W}} = \left\{\widetilde{W}_m : \widetilde{W}_m = \widetilde{w}_{j_1} \ldots \widetilde{w}_{j_d} \;\; \forall j_1, \ldots, j_d \in \{1, \ldots, n\} \text{ and } m = 1, \ldots, n^d\right\}$$

where $\widetilde{w}_i$ is the weights associated with the Gauss points along the ith axis of the hypercube. The expression for the integral in terms of the Gauss points is

$$\mathbf{A}_i^{(e)} = \sum_{i=1}^{d} \sum_{m \in \mathscr{I}(\mathscr{G}_p)} \widetilde{W}_m \left[\mathcal{N}^p(\widetilde{\eta})\right]_{\widetilde{\eta}=\hat{\eta}_m}^T [K_{e,i}] \left[\frac{\partial \mathcal{N}^p(\widetilde{\eta})}{\partial \eta_i}\right]_{\widetilde{\eta}=\hat{\eta}_m} \left[\frac{\partial \mathcal{N}^p(\widetilde{\eta})}{\partial \eta_i}\right]_{\widetilde{\eta}=\hat{\eta}_m}^T |\mathbf{J}(\widetilde{\eta})|_{\widetilde{\eta}=\hat{\eta}_m} \tag{5.29}$$

where $\mathscr{I}(\mathscr{G}_{\hat{\eta}})$ is the cardinality of the set $\mathscr{G}_{\hat{\eta}}$. The derivative of the shape functions $\mathcal{N}^p$ with respect to the global coordinates $\widetilde{\eta}$ has to go through a coordinate transformation which is written in terms of the inverse of the Jacobian matrix denoted by $[\mathbf{J}(\widetilde{\eta})]^{-1}$ which is well-established in the isoparametric finite element literature [Porter and Stirling, 1990]. From Eqn. (5.29) it is seen that we are trying to evaluate the random parameter K_e at the quadrature

integration points within the element domain. Hence, a better approximation of the random field would be obtained if the discrete spectral decomposition of the covariance function in Eqn. (5.3) is performed such that the eigenvector Φ represents the eigenmodes at the quadrature integration points. However, the additional computation cost has to be justified by the significance of the improvement in accuracy of the obtained solution. The next section deals with the solution methodology applied to the above discretized system to propagate the input parametric uncertainty to the system response and the evaluation of the second order response statistics.

5.4.3 Solution methodology

Here we present the solution methodology adopted in this study to solve the stochastic diffusion problem of the finite element discretized system. We present the setting for the Galerkin method with Polynomial Chaos Expansion (PCE) which can be used to represent the steady state diffusion equation with a finite order chaos expansion [Pettit and Beran, 2006, Ghanem and Spanos, 1991]. As has been discussed in the literature (e.g. [Keese, 2003]), the dimensionality of the linear system increases significantly with the order of chaos chosen and the dimension of the input stochastic space.

The assembly of the above element matrices to form the stochastic global system can be written as $\mathbf{A}(\theta) = \sum_{i=0}^{m} \mathscr{H}_i(\xi(\theta)) \left[\bigcup_{e\in\mathscr{E}} \mathbf{A}_i^{(e)}\right]$ from Eqn. (5.29) where $\mathbf{A}_i^{(e)}$ is the element level (e) matrix associated with the i-th KL mode of the random field, and $\mathscr{E}$ is the set of all elements of the finite element mesh on the spatial domain and $\mathscr{H}(\xi(\theta))$ are the stochastic basis functions which expresses the random field with iid random variables $\xi(\theta)$. Hence the Galerkin formulation at the stochastic level gives

$$\begin{aligned} \mathbb{E}\left[\left[\mathbf{v}^{q,M}\right]^T \mathbf{A}(\theta)\mathbf{u}^{q,M}\right] &= \mathbb{E}\left[\left[\mathbf{v}^{q,M}\right]^T \mathbf{Q}\right] \\ \text{where} \quad \mathbf{A} : \Theta^{(M)} \to \mathbb{R}^{n\times n};& \quad \forall \mathbf{v}^{q,M} \in \mathbb{R}^n \times L^2\left(\Theta^{(M)}, dP_\xi\right) \end{aligned} \tag{5.30}$$

where $\mathbb{E}[\bullet]$ is the expectation operator on the probability space, $\mathbf{u}^{q,M}$ is an assembly of the element block vectors $\mathbf{u}_e^{q,M}$ given in Eqn. (5.22) and $\mathbf{v}^{q,M}$ is the stochastic trial vector basis. Eqn. (5.30) leads to the following set of equations

$$\sum_{\alpha\in\mathscr{J}_{q,M}} \mathbb{E}\left[\mathbf{A}(\theta)\mathscr{H}_\alpha(\theta)\mathscr{H}_\beta(\theta)\right] \mathbf{u}_\alpha^{q,M} = \mathbb{E}\left[\mathscr{H}_\beta \mathbf{Q}\right] \tag{5.31}$$

If we denote $\underline{\mathbf{U}} = \left\{\mathbf{u}_\alpha^{q,M} : \alpha \in \mathscr{J}_{q,M}\right\}$, we have

$$\underline{\mathbf{A}}\,\underline{\mathbf{U}} = \underline{\mathbf{Q}} \tag{5.32}$$

where $\underline{\mathbf{A}}$ is the block-sparse system coefficient matrix and $\underline{\mathbf{Q}}$ is the right hand block vec-

tor. The block-sparse nature of the coefficient matrix is due to the fact that the Galerkin orthogonalization of the residual to the stochastic basis functions involve an integration in the stochastic space with the terms $H_{\alpha\beta\gamma} = \mathbb{E}\left[\mathscr{H}_\alpha(\theta)\mathscr{H}_\beta(\theta)\mathscr{H}_\gamma(\theta)\right]$. The $H_{\alpha\beta\gamma}$ is zero for most combinations of $\{\alpha, \beta, \gamma\}$. A particularly efficient way of tackling the expansion might be the use of double orthogonal polynomials for the random field in which case the coefficient matrix would be block-diagonal and the stochastic problem would be decoupled [Babuška *et al.*, 2005b]. Detailed discussion on the efficient solution of the linear system in Eqn. (5.32) is beyond the scope of the current work and hence the reader is referred to a review of the important literatures in this domain [Nouy, 2008, Schuëller, 2001].

5.5 Random boundary roughness

The randomness in the boundary surface is prevalent in many practical engineering applications and can be considered as one of the major source of uncertainty. Surface roughness has been accounted for by using various methods ranging from simple parameterization of surface inhomogeneities [Taylor, 1971, Richardson, 1971] to using fractals to represent the perturbations in the domain [Blyth and Pozrikidis, 2003]. An alternative approach is to assume that the detailed boundary topology is uncertain and to use random fields to model it. This description has been used in a number of studies which are briefly discussed here. Solution of PDEs on random domains was investigated in [Xiu and Tartakovsky, 2006] using a stochastic mapping of the body-fitted curvilinear coordinates. The extended finite element method (X-FEM) method has been extended to PDEs on random domain [Nouy *et al.*, 2008] and for tackling random heterogeneous material interfaces [Nouy and Clément, 2010]. This concept utilizes level set technique to implicitly represent the random geometry and then uses the classical spectral SFEM to solve the problem on a fixed finite element mesh. The method relies on representing the geometry and its randomness implicitly with random level-set functions. However, incorporating the randomness into the complex geometries with stochastic parametrization of random level set functions is not always a trivial exercise. Moreover, the random boundary may be realized with a random field model rather than just using random variables to model the stochastic level set functions. The method proposed in this work can potentially overcome these difficulties. Natural convection with random boundary topology has been tackled with a sparse-grid collocation technique [Ganapathysubramanian and Zabaras, 2007] where deterministic realizations of the stochastic problem have been solved at random sample points. Investigation of the transport phenomenon in rough walled tubes has been studied in [Tartakovsky and Xiu, 2006]. However integrating the treatment of these uncertainties in a generic manner within the stochastic spectral FE literature still remains a challenge. This is due to the fact that the stochastic mappings involved in these cases are particularly cumbersome to incorporate within the stochastic spectral Galerkin framework.

5.5.1 Problem definition in the random domain

A diffusion problem is considered here on a domain with random boundary perturbations such that $\mathscr{D}_\theta \subset \mathbb{R}^d$ where θ signifies the randomness component. Hence

$$\begin{aligned} \nabla(K\nabla u) &= Q \quad \text{on } \mathscr{D}_\theta \\ u &= G_c \quad \text{on } \Gamma_\theta^0 \\ \mathbf{n}.\nabla u = q_c \quad \text{on } \Gamma_\theta^1 \quad \text{and} \quad \mathbf{n}.\nabla u &= 0 \quad \text{on } \Gamma_\theta^2 \end{aligned} \tag{5.33}$$

where $\Gamma_\theta^1, \Gamma_\theta^2$ belongs to a part of the boundary $\partial\mathscr{D}_\theta$ which is random and $\Gamma_\theta^1 \cap \Gamma_\theta^2 = .$ Here $\mathbf{n}_1$ and $\mathbf{n}_2$ are the outward normals to the random boundary Γ_θ^1 and Γ_θ^2 respectively. The Dirichlet and the Neumann boundary conditions specified in the above equations are true for every sample realization of the random boundary, which put in another way states that G_c and q_c is constant for each random sample.

The weak formulation of the problem in Eqn. (5.33) expressed on the finite element mesh $\Delta(\mathscr{D}_\theta)$ is such that the solution is sought in $\bar{\mathbf{u}}_\theta = \{v_e(\chi^\theta) = \mathscr{N}(\chi^\theta)\mathbf{v}_\theta;\ \mathbf{v}_\theta \in \mathbf{R}^n\}$ where $\mathscr{N}(\chi^\theta)$ consists of spatial basis functions. For the sake of simplicity, if we consider Γ_1 to be a zero Neumann boundary for now, the following bilinear and linear forms are obtained

$$\left\{ \begin{aligned} \mathscr{B}_{\Delta(\mathscr{D}_\theta)}(u_e, v_e) &= \int_{\Delta(\mathscr{D}_\theta)} K_e \left(\nabla_{\chi^\theta}\mathscr{N}\mathbf{v}\right) \cdot \left(\nabla_{\chi^\theta}\mathscr{N}\mathbf{u}\right) d\mathscr{D}_\theta \\ \text{and} \quad \mathscr{L}_{\Delta(\mathscr{D}_\theta)}(v_e) &= \int_{\Delta(\mathscr{D}_\theta)} (\mathscr{N}\mathbf{v})\, Q d\mathscr{D}_\theta \\ \text{such that,} \quad \mathscr{B}_{\Delta(\mathscr{D}_\theta)}(u_e, v_e) &= \mathscr{L}_{\Delta(\mathscr{D}_\theta)}(v_e) \end{aligned} \right. \tag{5.34}$$

In the classical isoparametric FE formulation of the above integrals, the element domain is transformed to a master domain (for e.g. the domain $A''B''C''D''$ is transformed to $ABCD$ as in Fig. 5.2). Thus the integration is transformed to the master domain which can map any order of arbitrary shaped elements to the same order of a regular-shaped parent element. This facilitates easy implementation of a numerical quadrature scheme. It involves evaluating a Jacobian matrix $\mathbf{J}_\theta$ which transforms the differential volume $d\mathscr{D}_\theta$ in each realization of the random domain to its master domain as $d\mathscr{D}_\theta = \mathbf{J}_\theta d\mathscr{D}_M$. Also, the differential operator undergoes a transformation as $\nabla_{\chi^\theta} = \mathbf{J}_\theta^{-1}\nabla_\eta$. In the isoparametric FE formulation [Reddy, 1993], the degree p of the shape functions used to approximate the response field is the same as that used for the map of a given domain to its master domain. Hence Eqn. (5.34) can be

written as

$$\begin{cases} \mathscr{B}_{\Delta(\mathscr{D}_\theta)}(u_e, v_e) = \displaystyle\int_{\Delta(\mathscr{D}_M)} K_e \left(\mathbf{J}_\theta^{-1} \nabla_{\widetilde{\eta}} \mathscr{N}^p(\widetilde{\eta})\mathbf{v}\right) \cdot \left(\mathbf{J}_\theta^{-1} \nabla_{\widetilde{\eta}} \mathscr{N}^p(\widetilde{\eta})\mathbf{u}\right) \mathbf{J}_\theta d\mathscr{D}_M \\ \mathscr{L}_{\Delta(\mathscr{D}_\theta)}(v_e) = \displaystyle\int_{\Delta(\mathscr{D}_M)} \left(\mathscr{N}^p(\widetilde{\eta})\mathbf{v}\right) Q \mathbf{J}_\theta d\mathscr{D}_M \\ \text{such that,} \quad \mathscr{B}_{\Delta(\mathscr{D}_\theta)}(u_e, v_e) = \mathscr{L}_{\Delta(\mathscr{D}_\theta)}(v_e) \end{cases} \tag{5.35}$$

Here the Jacobian $\mathbf{J}_\theta$ is specific to each realization of the random boundary and has to be calculated for the resolution of the system at each point in the stochastic space. The Jacobian takes the form of $\mathbf{J}_\theta = \partial\chi^\theta / \partial\widetilde{\eta}$ where $\chi^\theta = \{\chi_1^\theta, \ldots, \chi_d^\theta\}$ denotes the vector of coordinate directions for each realization of the random domain and $\widetilde{\eta} = \{\widetilde{\eta}_1, \ldots, \widetilde{\eta}_d\}$ is the same in the master domain.

The above equation can be solved in this form using sampling techniques which solves the system for various realizations of the random boundary. Since the boundary perturbation has been modeled with a denumerable set of random variables, it is possible to obtain various realizations of the random field at chosen points in the stochastic space. Hence we can choose to solve this stochastic problem with various Monte Carlo simulations, response surface methodologies or sparse grid collocation techniques [Ganapathysubramanian and Zabaras, 2007].

An alternative to this approach is to solve the system using a unified approach where the solution can be expanded with a tensor product of the set of shape functions in the spatial domain and stochastic functions spanning the stochastic space. This is the framework of the stochastic Galerkin methods which is adopted in the following discussion.

5.5.2 Boundary roughness quantification

Modification of the boundary of a physical domain can result in the either of the following two scenarios: i) the elements in contact with the boundary surface (having one or more nodes on the boundary) can have their edges modified following the movement of the nodes, or ii) a set of elements may be moved along with the boundary in addition to a modification in shape. The scenario of perturbation of one particular element in the domain is graphically depicted in

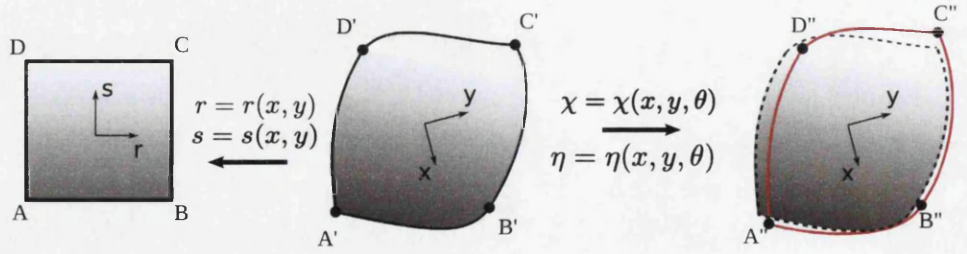

Figure 5.2: A quadrangular element from the finite element unstructured mesh in its perturbed configuration (marked in red). The leftmost figure denotes the master element and the middle figure denotes the deterministic element.

Fig. 5.2 while Fig. 5.3 illustrates the realizations of a perturbed boundary region of a physical domain. Let us denote the *deterministic* domain within the 'red' box in Fig. 5.3 as $\mathscr{D}_{\rm bc} \subset \mathscr{D}$ and the set of elements of the baseline model lying within this by the set $\Delta(\mathscr{D}_{\rm bc})$. We then specify the stochastic set $\Delta(\mathscr{D}_\theta)$ consisting of the random realizations of the elements in $\Delta(\mathscr{D}_{\rm bc})$. Figure 5.2 shows a sample realization of the configuration of an element in $\Delta(\mathscr{D}_\theta)$. A generic spatial domain meshed with quadrangular elements has been considered here. The mesh is assumed to be unstructured and hence the formulation can be trivially extended to the case of uniform mesh. The coordinate transformation from the deterministic to the master element is as given in Eqn. (5.27). The deterministic element in turn is transformed to the perturbed element $A''B''C''D''$ via the transformation

$$\chi_i(\theta) = Q_i^\theta(\eta_1, \ldots, \eta_d; \theta) \quad \forall\, i = 1, \ldots, d; \quad \text{and} \quad \Delta(\mathscr{D}_\theta) = \bar{\mathbf{Q}}^\theta(\Delta(\mathscr{D}_{\rm bc})) \tag{5.36}$$

where $\chi = \{\chi_1, \ldots, \chi_d\}$ is the set of independent coordinate directions specifying the points in the perturbed element and $\eta = \{\eta_1, \ldots, \eta_d\}$ denotes the same in the deterministic element domain.

The roughness of the boundary surface can be quantified with the correlation of the positional coordinates of the FE nodes of the elements in $\Delta(\mathscr{D}_\theta)$. The theoretical development of the discrete KL expansion, presented in Sec. 5.3.1, can be utilized in this context to represent this boundary randomness using a denumerable set of random variables. Here we use a covariance function $C(\mathbf{r}_1, \mathbf{r}_2)$ description of the input random field with the position coordinates ($\mathbf{r}_1, \mathbf{r}_2$ on $\mathscr{D}_{\rm bc}$) of the nodes of the element in the baseline deterministic domain $\mathscr{D}_{\rm bc}$. Following this a discrete spectral decomposition of C gives

$$\boldsymbol{C\phi_i} = \boldsymbol{\lambda_i \phi_i} \quad \textbf{with} \quad \mathbf{r} = \sum_{\mathbf{i=0}}^{\mathbf{p_M}} \boldsymbol{\phi_i \mathscr{H}_i(\xi)}, \quad \mathbf{r} \in \mathbb{R}^m \tag{5.37}$$

where $\mathbf{r}$ is the vector of the position coordinates of the nodes lying on the random boundary (or in the boundary region $\mathscr{D}_{\rm bc}$) approximated with M random variables with p_M-th order chaos expansion.

The parametrization of the element coordinates in the perturbed element in terms of the random variables ($\xi = \{\xi_1, \ldots, \xi_M\}$) used to model the boundary roughness would lead to the transformed coordinate vector $\boldsymbol{\chi}$ being expressed as $\boldsymbol{\chi} = \langle \boldsymbol{\chi} \rangle + \boldsymbol{\chi}'$ where $\langle \boldsymbol{\chi} \rangle$ is the deterministic component while $\boldsymbol{\chi}'$ are the zero mean perturbation components. The objective here is to obtain a mapping between the coordinates of the master element η and the samples of the perturbed configuration $\boldsymbol{\chi}$.

Thus we do not consider remeshing the domain for each random realization of its boundary. Only the perturbation of the coordinates of the nodes lying on the boundary region are incorporated into the formulation with a set of random variables. This is illustrated in Fig. 5.3

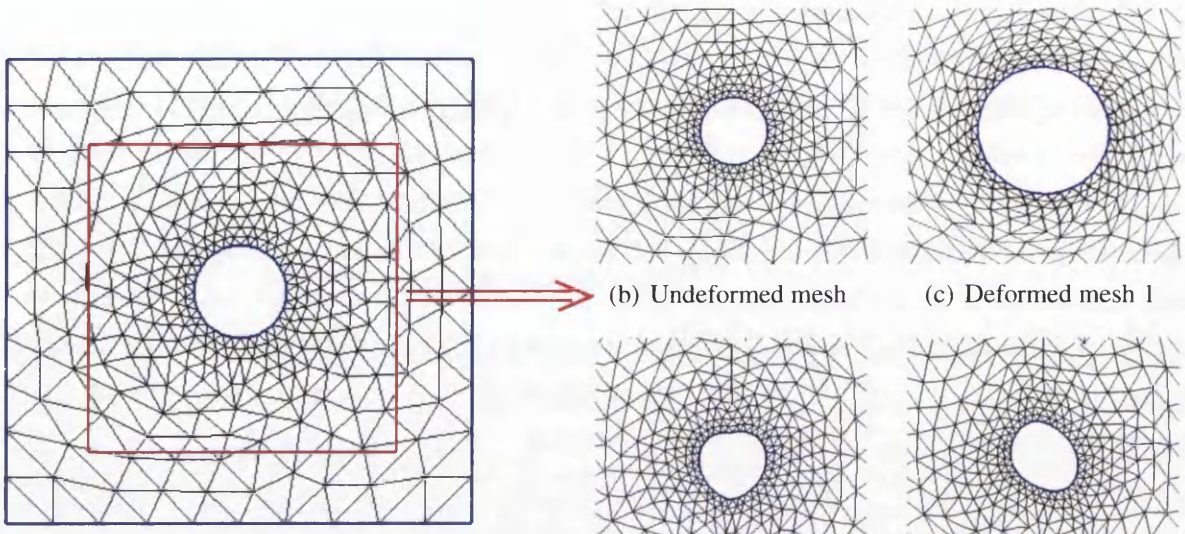

(a) Original configuration

(b) Undeformed mesh

(c) Deformed mesh 1

(d) Deformed mesh 2

(e) Deformed mesh 3

Figure 5.3: The original meshed configuration of a plate with a hole at the center ((a) and the realizations of the random geometrical deformation of the center hole. The refined mesh adjacent to the hole are shown before and after the random perturbation. The coarse mesh outside the marked rectangular region remains unchanged.

which shows a typical geometrical configuration of a plate with a hole at the center. Here the nodes lying inside the marked region are modeled with a set of random variables for the realization of the perturbed configurations while those outside it remains unchanged. Hence all the nodes in the region adjacent to the circle at the center of the plate are moved along with the boundary. The perturbation of these nodes can be modeled with the mapping described in Sec. 5.5.3. It might be mentioned here that the choice of the depth of the boundary region $\mathscr{D}_{\text{bc}}$ from the random boundary designated in the baseline model is governed by the degree of boundary perturbation considered for a particular meshed domain. If the boundary perturbation is small such that the random realizations of the boundary can be captured wholly by the elements lying on the boundary such that only the nodes lying on the boundary has to be modified, then it is sufficient to consider $\mathscr{D}_{\text{bc}}$ to be the boundary $\partial\mathscr{D}$ of the baseline model.

5.5.3 Mapping the random domain to the master domain

We denote the nodal coordinates of the deterministic element as the vector $\eta_{i_j} = \{\eta_{i_1}, \ldots, \eta_{i_{n_e}}\}\ \forall i = 1, \ldots, d$. For the deterministic case, the mapping of the master element (which we denote by $\mathscr{D}_M$, say) to the deterministic element is given as $\eta_i = \sum_{k=0}^{n_e} \mathscr{N}_k^p(\widetilde{\eta})\eta_{i_k} \quad \forall i = 1, \ldots, d$, where $\mathscr{N}^p = \{\mathscr{N}_1^p, \ldots, \mathscr{N}_{n_e}^p\}$ are the p-th order shape multidimensional Lagrange basis functions (n_e being the number of nodes per element). Hence, following Eqn. (5.36) we write

that

$$\eta_i = Q_i^M(\widetilde{\eta}_1, \ldots, \widetilde{\eta}_d) \quad \forall i = 1, \ldots, d; \quad \text{such that,} \quad \Delta(\mathscr{D}) = \bar{\mathbf{Q}}^M(\Delta(\mathscr{D}_M)) \tag{5.38}$$

which gives the mapping from the deterministic to the master element. Combining the above two equations we have

$$\Delta(\mathscr{D}_\theta) = \bar{\mathbf{Q}}^\theta \left(\bar{\mathbf{Q}}^M (\Delta(\mathscr{D}_M)) \right) \tag{5.39}$$

Thus the mapping from the master element to the perturbed element now involves a spatial as well as a stochastic transformation. Hence χ^θ, which denoted the coordinate directions for each sample realization of the random domain, is now be expressed as a function of a denumerable set of random variables used to model the boundary perturbations and the coordinate directions of the master element, i.e. $\chi(\widetilde{\eta}, \xi(\theta)) = \{\chi_1(\widetilde{\eta}, \xi(\theta)), \ldots, \chi_d(\widetilde{\eta}, \xi(\theta))\}$. As a result the interpolation of the spatial coordinates within the random element is given as a tensor double dot product

$$\chi_i(\widetilde{\eta}, \xi) = [\mathscr{N}(\widetilde{\eta}) \otimes \mathscr{N}_\theta(\xi)] : \left\{ \chi_i^{jk} \right\} = \underline{\underline{\mathbf{N}}}(\widetilde{\eta}, \theta) : \underline{\underline{\chi}}_i \quad \forall\, i = 1, \ldots, d \tag{5.40}$$

where $\underline{\underline{\chi}}_i$ is a second order tensor of the field χ_i at the nodal points in the tensor product space $\Delta(\mathscr{D}) \otimes \Theta^{(M)}$. If the matrix χ_i^{jk} is of dimension $n_e \times M$, where n_e is the number of FE nodes associated with the element, then it suggests that the coefficient associated with a particular node has M perturbation components. This suggests that the perturbed element can be described uniquely in a d-dimensional spatial domain and M-dimensional stochastic domain.

It is obvious from Eqn. (5.40) the tensor shape function $\underline{\underline{\mathbf{N}}}$ is stochastic in nature. To keep things simple, we consider the boundary roughness as the only source of uncertainty in the present case and ignore any effect of parametric or forcing randomness. The Jacobian $\mathbf{J}_\theta$ presented in context of the discussion of Eqns. (5.34)–(5.35) can now be expressed as a function of the input random variables as $\mathbf{J}_{\widetilde{\eta}}(\widetilde{\eta}, \xi(\theta)) = \partial\chi(\widetilde{\eta}, \xi(\theta))/\partial\widetilde{\eta}$. The differential volume $\Delta(\mathscr{D}_\theta)$ in the random boundary can be transformed to the master element as

$$\begin{aligned} d\mathscr{D}_\theta &= d\chi_i \ldots d\chi_d \quad \text{where} \quad d\chi_i = \frac{\partial \chi_i}{\partial \widetilde{\eta}} d\widetilde{\eta} \\ \text{following which,} \quad & d\{\boldsymbol{\chi}\} = [\mathbf{J}_{\widetilde{\eta}}(\widetilde{\eta}, \theta)]\, d\{\widetilde{\eta}\} \\ \text{Hence} \quad & \mathrm{d}\mathscr{D}_\theta = \det|\mathbf{J}_{\widetilde{\eta}}| d\widetilde{\eta}_1 \ldots d\widetilde{\eta}_d = \det|\mathbf{J}_{\widetilde{\eta}}| d\mathscr{D}_M \end{aligned} \tag{5.41}$$

The differential operator ∇_{χ^θ} in Eqn. (5.34) is transformed under the coordinate mapping as

$$\boldsymbol{\nabla}_{\boldsymbol{\chi}^\theta} = [\mathbf{J}_{\widetilde{\eta}}(\widetilde{\boldsymbol{\eta}}, \boldsymbol{\xi}(\boldsymbol{\theta}))]^{-1} \boldsymbol{\nabla}_{\widetilde{\eta}} \tag{5.42}$$

where $\nabla_{\tilde{\eta}}$ denotes the differential operator along the coordinate directions of the master element. For the implementation of the spectral Galerkin method it is essential to have a representation of the stochastic quantities in terms of polynomials of the input random variables. This allows efficient computation of the expectation of these stochastic polynomial functions. To this end, the expression for the elements of the Jacobian matrices are presented here as

$$(\mathbf{J}_{\tilde{\eta}}(\tilde{\eta}, \xi(\theta)))_{ij} = \left[\frac{\partial \mathscr{N}(\tilde{\eta})}{\partial \tilde{\eta}_j} \otimes \mathscr{N}_\theta(\xi)\right] : \underset{\sim}{\chi}_i \tag{5.43}$$

Taking $\mathscr{N}_{\theta_0} = 1$, the above Jacobian matrix $\mathbf{J}_{\tilde{\eta}}$ can be expressed as

$$\mathbf{J}_{\tilde{\eta}} = \mathbf{J}_{\tilde{\eta}_0} + \sum_{i=1}^{M} \mathscr{N}_{\theta i}(\boldsymbol{\xi}) \mathbf{J}_{\tilde{\eta}_i} \quad \text{where} \quad (\mathbf{J}_{\tilde{\eta}_i})_{mn} = \sum_{k} \frac{\partial \mathscr{N}_k(\tilde{\eta})}{\partial \tilde{\eta}_n} \left(\underset{\sim}{\chi}_m\right)_{ki} \tag{5.44}$$

It can be easily identified that $\mathbf{J}_{\tilde{\eta}_0}$ is the Jacobian associated with the transformation of the deterministic element to the parent element.

The inverse of the Jacobian matrix can be expressed with polynomial functions of the random variables using the Neuamnn type series expansion as

$$[\mathbf{J}(\tilde{\eta}, \xi(\theta))]^{-1} = \mathbf{J}_{\tilde{\eta}0}^{-1} \sum_{k=0}^{p} (-1)^k \left(\mathbf{J}_{\tilde{\eta}0}^{-1} \sum_{i} \mathscr{N}_{\theta_i}(\xi) \mathbf{J}_{\tilde{\eta}i}\right)^k = \sum_{k=0}^{p} \bar{\mathscr{H}}_k(\theta) \mathfrak{J}_{\tilde{\eta}_k} \tag{5.45}$$

where $\bar{\mathscr{H}}_k$ is the stochastic polynomial function which is obtained from combining the stochastic polynomials in the above equation. Of course $\bar{\mathscr{H}}_0 = 1$ and $\mathfrak{J}_{\tilde{\eta}_k}$ are the corresponding product of the Jacobian matices. The Neumann type series expansion has been performed under the assumption that the spectral radius of the matrix $\mathbf{J}_{\tilde{\eta}_0}$ is quite large when compared to the $\mathbf{J}_{\tilde{\eta}_i}$ components. This assumption is valid considering the fact that the major change in the elemental volume is captured in the transformation of the deterministic element to the master element (which is $A'B'C'D' \rightarrow ABCD$ in Fig. 5.2) while transformation from the deterministic to the stochastic element is small under the assumption of small random perturbation of boundary topology. Taking this into account, we can capture the transformation with a moderately low degree of Neumann expansion. In that case it is easy to track the polynomial of the random variables while implementing the finite order chaos expansion for the spectral Galerkin method.

In case, when the assumption regarding the spectral radius of $\mathbf{J}_{\tilde{\eta}_0}$ (which enables us to approximate the inverse with a truncated Neumann series) does not hold, the inverse has to be evaluated from the solution of the equation $\mathbf{J}_{\tilde{\eta}} \mathbf{J}_{\tilde{\eta}}^{-1} = \mathbf{I}$. We assume that the inverse of the Jacobian matrix can be expressed as a matrix series such that $\mathbf{J}_{\tilde{\eta}}^{-1} = \sum_{k=0}^{p} \mathscr{H}_k(\theta) \mathfrak{J}_{\tilde{\eta}_k}$ where $\mathfrak{J}_{\tilde{\eta}_k}$ are the undetermined matrix coefficients and $\mathscr{H}_k(\theta)$ are the multidimensional orthogonal polynomials spanning the stochastic Hilbert space. These can be evaluated if we apply

a Galerkin orthogonalization of the residual with respect to the orthogonal stochastic basis functions as

$$\left\langle \mathscr{H}_i(\theta), \mathbf{J}_{\tilde{\eta}} \left(\sum_{k=0}^{p} \mathscr{H}_k(\theta) \mathfrak{J}_{\tilde{\eta}_k} \right) \right\rangle_{L^2(\Theta^{(M)})} = \langle \mathscr{H}_i(\theta), \mathbf{I} \rangle_{L^2(\Theta^{(M)})} \tag{5.46}$$

$$\text{from which,} \quad \begin{bmatrix} \\ \overline{\mathbf{J}}^b_{\tilde{\eta}} \\ \\ \end{bmatrix} \begin{bmatrix} [\mathfrak{J}_{\tilde{\eta}_0}] \\ \vdots \\ [\mathfrak{J}_{\tilde{\eta}_p}] \end{bmatrix} = \begin{bmatrix} \mathbf{I} \\ \vdots \\ 0 \end{bmatrix} \tag{5.47}$$

where $\overline{\mathbf{J}}^b_{\tilde{\eta}}$ is the coefficient matrix composed of blocks of the Jacobian matrix series from Eqn. (5.44). The i, j block of this matrix is obtained as $[\overline{\mathbf{J}}^b_{\tilde{\eta}}]_{i,j} = \langle \mathscr{H}_i(\theta), \mathbf{J}_{\tilde{\eta}}(\theta) \mathscr{H}_j(\theta) \rangle_{L^2(\Theta^{(M)})}$ and $\langle \cdot, \cdot \rangle_{L^2(\Theta^{(M)})}$ denotes the inner product in the L^2 stochastic Hilbert space. Hence we have to solve for the block matrices $\mathfrak{J}_{\tilde{\eta}_k}$ from Eqn. (5.47) for each element which are included within the perturbed boundary region. It might be noted that the solution of the above matrix equation is trivially parallelizable since the column vectors of all the $\mathfrak{J}_{\tilde{\eta}_k}$ can be solved in parallel. This method is more expensive than the Neumann expansion method given in Eqn. (5.45), but it guarantees a good approximation of the inverse Jacobian under all conditions. Thus, in the present development we would consider that the inverse Jacobian matrix is approximated as a matrix series $\mathbf{J}^{-1}_{\tilde{\eta}} = \sum_{k=0}^{p} \bar{\mathscr{H}}_k(\theta) \mathfrak{J}_{\tilde{\eta}_k}$ where $\mathfrak{J}_{\tilde{\eta}_k}$ where $\bar{\mathscr{H}}_k(\theta)$ are the stochastic polynomials obtained from the Neumann expansion or the stochastic Galerkin method and $\mathfrak{J}_{\tilde{\eta}_k}$ are the corresponding matrix coefficients.

Recalling Eqn. (5.42), the transformation of the differential operator can be rewritten as

$$\nabla_{\chi^\theta} = \left(\sum_{k=0}^{p} \bar{\mathscr{H}}_k(\theta) \mathfrak{J}_{\tilde{\eta}_k} \right) \nabla_{\tilde{\eta}} \tag{5.48}$$

following from Eqn. (5.45). We note that the Jacobian matrix is expressed as a sum of Jacobian matrices weighted with stochastic polynomials as in Eqn. (5.44). The evaluation of the determinant of this random Jacobian matrix, as required in Eqn. (5.41), can be written explicitly in terms of a set of polynomial random functions as

$$\det|\mathbf{J}_{\tilde{\eta}}| = \sum_i \mathscr{H}^{\det}_i(\theta) \det|\mathbf{J}^{\pi}_{\tilde{\eta}_i}| \quad \text{with} \quad \mathscr{H}^{\det}_0 = 1 \tag{5.49}$$

where $\mathscr{H}^{\det}_{\tilde{\eta}_i}$ is the stochastic polynomial associated with the Jacobian $\mathbf{J}_{\tilde{\eta}}$. These polynomials are obtained by solving the determinant of a full rank Jacobian matrix and $\det|\mathbf{J}^{\pi}_{\tilde{\eta}_i}|$ is the combination of the Jacobian matrix with appropriate rearrangement of rows as per the coefficient random polynomial function. The detailed derivation to explicitly express the determinant of the sum of the series of the form $\det|\mathbf{J}_0 + \sum_i \alpha_i \mathbf{J}_i|$ with polynomial functions of the scalar coefficient α_i is provided in Appendix A.2. The maximum degree of the polynomial in α_i is

governed by the rank of the matrices $\mathbf{J}_i$.

The expression of the element level system matrices which are perturbed by random boundary fluctuations would involve products of random polynomial functions $\bar{\mathscr{H}}_i(\theta)$ and $\mathscr{H}_j^{\text{det}}(\theta)$ obtained from Eqns. (5.45) and (5.49). Introducing the notation $\mathscr{H}_k^S(\theta) = \bar{\mathscr{H}}_i\bar{\mathscr{H}}_j\mathscr{H}_l^{\text{det}}$, where k is the cardinality of the set $\mathscr{J}_{\mathscr{H}}$ which consists of an ordered set of the stochastic product functions $\mathscr{J}_{\mathscr{H}} = \{\mathscr{H}_k^S(\theta) = \bar{\mathscr{H}}_i\bar{\mathscr{H}}_j\mathscr{H}_l^{\text{det}} \;\; \forall\, i,j,l\}$

We discuss the relationship of the proposed methodology to the stochastic mapping technique implemented using the concept of boundary-conforming coordinate system introduced in [Xiu and Tartakovsky, 2006]. The latter utilizes the solution of Laplace equations to obtain the stochastic mapping of the random element boundaries to the deterministic domain. This concept relies on the assumption that the random boundary is realized with stochastic mapping of the structured body-fitted curvilinear coordinates. Thus the regularity requirements on the boundary applies to this case and in general the random mapping. In contrast, the proposed method is applicable to different types of physical domains $\mathscr{D} \in \mathbb{R}^d$ where the information of the positional coordinates of the set of finite element nodes lying on the boundary or a region adjacent to the boundary of the baseline model (usually the deterministic ideal domain) is the input to the stochastic model along with a covariance function describing the correlation of the nodal coordinates across the boundary region. For e.g. if the fluctuation of a portion of the domain boundary is described with body-fitted curvilinear coordinates $\bar{\mathbf{r}} \in \mathbb{R}^d$, then it is a simple exercise to obtain the coordinate transformation matrix $\mathbf{T}$ (and its inverse) such that $\mathbf{x} = \mathbf{T}\bar{\mathbf{r}}$ where $\mathbf{x}$ is the global Cartesian axes. The covariance function described with $C_a(\bar{\mathbf{r}}_1, \bar{\mathbf{r}}_2) = f(\Delta\bar{\mathbf{r}}/L_{\bar{\mathbf{r}}_c})$ is transformed to the Cartesian system as $C_a(\mathbf{x}_1, \mathbf{x}_2) = f(\Delta\{\mathbf{T}^{-1}\mathbf{x}\}/L_{\mathbf{x}_c})$ where $L_{\mathbf{x}_c}$ is the transformed correlation lengths along the Cartesian axes. The proposed method relies on the assumption that the boundary perturbations and in general, changes to the topology of the physical domain can be captured with perturbation of the elemental domains as shown in Fig. 5.3. However, this method would not be computationally meaningful in case of significant changes in the shape of the physical domain since the solution accuracy that would be obtained by transforming the mesh of the original domain may be unacceptable. Remeshing the domain, in such cases, would receive serious consideration. We have analyzed the accuracy of the solution obtained with the proposed method with respect to a benchmark brute force Monte Carlo simulation, for a given degree of input perturbation, in the results section later in this article.

5.5.4 Solution in tensor product space

The test functions for the weak formulation of the diffusion problem defined on a random domain would consist of all those functions which exist in the tensor product approximation space of the spatial basis functions and the stochastic polynomials. The solution is thus

approximated within the element domain as

$$u_e = [\mathscr{N}^p(\widetilde{\eta}) \otimes \mathscr{H}^{q,M}(\theta)] : \underline{\mathbf{u}} = \mathbf{N}_{\mathbf{H}}(\widetilde{\eta}, \theta) : \underline{\mathbf{u}} = \sum_{i=1}^{n_e} \sum_{j \in \mathscr{I}_m} \mathscr{N}_i^p(\widetilde{\eta}) \mathscr{H}_j^{q,M}(\theta) u_{ij} \qquad (5.50)$$

where $\mathscr{N}^p(\widetilde{\eta})$ denotes the p-th order spatial basis functions in the master domain and $\mathscr{H}^{q,M}$ are the q-th order orthogonal stochastic polynomials spanning the M dimensional input stochastic space and $\underline{\mathbf{u}}$ is a second order tensor of the unknown stochastic response quantities to be solved.

Thus the weak form of the diffusion equation defined on an element subjected to random boundary perturbations can be expressed on the tensor product space $\left\{\Delta(\mathscr{D}_M) \otimes \Theta^{(M)}\right\}$ with stochastic polynomial coefficient functions using Eqns. (5.48)–(5.50) as

$$\begin{aligned}
\mathscr{B}(u_e, v_e) &= \int_{\Theta^{(M)}} \sum_{i \in \mathscr{I}_{\mathscr{H}}} \mathscr{H}_i^S(\theta) \int_{\Delta(\mathscr{D}_M)} K_e \left(\mathfrak{J}_{\widetilde{\eta}_k} \nabla_{\widetilde{\eta}} \mathbf{N}_{\mathbf{H}} : \underline{\mathbf{v}}\right) \left(\mathfrak{J}_{\widetilde{\eta}_j} \nabla_{\widetilde{\eta}} \mathbf{N}_{\mathbf{H}} : \underline{\mathbf{u}}\right) \det|\mathbf{J}_{\widetilde{\eta}_l}^{\pi}| d\widetilde{\eta} dP_{\xi}(\theta) \\
\mathscr{L}(v_e) &= \int_{\Theta^{(M)}} \sum_{j} \mathscr{H}_{\widetilde{\eta}\xi_j}^{\det}(\theta) \int_{\Delta(\mathscr{D}_M)} \left(\mathbf{N}_{\mathbf{H}} : \underline{\mathbf{u}}\right) Q(\mathbf{r}_h) \det|\mathbf{J}_{\widetilde{\eta}\xi_j}^{\pi}| d\widetilde{\eta} dP_{\xi}(\theta)
\end{aligned} \qquad (5.51)$$

where $dP_{\xi}(\theta)$ is the joint probability measure of the vector of random variables ξ. The term $\mathscr{H}_k^S(\theta)$ is a compact notation of the product of stochastic polynomial functions as $\mathscr{H}_n^S = \mathscr{H}_i \mathscr{H}_j \mathscr{H}_{\widetilde{\eta}\xi_k}^{\det}$. The bilinear operator in the previous equation necessitates the evaluation of expectation of polynomials of random variables of the form $\mathbb{E}\left[\mathscr{H}_k^S \mathscr{H}_i^{q,M} \mathscr{H}_j^{q,M}\right]$. These are pre-calculated and plugged into the finite element code during the assembly of the large finite element system matrices. Alternatively, quadrature based integration schemes (such as the Gauss-Hermite quadrature) can be used to numerically evaluate the integrations in the stochastic space. However, for high dimensional stochastic problems this integration can have significant computational overhead. In such cases, the integral can be evaluated on a sparse grid of points in the stochastic space (for example using the Clenshaw-Curtis points). This can be made more efficient by using anisotropic grids in the stochastic space based on the important stochastic dimensions and implementing dimension adaptivity with nested quadrature schemes.

Equation (5.51) leads to a system of linear equations $\mathbf{AU} = \mathbf{F}$ of dimension $n_{\text{PC}} \times n_{\text{dof}}$ where n_{PC} is the number of terms of the PC expansion given by the formula $n_{\text{PC}} = \binom{M+q}{M}$ where M is the number of random variables and q is the order of chaos expansion. Each

element level matrix which is assembled to obtain the global system matrix $\mathbf{A}$ is obtained as

$$\left(\mathbf{A}^e_{K,L}\right)_{IJ} = \sum_{k\in\mathscr{J}_{\mathscr{H}}} \mathbb{E}\left[\mathscr{H}^S_k \mathscr{H}^{q,M}_K \mathscr{H}^{q,M}_L\right] \int_{\Delta(\mathscr{D}_M)} K_e \sum_{g=1}^{d}\left(\sum_{h=1}^{d}(\mathfrak{J}_{\widetilde{\eta}_k})_{gh}\nabla_{\widetilde{\eta}_h}\mathscr{N}^p_I\right)\cdot \left(\sum_{l=1}^{d}(\mathfrak{J}_{\widetilde{\eta}_k})_{gl}\nabla_{\widetilde{\eta}_l}\mathscr{N}^p_J\right)\det|\mathbf{J}^{\pi}_{\widetilde{\eta}_k}|\,d\widetilde{\eta}\,dP_\xi(\theta) \quad (5.52)$$

We present here an analysis of the computational complexity for the evaluation of the terms of the system matrix $\mathbf{A}$. If we assume that a n_{GQ} point Gauss-Legendre quadrature is utilized to perform the integration in the spatial domain and that the evaluation of the terms of the matrix in Eqn. (5.52) is given by n_s, then the evaluation of the system at each point in the stochastic space is given by $n^d_{\mathrm{GQ}}n_s$ where d is the number of dimensions in the spatial domain. If n_{pe} noded elements are used then the total cost of evaluating an element level matrix at one specific point in the stochastic space is given by $n^2_{pe}n^d_{\mathrm{GQ}}n_s$. If the random field is approximated with n_k stochastic functions i.e. $\mathscr{H}^S_k$ has n_k terms, and if the expectation terms associated with each system level term is pre-calculated then each block of the matrix $\mathbf{A}^e_{K,L}$ in Eqn. (5.52) is calculated with $n_k n^2_{pe}n^d_{\mathrm{GQ}}n_s$ operations. However, if a quadrature scheme is implemented in order to evaluate the stochastic integration operations during the evaluation of the system matrices, then the cost can be calculated as follows. If we assume that a n_q point quadrature scheme is chosen as per the weighting functions (i.e. Gauss-Hermite quadrature for Gaussian random variables or Gauss-Legendre quadrature for uniform random variables) then the cost is given as $n^M_q\left(n^2_{pe}n^d_{\mathrm{GQ}}n_s\right)$, where M is the number of random variables. As a result, pre-computing the expectation operators is going to be advantageous in most cases since n^M_q would almost always be greater than n_k. The value of n_k is governed by the chosen chaos order and the dimension of the approximating stochastic functions. Hence to evaluate the system matrix with 1 element using a q^{th} order chaos expansion in M dimensional stochastic space we have $n^2_{\mathrm{PC}}n^M_q\left(n^2_{pe}n^d_{\mathrm{GQ}}n_s\right)$. Thus the order of computational complexity grows as $\mathscr{O}(n^2_{\mathrm{PC}}n^M_q)$ with the stochastic dimension. Now a q point quadrature rule exactly integrates a function of order $\leq 2q-1$. Hence the number of quadrature points must increase with the order of chaos expansion.

Table 5.1 which gives the computational time to evaluate the element level system matrix using the Gauss-Hermite quadrature points as presented in the preceding paragraph. The calculations have been performed on 8 computational cores of identical capability with *multithreaded* FORTRAN 90 subroutines using gfortran compilers. It has been seen that we require at least 1 more quadrature point than the order of chaos expansion to obtain a good approximation of the stochastic integration (hence the boxes corresponding to high order chaos expansion with fewer quadrature points in Table 5.1 have been left blank). We see that the calculations approximately match the computational complexity orders calculated in the previous paragraph.

Table 5.1: Computational time (in secs) to obtain the system matrix **A** with multidimensional Gauss-Hermite quadrature points for the integration in stochastic space. The random boundary fluctuation has been represented with 4 independent Gaussian random variables in all the cases. The number of the Gauss-Hermite quadrature points used along each stochastic dimension is shown in the leftmost column and it is seen that the computational time increase exponentially with the order and number of quadrature points.

No. of quad points	PC order 2	PC order 4	PC order 6	PC order 8	PC order 10
5	0.4	7			
6	0.7	13			
8	2.2	41	374		
10	5.1	103	867	4319	
12	11	216	1817	9301	36797

The above discussion presents the general form of incorporating the description of random boundary perturbations, modeled with a set of independent identically distributed random variables, into the finite element formulation. Recalling the classification of parameter-based approximation of the field variable and the element geometry in finite element analysis [Zienkiewicz and Taylor, 1991], the isoparametric formulation is one in which the degree of interpolation (p) functions used to approximate the element geometry (G_p) and the unknown field (F_p) is the same, i.e. $G_p = F_p$. In the present formulation the element is approximated in the tensor product space of the spatial and stochastic domain. The approximation of the unknown quantity $\underset{=}{u}{}_p^{q,M}$ has been obtained in the spatial domain with p^{th} order spatial functions which is identical to that for the spatial geometrical approximation. However, the order of stochastic approximation q would be generally larger (or at best equal in few cases) to that used to approximate the random boundary. This implies that this is a *subparametric* formulation with respect to the stochastic approximation.

The transformation of the boundary integral terms for the Neumann part of the boundary Γ_θ^1 where a non-zero flux is imposed (as given in Eqn. (5.33)) is discussed here. This term is written as a boundary integral on the element (which lies on the perturbed geometry) as

$$\begin{aligned}\int_{\Theta^{(M)}} \oint_{\partial\Delta(\mathscr{D}_\theta)} \mathbf{n}\cdot\nabla u\Big|_{\partial\Omega_\theta} \mathbf{N_H} d\Omega_\theta dP_\xi(\theta) &= \int_{\Theta^{(M)}} \oint_{\partial\Delta(\mathscr{D}_\theta)} q_c \mathbf{N_H} d\Omega_\theta \, dP_\xi(\theta), \\ &= \int_{\Theta^{(M)}} \oint_{\partial\Delta(\mathscr{D}_M)} q_c \mathbf{N_H}(\widetilde{\eta}|_{\partial\Omega}, \xi) J_{\partial\Omega_\theta} d\Omega \, dP_\xi(\theta) \qquad (5.53)\end{aligned}$$

In the above equation $J_{\partial\Omega_\theta}$ denotes the stochastic Jacobian transformation of the stochastic elemental boundary $d\Omega_\theta$ to the master boundary $d\Omega$, $\mathbf{N_H}(\widetilde{\eta}|_{\partial\Omega}, \xi)$ is the stochastic shape functions (introduced in Eqn. (5.50)) defined on the boundary surface and q_c is the boundary flux given in Eqn. (5.33). All the earlier discussions on the Jacobian matrix for the transformation of the elemental random volume to its parent domain is also applicable here. The boundary flux term is imposed strictly on every stochastic sample realization and hence

any functional dependence of the flux on the boundary coordinates are transformed to the master domain using the isoparametric transformation introduced in Eqn. (5.40). Similarly, the Dirichlet boundary condition is imposed in the strict sense where $u = G_c$ on Γ_θ^0 for all $\theta \in \Theta^{(M)}$. Thus, with the isoparametric form, the implementation of the boundary condition follows from the previous theoretical development without additional mathematical complexity.

The proposed methodology enables the resolution of stochastic pde-s defined on domains with random boundary topology within the framework of stochastic spectral Galerkin methods. The solutions expressed with orthogonal polynomials from the finite dimensional stochastic Hilbert space requires the solution of large block sparse linear systems. This can be done with iterative Krylov solvers, as discussed in the following sections.

5.6 Unified treatment of parametric and boundary randomness

Here we present a unified treatment of the parametric and boundary uncertainty of the random field using the methodologies presented in Secs. 5.4 and 5.5. Assume that the parameter K in Eqn. (5.33) is random such that $K = K(\xi(\theta))$ where $\theta \in \Theta^{M_1}$ is an M_1 dimensional stochastic space for the parametric randomness. We utilize the boundary uncertainty description presented in the previous section where the solution is approximated in an M_2-dimensional stochastic space Θ^{M_2}. We assume that the random fields are stationary and square-integrable. This gives the bilinear and linear form on which is used as a starting point for the stochastic weak formulation on the domain with random boundary.

$$\mathscr{B}(u_e, v_e) = \int_{\Theta^{(\bar{M})}} \sum_{i \in \mathscr{I}_{q_1,M_1}} \mathscr{H}_i^S \int_{\Delta(\mathscr{D}_M)} \left(\sum_{k \in \mathscr{I}_{q_2,M_2}} \mathscr{H}^{q_2,M_2} K_i^e \right) (\mathfrak{J}_{\widetilde{\eta}_k} \nabla_{\widetilde{\eta}} \mathbf{N_H} : \underline{\mathbf{v}}) \cdot$$
$$(\mathfrak{J}_{\widetilde{\eta}_j} \nabla_{\widetilde{\eta}} \mathbf{N_H} : \underline{\mathbf{u}}) \det|\mathbf{J}^{\pi}_{\widetilde{\eta}_l}| d\widetilde{\eta} dP_{\xi_{M_1}} dP_{\xi_{M_2}}$$

$$\mathscr{L}(v_e) = \int_{\Theta^{(\bar{M})}} \sum_j \mathscr{H}^{\det}_{\widetilde{\eta}\xi_j}(\theta) \int_{\Delta(\mathscr{D}_M)} (\mathbf{N_H} : \underline{\mathbf{v}}) Q(\mathbf{r}_h) \det|\mathbf{J}^{\pi}_{\widetilde{\eta}\xi_j}| d\widetilde{\eta} dP_{\xi_{M_1}} dP_{\xi_{M_2}} \tag{5.54}$$

$$\text{where} \quad \mathbf{N_H}(\widetilde{\eta}, \xi_{M_1}, \xi_{M_2}) : \underline{\mathbf{u}} = \left[\mathscr{N}^{\mathrm{p}}(\widetilde{\eta}) \otimes \mathscr{H}^{\bar{\mathrm{Q}},\bar{\mathrm{M}}}(\xi_{M_1}, \xi_{M_2}) \right] : \underline{\mathbf{u}}$$

In the above equation, $\mathbf{N_H}(\widetilde{\eta}, \xi_{M_1}, \xi_{M_2})$ is the tensor product of the spatial and stochastic basis functions, $\mathscr{H}^{\bar{Q},\bar{M}}(\xi_{M_1}, \xi_{M_2})$ are the orthogonal polynomials constructed in the stochastic tensor product space $\Theta^{(M_1)} \times \Theta^{(M_2)}$ whose dimension is $M_1 \cup M_2$. Since the samples from $\Theta^{(M_1)}$ and $\Theta^{(M_2)}$ are taken to be independent of each other, the joint distribution is given by $dP_{\xi_{M_1}} dP_{\xi_{M_2}}$. The bilinear and linear forms in Eqn. (5.54) is defined on $\Delta(\mathscr{D}_M) \otimes \Theta^{(\bar{M})}$. The order of chaos expansion is chosen to be $\bar{Q}$ which is chosen based on the sensitivity of the

response to each stochastic dimension. Normally, dimensionally adaptive stochastic functions can produce optimal convergence of the stochastic solution with fewer basis functions. [Li and Ghanem, 1998, Blatman and Sudret, 2010].

The expression of the system matrix from Eqn. (5.54) can be written as

$$\left(\mathbf{A}^{e}_{K,L}\right)_{IJ} = \sum_{k\in\mathscr{J}_H} \mathbb{E}\left[\left(\mathscr{H}^{S}\mathscr{H}^{q_2,M_2}\right)_k \mathscr{H}^{\bar{Q},\bar{M}}_{K}\mathscr{H}^{\bar{Q},\bar{M}}_{L}\right] \int_{\Delta(\mathscr{D}_M)} K^{e}_{k} \sum_{g=1}^{d}\left(\sum_{h=1}^{d}(\mathfrak{J}_{\tilde{\eta}_k})_{gh}\nabla_{\tilde{\eta}_h}\mathscr{N}^{p}_{I}\right)\cdot \left(\sum_{l=1}^{d}(\mathfrak{J}_{\tilde{\eta}_k})_{gl}\nabla_{\tilde{\eta}_l}\mathscr{N}^{p}_{J}\right)\det|\mathbf{J}^{\pi}_{\tilde{\eta}_k}|d\tilde{\eta}dP_{\xi_{M_1}}dP_{\xi_{M_2}} \tag{5.55}$$

where $\mathscr{J}_H$ is the cardinality of the set $H = \left\{\mathscr{H}^{S}_{i}\mathscr{H}^{q_2,M_2}_{j} \text{ for all } i \in \mathscr{J}_{q_1,M_1} \text{ and } j \in \mathscr{J}_{q_2,M_2}\right\}$. This leads to the linear system of equations of the form $\mathbf{AU} = \mathbf{F}$ where the dimension of system depends on the total number of random variables $\bar{M}$ and the order of chaos expansion $\bar{Q}$ chosen for the solution. The expectations $\mathbb{E}[\cdot]$ of the stochastic polynomials has to be precomputed and plugged in the solver for the efficient evaluation of the linear system. This gives a unified framework within which the diffusion problem with parametric uncertainty can be tackled on a domain which has random boundary fluctuations.

5.7 Results

We present the numerical experiments performed with the methodologies presented in the previous sections to demonstrate their applicability in practical cases. The results for the spectral decomposition of the covariance kernel using the discrete representation of the covariance kernel at the nodal points in the spatial domain is presented in Sec. 5.7.1. Also, a comparison of this method with the FE type solution of the covariance kernel, as presented in Sec. 5.3.2, is also given in Sec. 5.7.1 which demonstrates the accuracy of the proposed method. Following this, the steady state diffusion system with parametric uncertainty has been analyzed in Sec. 5.7.2 where FE shape functions have been utilized to interpolate the discrete random field within each element domain. Following this the unsteady response of a dynamic diffusion system on a domain with random boundary fluctuations and its comparison with direct MCS solution has been given.

5.7.1 Discrete random field representation

In this section we present the results pertaining to the discretization of the random field with the 'discrete KL expansion' as presented in Sec. 5.3.1. We have seen that the discrete covariance matrix can be constructed with the finite element mesh and the principal eigen modes can be identified from this matrix. The random field is hence expressed as a sum of the eigen

components evaluated at the nodal points. Following this the random field is interpolated inside the element using FE shape functions.

Here we consider a lognormal random field which has been approximated in the spatial domain with finite order Hermite polynomials constructed with a set of Gaussian iid random variables. The convergence of the lognormal field with various parameters such as the input stochastic dimension, order of Hermite polynomials and mesh parameter size has been studied here. An error metric has been constructed for this purpose which is defined as

$$\varepsilon = \frac{\|C_a^{\text{exact}} - C_a^{\text{approx}}\|_{\text{F}}}{\|C_a^{\text{exact}}\|_{\text{F}}} \tag{5.56}$$

where C_a^{exact} is an accurate description of the covariance kernel constructed over the spatial domain at all the Gauss integration points of the elements. This C_a^{exact} is the original covariance function used to describe the random field. The approximated covariance kernel C_a^{approx} has been synthesized from the discrete random field at the Gauss points and the relative error has been studied. Thus ε denotes the accuracy of the approximate covariance function to the target kernel and has been used to ascertain the accuracy of simulated stochastic fields [Sakamoto and Ghanem, 2002]. Also, ε can be an estimate of the norm of the approximation error on the entire domain when considering the full covariance matrix or as cell values computed within each element of the finite element mesh if, for example, we consider the covariance matrix to be constructed at the quadrature integration points within each element.

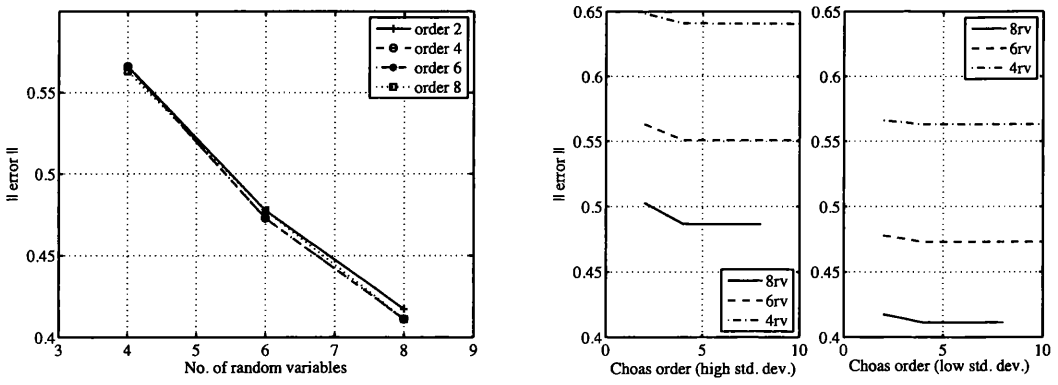

(a) Convergence of the error with input stochastic space dimension.

(b) Convergence of the error with chaos order.

Figure 5.4: Convergence of the Frobenius error norm of the covariance matrix with the order of Chaos expansion and the input stochastic dimension. The values of standard deviation are $\{0.10, 0.20\}$ (low and high respectively).

Here the exact covariance function has been synthesized in two different ways to highlight the convergence of the approximate random field with respect to various approximating parameters. One method uses the exact covariance matrix from the original description of the covariance function over the entire physical domain at the discrete nodal locations. We have

used an exponential covariance function for this purpose as $C_a^{\text{exact}} = \exp(-\|\mathbf{r}_1 - \mathbf{r}_2\|/\mathbf{L}_r)$ where $\mathbf{L}_r$ is the correlation length of the underlying Gaussian random field. Using this description, the behavior of the error norm in Eqn. (5.56) is presented in Fig. 5.4. The figure shows the error with increasing number of random variables used to model the stochastic lognormal field and different order of chaos functions used to express the lognormal field with multidimensional Hermite polynomials of a set of independent Gaussian random variables. Figure 5.4(a) highlights the improvement in accuracy obtained with increasing dimension of the input stochastic field and also shows the effect of the order of chaos expansion on the stochastic field. Figure 5.4(b) shows the effect of increasing the variability of the input stochastic field, and demonstrates that just increasing the order of the chaos expansion do not give great improvements in the accuracy of the approximate random field. Hence optimal convergence of the approximate random field is obtained by simultaneously controlling the dimension and the order of chaos such that the highest gradient of the error curve is obtained.

It is desirable however to obtain an understanding of the improvement in random field approximation with the increasing order of chaos expansion when a particular dimension of the input random field has been specified. Hence we now construct $C_a^{M,\text{exact}}$ which is the exact covariance kernel of the lognormal random field represented with M iid Gaussian random variables i.e. the covariance matrix

$$C_a^{M,\text{exact}} = \mathbb{E}\left[\left\{\exp\left(\bar{\mathbf{a}}_0 + \sum_{i=1}^{M}\xi_i\widetilde{\mathbf{a}}_i\right) - \mu_{\text{exp}}\right\}^T\left\{\exp\left(\bar{\mathbf{a}}_0 + \sum_{i=1}^{M}\xi_i\widetilde{\mathbf{a}}_i\right) - \mu_{\text{exp}}\right\}\right]$$

where $\mu_{\text{exp}} = \mathbb{E}\left[\exp\left(\bar{\mathbf{a}}_0 + \sum_{i=1}^{M}\xi_i\widetilde{\mathbf{a}}_i\right)\right]$ is the mean of the exponential field. Using simple algebraic manipulations and simplifying these expressions for each (p,q)-th element of the matrix $C_a^{M,\text{exact}}$ we have

$$[C_a^{M,\text{exact}}]_{p,q} = \exp\left([\bar{\mathbf{a}}_0]_p + [\bar{\mathbf{a}}_0]_q\right)\left[\exp\left(\sum_{i=1}^{M}\frac{1}{2}([\widetilde{\mathbf{a}}_i]_p + [\widetilde{\mathbf{a}}_i]_q)^2\right) - \exp\left(\sum_{i=1}^{M}\frac{1}{2}([\widetilde{\mathbf{a}}_i]_p^2 + [\widetilde{\mathbf{a}}_i]_q^2)\right)\right] \tag{5.57}$$

Here $[\bar{\mathbf{a}}_0]_p$ and $[\widetilde{\mathbf{a}}_i]_p$ denotes the p-th component of the deterministic and perturbation parts of the random field vector. The value of M is fixed at the specific input stochastic dimension. Hence the error constructed with this synthesized 'exact' covariance matrix using Eqn. (5.56) would highlight the approximation accuracy obtained with successive p-refinements of the stochastic space. Figure 5.5(a) gives the convergence of the lognormal random field with respect to the chaos order which shows an exponential convergence of the error. The three different curves correspond to the different dimensions (4,6,8) of the input stochastic space. Figure 5.5(b) shows the same convergence behavior but for different input variability of the random field. It shows that higher order chaos functions have to be utilized to get desired accuracy levels for higher input standard deviation.

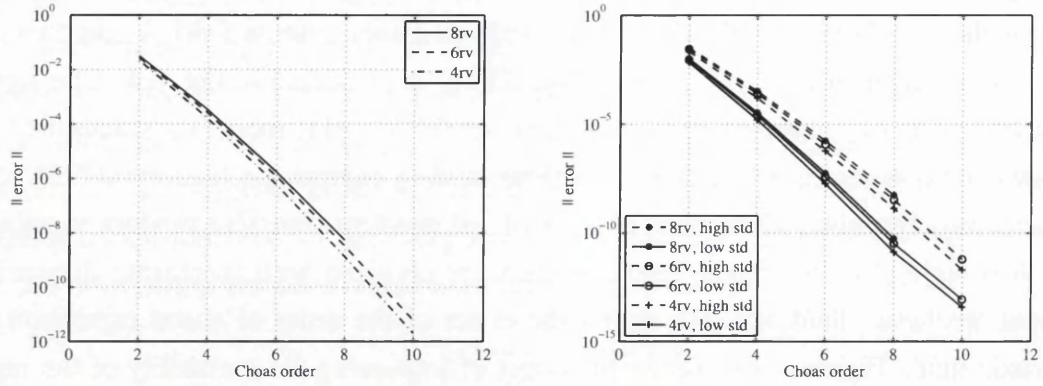

(a) Error convergence with chaos order

(b) Comparison of convergence behaviour for different input variability

Figure 5.5: Convergence of the Frobenius error norm of the covariance matrix with respect to the chaos order, input stochastic dimension and variability of the random field. The values of standard deviation are $\{0.10, 0.20\}$ (low and high respectively).

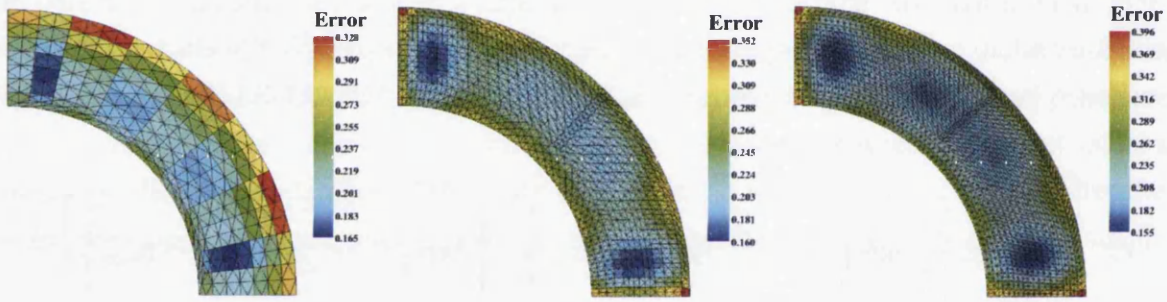

(a) h_{min} = 6.6, 4 rv

(b) h_{min} = 2.9, 4 rv

(c) h_{min} = 1.9, 4 rv

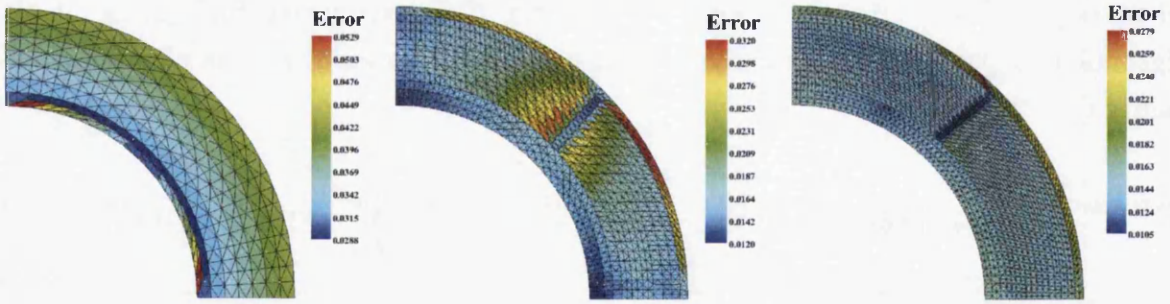

(d) h_{min} = 6.6, 200 rv

(e) h_{min} = 2.9, 200 rv

(f) h_{min} = 1.9, 200 rv

Figure 5.6: The spatial distribution of the L^2 error in approximating the input random field with two different stochastic space dimensions 4 and 200 ('rv' in the figure captions, denotes random variables) for a fixed value of correlation length and three different mesh resolutions in ascending order $h_{min} = 6.6, 2.9, 1.9$

We have presented in Fig. 5.6 the error in the covariance kernel in each element of the FE mesh on the spatial domain for different dimensions of the input stochastic space and mesh parameter sizes. The exact and the synthesized covariance kernels have been obtained at the Gauss quadrature points inside each element and the Frobenius norm of these matrices gives

the approximation error inside each elemental domain. The figures show that as the mesh is refined (or as h_{min} is reduced) the order of accuracy improves appreciably. Also, since the mesh has been deliberately taken to be unstructured, the particular elements in the mesh which are larger and more skewed have a higher value of error. Also, the improvement in the accuracy of the error as the stochastic dimension is increased (from 4 in Figs. 5.6(a)–5.6(c), to 200 in Figs. 5.6(d)–5.6(f)) is highlighted. This colormap shows that as the mesh is refined the 'blue' patches increases, which indicate an improved approximation of the covariance function.

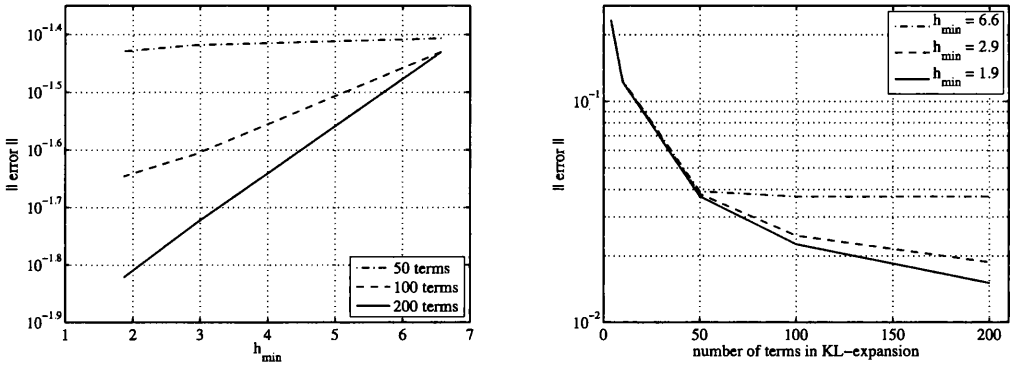

(a) Error convergence with mesh parameter size (b) Error convergence with the input stochastic space dimension

Figure 5.7: Error in the discretization of the covariance kernel for different mesh parameter size (h_{min}) and dimension of the input stochastic space.

Figure 5.7 shows the convergence trend of the error in the covariance kernel with decreasing mesh parameter h_{min} and increase in dimension of the stochastic space. The plotted error is a weighted average of the errors (ε^e) shown as cell values in the colormap in Fig. 5.6, so that it can be written as $\|\text{error}\| = (\sum_i A_i^e \varepsilon_i^e) \,/\, (\sum_i A_i^e)$. It shows that exponential convergence is achieved with h_{min} and the slope is steepest for the highest input stochastic dimension. Similar behavior is observed for the study of convergence of error with increasing input stochastic dimension for a fixed mesh parameter h_{min} which shows that higher accuracy is obtained for fine mesh.

Figure 5.8 shows some realizations of the lognormal random diffusion coefficient obtained with different number of terms retained in the discrete KL expansion of the covariance function. Here we have chosen the decreasing correlation lengths for the random fields approximated with 4 and 20 random variables. The plots in the first row, Fig. 5.8(a), gives the stochastic field modeled with 4 random variables while those on the second row, Fig. 5.8(b), gives the stochastic field constructed with 20 random variables. The latter shows a greater degree of variation in the random field realizations than the former.

Figure 5.9 shows the eigenmodes of the spectral decomposition of an exponential covariance kernel (C_{exp}), ((a)–(g)) and the modes for a triangular covariance kernel (C_{tri}) ((h)–(n))

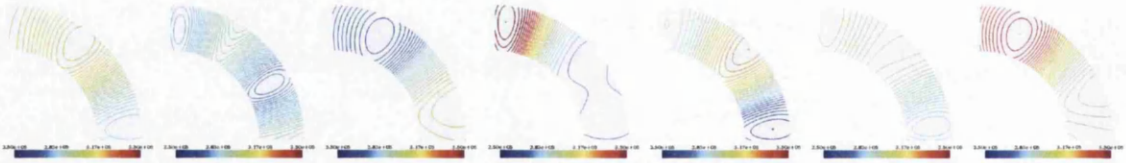

(a) Lognormal random field modeled with 4 random variables

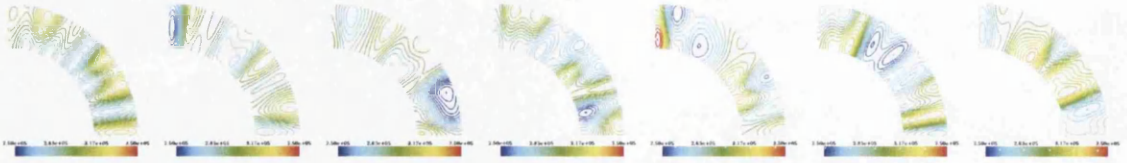

(b) Lognormal random field modeled with 20 random variables

Figure 5.8: The spatial distribution of the sample realizations of the lognormal stochastic diffusion coefficient modeled with (a) 4 and (b) 20 independent identically distributed Gaussian random variables for exponential covariance kernel with different (decreasing) correlation length. The lognormal field is expressed with with 4th order Hermite polynomials. The colorbar limits are $2.5\exp(+05)$ (minimum) and $3.5\exp(+05)$ (maximum) for each subfigure.

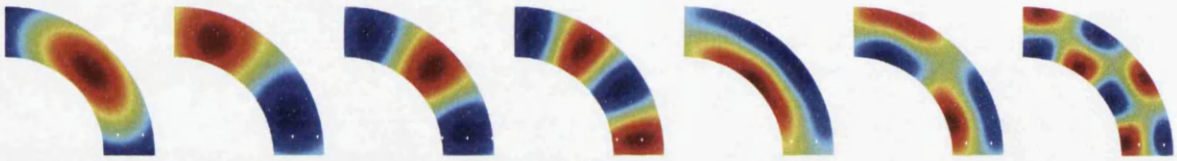

(a) Mode 01 (b) Mode 02 (c) Mode 03 (d) Mode 04 (e) Mode 08 (f) Mode 10 (g) Mode 14

(h) Mode 01 (i) Mode 02 (j) Mode 03 (k) Mode 04 (l) Mode 08 (m) Mode 10 (n) Mode 14

Figure 5.9: The orthonormalized eigenmodes associated with the discrete Karhunen-Loève expansion of the exponential covariance kernel. (a)–(g) are the eigenmodes for an exponential covariance kernel while (h)–(n) are the eigenmodes for a triangular covariance kernel. The correlation length has been taken as $[l_r/4,\ l_c/8]$ in both the cases where l_r and l_c are the radial and circumferential characteristic lengths associated with the annular circular arc.

evaluated with the discrete KL expansion method where

$$C_{\text{exp}} = \exp(-\left\|\mathbf{r}_1 - \mathbf{r}_2\right\| / \mathbf{L}_r) \quad \text{and} \quad C_{\text{tri}} = 1 - \left\|\mathbf{r}_1 - \mathbf{r}_2\right\| / \mathbf{L}_r$$

The correlation length has been chosen to be $\mathbf{L}_r = [l_r/4,\ l_c/8]$ where the components of $\mathbf{L}_r$ gives the correlation length along the radial and circumferential directions of the annular circular arc respectively and $\|\cdot\|$ denotes the L^2 norm.

While in the above example the description of the random fields was provided with the L^2 norm of the distance between the points on the physical domain, the proposed method of ob-

taining the eigenfunctions at discrete points on the spatial domain (as presented in Sec. 5.3.1) can handle a variety of covariance descriptions of the random field on any arbitrary shaped geometry. We present here a comparison of a random field model on a corrugated panel which has been described with two different covariance functions. The L^1 norm is utilized to define the distance between two points of the panel along the corrugation (like the 'blue' curve if Fig. 5.1(c)) in contrast to the L^2 norm or the Euclidean length (indicated by the 'red' curve). The models utilize these norms in the covariance function definition on the corrugated geometry. Figure 5.10(a) shows a typical meshed corrugated panel over which a paramter is assumed to be randomly distributed. Figures 5.10(b)–5.10(c) show the top view of the plots of the random elastic stiffness over the entire domain. The shaded grey area of the plot is the top view of the original undeformed corrugated panel on top of which a deformed colormap of the panel has been superimposed. The deformed colormap has been constructed such that

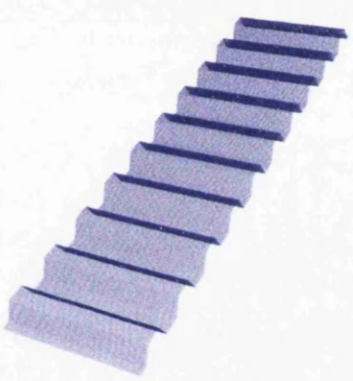

(a) A typical meshed corrugated panel with C^0 continuity of geometrical parameters across the corrugated edges.

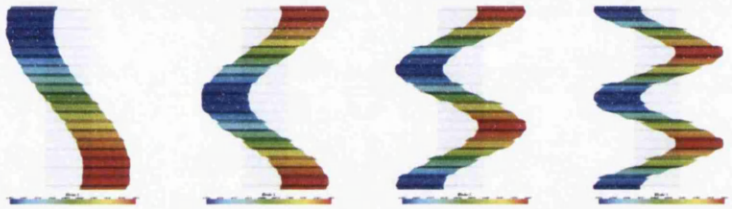

(b) Modes: $\{2, 3, 4, 5\}$ for L^1 norm of the correlation length

(c) Modes: $\{2, 3, 4, 5\}$ for L^2 norm of the correlation length

Figure 5.10: The various normalized eigen modes associated with the covariance function description of the random field over the spatial domain of a corrugated panel. The plots in (b) is for the case of L^1 norm of the length used in the covariance function while those in (c) is for L^2 norm. The latter set of curves is smoother at the edges than the former set.

the various eigen functions associated with the discrete KL expansion are plotted as sideways displacements of the nodal values of the eigenfunctions of the covariance function. The plots in Fig. 5.10(b), correspond to the L^1 norm of lengths used in the covariance function, while those in Fig. 5.10(c) are for the L^2 norm of length. For the covariance function defined with the L^2 norm, the eigen functions are smoother at the edges of the corrugation (which is C^0 continuous) compared to the eigenfunctions obtained for the case of L^1 norm.

Figure 5.11 gives a comparison of the eigenvalues of the spectral decomposition of the covariance function of the input random field over the spatial domain. The integral equation in Eqn. (2.6) has been decomposed using the discrete representation of the covariance kernel

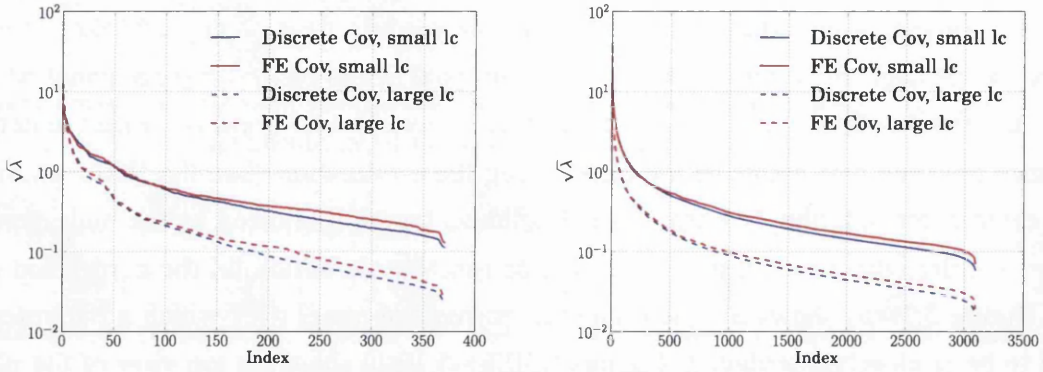

(a) Course mesh

(b) Fine mesh

Figure 5.11: Comparison of the descending eigenvalue sepctrum associated with the exponential covariance kernel with 2 different mesh resolutions of the random parametric field obtained with the discrete KL expansion method (marked as 'Discrete Cov') and the FE type solution technique (marked as 'FE Cov'). Two different correlation lengths $L/4$ and $L/20$ have been considered here which corresponds to the 'large lc' and 'small lc' respectively. The input standard deviation is $\sigma_a = 0.5$

given in Sec. 5.3.1 and using the Galerkin method as in Sec. 5.3.2. The eigenvalue spectrum shows that the eigenvalue approximations are in good agreement at least up to the first few hundred indices and the approximation is imporved as the mesh resolution is improved. Also, for small correlation lengths and coarse meshes (as seen in Fig. 5.11), the deviation is more pronounced. This suggests that for a low-order approximation of the random field with the KL eigen-functions, the 'discrete KL expansion' performs quite well.

Figure 5.12 shows the error in resolving the Fredholm integral equation using the methods of KL expansion at discrete points in the spatial domain and the FE type solution techniques. The spectral decomposition has been performed on the domain with two different mesh resolutions which corresponds to the curves shown in Fig. 5.11. The relative error has been estimated with respect to an exact covariance matrix formed for the Gaussian quadrature integration points within each element and comparing the results with an approximate covariance matrices constructed with the random field representation obtained using the discrete type KL and the Galerkin type KL resolution methods. This is as per Eqn. (5.56). Here we consider two different mesh resolutions, a coarse mesh and a refined one as shown in the figures. The results indicate that good levels of approximation is obtained with both methods and the level of accuracy is comparable. Of course, the level of error decreases as the mesh is refined. It is seen that overall the FE method performs slightly better in certain elements than the discrete KL, however the level of error is generally acceptable.

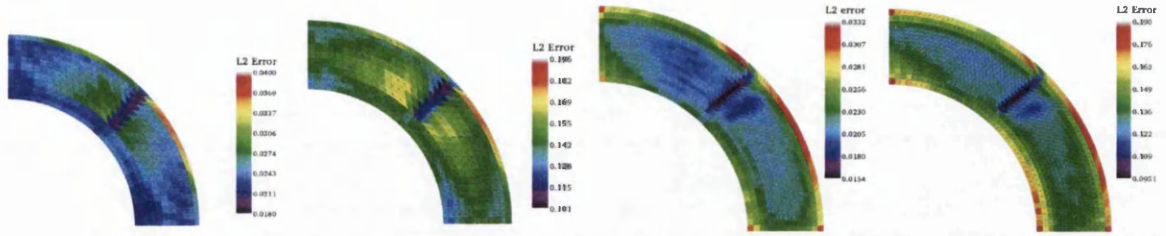

(a) Discrete KL, coarse mesh, cl= $L/4$ (b) Discrete KL, coarse mesh, cl= $L/20$ (c) Discrete KL, fine mesh, cl= $L/4$ (d) Discrete KL, fine mesh, cl= $L/20$

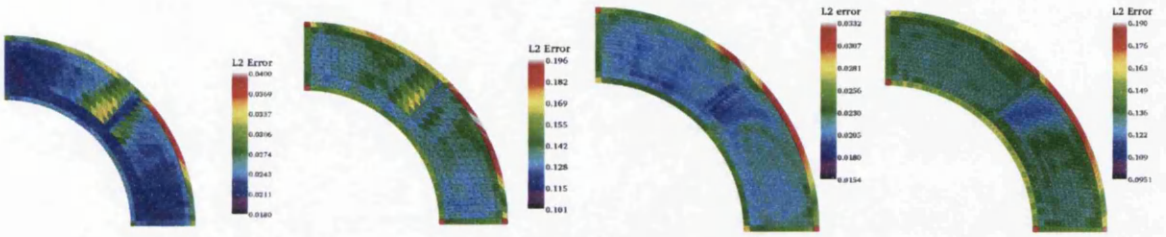

(e) Galerkin KL, coarse mesh, cl= $L/4$ (f) Galerkin KL, coarse mesh, cl= $L/20$ (g) Galerkin KL, fine mesh, cl= $L/4$ (h) Galerkin KL, fine mesh, cl= $L/20$

Figure 5.12: Comparison of the L^2 error of the covariance matrices constructed with the random field obtained from the KL eigenfunctions. The KL eigenfunctions have been resolved with the proposed 'Discrete' spectral decomposition and the FE-type 'Galerkin' method. Two different mesh resolutions have been considered here as indicated by the 'coarse' and the 'fine' mesh. *'cl'* denotes the correlation length of the input parametric random field and two distinct values have been used, $L/4$ and $L/20$ where L is the characteristic length of the domain.

5.7.2 System response

We present here numerical examples to demonstrate the applicability of the methods proposed in Secs. 5.4 and 5.5 for handling parametric uncertainty with discrete representation of the random field and for tackling the diffusion equation on a domain with random boundary fluctuations. The results for the steady state diffusion equation with parametric uncertainty is presented next. Following this, the case of unsteady diffusion on a domain with a random boundary has been studied.

Steady State System Response

We present here the results obtained for a steady state diffusion problem with random log-normal diffusivity coefficient. The covariance function is assumed to be exponential with the correlation length, 'cl', defined as the L^2 norm of the difference in position coordinates of FE nodes, where cl=$L/20$.

Figure 5.13(a) is a schematic diagram of the steady state physical system with the source and sink terms denoting the input flux to the system and the dissipation from the system respectively. Figure 5.13(b) shows the various sample realizations of the steady state system response with random diffusion coefficient. The configuration of the deterministic system is

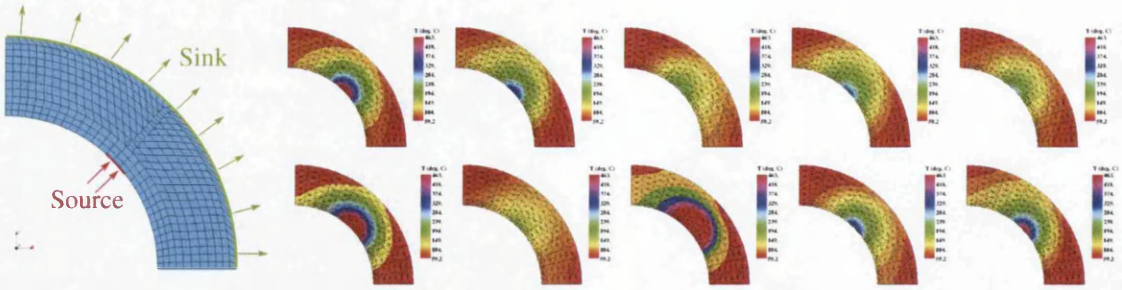

(a) Configuration of the steady state physical system

(b) Sample realizations of the steady state response of the randomly parametrized system

Figure 5.13: The configuration of the steady state physical system with the boundary conditions implemented at the displayed locations. The various sample realizations of the steady state response for a lognormal input random parameter approximated with 20 random variables is been shown in (b).

such that the response is symmetrical in the angular direction. However, due to the random diffusion coefficient we obtain different non-symmetrical distributions of the response over the spatial domain.

Figure 5.14 shows the statistics of the response over the spatial domain. Figure 5.14(a) shows the contour plot of the deterministic response and compares it to the mean and standard deviation of the response given in Figs. 5.14(b) and 5.14(c) respectively. The results show that

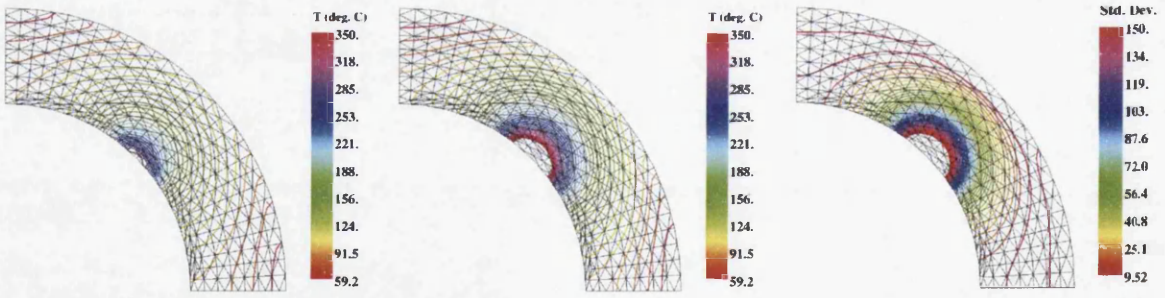

(a) Deterministic steady state response

(b) Mean Steady State response

(c) Standard deviation of the steady state response

Figure 5.14: The spatial distribution of the steady state response field.

the mean response is symmetric in the angular direction. Also for the lognormal distribution of the random field the mean response shows that more energy is concentrated near the source flux. This signifies that the dissipation of energy is not as efficient as in the deterministic case. The plot for the standard deviation also shows the highest variability of the response near the source.

Unsteady response on random domain

We take an example of an unsteady diffusion system in this study to demonstrate the methodology proposed in Sec. 5.5 for handling random boundary roughness within the finite element framework. Following from Eqn. (5.18), we write the unsteady diffusion equation on the random domain as

$$\begin{cases} C\dot{T}(t) + \nabla(K\nabla T(t)) = Q(t) \quad \text{on } \mathscr{D}_\theta; \quad \text{t} \in [0, \text{T}] \\ T(t) = G_c \quad \text{on } \Gamma_\theta^0; \\ \mathbf{n}_1 \cdot \nabla T(t) = q_1(t) \quad \text{on } \Gamma_\theta^1 \\ \mathbf{n}_2 \cdot \nabla T(t) = q_2(t) \quad \text{on } \Gamma_\theta^2 \\ \text{and} \quad T(t=0) = T_0 \quad \text{on } \mathscr{D}_\theta \end{cases} \tag{5.58}$$

where Γ_θ^1 is the 'red' part of the boundary in Fig. 5.16(a) which supplies the input flux to the system and Γ_θ^2 denotes the 'green' portion of the boundary which dissipates energy. G_c is the prescribed value of the Dirichlet boundary condition and q_1 and q_2 are the boundary flux terms. T_0 is the initial condition. The above equation indicates that the initial and boundary conditions are prescribed on the boundary for every sample realization of the random boundary. The time integration is carried out using the Euler's central difference scheme which is an implicit time stepping algorithm with a fixed time step size. The upper bound on the step size is governed by the dynamic characteristics of the transient system and has been chosen to be sufficiently small to ensure stability and convergence.

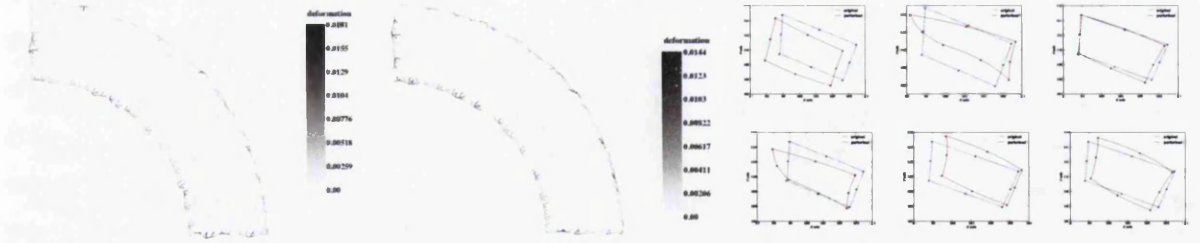

(a) Sample 1 (b) Sample 2 (c) Perturbed configurations of an element

Figure 5.15: (a)–(b) Sample realization of the domain with random boundary. The boundary fluctuations have been modeled as Gaussian random field with an exponential covariance which incorporates the correlation of the position coordinates of the nodes of the element lying on the boundary. The input standard deviation is $\sigma_a = 0.5$. (c) shows the various sample realizations of the perturbations of an element lying on the boundary of the domain shown in (a)– (b). The 'blue' colored element constitutes the baseline model while the 'red' colored ones are the various perturbed configurations.

Figure 5.15 shows two sample realizations of domains with random boundary. The boundary fluctuation has been modeled as a Gaussian random field and described with an exponential covariance function between the coordinates of the nodes of the element lying on the

boundary. The correlation length has been chosen as $L/4$ where L is the characteristic length of the domain. The discretized model of the random field has been represented with 20 random variables.

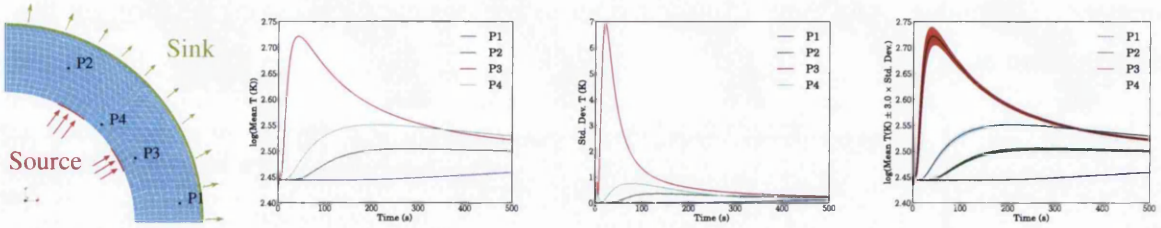

(a) Configuration of the transient system (b) Mean Response (c) Standard Deviation (d) Mean $\pm 3\times$ Std. Dev.

Figure 5.16: (a) Configuration of the unsteady diffusion system (b) & (c) Time history of the mean and standard deviation σ of the response at arbitrarily chosen points in the domain. (d) Mean with $\pm 3 \times \sigma_a$ envelope around it. The input standard deviation is $\sigma_a = 0.5$

The plot in Fig. 5.16(a) shows the configuration of the transient dynamic system on a random domain (the sample realizations of which has been shown in Fig. 5.15) with the 'red' arrows indicating the region of input energy while the 'green' arrows indicate the boundary from which energy is dissipated. The profile of the input energy can be written as $q_1 = Q_0 exp(-c_t t)$ where Q_0 is the flux at $t = 0$ and $c_t > 0$ is a constant signifying the exponential rate of decay of the input flux with time t. Here c_t has been chosen to be 0.3. Also, the output flux is given by $q_2(t) = C_h(T - T_a)$ where C_h is a positive constant with T being the response field and $T_a = 278$ is a fixed constant. Thus the rate of dissipation of energy is given by the difference $T - T_a$. The initial conditions has been chosen as $T(t = 0) = 278$. The time integration has been carried out over the interval $t = [0, 500]$ seconds. The mean and standard deviation of the response has been plotted in Figs. 5.16(b) and 5.16(c) which gives the time histories of the above response statistics at arbitrarily chosen points in the domain. Figure 5.16(d) gives the mean plotted with $\pm 3 \times \sigma$ envelope around it. Given the initial and boundary conditions, it is expected that the response would first increase with the input flux and then gradually decay and tend towards a uniform value over the entire domain.

Figure 5.17 gives the snapshots of the statistics of unsteady response plotted in the *mean* random domain at time intervals shown in the figure. Figure 5.17(a) shows that the response first grows with time at the positions of input flux and slowly decays with the time as the input flux decreases. The standard deviation plots in Figs. 5.17(b) when compared with the plot in Fig. 5.16(c) shows that evolution of the standard deviation of the response field follows the mean response pattern closely. However, it can be observed that as the response decays, the highest standard deviation is concentrated in the regions of the input flux along the radial direction of the circular arc. This is expected since the randomness in the boundary edges propagated to the response and evolving in time would be concentrated along the dominant directions of the spatial gradient of the solution (which is the radial direction in this case).

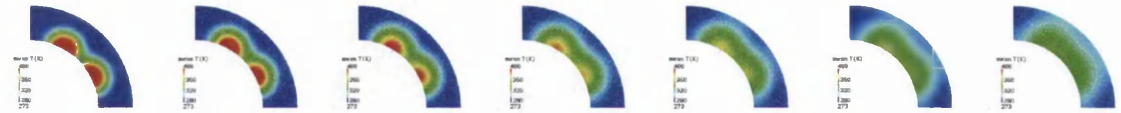

(a) Mean response at $t = \{125, 175, 225, 275, 325, 375, 450\}$ seconds

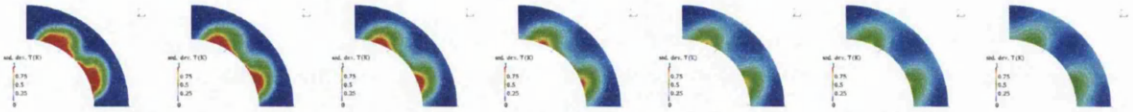

(b) Standard deviation of the response at $t = \{125, 175, 225, 275, 325, 375, 450\}$ seconds

Figure 5.17: Transient response of the mean and standard deviation (σ_T) of the stochastic field on a domain with random boundary under the action of external input flux. The boundary fluctuations have been modeled as Gaussian random field with an exponential covariance which incorporates the correlation of the position coordinates of the nodes of the element lying on the boundary. 20 iid Gaussian random variables have been used to model the random boundary. The input standard deviation is $\sigma_a = 0.5$

The convergence property of the linear system to be solved at each time step is studied here with regards to the number of iterations required for the solution to converge to a desired accuracy. Since the dimension of the linear system resulting from the finite order chaos expansion of the dynamical response grows exponentially with the stochastic space dimension and the order of chaos, implementation of sparse matrix factorization algorithms for the solution of the linear system becomes memory intensive and thus quite expensive. The Krylov iterative solvers, on the other hand, has the advantage of speeding up the linear system solution by projecting the solution in a finite dimensional Krylov subspace using orthogonal vectors. The conjugate gradient (CG) algorithm has been used here in conjunction with block diagonal preconditioners [Pellissetti and Ghanem, 2000] for the linear system solution at each time step. Additionally it offers the advantage of using the solution obtained at the previous time step as a starting guess for the solution at the current time step. This is usually very efficient especially when the time step size is small such that the change in the solution vector from the previous time step to the current one is not very large. Here we present the calculations that have been performed with different orders of expansion of the solution with the orthogonal Hermite polynomials and different values of input standard deviation of the random field.

Figure 5.18 shows the plots of the residuals given in Table 5.2 for two different value of input standard deviation of the random field. It shows that more iterations are necessary when the order chaos expansion of the solution is increased and also for an increase in the input variability of the random field. It also shows the efficacy of the preconditioning technique which enables rapid convergence to the solution even for cases of high standard deviation and input variability where the cost for the case of 'Without Preconditioner' becomes prohibitively high. This demonstrates the applicability of the preconditioning technique for the proposed formulation to solve problems on domains with arbitrary perturbations.

Table 5.3 shows a comparison of the L^2 relative error of the mean and standard devia-

Table 5.2: Convergence behaviour of the Conjugate Gradient Method with and without block-diagonal preconditioners for solving the linear system obtained from the block sparse coefficient matrix for the diffusion operator on a domain with random boundary

	Without Preconditioner				With Preconditioner			
PC	Std Dev 0.25		Std Dev 0.50		Std Dev 0.25		Std Dev 0.50	
order	Residual	Iter.	Residual	Iter.	Residual	Iter.	Residual	Iter.
2	7.91×10^{-6}	34	8.85×10^{-6}	41	9.73×10^{-6}	5	4.45×10^{-6}	9
4	9.62×10^{-6}	99	6.62×10^{-6}	144	4.76×10^{-6}	7	5.42×10^{-6}	25
6	8.99×10^{-6}	366	3.26×10^{-2}	500	6.95×10^{-6}	10	7.19×10^{-6}	68
8	5.87×10^{-4}	500	7.47×10^{-1}	500	6.77×10^{-6}	14	7.12×10^{-6}	184

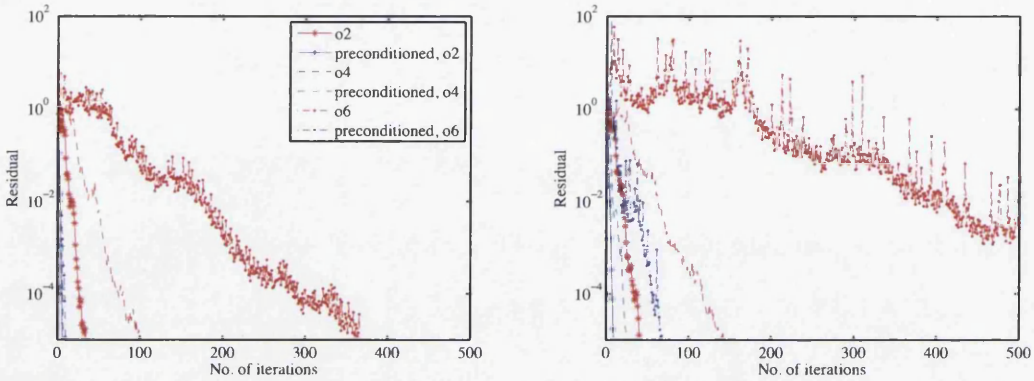

(a) Residual for CG iterations for input std. dev. 0.25

(b) Residual for CG iterations for input std. dev. 0.50

Figure 5.18: Convergence of the solution using iterative conjugate gradient (CG) scheme with and without the use of preconditioners (block-diagonal) for different orders of expansion of the solution in the stochastic Hilbert space and for two different values of input standard deviation of the random field, $\sigma_a = \{0.25, 0.50\}$.

Table 5.3: Convergence of the relative L^2 error of the mean and variance of the response with respect to the direct Monte Carlo simulation results and its relation with the residual error of the linear system for various orders of chaos expansion of the response of the diffusion system on a domain with random boundary.

PC	Input Standard Deviation 0.25			Input Standard Deviation 0.50		
order	Residual	Err (Mean)	Err (Variance)	Residual	Err (Mean)	Err (Variance)
2	7.91×10^{-6}	9.87×10^{-5}	3.51×10^{-3}	8.85×10^{-6}	4.99×10^{-4}	1.64×10^{-2}
4	8.62×10^{-6}	2.53×10^{-5}	3.30×10^{-3}	6.62×10^{-6}	1.33×10^{-4}	1.03×10^{-2}
6	9.39×10^{-6}	2.56×10^{-5}	3.30×10^{-3}	4.62×10^{-4}	9.4×10^{-5}	3.4×10^{-3}
8	5.13×10^{-6}	2.55×10^{-5}	3.30×10^{-3}	3.09×10^{-2}	6.96×10^{-5}	4.0×10^{-3}
10	9.77×10^{-6}	2.57×10^{-5}	3.30×10^{-3}	1.19	7.39×10^{-4}	2.54×10^{-2}

tion of the response on the domain with random boundary obtained with various orders of chaos expansion of the solution. The direct MCS with 10,000 samples has been taken as the benchmark solution here with respect to which the L^2 relative error has been constructed. The comparison of the various levels of residual of the linear system with the L^2 relative

error highlights the important aspect of convergence of the solution with the order of chaos expansion. It can be seen from the table that for an input standard deviation of $\sigma_a = 0.25$ and for residuals of the order of $\approx 10^{-6}$, the relative error gives a satisfactory level of convergence of the mean and standard deviation of the solution from the 4th order chaos. However, for the case of $\sigma_a = 0.50$ it is seen that for low order chaos and for residuals of $\approx 10^{-6}$ (which is rapidly reached since the dimension of the linear system is quite small for low order chaos), the levels of relative error are larger than its higher order counterparts. For the higher order chaos, it is seen that relatively high levels of residuals produces accuracy levels of $\approx 10^{-4} - 10^{-5}$ and $\approx 10^{-2} - 10^{-3}$ for the mean and standard deviation respectively.

5.8 Summary

The numerical method proposed here is an unified approach to solve the partial differential equations with random parameters on spatial domains having random boundary. The parametric field has been modeled with a finite set of random variables and a set of eigenvectors obtained from a discrete spectral decomposition of a covariance matrix. The random parametric field has been approximated on the nodes of an unstructured finite element mesh and has been interpolated at the quadrature points using the finite element shape functions. The parametric uncertainty has been modeled with random variables within the probabilistic framework and has been integrated with the isoparametric finite element formulation using stochastic mapping of the perturbed elements to the corresponding master element. The salient features of the present work can be summarized as:

- A discrete spectral decomposition of the covariance matrix to obtain the Karhunen-Loève expansion of the random field has been proposed here which evaluates the random field at the discrete finite element nodes of an unstructured mesh. The accuracy of this expansion for different mesh resolutions and orders of chaos expansion has been studied with a measure of the relative error and has been compared with a Galerkin type solution of the covariance kernel. The proposed method is not restricted to the case of uniform mesh and covers the various descriptions of the covariance function on general geometrical domains.

- The random field is approximated with the same order of spatial basis functions as the response quantity and its value at the quadrature integration points within the element are interpolated explicitly. While this increases the number of quadrature points required for integration over the spatial domain, this allows the proposed description of the random field to be utilized when using higher-order finite element basis functions.

- The explicit expressions for the coefficients of the lognormal random field have been derived in the Appendix A.1. This enables rapid evaluation of the coefficients of the

lognormal field with Hermite polynomials of independent identically distributed Gaussian random variables.

- Partial differential equation on domains with random boundary has been studied within the probabilistic framework where the boundary has been parametrized with a denumerable set of independent identically distributed random variables in conjunction with the discrete spectral components of the input covariance function. A stochastic isoparametric mapping has been proposed which maps the perturbed elements of the unstructured mesh to the corresponding master element. Tensors of stochastic shape functions have been utilized to approximate the solution within the stochastic spectral Galerkin method. The mapping of the differential operators and the associated Jacobian matrices have been expressed explicitly with random polynomials in order to facilitate prior computation of the expectations of stochastic polynomials.

- The computational complexity associated with the evaluation of the integrals in the weak formulation using the full stochastic tensor quadrature grows exponentially with the dimension and order of chaos expansion of the random field. Calculations in Table 5.1 and Sec. 5.5.4 illustrates this fact. Thus while this may be applicable for low dimensional stochastic problems with low input variability, precomputing the tensor inner products is essential even for moderate orders of chaos expansion.

- The determinant of a matrix series with stochastic coefficients has been calculated explicitly in terms of random polynomials in Sec. A.2 which enables us to pre-calculate the expectations of the stochastic polynomials.

- The statistics of the unsteady time domain response of a diffusion problem on a domain with random boundary has been solved with the proposed methodology in conjunction with the implicit central difference time stepping algorithm. The input randomness has been modeled as Gaussian random field with 20 random variables. This shows the applicability of the proposed methodology to efficiently use the stochastic isoparametric mapping to solve complex linear systems.

- The accuracy of the response statistics obtained with the proposed method for solving problems on random domain has been studied with respect to brute force Monte Carlo simulations (which serves as the benchmark solution) for various order of chaos expansions, number of quadrature integration points and the corresponding computational cost.

- The convergence of the solution of the symmetric positive definite linear system, resulting from the weak formulation of the partial differential equation on a domain with random boundary, is shown in Table 5.3. This demonstrates the efficiency of the Krylov

type iterative solvers in context of solving the large block sparse linear systems obtained for the random boundary problem in conjunction with block diagonal preconditioning techniques.

Thus results and the above discussions demonstrate the applicability and numerical accuracy of the proposed methodology to resolve the response of randomly parametrized linear systems on spatial domains with random boundary. The discrete spectral resolution of the covariance matrix gives an accurate representation of the random field, which allows us to compute the KL eigenmodes for all practical descriptions of the covariance functions of the random field on all geometrical domains. For the case of domains with random topology, using the deformation of the meshed region adjacent to the boundary surface, it is possible to capture the boundary deformation without remeshing each random realization of the domain. For low order chaos expansion and small input stochastic space dimensions, quadrature schemes may be implemented with the stochastic Galerkin scheme. However, for moderate/high dimensional stochastic problems with comparable order of chaos expansion, precomputing the statistics of the stochastic polynomials is the computationally feasible approach. This has been discussed in detail in Sec. 5.5.

The curse of dimensionality associated with the stochastic spectral Galerkin methods is still a major concern and would be addressed in the following chapter in context of resolution of the unsteady response of dynamical systems where it becomes particularly significant. This is so because when using any time integration technique to obtain the time evolution of the stochastic response, it becomes necessary to solve a large dimensional system at every time step. Hence we have approximated the dominant subspace in which the solution exists with a set of precomputed stochastic basis functions. This has been discussed in detail in the next chapter.

Chapter 6

Transient response analysis of randomly parametrized finite element systems based on approximate balanced reduction

6.1 Introduction

While the previous chapter was concerned with the development of a generic method to incorporate the input uncertainty on arbitrarily shaped domains into the weak SFEM formulation, the concern for the curse of dimensionality arising from the spectral Galerkin method applied to these problems is still a cause for concern. Hence we develop a model order reduction method applicable for the resolution of unsteady response of uncertain systems with the stochastic spectral Galerkin method. This chapter is concerned with the resolution of the large-scale randomly parametrized linear time-invariant (LTI) systems using efficient reduced order modeling techniques. We recount that the Galerkin-type methods [Ghanem and Spanos, 1991, Xiu and Karniadakis, 2002, Matthies and Keese, 2005] developed with differing choices of the approximation basis, systematically gives good accuracy of the approximate solution statistics and allows the response to be expressed explicitly in terms of the basic input random variables. Their principle drawback lies in the fact that the dimension of the resulting system of linear equations is huge. The difficulty to build efficient preconditioners and memory requirements associated with these techniques still pose a challenge and is an active area of research.

As has been discussed in context of model order reduction for large stochastic linear systems in Sec. 1.4, the additional computational overhead associated with obtaining the response statistics of the randomly parametrized systems have motivated researchers to look into various model reduction techniques for the numerical solution of SPDE. A review of some of these techniques can be found in [Nouy, 2009, Keese, 2003]. Some of these techniques attempt to perform a spectral (Hilbert Karhunen-Loève) decomposition of the stochastic solu-

tion to obtain the set of basis functions [Doostan *et al.*, 2007] or use a low-order Neumann expansion scheme to compute a estimation of the correlation structure of the response vector [Matthies and Keese, 2005]. These belong to the class of *a-posteriori* model reduction since the optimal basis is calculated from a primary approximation of the statistics of the stochastic response. On the other hand the *a-priori* model reduction schemes in context of Galerkin spectral stochastic methods evaluate the stochastic basis functions for approximating the solution using well defined optimality criterion. Methods belonging to this category are Generalized Spectral Decomposition [Nouy, 2008] and the so called Reduced Basis methods [Boyaval *et al.*, 2009].

On the other hand, the problem of reduced order modeling for linear time invariant systems (LTI) has been studied widely within the scope of control literature [Antoulas *et al.*, 2001, Gugercin and Antoulas, 2004]. The foundation for the minimal realization of LTI systems using balanced truncation has been laid in [Moore, 1981] which is a principal components analysis of the LTI system using the concept of observability and controllability Gramians. Among the vast range of other model reduction techniques for LTI systems we refer to the singular value decomposition based approaches [van der Veen *et al.*, 1993], the classical moment matching techniques [Grimme, 1997] and singular perturbation technique [Kokotovic *et al.*, 1976] for the attention they have received. Model reduction for systems with random inputs modeled as stochastic processes have been studied in [Benner and Damm, 2011, Beck *et al.*, 1996].

The objective of this study is to approach model reduction from a systems perspective where the complete information of the LTI system is available in the form of a finite element model obtained from applying the stochastic spectral Galerkin method to a randomly parametrized stochastic partial differential equation. These systems typically have very large dimension and it is a challenge to realize their transient response statistics with an appropriate reduced order model. This has remained a sparsely studied topic in the model reduction literature for large dynamical systems and forms the focus of the present work. This belongs to a class of an *a-priori* model reduction technique. The motivation of the work is provided by the fact that the statistics of the dynamical response of the randomly parametrized LTI system can be approximated by retaining only the dominant dynamical coupling characteristics between the specified input and desired outputs of the system.

For this we have looked at the dominant eigen components of the symmetric, positive definite controllability Gramian of the randomly parametrized system. Under the assumption that we are dealing with a stable LTI system, the dominant eigen modes of the stochastic controllability Gramian can provide a reduced subspace in which the dynamic response can be approximated with good accuracy. The extension of the idea of dominant modes of the controllability Gramian to the spectral stochastic Galerkin framework classically employed for the propagation of the input parametric uncertainty to the system response would give

the justification of using the method for large-scale randomly parametrized FE systems. The matrix Lyapunov equations involved in resolving the stochastic controllability Gramian can be quite expensive and hence alternative numerical schemes for approximate solutions of these equations have to be investigated.

This chapter is organized as follows. In Sec. 6.2 we introduce the model reduction problem for the resolution of the time domain response of LTI systems and give an overview of some model reduction strategies. Section 6.3 gives the model reduction for technique for stochastic dynamical systems. It discusses the idea of the minimal realization of the dynamical system based on the principal modes of the controllability Gramian and discusses the numerical methods for evaluating the principal components of this Gramian based on Arnoldi's algorithm. Section 6.4 demonstrates the proposed method with numerical examples of a transient advection-diffusion-reaction system and a pure diffusion problem. Section 6.5 gives the summary and the principal contributions of this work.

6.2 Background of model order reduction for dynamical systems

We consider a dynamical system in the state space form obtained from the finite element model of a physical LTI system as

$$\mathbf{C}\dot{\mathbf{X}}(t) = \mathbf{A}\mathbf{X}(t) + \mathbf{B}\mathbf{f}(t) \tag{6.1}$$

where $\mathbf{X}(t) \in \mathbb{R}^n$ is the vector of the state variables, $\mathbf{A}, \mathbf{C} \in \mathbb{R}^{n\times n}$ are the system matrices and $\mathbf{B} \in \mathbb{R}^{n\times p}$ is the matrix associated with the locations of a finite number p of inputs $\mathbf{f}(t) = \{f_1(t), \ldots, f_p(t)\}$. It is assumed here that the system matrices $\mathbf{A}$ and $\mathbf{C}$ are large and sparse in nature, which is the case for finite element implementation with finite order piecewise polynomials. The objective of most model reduction techniques is to obtain a good low order approximation of the solution of Eqn. (6.1) by identifying a dominant subspace in which the time varying response of the system exists.

Model reductions in context of state space systems have been widely studied for many decades [Gugercin and Antoulas, 2004]. Classical control theory literature relies on two key concepts for a low order realization of the plant mode. These are the principal component analysis and the singular value decomposition. If we consider a set of outputs of an unsteady state space system at discrete points in time as $\bar{\mathbf{X}} = \{\mathbf{X}(t_1), \mathbf{X}(t_2), \ldots, \mathbf{X}(t_m)\}$ where $\bar{\mathbf{X}} \in \mathbb{R}^{n\times m}$ then using the concept of principal component analysis it is possible to construct a alternative set of basis vectors $\mathbf{U} = \{U_1, \ldots, U_q\}$ such that $\mathbf{U} \in \mathbb{R}^{n\times q}$ where $q << n$. The response vector can be expressed in these bases as $\mathbf{x} = \sum_{i=1}^{q} U_i x_i$ and its time derivative as

$\dot{\mathbf{x}} = \sum_{i=1}^{q} U_i \dot{x}_i$. Using this, we can transform the equation in this reduced basis as

$$\mathbf{U}^T\mathbf{C}\,\mathbf{U}\dot{\mathbf{x}}(t) = \mathbf{U}^T\mathbf{A}\,\mathbf{U}\mathbf{x}(t) + \mathbf{U}^T\mathbf{B}\mathbf{f}(t) \tag{6.2}$$

where $\mathbf{x} = \{x_1, \ldots, x_q\} \in \mathbb{R}^q$ are the undetermined coefficients associated with the reduced basis. However, the solution vectors at discrete points in time are not known a-priori and hence it is not possible to ascertain the bases of a minimal order model directly. As a result we resort to the information available to us in the form from the mathematical model for of the dynamical characteristics of the LTI state space system.

6.2.1 Overview of the model reduction strategies

Model reduction schemes for large large LTI systems based on balancing [Beck *et al.*, 1996] aims to preserve invariant properties of the strong input-output dynamical coupling of the LTI system. This approach is of particular relevance in the present context and we briefly discuss the method here. We consider an LTI system as

$$\begin{cases} \dot{\mathbf{X}} = \mathbf{A}\mathbf{X} + \mathbf{B}\mathbf{f} \\ \mathbf{Y} = \mathbf{E}\mathbf{X} \end{cases} \tag{6.3}$$

with $\mathbf{A} \in \mathbb{R}^{n\times n}$, $\mathbf{B} \in \mathbb{R}^{n\times p}$, $\mathbf{E} \in \mathbb{R}^{m\times n}$ where p and m are the number of inputs and outputs respectively. The system is subjected to a sequence of p inputs in $\mathbf{f}(t) = \mathbf{e}_i\delta(t),\ 1 \geqslant i \geqslant p$ such that $\delta(t)$ are unit impulse functions and $\mathbf{e}_i$ is the i-th column of the $p \times p$ identity matrix. We consider a set of such sequence of p inputs. If an impulse response matrix of the state space system is considered which consists of k response vectors denoted by $\bar{\mathbf{X}}(t) \in \mathbb{R}^{n\times k}$, we can construct a Gramian of the state response as

$$\mathbf{P}^2 = \int_{t_1}^{t_2} \bar{\mathbf{X}}(t)\bar{\mathbf{X}}^T(t)dt \tag{6.4}$$

Here $\mathbf{P}^2$ is a real symmetric matrix which is termed as the controllability Gramian for state space systems in the control literature [Moore, 1981]. It has been shown that the system is controllable if and only if the matrix $\mathbf{P}^2$ is a full rank matrix. Controllability in this context is defined as the ability to take the system from some initial state $\mathbf{X}(t_0)$ to a final state $\mathbf{X}(t_1)$ with an input signal. For controllable systems, $\mathbf{P}^2$ is a positive semi-definite matrix. An eigen decomposition of this Gramian $\mathbf{P}^2$ gives

$$\mathbf{P}^2 = \mathbf{\Phi}\Lambda^2\mathbf{\Phi}^T\ ; \quad \mathbf{\Phi} \in \mathbb{R}^{n\times n}, \quad \Lambda^2 = \text{diag}\left\{\lambda_1^2, \ldots, \lambda_n^2\right\} \tag{6.5}$$

where $\lambda_1^2 \geqslant \lambda_2^2 \geqslant \ldots \geqslant \lambda_n^2 \geqslant 0$ is a non-negative definite sequence of eigenvalues and $\mathbf{\Phi} = \{\phi_1, \ldots, \phi_n\}$ is a matrix of mutually orthogonal eigenvectors such that $\mathbf{\Phi}^T\mathbf{\Phi} = \mathbf{I}$. If

we denote the class of all piecewise continuous input functions in $\mathbf{f}(t) = \{f_1(t), \ldots, f_p(t)\}$ within a unit circle such that $\left(\int_0^T \|f_i(t)\|^2 \, dt\right)^{1/2} \leqslant 1, \ \forall i$ and the set of state responses to these functions denoted as $\underline{\mathbf{U}}$ then

$$\underline{\mathbf{U}} = \left\{ \mathbf{X} \in \mathbb{R}^n : \mathbf{X} = \int_0^T \psi(t,\tau)\mathbf{B}\mathbf{f}(\tau) d\tau \right\} \tag{6.6}$$

where $\psi(t,\tau)$ is the state-transition matrix from τ to t. Referring back to Eqn. (6.4) it can be shown that $\underline{\mathbf{U}} \in \mathbb{R}^n$ is an ellipsoid whose principal axes lengths are the singular values λ_i of the controllability Gramian $\mathbf{P}^2$. For state space systems (as given in Eqn. (6.1)), it can be seen that the state-transition matrix is given as $\psi(t,\tau) = \exp\{\mathbf{A}(t-\tau)\}$. For stable systems where the eigenvalues of the system matrix A lies in the left half plane, $\mathbf{P}^2$ converges to a steady state matrix as $t \to \infty$, i.e. the controllability Gramian is given as

$$\mathbf{P}^2 = \int_0^\infty \exp\{\mathbf{A}\, t\}\, \mathbf{B}\mathbf{B}^T \exp\left\{\mathbf{A}^T t\right\} dt \tag{6.7}$$

where $\mathbf{P}^2$ is a stable matrix. The Gramian $\mathbf{P}^2$ contains the strong coupling characteristics between the input and the output of the state space system. Hence the principal components of the matrix Gramian $\mathbf{P}^2$ would give a dominant subspace in which the solution of the state space system lies. And this idea can potentially be used for the model order reduction of the large transient dynamic systems.

Usually two Gramians of the state space system is considered while implementing the idea of balanced truncation. These are the controllability Gramian $\mathbf{P}^2$ and the observability Gramian $\mathbf{Q}^2$. These Gramians determine the observable and controllable characteristics of the system which are mathematical duals. For the continuous time LTI systems these Gramians can be resolved from the solution of the coupled *Lyapunov* equations as

$$\begin{cases} \mathbf{A}\mathbf{P}^2 + \mathbf{P}^2\mathbf{A}^T = -\mathbf{B}\mathbf{B}^T \\ \mathbf{A}^T\mathbf{Q}^2 + \mathbf{Q}^2\mathbf{A} = -\mathbf{E}^T\mathbf{E} \end{cases} \tag{6.8}$$

Under the assumption of A being stable, the Gramians $\mathbf{P}^2$ and $\mathbf{Q}^2$ are positive semi-definite amenable to the factorization $\mathbf{P}^2 = \mathbf{P}_c^T\mathbf{P}_c$ and $\mathbf{Q}^2 = \mathbf{Q}_o^T\mathbf{Q}_o$ (which are referred to as the Cholesky factors of the Gramians). The *Hankel singular values* of the system are defined as

$$\mathbf{P}_c\mathbf{Q}_o^T = \begin{bmatrix} \mathbf{U}_1 & \mathbf{U}_2 \end{bmatrix} \begin{bmatrix} \Sigma_1 & 0 \\ 0 & \Sigma_2 \end{bmatrix} \begin{bmatrix} \mathbf{V}_1^T \\ \mathbf{V}_2^T \end{bmatrix} \tag{6.9}$$

where the diagonal matrices Σ_1 and Σ_2 consists of descending order of singular values $\sigma_i > \sigma_{i+1}$ of the matrices $\mathbf{P}_c\mathbf{Q}_o^T$. If the number of Hankel singular values chosen to represent the reduced order system is restricted to r then the reduced order model can be realized with r

components of the vectors $\mathbf{U}_r$ and $\mathbf{V}_r^T$. This consists the idea of balanced truncation where the least controllable and observable states are rejected via a similarity transformation which balances the system. In other words, a state-space realization is sought so that the controllability and observability Gramians are diagonalized and equal to the Hankel singular values. The balanced truncation approach leads to a model reduction approach which captures the transient behavior of the system satisfactorily but fails to capture the steady state response with sufficient accuracy. To overcome this, the method of singular perturbation approximation expands the solution to have zero error under steady state condition [Liu and Anderson, 1989, Kokotovic *et al.*, 1987]. But this approach is computationally expensive since it involves the solution of the matrix Lyapunov equations which involve a computational cost of $\mathcal{O}(n^3)$.

Another significant model reduction approach which has been the subject of rigorous research is based on the Krylov subspace approximation of the transfer functions of the state-space systems [Grimme, 1997, Bai, 2002]. The primary aim of these model reduction schemes is to obtain a good approximation of the dynamical characteristics (transfer function) of the system over a wide frequency range of the problem. This is achieved by expanding the moments of the transfer function with respect to the Laplace variable (or the shifted Laplace variable) and matching at least the low order the moments this expansion. If we consider an LTI state space system in Eqn. (6.3), its frequency domain input-output relationship is captured by the relationship $\hat{\mathbf{Y}}(s) = \mathbf{H}(s)\hat{\mathbf{F}}(s)$ where the transfer function $\mathbf{H}(s)$ is given by

$$\mathbf{H}(s) = \mathbf{E}\left(s\mathbf{I} - \mathbf{A}\right)^{-1}\mathbf{B} \quad s \in \mathbb{C}. \tag{6.10}$$

Here $\mathbf{H}(s)$ is a rational function of the Laplace variable s. It is assumed that the pencil $(s\mathbf{I}-\mathbf{A})$ is regular [Freund, 2000]. The transfer function is expanded as moments of s (or multipoint expansions about $(s - s_i)$) and the objective is to match the first q moments using a projection $\mathcal{P} = \mathbf{U}\mathbf{W}^T \in \mathbb{R}^{n\times n}$ with $\mathbf{U}, \mathbf{W} \in \mathbb{R}^{n\times q}$ being biorthogonal matrices such that $\mathbf{W}^T\mathbf{U} = \mathbf{I}$. The reduced order model is hence obtained as the projection of the solution on $\mathbf{U}$ and the residual being orthogonal to the space spanned by $\mathbf{W}$ as

$$\begin{cases} \mathbf{W}^T\mathbf{U}\dot{\mathbf{x}} = \mathbf{W}^T\mathbf{A}\mathbf{U}\mathbf{x} + \mathbf{W}^T\mathbf{B}\mathbf{f} \\ \mathbf{Y} = \mathbf{E}\mathbf{U}\mathbf{x} \end{cases} \tag{6.11}$$

where the solution is given by $\mathbf{X} = \mathbf{U}\mathbf{x}$. The block Krylov subspace projection technique is utilized to evaluate $\mathbf{U}$ and $\mathbf{W}$ such that the first few moments of the solution are approximated accurately

$$\begin{aligned} &\text{colsp}\left[\mathbf{U}\right] \text{ spans } \mathcal{K}_q\left(\mathbf{A}, \mathbf{B}\right) \\ &\text{colsp}\left[\mathbf{W}\right] \text{ spans } \mathcal{K}_q\left(\mathbf{A}^T, \mathbf{E}^T\right) \end{aligned} \tag{6.12}$$

The general proof of the moment matching properties of U and W has been provided in

[Grimme, 1997]. Asymptotic Waveform Evaluation (AWE) [Pillage and Rohrer, 1990], Arnoldi based algorithm [Freund, 1999], Lanczos method [Bai, 2002], Padé via Lanczos (PVL) [Feldmann and Freund, 1995] can perform single input single output system (SISO) reduction by matching the first few moments of the rational transfer function.

6.3 Randomly parametrized linear time invariant system

We consider a bounded domain $\mathscr{D} \in \mathbb{R}^d$ with piecewise Lipschitz boundary $\partial\mathscr{D}$, where $d \leq 3$ is the spatial dimension and $t \in \mathbb{R}^+$ is the time. We consider here a linear stochastic dynamical system with parametric uncertainty as

$$\frac{\partial x(\mathbf{r},t;\theta)}{\partial t} = \nabla\left(k(\mathbf{r},\theta)\nabla x(\mathbf{r},t;\theta)\right) + f(\mathbf{r},t) \quad \mathbf{r} \in \mathscr{D},\ t = [0,T] \tag{6.13}$$

where the $k(\mathbf{r},\theta) : \mathbb{R}^d \times \theta \rightarrow \mathbb{R}$ is a square integrable random field in the probability space $(\Theta, \mathscr{F}, P)$ and $f(\mathbf{r},t) \in \mathbb{R}$ is the deterministic time varying external forcing function. The objective is to solve for the stochastic transient system response $x(\mathbf{r},t;\theta)$ which exists in the tensor product Hilbert space $H(\mathscr{D} \times \Theta \times T)$. A finite element discretization of the spatial domain results in the set of elements $S_e = \{\Delta(\mathscr{D}_h) : \bigcup \Delta(\mathscr{D}_h) = \mathscr{D}\}$ where h is the mesh parameter size. We assume that the discretized stochastic field is expressed at the n_e nodal points within each element of the FE mesh as $\mathbf{k}^e(\theta) \in \mathbb{R}^{n_e}$ and is interpolated inside the element domain with the spatial basis function as

$$k^e(\mathbf{r},\theta) = [N(\mathbf{r})]^T\,\mathbf{k}^e(\theta) = [N(\mathbf{r})]^T \sum_{i=0}^{p_k} \hat{\boldsymbol{k}}_i^e \mathscr{H}_i(\theta) \tag{6.14}$$

where $\hat{\boldsymbol{k}}_i^e \in \mathbb{R}^{n_e}\ \forall i = 1,\ldots,p_k$, $[N(\mathbf{r})]$ is the vector of FE shape functions belonging to the Sobolev space $S^{k,2} \subset L^2(\Delta(\mathscr{D}_h))$ which are C^k-continuous within the element domain, $k \geqslant 1$. Also, $\mathscr{H}(\boldsymbol{\xi}(\theta)) = \{\mathscr{H}_1(\boldsymbol{\xi}(\theta)),\ldots,\mathscr{H}_{p_k}(\boldsymbol{\xi}(\theta))\}$ are the orthogonal stochastic polynomials which model the input parametric uncertainty in the finite dimensional stochastic space. This leads to the stochastic finite element linear system as

$$\mathbf{C}\dot{\mathbf{X}}(t;\theta) = \mathbf{K}(\theta)\mathbf{X}(t;\theta) + \bar{\mathbf{B}}\mathbf{f}(t) \tag{6.15}$$

$$\text{or,}\quad \dot{\mathbf{X}}(t;\theta) = \mathbf{A}(\theta)\mathbf{X}(t;\theta) + \mathbf{B}\mathbf{f}(t) \tag{6.16}$$

To keep the discussions simple, it is assumed that the forcing function $\mathbf{f}(t)$ is deterministic in nature. Here $\mathbf{K}(\theta)$ or $\mathbf{A}(\theta)$ are the system matrices for each stochastic sample realization $\theta \in \Theta^{(M)}$. It can be seen from the above equation that we have changed the descriptor form of the linear system in Eqn. (6.15) to the standard form in Eqn. (6.16) where $\mathbf{A}(\theta) = \mathbf{C}^{-1}\mathbf{K}(\theta)$ and $\mathbf{B} = \mathbf{C}^{-1}\bar{\mathbf{B}}$. Doing this has its disadvantages which might seriously affect the

efficiency of the solver. However, we have used the standard form of Eqn. (6.16) for the time being to facilitate ease of theoretical discussion without making the notation too complicated. We would include in the subsequent section the methods to deal with the descriptor systems within a completely generic framework (given in Sec. 6.3.4). Here $\bar{\mathbf{B}}$ is the input distribution array and hence $\mathbf{B} \in \mathbb{R}^{n \times p}$ is associated with the p inputs to the system. The inputs are modeled via $\mathbf{f}(t) = \{f_1(t), \ldots, f_p(t)\} \in \mathbb{R}^p$. The stochastic matrix and $K(\theta)$ are expressed in the series expansion form as

$$\mathbf{K}(\theta) = \mathbf{K}_0 + \sum_{i=i}^{P_k} \mathbf{K}_i \mathscr{H}_i(\boldsymbol{\xi}(\theta)) \tag{6.17}$$

where $\mathbf{K}_0 \in \mathbb{R}^{n \times n}$ is the matrix belonging to the baseline model (with the associated stochastic functions being equal to 1) while $\mathbf{K}_i$ are the perturbation matrices associated with the stochastic functions in $\mathscr{H}(\boldsymbol{\xi}(\theta))$. The input parametric uncertainty is modeled within the probabilistic framework with iid random variables $\boldsymbol{\xi}(\theta) \in \mathbb{R}^M$. Hence the global input stochastic space is a M dimensional hyperspace $\Theta^{(M)} \subset \Theta$.

6.3.1 Minimal realization of the randomly parametrized dynamical system

The state transition matrix $\boldsymbol{\Psi}(t, \tau; \theta)$ of the stochastic LTI system would incorporate the input parametric uncertainty in $\boldsymbol{\xi}(\theta) \in \mathbb{R}^M$. Hence $\boldsymbol{\Psi}(t, \tau; \theta) : \mathbf{X}(\tau; \theta) \mapsto \mathbf{X}(t; \theta)$ for each $\theta \in \Theta^{(M)}$. The controllability Gramian of this system $\mathbf{P}^2(\theta) \in \mathbb{R}^{n \times n}$ can be realized for each point in the M dimensional stochastic input space $\Theta^{(M)}$. Our aim here is to obtain the dominant stochastic modes of the controllability Gramian and the solution of the stochastic system would be projected on to these basis functions.

The stochastic controllability Gramian for the randomly parametrized LTI system in Eqn. (6.16) obeys the Lyapunov equation for each sample θ as

$$\mathbf{A}(\theta)\mathbf{P}^2(\theta) + \mathbf{P}^2(\theta)\mathbf{A}^T(\theta) + \mathbf{B}\mathbf{B}^T = 0\,; \quad \text{where } \mathbf{P}^2(\theta) \in \mathbb{R}^{n \times n}\ \forall\ \theta \in \Theta^{(M)} \tag{6.18}$$

where the stochastic coefficient matrix $\mathbf{A}(\theta)$ can be written in the series expandable form as $\mathbf{A}(\theta) = \sum_{i \in \mathscr{I}_{\mathscr{H}}} \mathbf{A}_i \mathscr{H}_i(\boldsymbol{\xi}(\theta))$ with $\mathbf{A}_i \in \mathbb{R}^{n \times n}\ \forall i$. Hence the dominant modes of $\mathbf{P}^2(\theta)$ would be obtained in $\mathbb{R}^n$ for every random sample realization in $\Theta^{(M)}$. Here we take $\mathbf{X}(t; \theta) \in \mathbb{R}^n$ to denote the stochastic system solution for every random sample $\theta \in \Theta^{(M)}$ at all points in time $t \in [0, T]$. If we use a separable representation of this space in the form $H(T) \otimes H(\mathbb{R}^n \times \Theta^{(M)})$, the stochastic system response $\mathbf{X}(t, \theta) \in \mathbb{R}^n$ at time t can be represented as

$$\mathbf{X}(t; \theta) = \sum_{i=0}^{n_r} \alpha_i(t) U_i(\theta)\,; \quad \text{such that } U_i(\theta) : \mathbb{R}^n \times \theta \to \mathbb{R}^n,\ \alpha_i : T \to \mathbb{R} \quad \forall i \tag{6.19}$$

where $\mathbf{U}(\theta) = \{U_0, \ldots, U_{n_r}\}$ are the n_r stochastic reduced basis of the linear system and $\alpha = \{\alpha_1, \ldots, \alpha_{n_r}\}$ is the map of the time dependent stochastic coefficients to n_r undetermined coefficients. The identification of the principle modes $\mathbf{U}$ can be performed from the spectral decomposition of the stochastic Gramian $\mathbf{P}^2(\theta)$ using methods such as stochastic sampling. The simplest sampling based technique is the Monte Carlo method where the principal modes of $\mathbf{P}^2(\theta)$ for each stochastic sample θ of an ensemble of N random samples in $\Theta^{(M)}$ is solved to obtain $\mathbf{U}_\theta \in \mathbb{R}^{n \times n_r}$ for each random realization θ. Assuming that these modes are associated with the most dominant spectral components, we can expand them with orthogonal polynomials spanning the stochastic Hilbert space as $U_i(\theta) = \sum_{j=0}^{p} U_{ij} \mathscr{H}_j(\boldsymbol{\xi}(\theta))$ such that

$$U_{ij} = \frac{\langle \mathscr{H}_j(\boldsymbol{\xi}(\theta)), U_i(\theta) \rangle_{L^2(\Theta^{(M)})}}{\langle \mathscr{H}_j^2(\boldsymbol{\xi}(\theta)) \rangle_{L^2(\Theta^{(M)})}} \; ; \quad U_{ij} \in \mathbb{R}^n \tag{6.20}$$

However, this method is not favorable since obtaining ensemble of $U_i(\theta)$ for every random realization θ is computationally quite expensive. It is possible to use efficient stochastic sampling based techniques or other surrogate modeling to improve the evaluation of these bases functions [Ma and Zabaras, 2009].

A closer look into the problem of identification of the dominant modes of the stochastic transient system reveals that it is necessary to evaluate a vector basis $\mathbf{U}^r = \left[U_1^r, \ldots, U_{n_r}^r\right]$ such that it captures the solution of the stochastic finite element system within the time interval $t = [0, T]$ with sufficient accuracy. Hence, if we start with a generic framework of decomposition of the tensor product Hilbert space in which the stochastic transient solution exists (considered in the context of Eqn. (6.19)) with a set of basis functions, we can write

$$\mathbf{X}(t, \theta) = \sum_{i \in \mathscr{I}_\alpha} \sum_{j \in \mathscr{I}_\mathscr{H}} \alpha_i \mathscr{H}_j(\theta) U_{ij}^r \tag{6.21}$$

where $U_{ij}^r \in \mathbb{R}^n$ are the reduced basis functions on which the solution is projected, $\mathscr{I}_\alpha$ and $\mathscr{I}_\mathscr{H}$ are the cardinality of the sets consisting of the undetermined coefficients α and the orthogonal stochastic functions $\mathscr{H}_j(\theta)$ respectively. The residual $\mathbf{R}(t; \theta) \in \mathbb{R}^n$, $\forall \theta \in \Theta^{(M)}$ associated with the stochastic transient FE linear system (given in Eqn. (6.15)) is given as

$$\mathbf{R}(t; \theta) = \mathbf{C}\dot{\mathbf{X}}(t; \theta) + \mathbf{K}(\theta)\mathbf{X}(t; \theta) - \bar{\mathbf{B}}\mathbf{f}(t) \tag{6.22}$$

Here we apply the stochastic Galerkin method where the residual is made orthogonal to the basis U^r in $\mathbb{R}^n$ and the finite order orthogonal basis functions $\mathscr{H}(\theta)$ spanning the stochastic subspace $\Theta^{(M)}$. This can be written as

$$\left\langle \mathscr{H}_i(\theta) U_j^r, \mathbf{R}(t, \theta) \right\rangle_{\mathbb{R}^n \times L^2(\theta^{(M)})} = 0 \quad \forall i \in \mathscr{I}_\mathscr{H}, \; \forall j \in \mathscr{I}_\alpha, \text{ and } \forall t \in [0, T] \tag{6.23}$$

where $\mathbf{R}(t, \theta) : \mathbb{R}^n \times \Theta^{(M)} \rightarrow \mathbb{R}^n$ is the residual of the linear system given in Eqn. (6.22).

The identification of the dominant basis U^r has to be determined which is the focus of the following sections.

6.3.2 Vectorization of stochastic Lyapunov matrix equations

To obtain the reduced basis as discussed in Eqn. (6.21) we focus on the stochastic controllability Gramian considered in Eqn. (6.18). The stochastic realizations of the Gramian of the stochastic time varying linear system satisfies Eqn. (6.18). The random quantity $\mathbf{P}^2(\theta)$ can be expressed as a series expansion of finite order chaos expansion in the stochastic Hilbert space with orthogonal polynomials as

$$\mathbf{P}^2(\theta) = \sum_{i \in \mathscr{I}_{\mathscr{H}}} \mathbf{P}_i \mathscr{H}_i(\boldsymbol{\xi}(\theta)) \tag{6.24}$$

The Lyapunov equation involving this stochastic controllability Gramian $\mathbf{P}^2(\theta)$ can be solved with the Galerkin method using this expansion. Applying the Galerkin orthogonalization of the residual to the orthogonal stochastic basis we have

$$\left\langle \mathscr{H}_i(\boldsymbol{\xi}(\theta)), \left(\mathbf{A}(\theta)\mathbf{P}^2(\theta) - \mathbf{P}^2(\theta)\mathbf{A}^T(\theta) + \mathbf{B}\mathbf{B}^T\right) \right\rangle_{L^2(\theta^{(M)})} = 0 \; ; \quad \forall \, i \in \mathscr{I}_{\mathscr{H}} \tag{6.25}$$

In order to facilitate the matrix equation (such as the one given in Eqn. (6.18)) to be expressed as a set of linear equations, we use to the linear map $vec(\cdot)$ which describes a one to one mapping a set of k column vectors in the $n \times k$-dimensional matrix to a vector in the nk-dimensional space and is expressed as $vec(\mathbf{V}_{n\times k}) = [V_{11}, \ldots, V_{n1}, \ldots, V_{1k}, \ldots, V_{nk}]$. Using this linear map and the associated identities i.e. $vec(\mathbf{AXB}) = (\mathbf{B}^T \otimes \mathbf{A})vec(\mathbf{X})$, we can write Eqn. (6.18) as

$$\begin{aligned} & vec\left(\mathbf{A}(\theta)\mathbf{P}^2(\theta) + \mathbf{P}^2(\theta)\mathbf{A}^T(\theta) + \mathbf{B}\mathbf{B}^T\right) = 0 \\ \text{or,} \quad & \left[\mathbf{I} \otimes \mathbf{A}(\theta) + \mathbf{A}(\theta) \otimes \mathbf{I}\right] vec\left(\mathbf{P}^2(\theta)\right) = -vec\left(\mathbf{B}\mathbf{B}^T\right) \end{aligned} \tag{6.26}$$

where $\mathbf{I} \in \mathbb{R}^{n\times n}$ is the identity matrix. Using this we can transform the expansion of the stochastic Gramian in Eqn. (6.24) to

$$vec(\mathbf{P}^2(\theta)) = \sum_{i \in \mathscr{I}_{\mathscr{H}}} vec(\mathbf{P}_i)\mathscr{H}_i(\boldsymbol{\xi}(\theta)) \tag{6.27}$$

This vector form of the equation is utilized in the Galerkin framework in an identical manner

as shown in Eqn. (6.25) which can be written as

$$\left\langle \mathscr{H}_i(\boldsymbol{\xi}(\theta)), \left(\mathbf{A}(\theta) \sum_{i \in \mathscr{I}_{\mathscr{H}}} vec(\mathbf{P}_i) \mathscr{H}_i(\boldsymbol{\xi}(\theta)) \right) \right\rangle_{L^2(\theta^{(M)})} = - \left\langle \mathscr{H}_i(\boldsymbol{\xi}(\theta)), vec(\mathbf{B}\mathbf{B}^T) \right\rangle_{L^2(\theta^{(M)})} \quad \forall\, i \in \mathscr{I}_{\mathscr{H}} \tag{6.28}$$

where $\mathbf{A}(\theta) = [\mathbf{I} \otimes A(\theta) + A(\theta) \otimes \mathbf{I}]$. This gives a linear system of the form

$$\begin{bmatrix} \mathbf{A}_{11} & \mathbf{A}_{12} & \cdots & \mathbf{A}_{1p} \\ \mathbf{A}_{21} & \mathbf{A}_{22} & & \vdots \\ \vdots & & \ddots & \vdots \\ \mathbf{A}_{p1} & \cdots & \cdots & \mathbf{A}_{pp} \end{bmatrix} vec \left(\begin{bmatrix} \mathbf{P}_1 \\ \vdots \\ \vdots \\ \mathbf{P}_p \end{bmatrix} \right) = vec \left(\begin{bmatrix} -\mathbf{B}\mathbf{B}^T \\ 0 \\ \vdots \\ 0 \end{bmatrix} \right) \tag{6.29}$$

where the matrix blocks $\mathbf{A}_{ij} = \langle \mathscr{H}_i(\boldsymbol{\xi}(\theta)) \mathscr{H}_j(\boldsymbol{\xi}(\theta)), [\mathbf{I} \otimes \mathbf{A}(\theta) + \mathbf{A}(\theta) \otimes \mathbf{I}] \rangle_{L^2(\theta^{(M)})}$ involve inner product of the set of stochastic polynomials in $\mathscr{H}(\boldsymbol{\xi}(\theta))$. $\mathbf{P}_i$ are block matrices as given in Eqn. (6.24) and the right hand side of the equation has only its first block as nonzero, while the rest are zero since $\mathrm{E}[\mathscr{H}_i(\theta)] = 0 \ \forall i \neq 0$. The above system of linear matrix equations can be solved using solvers based on matrix factorization or Krylov based methods. For example, the Bartels-Stewart method [Bartels and Stewart, 1972] or the Hammarling method [Hammarling, 1982] involves reducing the coefficient matrix to a real Schur form which involves a computational cost of $\mathscr{O}(N^3)$ where N is the dimension of the linear system. In the vectorized form, as shown in Eqns. (6.26) and (6.29), the dimension of the linear system to be solved is given as $N = n^2 n_p$ where n_p is given by the dimension of the stochastic system M and order of chaos expansion chosen p as $n_p = \binom{M}{p}$. After solving for the vectorized Lyapunov Gramian, the Gram matrix $\mathbf{P}^2(\theta)$ can be reconstructed using the inverse mapping of the linear map used in Eqn. (6.27). Hence solving the full vectorized Lyapunov equation can become extremely expensive even for moderate dimensions of input stochastic space.

6.3.3 Approximating the stochastic Gramian of the random system response

A closer look at the stochastic Gram matrix $\mathbf{P}^2(\theta)$ reveals that for every random sample θ it can be written in $t = [0, \infty)$ as

$$\mathbf{P}^2(\theta) = \int_0^\infty \exp\{\mathbf{A}(\theta)\, t\}\, \mathbf{B}\mathbf{B}^T \exp\{\mathbf{A}^T(\theta)\, t\}\, dt \tag{6.30}$$

Since the exponential term could be represented in a series expandable form with stochastic coefficients, a general representation of this stochastic Gramian can be written as $\mathbf{P}(\theta) = \sum_{i=0}^{n_a} \bar{\lambda}_i(\theta) \bar{\mathbf{P}}_i$ like the expression in Eqn. (6.24). It is seen that that the time domain solution

of the randomly parametrized system in Eqn. (6.16) exists in the tensor product space $\mathcal{S}^{n,\theta}$ given by

$$\mathcal{S}^{n,\theta} := \mathbb{R}^n \otimes L^2(\Theta^M) \tag{6.31}$$

where $\mathbb{R}^n$ contains the solution at the n finite element nodes and $L^2(\Theta^{(M)})$ is a function space of the M-dimensional stochastic space defined by the iid random variables used to model the input uncertainty. Assuming that we choose n_a stochastic basis functions spanning an n_a dimensional subspace of the stochastic functions space $L^2(\Theta^{(M)})$ as $\mathscr{H}(\boldsymbol{\xi}(\theta)) = \{\mathscr{H}_0(\boldsymbol{\xi}(\theta)), \ldots, \mathscr{H}_{n_a}(\boldsymbol{\xi}(\theta))\}$, we can express the solution vector at time t as

$$\begin{aligned} \mathbf{X}(t,\theta) &= \sum_{i=1}^{n}\sum_{j=0}^{n_a} \mathbf{e}_i \mathscr{H}_j(\boldsymbol{\xi}(\theta)) x_{i,j} \quad \text{where} \quad \mathbf{e}_i \in \mathbb{R}^n \\ \text{or,} \quad \mathbf{X}(t,\theta) &= \underline{\mathbf{X}}(t)\mathscr{H}(\boldsymbol{\xi}(\theta)) \end{aligned} \tag{6.32}$$

where $\underline{\mathbf{X}} \in \mathbb{R}^{n \times n_a}$ is a second order tensor associated with the canonical bases $\mathbf{e}_i$ of the Euclidean space $\mathbb{R}^n$ and $\mathscr{H}(\boldsymbol{\xi}(\theta))$ is the basis of the stochastic subspace spanned by the polynomial function elements of it. Now we apply the stochastic Galerkin method where the residual of the linear system is made orthogonal to the stochastic basis functions. Thus from Eqn. (6.16) we write

$$\begin{aligned} &\left\langle \mathscr{H}_i(\boldsymbol{\xi}(\theta)), \left\{ \dot{\underline{\mathbf{X}}}(t)\mathscr{H}(\boldsymbol{\xi}(\theta)) - \mathbf{A}(\theta)\underline{\mathbf{X}}(t)\mathscr{H}(\boldsymbol{\xi}(\theta)) + \mathbf{B}\mathbf{f}(t) \right\} \right\rangle_{L^2(\theta)} = 0 \\ &\text{which gives,} \quad \dot{\mathcal{X}}(t) = \mathcal{A}\mathcal{X}(t) + \mathcal{B}\mathcal{F}(t) \end{aligned} \tag{6.33}$$

where $\mathcal{A} \in \mathbb{R}^{N_a \times N_a}$ is a block sparse finite element system obtained with the finite order chaos expansion with stochastic Galerkin method. The objective of the model reduction scheme is to identify a dominant basis for the second order tensor $\underline{\mathbf{X}}$ with which the solution can be accurately approximated with lesser computational effort.

If the second order tensor $\underline{\mathbf{X}}$ is vectorized as $X_{\text{vec}} = vec(\underline{\mathbf{X}}) \in \mathbb{R}^{N_a}$ (where $N_a = n.n_a$), then it is possible to construct a squared Gram matrix $\overline{\mathbf{W}}^2$ for the solution approximated in the tensor product space $S^{n,\theta}$ as

$$\overline{\mathbf{W}}^2 = \int_0^T \{X_{\text{vec},1}(t), \ldots, X_{\text{vec},p}(t)\} \{X_{\text{vec},1}(t), \ldots, X_{\text{vec},p}(t)\}^T dt \tag{6.34}$$

where $\overline{\mathbf{W}}^2 \in \mathbb{R}^{N_a \times N_a}$ is a Gramian of the system in the tensor product space spanned by $\{\mathbf{e}_1, \ldots, \mathbf{e}_n\} \otimes \mathscr{H}(\boldsymbol{\xi}(\theta))$ and $\{X_{\text{vec},1}(t), \ldots, X_{\text{vec},p}(t)\}$ is a collection of p vectors each of dimension N_a which represent solutions at time t. From this discussion it is clear that the stochastic Gramian $\overline{W}^2$ in Eqn. (6.36) is exact for the chosen order of chaos in expressing the solution of the randomly parametrized system in the tensor product space denoted by $\mathcal{S}^{n,\theta}$ in

Eqn. (6.31). It is readily seen that the Gramian $\overline{\mathbf{W}}^2$ satisfies the Lyapunov equation

$$\mathcal{A}\overline{\mathbf{W}}^2 + \overline{\mathbf{W}}^2\mathcal{A}^T = \mathcal{B}\mathcal{B}^T \tag{6.35}$$

The above is a matrix equation of dimension $N_a \times N_a$ which is significantly larger than the size of the baseline finite element system. The dimension increases exponentially with the order of chaos and the dimension of the input stochastic space. The solution of this matrix equations can be performed with the available Lyapunov equation solver [Penzl, 1998]. However, these solvers are computationally expensive and do not take advantage of the sparsity of the system matrices which is always obtained for large FE systems.

Once the matrix equation has been solved to obtain the Gramian $\overline{\mathbf{W}}^2$, the spectral decomposition of the latter gives the dominant eigenmodes of the Gramain. These eigenmodes form the basis functions of the reduced subspace in which the solution is sought [Laub *et al.*, 1987]. The stochastic system solution with a finite order chaos expansion in $t = [0, T]$ can be approximated with the dominant modes obtained from the eigen decomposition of $\overline{\mathbf{W}}^2$ such that

$$\overline{\mathbf{W}}^2 = \overline{\mathbf{\Phi}}\mathbf{\Lambda}\overline{\mathbf{\Phi}}^T \tag{6.36}$$

Here $\overline{\mathbf{\Phi}}_P = \left\{\overline{\phi}_i : \overline{\phi}_i^T\overline{\phi}_j = \delta_{ij},\ \overline{\phi}_i \in \mathbb{R}^{N_a}\ \forall\ i,j = 1,\ldots,n_r\right\}$ where n_r denotes the reduced number of eigen modes chosen from the eigenvalue decomposition of $\overline{\mathbf{W}}^2$. The eigenvectors $\overline{\phi}_i \in \mathbb{R}^{N_a}$ can be transformed via the inverse vectorization operator to the matrix $\overline{\boldsymbol{\phi}}_{i,n_a} \in \mathbb{R}^{n\times n_a}$ as $\overline{\boldsymbol{\phi}}_{i,n_a} = vec^{-1}(\overline{\phi}_i)\ \forall\ 1 \geqslant i \geqslant n_r$ such that $\overline{\boldsymbol{\phi}}_i = \left[\overline{\phi}_{i,1}\cdots\overline{\phi}_{i,n_a}\right]$ where $\overline{\phi}_{i,j} \in \mathbb{R}^n\ \forall\ j = 1,\ldots,n_a$. These, when used as the basis in $\mathbb{R}^{n\times n} \times \Theta^{(M)}$ on which the solution $\mathbf{X}(t;\theta)$ is projected, give

$$\mathbf{X}(t,\theta) = \sum_{i=1}^{n_r}\alpha_i(t)\sum_{j=1}^{n_a}\overline{\phi}_{i,j}\mathscr{H}_j(\boldsymbol{\xi}(\theta)) \tag{6.37}$$

Here the coefficients α_i capture the time varying component of the solution. A careful observation shows that the reduced order model of the system response is based on identifying the principal modes on which the solution can be projected in the tensor product space $\mathcal{S}^{n,\theta}$ (as given in Eqn. (6.31)). Increasing the order of the minimal realization, i.e. using a higher number of basis functions $\overline{\boldsymbol{\phi}}_{i,n_a}$ from the spectral decomposition of $\overline{W}^2$ does not increase the order of chaos functions used in approximating the solution. It only provides a better approximation of the solution in the stochastic space in which the Gramian $\overline{W}^2$ has been conceived.

Now solving the eigenvalue problem to identify the principal modes of the solution can become quite expensive when dealing with large finite element systems and even a moderate dimensional stochastic space. The primary obstacle is the solution of the matrix Lyapunov equations followed by the solving for the dominant eigenmodes of the Gramian. This serves as the motivation to look for alternate techniques to identify the principal modes of the Gramian

of the stochastic state space system [Li and White, 2002].

It might be noted here that we do not actually require the estimate of the Gramian $\overline{\mathbf{W}}^2$, rather it is only necessary to obtain the principal modes of this Gramian. This motivates us to seek a low-rank approximation $\overline{\mathbf{W}}_*^2$ of the Gramian such that $\left\|\overline{\mathbf{W}}^2 - \overline{\mathbf{W}}_*^2\right\|_{\mathrm{F}}$ is minimized where $\|\cdot\|_{\mathrm{F}}$ denotes the Frobenius matrix norm. This has been looked at in the following section.

6.3.4 Arnoldi's method for decomposition of Gram matrix

An eigenvalue decomposition of the matrix $\overline{\mathbf{W}}^2$ is given in Eqn. (6.36) where the eigenvalues in the diagonal matrix Λ is assumed to be ordered as $|\lambda_1| \geqslant \ldots \geqslant |\lambda_{N_a}|$. If we choose only the first n_r modes from this set then the approximate Gramian is given as $\overline{\mathbf{W}}_*^2 = \overline{\mathbf{\Phi}}_{n_r} \mathbf{\Lambda}_{n_r} \overline{\mathbf{\Phi}}_{n_r}$. If we choose a basis $\mathbf{U}_{n_r} \in \mathbb{R}^{N_a \times n_r}$ on which the Gramain $\overline{\mathbf{W}}^2$ is projected, we can write the Lyapunov equation in Eqn. (6.35) as

$$\mathbf{U}_{n_r}^T \mathcal{A} \mathbf{U}_{n_r} \mathcal{W} + \mathcal{W} \mathbf{U}_{n_r}^T \mathcal{A}^T \mathbf{U}_{n_r} = -\mathbf{U}_{n_r}^T \mathcal{B}\mathcal{B}^T \mathbf{U}_{n_r} \tag{6.38}$$

Using this, the approximate Gramian is given by $\overline{\mathbf{W}}_*^2 = \mathbf{U}_{n_r} \mathcal{W} \mathbf{U}_{n_r}^T$. The accuracy of the solution is governed by the selection of the basis $\mathbf{U}_{n_r}$ which should span the same n_r dimensional subspace as that spanned by the vectors in $\overline{\mathbf{\Phi}}_{n_r}$.

This motivates us to identify the subspace associated with the dominant modes of the stochastic system matrices present in the Lyapunov equations. We start with the m-dimensional Krylov subspace associated with the system matrices obtained after applying the stochastic Galerkin method as

$$\mathcal{K}^m \{\mathcal{A}, \mathcal{B}\} = \text{span} \left\{\mathcal{B}, \mathcal{A}\mathcal{B}, \mathcal{A}^2\mathcal{B}, \ldots, \mathcal{A}^{m-1}\mathcal{B}\right\} \tag{6.39}$$

For $\mathcal{B} \in \mathbb{R}^{n \times q}$ with q inputs, the block Krylov method would be considered where the dimension of the Krylov space would become $m \times q$. The block Arnodli algorithm [Wilkinson, 1988] is used to calculate the orthonormal basis Q spanning the m dimensional dominant eigen space. This consists of the following steps

Estimation of the Arnoldi-Lyapunov bases for reduced order modeling of stochastic system

1. *Initialize* $\mathbf{Q} = [\mathbf{Q}_1]$ *such that* $\mathbf{Q}_1 \in \mathbb{R}^{n \times q}$ *with an orthogonal basis spanning the column space of* $\mathcal{B}$.

2. *Calculate the orthogonal bases spanning the* n_k *dimensional block Krylov space given by*

$$\mathcal{K}_{n_k}(\mathcal{A}, \mathcal{B}) = \textit{span} \left\{\mathcal{B}, \mathcal{A}\mathcal{B}, \mathcal{A}^2\mathcal{B}, \ldots, \mathcal{A}^{n_k-1}\mathcal{B}\right\}$$

using a Gram-Schmidt process or a modified Gram-Schmidt process to get the set of orthogonal vector basis $\mathbf{Q} = \{\mathbf{Q}_1, \mathbf{Q}_2, \ldots, \mathbf{Q}_{n_k}\}$ *where* $\mathbf{Q}_i \in \mathbb{R}^{n \times q}\, \forall i = 1, \ldots, n_k$.

3. *To use an error indicator as a stopping criterion, use the following steps*

   (a) *Calculate the block upper Hessenberg matrix* $\mathcal{A}_{qn_k} \in \mathbb{R}^{qn_k \times qn_k}$ *such that* $\mathcal{A}_{qn_k} = \mathbf{Q}^T \mathcal{A} \mathbf{Q}$. *Denoting the residual of the Lyapunov equation as* $\mathcal{R}(\overline{\mathbf{W}}_*^2) = \mathcal{A}(\mathbf{Q}\overline{\mathbf{W}}_*^2\mathbf{Q}^T) + (\mathbf{Q}\overline{\mathbf{W}}_*^2\mathbf{Q}^T)\mathcal{A}^T + \mathcal{B}\mathcal{B}^T$ *we apply a Galerkin type orthogonalization of the residual to the Krylov space* $\mathcal{K}_{n_k}(\mathcal{A}, \mathcal{B})$ *to obtain the problem statement*

   $$\text{find } \overline{\mathbf{W}}_*^2 \text{ such that } \mathbf{Q}^T \mathcal{R}(\overline{\mathbf{W}}_*^2)\mathbf{Q} = 0$$

   This gives an estimate of the reduced Lyapunov solution vector $\overline{\mathbf{W}}_*^2$

   (b) *If the residual norm* $\left\|\mathcal{R}(\overline{\mathbf{W}}_*^2)\right\|_{\mathrm{F}} > \epsilon$, *increase the value of* n_k *and include more Krylov bases from step* 2 *and repeat the previous steps.*

4. *Obtain the reduced order Lyapunov solution as* $\mathbf{Q}\overline{\mathbf{W}}_*^2\mathbf{Q}^T$.

It has been shown in [Jaimoukha and Kasenally, 1994] that the Galerkin type orthogonalization of the residual to the orthogonal basis $\mathbf{Q}$ as $\mathbf{Q}^T\mathcal{R}(\mathcal{X}_{qn_k})\mathbf{Q} = 0$ is satisfied if and only if $\overline{\mathbf{W}}_*^2$ satisfies the reduced Lyapunov equation

$$\mathcal{A}_{qn_k}\overline{\mathbf{W}}_*^2 + \overline{\mathbf{W}}_*^2\mathcal{A}_{qn_k}^T + \mathcal{B}_{qn_k}\mathcal{B}_{qn_k}^T = 0 \tag{6.40}$$

where $\mathcal{B}_{qn_k} = \mathbf{Q}^T\mathcal{B}$. The orthogonal basis $\mathbf{Q} \in \mathbb{R}^{n \times qn_k}$ spanning the Krylov subspace approximates the Gram matrix $\overline{\mathbf{W}}^2$ as

$$\overline{\mathbf{W}}^2 = \mathbf{Q}\overline{\mathbf{W}}_*^2\mathbf{Q}^T \tag{6.41}$$

We can use these orthogonal basis functions to approximate the solution of the linear system in Eqn. (6.33). Approximating $\mathcal{X}(t) = \mathbf{Q}\mathcal{X}_{qn_k}(t)$ and $\dot{\mathcal{X}}(t) = \mathbf{Q}\dot{\mathcal{X}}_{qn_k}(t)$ we have the linear system as

$$\dot{\mathcal{X}}_{qn_k}(t) = \mathcal{A}_{qn_k}\mathcal{X}_{qn_k}(t) + \mathcal{B}_{qn_k}(t) \tag{6.42}$$

The above system can be resolved with any time integration scheme such as the explicit Runge-Kutta type methods or the implicit time stepping schemes (such as Euler's method).

The error estimation procedure which is used as a stopping criterion to restrict the Krylov space dimension to an optimum value is a computationally expensive procedure which has a computational complexity of $\mathcal{O}((qn_k)^3)$. Hence in the above discussed Arnoldi algorithm, the error estimation step is included not after every step of the block Krylov basis evaluation but only after certain manually chosen intervals to enhance the computational efficiency of the method.

For descriptor systems of the form given in Eqn. (6.15) it is not always computationally advantageous to take the inverse of the $\mathcal{C}$ matrix and take the equation in standard form as given in Eqn. (6.16). This makes the system lose its sparsity pattern and hence the storage requirement for the matrix $\mathbf{A}$ in Eqn. (6.33) becomes huge. This is especially disadvantageous when solving the randomly parametrized system with the stochastic Galerkin method which results in a block sparse coefficient matrix composed of the individual blocks of the system matrix. Hence the descriptor form is more suitable especially for FE linear systems. The Lyapunov theory for descriptor systems is available [Takaba *et al.*, 1995, Ishihara and Terra, 2003], but it requires extensive matrix-matrix products which destroys the desired sparsity of the system once again. Noting that the parametric uncertainty in the system is present in the form of the random diffusion coefficient only, it is readily seen that using the spectral Galerkin method we get a matrix $\mathcal{C}$ which is block diagonal in nature. The product of a block-diagonal matrix and another block-sparse matrix preserves the block sparse nature of the latter matrix. Thus storing the inverse of the matrix essentially requires the storing of just the deterministic baseline matrix as $\mathbf{C}^{-1}$ and the block diagonal inverse of the matrix $\mathcal{C}$ is given as $[\mathcal{C}^{-1}]_{ii} = \left(1/\left\langle \mathscr{H}_i \right\rangle^2\right) \mathbf{C}^{-1}$ where $[\mathcal{C}^{-1}]_{ii}$ is the i-th diagonal block of $\mathcal{C}^{-1}$. This is an advantageous situation for the implementation of the Krylov based methods. Hence the Krylov space can be formed such that the $\mathcal{C}$ matrix is used as a preconditioner, i.e.

$$\mathcal{K}_{n_k}\left(\mathcal{C}^{-1}\mathcal{K}, \mathcal{C}^{-1}\bar{\mathcal{B}}\right) = \text{span}\left\{\mathcal{C}^{-1}\bar{\mathcal{B}}, \left(\mathcal{C}^{-1}\mathcal{K}\right)\mathcal{C}^{-1}\bar{\mathcal{B}}, \left(\mathcal{C}^{-1}\mathcal{K}\right)^2\mathcal{C}^{-1}\bar{\mathcal{B}}, \ldots, \left(\mathcal{C}^{-1}\mathcal{K}\right)^{n_k}\mathcal{C}^{-1}\bar{\mathcal{B}}\right\} \tag{6.43}$$

The modified Gram-Schmidt orthogonalization applied to these basis vectors would create an orthonormal basis $\mathbf{Q}_d$ which gives the upper Hessenberg matrix $\mathcal{A}_{qn_k} = \mathbf{Q}_d^T\left(\mathcal{C}^{-1}\mathcal{K}\right)\mathbf{Q}_d^T$. Thus the descriptor system, when solved with this vector basis gives

$$\mathcal{C}_{qn_k}\dot{\mathcal{X}}_{qn_k} = \mathcal{K}_{qn_k}\mathcal{X}_{qn_k}(t) + \bar{\mathcal{B}}_{qn_k}(t) \quad \text{where} \quad \mathcal{C}_{qn_k} = \mathbf{Q}_d^T\mathcal{C}\mathbf{Q}_d\,;\ \mathcal{K}_{qn_k} = \mathbf{Q}_d^T\mathcal{K}\mathbf{Q}_d \tag{6.44}$$

The original solution is obtained using the transformation $\mathcal{X}(t) = \mathbf{Q}_d\mathcal{X}_{qn_k}(t)$. In the following section we discuss the method for updating the dominant subspace which involves a recalculation of the basis functions using a restarted Arnoldi algortihm.

6.3.5 Implicit restarting of Arnoldi-Lyapunov basis evaluation

The Arnoldi vectors derived using the Arnodi-Lyapunov algorithm relies on the system solution of the LTI finite element system with a finite order chaos expansion using a time integration technique. An implicit time marching algorithm, such as Euler's central difference scheme relies on evaluating the forcing terms and the response quantities at the center of each time step. Let us consider a transient LTI diffusion system (in the descriptor form) with a random diffusion coefficient (given in Eqn. (6.15)) expressed with finite order chaos expansion

of the input random variables as

$$\mathcal{C}\dot{\mathcal{X}}(t) + \mathcal{K}\mathcal{X}(t) = \bar{\mathcal{B}}\mathcal{F}(t) \tag{6.45}$$

Solving this system with Euler's central difference scheme, we choose to divide the time domain of interest into a finite number of divisions. The time step size is governed by the dynamics of the system and is chosen such that it is within the characteristic time length of the dynamic system. The linear system giving the solution at $t = T_{n+1}$ is

$$\left([\mathcal{C}] + [\mathcal{K}]\frac{\Delta t}{2}\right)\mathcal{X}_{n+1} = F_{n+1}\left(\mathcal{F}(T_{n+1}), \mathcal{F}(T_n), \mathcal{X}_n, \mathcal{C}, \mathcal{K}, \bar{\mathcal{B}}\right) \tag{6.46}$$

where the forcing at the step T_{n+1} is given by a combination of the forcing at steps T_{n+1} and T_n along with the response at previous step n given by $\mathcal{X}_n$. The Arnoldi-Lyapunov algorithm given in Sec. 6.3.4 starts with the matrices $\mathcal{C}, \mathcal{K}$ and $\bar{\mathcal{B}}$ to evaluate the dominant basis with which the LTI system solution can be approximated. However, as the time marching algorithm tries to capture long time integration response, it might occur for rapidly changing systems that the basis functions fail to capture the response with sufficient accuracy or the solution might diverge altogether. A recalculation of the Arnoldi bases under such conditions would avoid a breakdown of the proposed scheme in Sec. 6.3.4.

To implement this, we consider the right hand side of the linear system in Eqn. (6.46) obtained with Euler's central difference scheme. Thus

$$\left([\mathcal{C}] + [\mathcal{K}]\frac{\Delta t}{2}\right)\mathcal{X}_{n+1} = \bar{\mathcal{B}}\left(\frac{\mathcal{F}_{n+1} + \mathcal{F}_n}{2}\right) + \bar{\mathcal{X}}_n \quad \text{where} \quad \bar{\mathcal{X}}_n = \left([\mathcal{C}] + [\mathcal{K}]\frac{\Delta t}{2}\right)\mathcal{X}_n \tag{6.47}$$

The Arnoldi-Lyapunov algorithm is initialized to evaluate the basis functions of the dominant Krylov subspace $\mathcal{K}_{n_k}\left(\mathcal{C}^{-1}\mathcal{K}, \mathcal{C}^{-1}\mathcal{B}\right)$. But additional information on the right side of Eqn. (6.47) is available in the form of the vector $\bar{\mathcal{X}}_n$. This can be incorporated into the Arnoldi basis calculation to obtain a better estimate of reduced subspace in which the solution exists.

For the sake of simplicity, first we refer to the baseline LTI system in Eqn. (6.3), in which, the state transition matrix, given as $\psi(t, \tau)$, takes the form of $\exp\{\mathbf{A}(t-\tau)\}$. This is utilized to get the response of the system at time t subject to an initial condition $\mathbf{X}_0$ as $\mathbf{X}(t) = \psi(t, t_0)\mathbf{X}_0$ with $t_0 = 0$. Hence the response of the LTI system at every $t \in [0, \infty)$ to the initial condition specified by $\mathbf{X}(t_0)$ and the forcing $\mathbf{Bf}(t)$ is given as

$$\mathbf{X}(t) = \psi(t, t_0)\mathbf{X}_0 + \int_0^t \psi(t, \tau)\mathbf{Bf}(\tau)d\tau \tag{6.48}$$

In absence of a forcing term, i.e. if $\mathbf{f}(\tau) = 0$, and with a prescribed initial condition $\mathbf{X}_0$, the response $\mathbf{X}(t)$ would only consist of $\mathbf{X}(t) = \mathbf{X}_0\exp\{\mathbf{A}t\}$. Here we note the identity $(G * \delta) = G$ for any bounded function G and unit impulse (or delta) function δ, where '$*$'

denotes the convolution operation. Using this the response $\mathbf{X}(t)$ in the above equation can be written as

$$\mathbf{X}(t) = \psi(t,\tau) * (\mathbf{X}_0\delta(\tau) + \mathbf{B}\mathbf{f}(\tau)) = \psi(t,\tau) * [\mathbf{X}_0 \;\; \mathbf{B}]\,[\delta(\tau) \;\; \mathbf{f}(\tau)]^T \tag{6.49}$$

where $\delta(t)$ is the delta distribution, $[\mathbf{X}_0 \;\; \mathbf{B}] \in \mathbb{R}^{n\times(q+1)}$ is the matrix combining the vector $\mathbf{X}_0 \in \mathbb{R}^n$ and matrix $\mathbf{B} \in \mathbb{R}^{n\times q}$, while $[\delta(\tau) \;\; \mathbf{f}(\tau)] \in \mathbb{R}^{q+1}$ is the combined vector of the delta function and the q input functions. Assuming that the system is stable under the action of all piecewise continuous bounded functions in $[0,T]$, we can identify a modified Gram matrix which satisfies the Lyapunov equations

$$\mathbf{A}\overline{\mathbf{W}}_m^2 + \overline{\mathbf{W}}_m^2\mathbf{A}^T + \mathbf{B}_x\mathbf{B}_x^T = 0 \tag{6.50}$$

where $\mathbf{B}_x = [\mathbf{X}_0 \;\; \mathbf{B}] \in \mathbb{R}^{n\times(q+1)}$. This form is particularly conducive for constructing (or restarting) the Arnoldi-Lyapunov algorithm discussed in Sec. 6.3.4. We can now incorporate the vector of the initial condition to the force locator matrix $\mathbf{B}$ which would be taken into account while constructing the block Krylov bases with the force locator matrix $\mathbf{B}_x$.

Extension of the above discussion to the randomly parametrized LTI system in Eqn. (6.33) is straightforward. It is seen that the modified block Krylov algorithm restarted at an arbitrary time step t_{r+1} where the solution $\mathcal{X}_r = \mathcal{X}(t = t_r)$ at the step t_r is available would consider the matrix $\mathcal{B}_x = [\mathcal{X}_r \;\; \mathcal{B}]$ and form the Krylov bases as

$$\mathcal{K}_{n_k}^r(\mathcal{A}, \mathcal{B}_x) = \text{span}\left\{\mathcal{B}_x, \mathcal{A}\mathcal{B}_x, \mathcal{A}^2\mathcal{B}_x, \ldots, \mathcal{A}^{n_k-1}\mathcal{B}_x\right\} \tag{6.51}$$

Additionally, when we start the Krylov basis evaluation with initial condition set to zero, the above Krylov space is equivalent to the one obtained with $\mathcal{K}_{n_k}^r(\mathcal{A}, \mathcal{B}_x)$ as given in Sec. 6.3.4.

Thus the scheme of restarting the Arnoldi-Lyapunov vector estimation implicitly after finite intervals of time consists of the following steps

Implicit restarting of Arnoldi-Lyapunov basis evaluation for time integration

1. *Initialize the global error indicator ε_g, the Arnoldi-Lyapunov convergence criterion ϵ_{AL}, implement the prescribed initial condition $\mathcal{X}_r = \mathcal{X}_0$, initialize $r = 0$.*

2. *Set up the LTI system using the central difference the time marching algorithm (as per Eqn. (6.46)) and implement the initial and boundary conditions. Begin evaluation of the Arnoldi vectors on which the solution would be projected as follows:*

   (a) *Set $\mathbf{Q} = \mathbf{Q}_1$ such that $\mathbf{Q}_1$ are the orthogonal basis spanning the column space of*

$$\mathcal{B}_x = [\mathcal{X}_r \;\; \mathcal{B}] \in \mathbb{R}^{n\times(q+1)}. \tag{6.52}$$

(b) *Initialize n_k and calculate the orthogonal bases spanning the n_k dimensional block Krylov space given by*

$$\mathcal{K}_{n_k}(\mathcal{A}, \mathcal{B}_x) = span\left\{\mathcal{B}_x, \mathcal{A}\mathcal{B}_x, \mathcal{A}^2\mathcal{B}_x, \ldots, \mathcal{A}^{n_k-1}\mathcal{B}_x\right\}$$

using a modified Gram-Schmidt process to get the set of orthogonal vector basis $\mathbf{Q} = \{\mathbf{Q}_1, \mathbf{Q}_2, \ \ldots, \mathbf{Q}_{n_k}\}$ where $\mathbf{Q}_i \in \mathbb{R}^{n\times q}\ \forall i = 1, \ldots, n_k$.

(c) *The error indicator to evalaute the optional Krylov space dimension is determined as*

i. *Evaluate block upper Hessenberg matrix $\mathcal{A}_{qn_k} = \mathbf{Q}^T\mathcal{A}\mathbf{Q}$; $\mathcal{A}_{qn_k} \in \mathbb{R}^{qn_k\times qn_k}$ along with the Lyapunov residual $\mathcal{R}(\overline{\mathbf{W}}_*^2) = \mathcal{A}(\mathbf{Q}\overline{\mathbf{W}}_*^2\mathbf{Q}^T) + (\mathbf{Q}\overline{\mathbf{W}}_*^2\mathbf{Q}^T)\mathcal{A}^T + \mathcal{B}\mathcal{B}^T$.*

ii. *Apply Galerkin type orthogonalization of the residual to the Krylov space $\mathcal{K}_{n_k}(\mathcal{A}, \mathcal{B})$:*

$$find\ \overline{\mathbf{W}}_*^2\ such\ that\ \mathbf{Q}^T\mathcal{R}(\overline{\mathbf{W}}_*^2)\mathbf{Q} = 0$$

This gives an estimate of the reduced Lyapunov solution vector $\overline{\mathbf{W}}_*^2$

iii. *If the residual norm $\left\|\mathcal{R}(\overline{\mathbf{W}}_*^2)\right\|_{\mathrm{F}} > \epsilon_{AL}$, increase the value of n_k and include more Krylov bases from step 3 and repeat the previous steps.*

(d) *Project the solution on the Arnoldi-Lyapunov vectors as $\mathcal{X}(t) = \mathbf{Q}\mathcal{X}_{qn_k}(t)$ and solve the LTI system using the central difference scheme at subsequent time steps as*

$$\mathbf{Q}^T\left([\mathcal{C}] + [\mathcal{K}]\frac{\Delta t}{2}\right)\mathbf{Q}\bar{\mathcal{X}}_{n+1} = \mathbf{Q}^T F_{n+1}\left(\mathcal{F}(T_{n+1}), \mathcal{F}(T_n), \mathbf{Q}\bar{\mathcal{X}}_n, \mathcal{C}, \mathcal{K}, \bar{\mathcal{B}}\right) \tag{6.53}$$

with the solution at discrete time steps given by $\mathcal{X}_{n+1} = \mathbf{Q}\bar{\mathcal{X}}_{n+1}$.

(e) *Calculate the L^2 norm of the residual vector of the LTI system at time step T_{n+1} given by*

$$\mathcal{R}_{n+1} = \left([\mathcal{C}] + [\mathcal{K}]\frac{\Delta t}{2}\right)\mathcal{X}_{n+1} - F_{n+1}\left(\mathcal{F}(T_{n+1}), \mathcal{F}(T_n), \mathbf{Q}\mathcal{X}_n, \mathcal{C}, \mathcal{K}, \bar{\mathcal{B}}\right) \tag{6.54}$$

as $\|\mathcal{R}_{n+1}\|_2$.

(f) *If $\|\mathcal{R}_{n+1}\|_2 > \varepsilon_g$ then go to step 2 of the algorithm and restart the calculation of the Arnoldi-Lyapunov basis evaluation with $\mathcal{X}_r = \mathcal{X}_n$. Otherwise if $\|\mathcal{R}_{n+1}\|_2 \leqslant \varepsilon_g$, goto step (d) and carry on with the time marching algorithm.*

3. *The solution vector at the discrete time steps $i = 1, 2, \ldots, n$ is given given by the vectors $\mathcal{X}_i$.*

The above algorithm ensures that the accuracy of the solution of the randomly parametrized LTI system obtained at all time steps do not fall below the prescribed value ε_g. The check for the residual of the linear system for the implicit restarting can be performed after every few time steps as governed by the accuracy requirement of the problem and also the consideration for the additional cost associated with the residual evaluation. It might be pointed out the choice of the number of Arnoldi-Lyapounov basis functions and the frequency of restart are interrelated for stable time evolving systems. Choosing a large number of Arnoldi-Lyapunov bases can ensure good approximation accuracy of the solution over a long time integration, however, an additional cost is associated with it. On the other hand, evaluation of a revised set of Arnoldi-Lyapunov vectors also increases the computational overhead of the solver. Hence the choice of the number of Arnoldi-Lyapunov vector basis (i.e. the reduced subspace dimension) and the interval after which the Arnoldi-Lyapunov basis estimation is restarted are complimentary aspects of the numerical algorithm and has to be judiciously chosen to optimize the efficiency of the solver.

6.4 Numerical results

In this section we present the results obtained from the numerical simulation of the transient response of various randomly parametrized LTI dynamical systems whose solution has been obtained with the proposed reduced Arnoldi-Lyapunov basis vectors spanning a dominant subspace of the solution.

6.4.1 Advection-diffusion-reaction system

Here consider the finite element simulation of a large advection-diffusion-reaction system to demonstrate the applicability of the proposed Arnoldi-Lyapunov reduced basis for the resolution of its time domain response. We consider the geometrical properties of the advection-diffusion-reaction system as described in [Parés *et al.*, 2008] such that the physical domain $\mathscr{D} \in \mathbb{R}^2$ is a square contained in $[0,1] \times [0,1]$ and the time domain of interest is $t = [0, 0.03]$. The coordinate axes are denoted by (r, s). The governing equation is given as

$$\begin{aligned} &\dot{x} - \nabla\left(k(\theta)\nabla x\right) + c \cdot \nabla x + \sigma x = f \\ &x = 0 \text{ on } \partial\mathscr{D} \times t \\ &x = 0 \text{ on } \mathscr{D} \times \{0\} \end{aligned} \tag{6.55}$$

where the diffusion coefficient has been modeled as a lognormal random field with mean value of 1.0 and standard deviation of 0.5. The constant c is chosen to be spatially varying as $c = 250\left(s - \frac{1}{2}, \frac{1}{2} - r\right)$ and $f(r, s, t) = 100$ on the square sub-domain $[0.7, 0.8] \times [0.7, 0.8]$. This emulates a velocity field which rotates in the clockwise direction with its centre at $\left(\frac{1}{2}, \frac{1}{2}\right)$.

The physical domain has been meshed with isoparametric quadrangular elements of order 2 and the time range of interest $t = [0, 0.03]$ has been divided into 100 uniform intervals.

The random field $k(\theta)$ is characterized with an exponential covariance kernel. The finite dimensional representation of the random field is given with 4 iid random variables $\boldsymbol{\xi}(\theta) = \{\xi_1, \ldots, \xi_4\}$ with Hermite chaos. The finite element treatment of the stochastic dynamical system given in Eqn. (6.55) results in system matrices of the form

$$\mathbf{C}\dot{\mathbf{X}}(t;\theta) + \mathbf{K}(\theta)\mathbf{X}(t;\theta) = \bar{\mathbf{B}}f(t) \tag{6.56}$$

where $\mathbf{K}(\theta) = \sum_{i=0}^{M} \mathbf{K}_i \mathscr{H}_i(\boldsymbol{\xi}(\theta))$ is the series representation of the system matrix with a random diffusion coefficient. A stochastic Galerkin projection of the solution on the orthogonal basis functions $\mathscr{H}(\boldsymbol{\xi}(\theta)) = \{\mathscr{H}_0(\boldsymbol{\xi}(\theta)), \ldots, \mathscr{H}_p(\boldsymbol{\xi}(\theta))\}$ leads to a block sparse system of equations as

$$\left\langle \mathscr{H}_i(\boldsymbol{\xi}(\theta)), \left(\mathbf{C}\dot{\mathbf{X}}(t,\theta) + \mathbf{K}(\theta)\mathbf{X}(t,\theta) - \bar{\mathbf{B}}f(t)\right)\right\rangle_{L^2(\theta)} = 0\,; \quad \forall i = 0, \ldots, p$$

$$\text{which gives} \quad \mathcal{C}\dot{\mathcal{X}}(t) + \mathcal{K}\mathcal{X}(t) = \bar{\mathcal{B}}f(t) \tag{6.57}$$

where $\mathcal{C}$ is a block diagonal matrix, with $\mathcal{K}$ being a block sparse matrix and $\mathcal{X}(t)$ is a $n \times p$ vector denoting the stochastic system response, where n is the number of degrees of freedom associated with the finite element system. It can be seen from the above equations that the system given in Eqn. (6.55) gives rise to an unsymmetrical coefficient matrix $\mathbf{K}(\theta)$ and hence $\mathcal{K}$. Here we have chosen 4-th order stochastic Hermite polynomials basis with which the solution has been approximated.

(a) $t = 1T_{\text{tot}}/5$ (b) $t = 2T_{\text{tot}}/5$ (c) $t = 3T_{\text{tot}}/5$ (d) $t = 4T_{\text{tot}}/5$ (e) $t = 5T_{\text{tot}}/5$

Figure 6.1: Reference solution of the deterministic model of the advection-diffusion-reaction problem on a square domain.

Figure 6.1 shows the response of the baseline (deterministic) dynamic advection-diffusion-reaction system subjected to deterministic externel forcing as described in context of Eqn. (6.55) at 5 discrete points in time. The time domain response has been resolved with the central difference scheme.

Figures 6.2 and 6.3 shows the response statistics, i.e. the mean and the standard deviation respectively, of the response of the randomly parametrized system resolved with polynomial

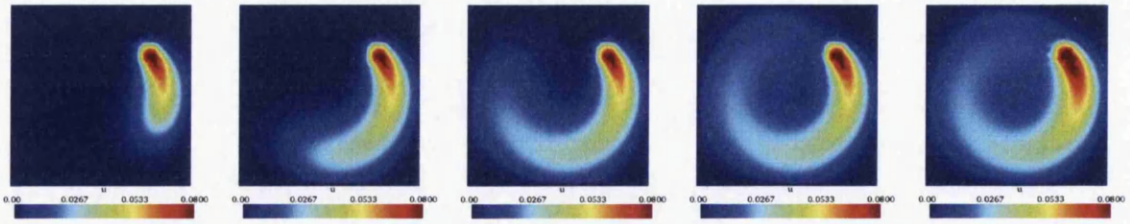

(a) $t = 1T_{\text{tot}}/5$ (b) $t = 2T_{\text{tot}}/5$ (c) $t = 3T_{\text{tot}}/5$ (d) $t = 4T_{\text{tot}}/5$ (e) $t = 5T_{\text{tot}}/5$

Figure 6.2: Mean response of the stochastic model problem with a lognormal random diffusion coefficient using a 4-th order Polynomial Chaos expansion.

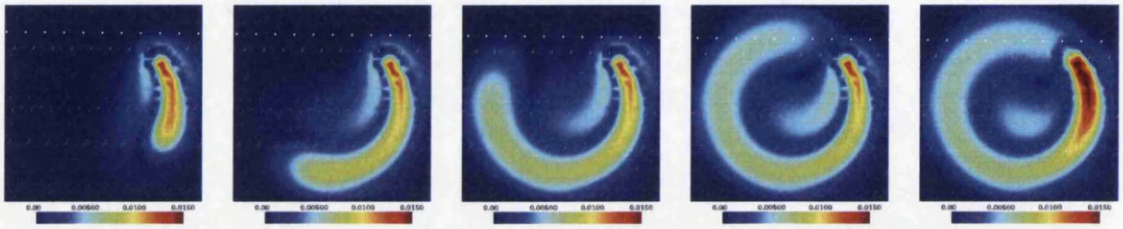

(a) $t = 1T_{\text{tot}}/5$ (b) $t = 2T_{\text{tot}}/5$ (c) $t = 3T_{\text{tot}}/5$ (d) $t = 4T_{\text{tot}}/5$ (e) $t = 5T_{\text{tot}}/5$

Figure 6.3: Standard deviation of the response of the stochastic model problem with a lognormal random diffusion coefficient using a 4-th order Polynomial Chaos expansion.

chaos expansion under the action of the deterministic external forcing. We have used 4-th order Hermite chaos for a 4 dimensional input stochastic space represented with 4 independent identically distributed random variables.

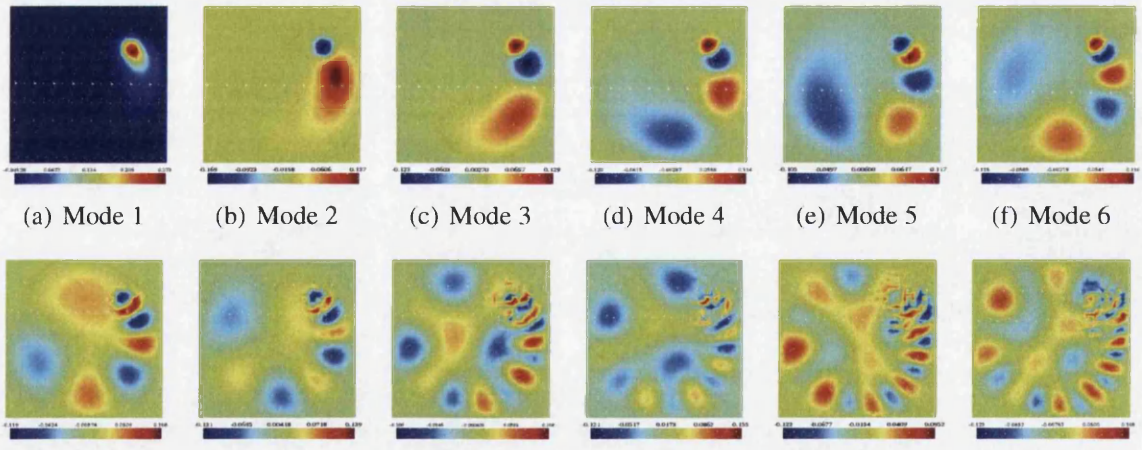

(a) Mode 1 (b) Mode 2 (c) Mode 3 (d) Mode 4 (e) Mode 5 (f) Mode 6

(g) Mode 8 (h) Mode 10 (i) Mode 19 (j) Mode 21 (k) Mode 26 (l) Mode 31

Figure 6.4: Various eigenmodes of the complete Gramian of the response of the baseline (deterministic) advection-diffusion-reaction system.

Figure 6.4 gives the first few eigenmodes of the controllability Gramian $\overline{\mathbf{W}}^2$ of the deterministic dynamical system. Here the estimation of the eigenvectors associated with the largest eigenvalues is exact since the Gramian has been calculated first following which we have performed an eigenvalue analysis of the deterministic Gramian. It can be seen that the

first eigenmode almost replicate the solution at the very early time steps. Gradually the modes become more complex and exhibit an anticlockwise rotation pattern. All the modes presented in this figure are orthogonal to each other and have been normalized.

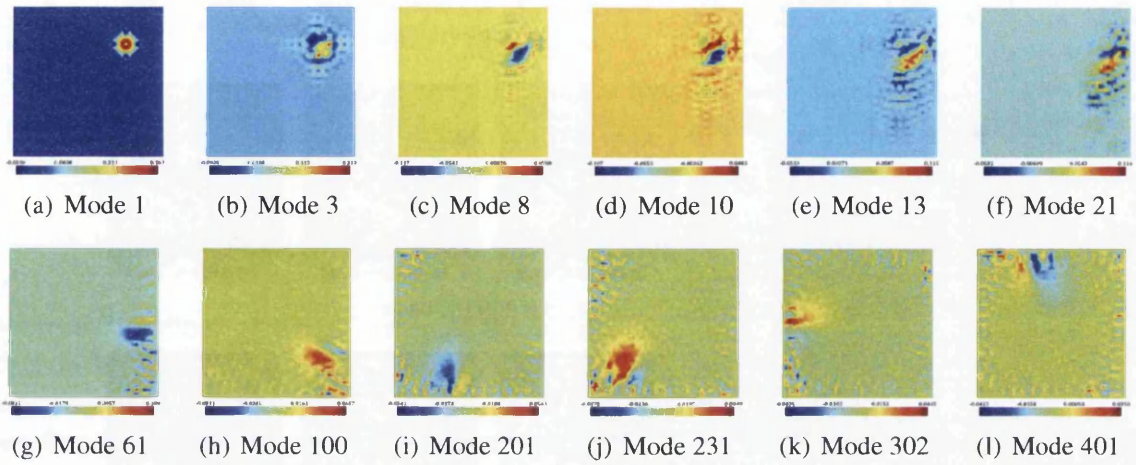

(a) Mode 1 (b) Mode 3 (c) Mode 8 (d) Mode 10 (e) Mode 13 (f) Mode 21

(g) Mode 61 (h) Mode 100 (i) Mode 201 (j) Mode 231 (k) Mode 302 (l) Mode 401

Figure 6.5: Plots of the mean of the various basis functions spanning the dominant subspace of the stochastic controllability Gramian of the randomly parametrized linear system calculated with an iterative Krylov method implemented within the scope of Arnoldi's algorithm.

We give the mean Arnoldi-Lypaunov basis vectors of the randomly parametrized dynamical system in Fig. 6.5 which have been calculated using the algorithm presented in Sec. 6.3.3. The basis vectors span the dominant eigen space of the stochastic controllability Gramian. These vectors are orthonormalized and are used to model the reduced order response of the dynamical system. It is seen that these modes are significantly different from the ones presented in Fig. 6.4. However, it is still apparent that a clockwise rotation pattern is exhibited as the mode number increases. The solution to the randomly parametrized advection-diffusion-reaction system is approximated with a subset of Arnoldi-Lyapunov basis vectors and the accuracy of the solution has been compared with respect to the dimension of the reduced space in which the solution is sought.

Figure 6.6 gives the mean response of the stochastic LTI system calculated with the 4-th order chaos expansion of the input iid random variables. The mean response has been evaluated with an increasing subset of Arnoldi-Lyapunov basis vectors and have been studied for their accuracy. Here the mean response with 4-th order chaos has been approximated successively with $150, 300, 400$ and 600 basis functions and Figs. 6.6(a)–6.6(d) shows the improved accuracy of the solution as the number of Arnoldi-Lyapunov basis vectors are increased. These have been compared to the full system solution without a reduced subspace projection which has been shown in Fig. 6.6(e). The plots indicate that with fewer basis vectors, the solutions at early time steps are accurate but the time evolution of the solution stops altogether after a finite interval of time. For example the mean response calculated with 150 modes stops evolving in time from $t = 2T_{\text{tot}}/5$ onwards. When using a higher number of

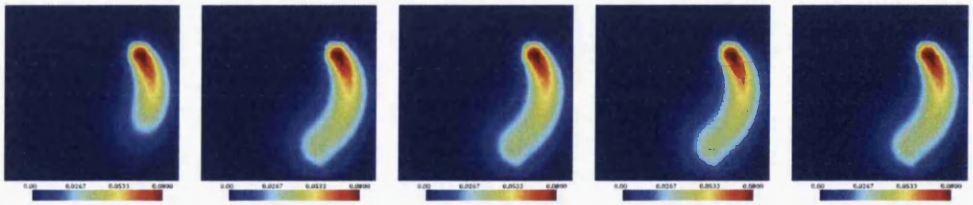

(a) Mean calculated with 150 PC basis

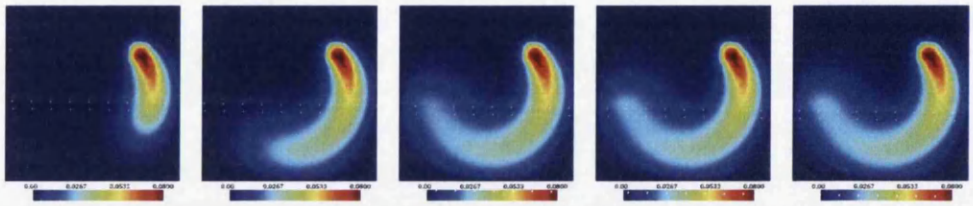

(b) Mean calculated with 300 PC basis

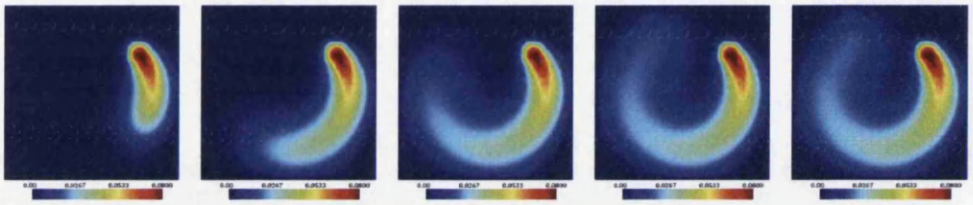

(c) Mean calculated with 400 PC basis

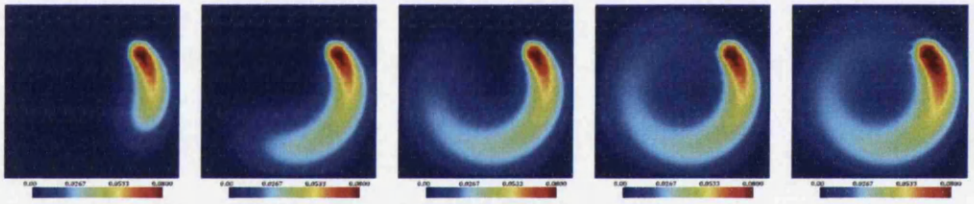

(d) Mean calculated with 600 PC basis

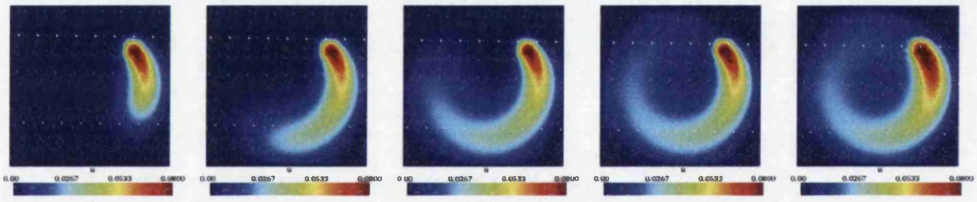

(e) Mean of the full system PC solution

Figure 6.6: Approximate mean response calculated with various reduced number of Arnoldi-Lyapunov basis vectors spanning the dominant subspace associated with the stochastic Gramian of the randomly parametrized linear system. The basis functions were calculated with an iterative Krylov method implemented within the scope of Arnoldi's algorithm. The responses are shown at different instances of time $t = iT_{\text{tot}}/5$ with $i = 1, \ldots, 5$ along each row.

modes, say 300 the solution grows until $t = 3T_{\text{tot}}/5$ after which it becomes stagnant, while the response with 600 modes captures almost the entire time varying solution.

To quantify the approximation error in obtaining the transient response of the LTI system with a reduced number of Arnoldi-Lyapunov basis vectors, we construct a relative error

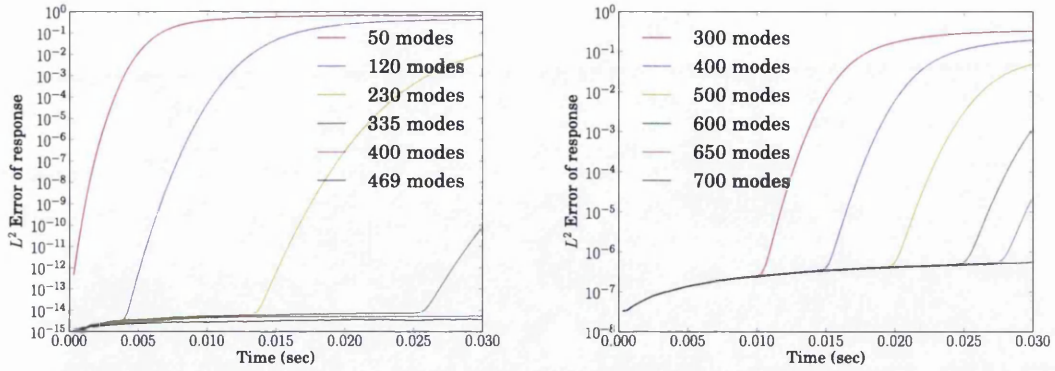

(a) L^2 error, deterministic system

(b) L^2 error, stochastic system

Figure 6.7: Plots of the L^2 error of the reduced basis transient solution vector with respect to the complete solution obtained with a time marching algorithm for two different cases: deterministic system (a) without considering any parametric uncertainty and randomly parametrized system (b) with finite order chaos expansion of the solution vector.

indicator which is defined as follows

$$\varepsilon_n^m = \frac{\left\| \mathcal{X}_n^{\text{red},m} - \mathcal{X}_n^{\text{full}} \right\|_2}{\left\| \mathcal{X}_n^{\text{full}} \right\|_2} \tag{6.58}$$

where $\mathcal{X}_n^{\text{full}}$ is the full system solution at time step n, $\mathcal{X}_n^{\text{red},m}$ is the approximate solution at time step n computed with m Arnoldi-Lyapunov vectors and $\|\cdot\|_2$ denotes the L^2 vector norm. Hence the relative error norm is a function of the dimension of the reduced subspace in which the solution is sought and varies with time.

Figure 6.7 shows the plot of this relative error norm ε_n^m on the time range of interest $t = [0, 0.03]$s with different orders of approximation of the response vector. Fig. 6.7(a) shows the error in approximating the deterministic solution with the Gramian of the deterministic transient response while Fig. 6.7(b) gives the same for the randomly parametrized system with the stochastic Gramian. Of course in the latter case the dimension of the linear system is significantly larger and hence a higher number of basis vectors are required to satisfactorily capture the system response over the entire time range. Additionally, it is seen that the approximation error obtained for the deterministic transient system is many orders of magnitude lower than that for the stochastic system. This is expected since the dimension of the stochastic linear system is much higher than the deterministic one. Hence the approximation error is comprised of the error in the tensor product of the finite dimensional stochastic subspace spanned by the orthogonal polynomial chaos functions and the vector space associated with the FE discretization. From Fig. 6.6 it is seen that the maximum approximation accuracy (of the order of 10^{-15}) is obtained at all time steps with approximately 400 modes while for the stochastic system the maximum approximation accuracy (of the order of 10^{-7}) is obtained with approximately 700 modes. This leads to a significant improvement in the computa-

tional efficacy of the time stepping algorithm since a good approximation of the stochastic response expressed with the finite order chaos expansion is obtained with only a few basis functions. For example, the finite element discretization of the advection-diffusion-reaction problem leads to a linear system of dimension ≈ 2000. With 4-th order chaos expansion in 4 dimensional stochastic space, we have to solve a $\approx 1.4 \times 10^5$ dimensional block sparse linear system at each time step. In contrast, it is seen that 700 Arnoldi-Lyapunov vectors provide us with a solution of accuracy 10^{-7} at all time steps.

Figure 6.8 gives the standard deviation of the response of the stochastic LTI system calculated with the 4-th order chaos expansion of the input iid random variables. The response standard deviation has been evaluated with an increasing subset of Arnoldi-Lyapunov basis vectors (such as $150, 300, 400$ and 600) and have been studied for their accuracy as given in Figs. 6.8(a)–6.8(d). These show the improved accuracy of the solution as the number of basis vectors are increased. These have been compared to the full system solution without a reduced subspace projection which has been shown in Fig. 6.8(e). The plots indicate that with fewer basis functions, the solutions at early time steps are accurate but the time evolution of the solution stops altogether after a finite interval of time. This behavior is consistent and similar to that obtained for the mean response given in Fig. 6.6. For example the standard deviation of the response calculated with 150 modes is found to become stagnant from $t = 2T_{\text{tot}}/5$ onwards which is similar to the behavior of the mean response of the system as shown in Fig. 6.6. Again, using a higher number of modes, say 300, the solution grows till $t = 3T_{\text{tot}}/5$ after which it becomes stagnant, while the response with 600 modes captures almost the entire time varying solution.

The results demonstrate the applicability of the proposed method for the reduced order realization of the stochastic system response using the principal Arnoldi-Lyapunov modes associated with the stochastic controllability Gramian. It should also be noted that the system being solved here (i.e. the linear system given in Eqn. (6.57)) is unsymmetrical due to the presence of the non self-adjoint advection term. The numerical results of the approximation of the stochastic response with the reduced number of modes indicates that the method is not limited to symmetric systems but is also effective for unsymmetrical cases which are generally more complicated to handle.

6.4.2 Pure diffusion with boundary terms

We study another example problem here which consists of a randomly parametrized unsteady diffusion system to demonstrate the applicability of the model reduction technique that has been proposed here. The physical configuration of the problem is defined on a circular arc-like domain which is shown in Fig. 6.9(a). The governing equation for this unsteady diffusion

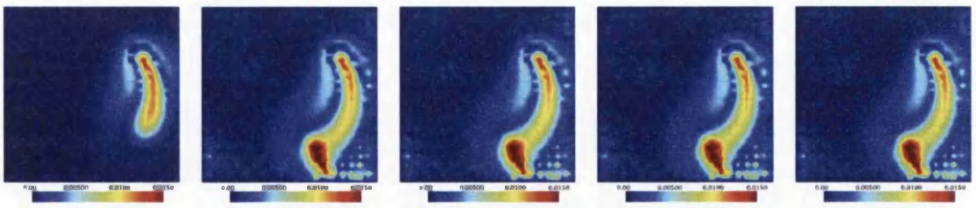

(a) Standard deviation calculated with 150 PC basis

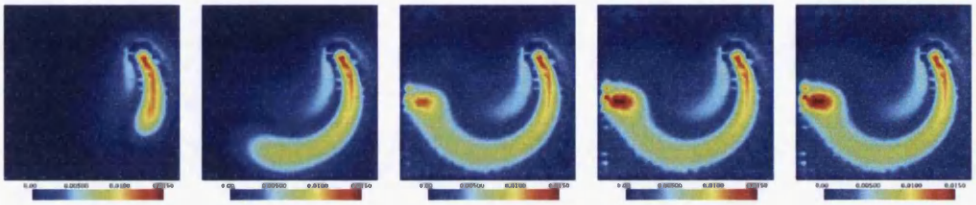

(b) Standard deviation calculated with 300 PC basis

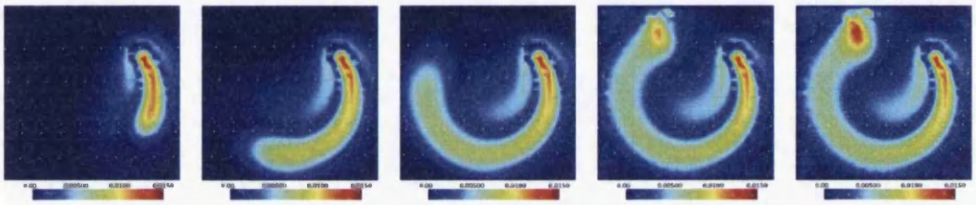

(c) Standard deviation calculated with 400 PC basis

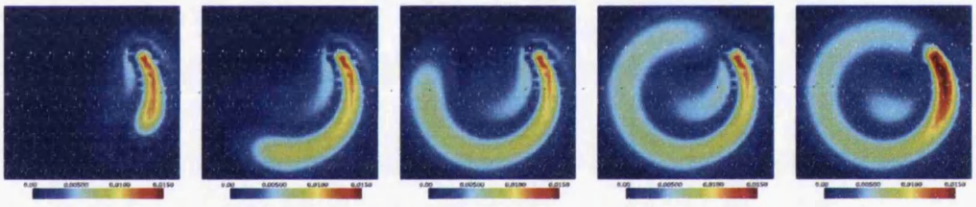

(d) Standard deviation calculated with 600 PC basis

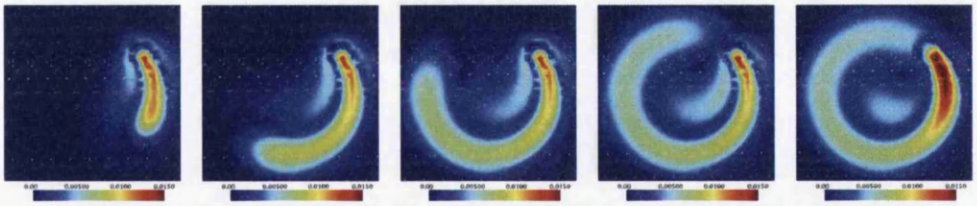

(e) Standard deviation of the full system PC solution

Figure 6.8: Approximation of the standard deviation of the response calculated with various reduced number of Arnoldi-Lyapunov basis vectors spanning the dominant subspace associated with the stochastic Gramian of the randomly parametrized linear system. The basis functions were calculated with an iterative Krylov method implemented within the scope of Arnoldi's algorithm. The responses are shown at different instances of time $t = iT_{\text{tot}}/5$ with $i = 1, \ldots, 5$ along each row.

equation is given as

$$\begin{gathered} c\dot{x}(t;\theta) - \nabla\left(k(\theta)\nabla x(t;\theta)\right) = 0 \quad \text{on } \mathscr{D} \quad \forall\, \mathrm{t} \in [0, \mathrm{T}] \\ \mathbf{n}_1.\nabla x(t;\theta) = f_1(t) \quad \text{on } \Gamma^1 \quad \text{and} \quad \mathbf{n}_2.\nabla x(t;\theta) = f_2(t) \quad \text{on } \Gamma^2 \quad \forall\, \theta \in \Theta \\ \text{and} \quad x(t=0;\theta) = x_0 \quad \text{on } \mathscr{D} \quad \forall\, \theta \in \Theta \end{gathered} \tag{6.59}$$

where Γ^1 is the 'red' part of the boundary in Fig. 6.9(a) which supplies the input flux to the system and Γ^2 denotes the 'green' portion of the boundary which dissipates energy. Thus this is a mixed boundary condition problem with the Γ^1 having a Neumann boundary while Γ^2 consists of Robin boundary conditions. The above equation indicates that the initial and boundary conditions are prescribed on the boundary for every sample realization of the randomly parametrized system. The time integration is carried out using the implicit Euler's central difference scheme with a time step size whose upper bound is governed by the dynamic characteristics of the transient system and has been chosen to be sufficiently small to ensure stability and convergence. The time range of interest for this problem is $t = [0, 500]$s. The boundary source term consists of an exponentially decaying flux modeled as $f_1(t) = \bar{f}_1 e^{-c_d t}$ where c_d is a positive constant while the dissipation boundary term has been modeled as $f_2(t) = \bar{f}_2(x(t;\theta) - x_\infty)$ where x_∞ is a constant. We have chosen the constants x_0 (the initial condition) and x_∞ to be equal to 273. This results in the linear system of equations

$$\mathbf{C}\dot{\mathbf{X}}(t;\theta) + \mathbf{K}(\theta)\mathbf{X}(t;\theta) + \mathbf{H}\mathbf{X}(t;\theta) = \bar{\mathbf{B}}\mathbf{f}(t) \tag{6.60}$$

where $\bar{\mathbf{B}} \in \mathbb{R}^{n\times 2}$ is the locator matrix associated with the forcing vector $\mathbf{f}(t) = \{f_1(t),\ f_2(t)\}$ and $\mathbf{H}$ is a boundary contribution matrix obtained from the finite element method applied to the boundary term $\bar{f}_2(x(t;\theta))$ depending on the field value $x(t,;\theta)$ at the boundary. Hence the block Krylov method (as detailed in Sec. 6.3.4) of order n_k would consist of $2n_k$ vectors of length n where the latter is the number of degrees of freedom obtained from the FE discretization. After applying the stochastic Galerkin method with finite order chaos expansion of the stochastic solution vector we obtain

$$\mathcal{C}\dot{\mathcal{X}}(t) + \mathcal{K}\mathcal{X}(t) + \mathcal{H}X(t) = \bar{\mathcal{B}}\mathcal{F}(t) \tag{6.61}$$

where $\mathcal{C}$ and $\mathcal{H}$ are block diagonal matrices, while $\mathcal{K}$ is a block sparse matrix. It might be noted here that the system matrices obtained are symmetric, which was not the case in the advection-diffusion-reaction problem given in Sec. 6.4.1.

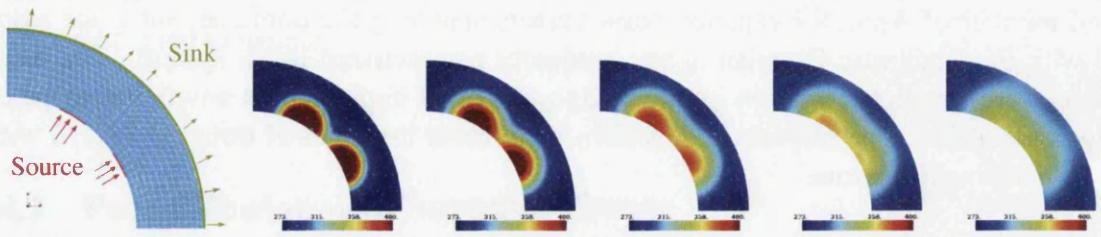

(a) Configuration of the transient system

(b) Solution at five different instance of time $t = iT_{\text{tot}}/5$ where $i = 1, \ldots, 5$.

Figure 6.9: Configuration of the LTI system under the action of external forcing functions along with the reference solution of the baseline (deterministic) model for the trasient diffusion problem.

Figure 6.9 gives the reference solution of the baseline (deterministic) model (schematic diaGram shown in Fig. 6.9(a)) at 5 different instants of time which shows the energy input to the system at the two locations of the inner circumference gradually being dissipated via the outer circumferential edge. The various eigenmodes associated with the largest eigenvalues of

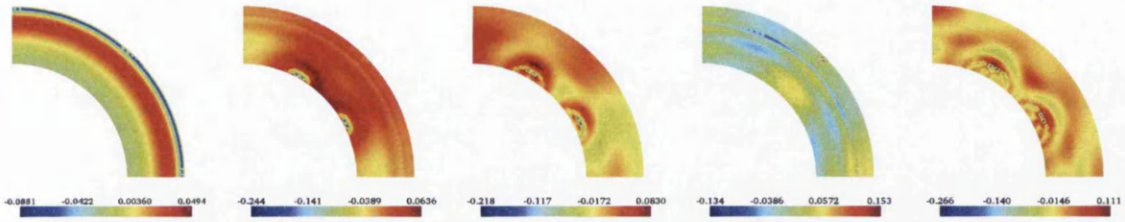

(a) Mode 03 (b) Mode 12 (c) Mode 20 (d) Mode 23 (e) Mode 28

Figure 6.10: Various eigenmodes of the complete controllability Gramian of the baseline (deterministic) diffusion system with boundary forcing terms.

the controllability Gramian of this deterministic model are shown in Fig. 6.10 which has been computed after the controllability Gramian matrix has been solved from the Lyapunov equation. Hence this method is extremely expensive and hence the dominant Arnoldi-Lyapunov

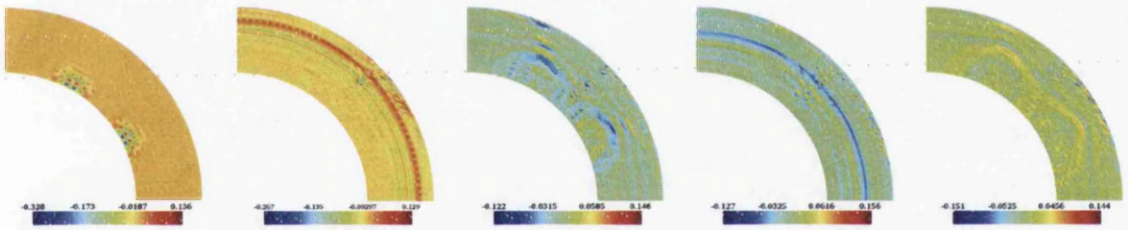

(a) Mode 03 (b) Mode 40 (c) Mode 65 (d) Mode 69 (e) Mode 80

Figure 6.11: Various Arnoldi-Lyapunov eigenmodes of the controllability Gramian obtained with a block Krylov method applied to the baseline (deterministic) diffusion system with boundary forcing terms.

eigenvectors have been calculated from the block Krylov space using the algorithm detailed in Sec. 6.3.4. It can be seen that the block Krylov modes are generally not close to the eigenmodes of the controllability Gramian, but a closer scrutiny reveals that the Arnoldi-Lyapunov modes are seen to be associated with the impulse response of the block forcing imposed on the system via the matrix $\bar{\mathcal{B}}$.

Now, for the randomly parametrized diffusion system calculating the controllability Gramian becomes prohibitively expensive and hence the dominant Arnoldi-Lyapunov vectors are calculated using the Arnoldi's algorithm for the Lyapunov matrix equations in the tensor product space of the vector of finite element nodal degrees of freedom and the finite order chaos expansion of the stochastic space. The mean of these eigenvectors are shown in Fig. 6.12 which again exhibits a similar patter with respect to the forcing imposed at the boundary to those shown in Figs. 6.10–6.11.

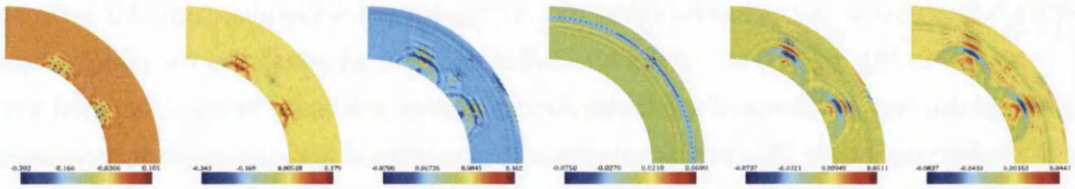

(a) Mode 05 (b) Mode 12 (c) Mode 24 (d) Mode 46 (e) Mode 60 (f) Mode 70

Figure 6.12: Plots of the mean of the various Arnoldi-Lyapunov eigenmodes of the stochastic controllability Gramian approximated with finite order chaos expansion of the randomly parametrized diffusion system with boundary forcing terms.

(a) Mean response, 100 modes.

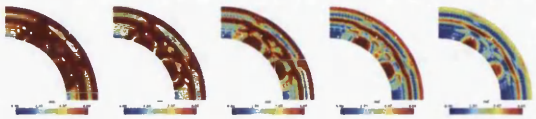

(f) Standard deviation of response, 100 modes.

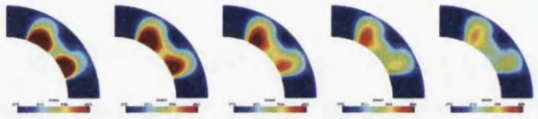

(b) Mean response, 200 modes.

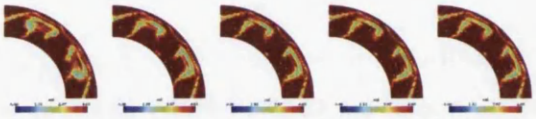

(g) Standard deviation of response, 200 modes.

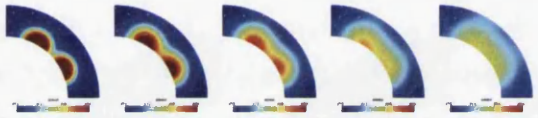

(c) Mean response, 400 modes.

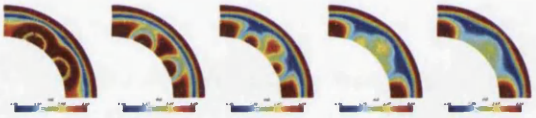

(h) Standard deviation of response, 400 modes.

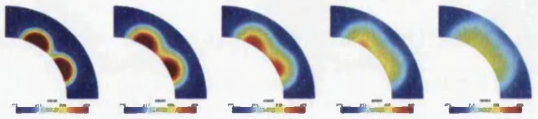

(d) Mean response, 500 modes.

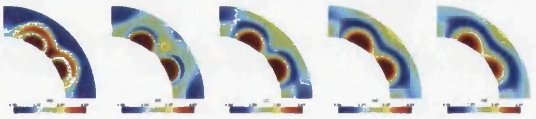

(i) Standard deviation of response, 500 modes.

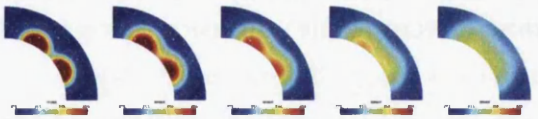

(e) Mean response of the full system solution shown at five different instances of time $t = iT_{\text{tot}}/5$ where $i = 1, \ldots, 5$.

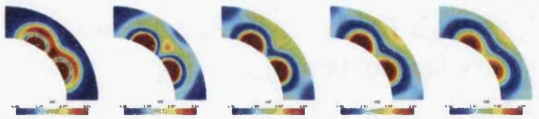

(j) Standard deviation of the response of the full system solution shown at five different instances of time $t = iT_{\text{tot}}/5$ where $i = 1, \ldots, 5$.

Figure 6.13: Plots of the mean (left column) and standard deviation (right column) of the response to the randomly parametrized diffusion system under the action of the boundary forcing terms. The statistics of the response obtained with various reduced order models (realized with the Arnoldi-Lyapunov eigenmodes) of the system are shown here. The bottom most row gives the mean and standard deviation of full system response which is treated as the benchmark solution. The stochastic solutions in all these cases have been approximated with a 4-th order chaos expansion for a 4-dimensional input space.

The statistics of the solution of the transient diffusion system under the action of time varying boundary forcing terms is shown in Fig. 6.13 which compares the accuracy of the

solution obtained with increasing the dimension of the reduced subspace in which the solution is sought, i.e. as the number of Arnoldi-Lyapunov basis vectors are increased. It can be seen that for low order approximations with only 100 eigenmodes, the solution fails to give any reasonable response statistics, while as more basis functions are included to construct the approximate solution the accuracy of the response increases. It can also be noted that as the higher order statistics of the solution are sought, it becomes necessary to incorporate additional modes into the reduced order model. It should however, be noted that increasing the number of Arnoldi-Lyapunov basis functions does not mean an increase in the degree of the stochastic chaos functions used to approximate the solution vector. It can be seen that even the low order approximations of the solution with the Arnoldi-Lyapunov basis vectors gives the solution with the 4-th order chaos expansion. However, the higher order statistics of the response necessitates additional terms associated with the 4-th degree stochastic polynomial terms in order to obtain a good approximation of the response.

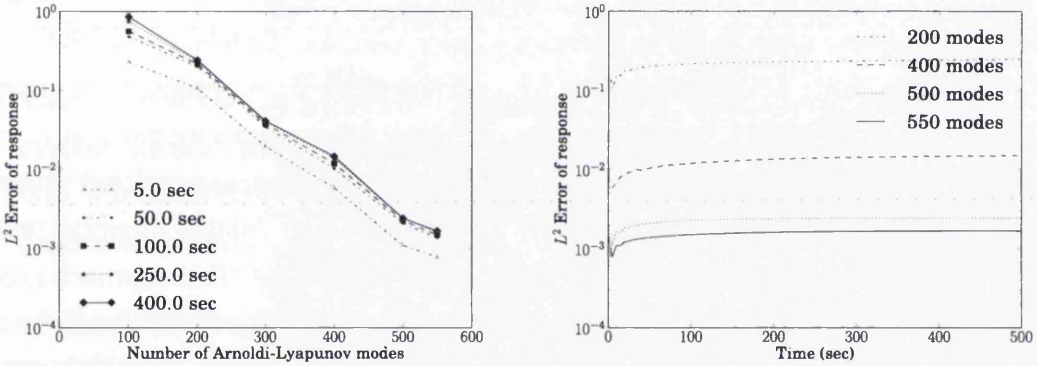

(a) L^2 norm of the error of the stochastic solution vector specific values of t for increasing number of Arnoldi-Lyapunov modes.

(b) L^2 norm of the error of the stochastic solution at all t

Figure 6.14: Plots of the L^2 errors of the stochastic solution vector for various dimension of the reduced subspace in which the solution is approximated. The reduced subspace dimension is determined by the number of Arnoldi-Lyapunov basis functions used to approximate the controllability Gramian with finite order chaos expansion.

Figure 6.14 gives the L^2 error of the approximate solution vector with respect to the full system solution (as described by Eqn. (6.58)) when using a 4-th order chaos expansion with different reduced order models of the randomly parametrized diffusion system. We present the convergence rate of the solution with the number of approximating Arnoldi-Lyapunov vectors at various instances in time (such as $t = [5, 50, 100, 250, 400]$ seconds) in Fig. 6.14(a) which shows a nearly exponential convergence. The L^2 error norm at all instances of time is shown in Fig. 6.14(b) which shows that the error increases slightly as the value of t increases. Thus, increasing the number of Arnoldi-Lyapunov modes leads to a rapid improvement in the solution accuracy.

6.5 Summary

A computationally efficient scheme of resolution of the transient response of numerical models of large scale randomly parametrized dynamical systems has been proposed. The methodology relies on obtaining a minimal order realization of the linear time invariant system based on the idea of preserving the strong dynamical coupling of the specified input-output characteristics of the system. The uncertainty associated with the random input parameters is propagated to the system response using the established framework of stochastic spectral Galerkin method. The resulting linear system due to the application of this method is orders of magnitude larger than the baseline FE linear systems and model reduction techniques are very important in this context. The transient response of the randomly parametrized linear system has been approximated with a denumerable set of dominant dynamical modes obtained from the spectral decomposition of the stochastic controllability Gramian.

The controllability Gramian satisfies the stochastic Lyapunov equation which requires the resolution of a matrix equation of significant dimension. Different methods of resolution of this stochastic matrix equation using a stochastic sampling based technique to the series expansion of the stochastic Gram matrix with orthogonal stochastic polynomials and applying the 'vec' transformation have been discussed. However, the computational cost associated with these methods becomes prohibitively large even for moderate dimensional systems. Hence an alternative method of approximating the stochastic controllability Gramian with a reduced number of Arnoldi-Lyapunov vector bases has been proposed. This approach avoids the full solution of the stochastic Lyapunov equation and approximates the dominant invariant subspace associated with spectral components of the stochastic controllability Gramian. The algorithm approximating the transient stochastic response with the Arnoldi-Lyapunov basis vectors in conjuction with an implicit time stepping scheme has been detailed. Additionally, to enhance the stability and convergence properties of the time integration scheme further, especially for long time integration problems, a restarted Arnoldi-Lyapunov basis vector estimation has been proposed. The latter relies on reinitializing the reduced-order basis evaluation after finite intervals of time based on the solution of the dynamic system obtained at that time step. The theoretical justification for the implicit restarting of the basis evaluation has been discussed. Finally the steps of the algorithm have been detailed in an itemized algorithm. The proposed reduced order modeling of the randomly parametrized system with Arnoldi-Lyapunov vectors basis has been demonstrated with examples of an advection-diffusion-reaction problem on a regular square domain and a pure diffusion problem with boundary forcing terms on a circular arc-shaped domain.

The salient features of the work presented here are

- A randomly parametrized large-scale linear time invariant finite element system has been considered and a computationally efficient minimal realization scheme to obtain

the transient response of this system has been studied.

- The minimal realization of the LTI system has been obtained from the dominant spectral components of the stochastic controllability Gramian.
- The theoretical and implementational aspects of different methods of resolution of the principal modes of the stochastic controllability Gramian has been provided and analyzed for their computational overhead.
- To mitigate the cost associated with the solution of the large dimensional matrix equations, the Arnoldi-Lyapunov basis spanning the dominant space associated with the spectral components of the stochastic controllability Gramian has been investigated.
- The computationally efficient methodology to resolve the transient response of the LTI system with an Arnoldi-Lyapunov vector basis has been highlighted in an algorithm.
- An implicit scheme of restarting the determination of the Arnoldi-Lyapunov vector basis has been proposed and the theoretical justification for this has been detailed.
- The minimal realization of the dynamic characteristics of the randomly parametrized system has been illustrated with two stochastic finite element problems in conjunction with a spectral Galerkin approach which demonstrates the applicability of the reduced order evaluation of the transient response of large computational models.

Thus the numerical results demonstrate the applicability of the proposed methodology to large scale randomly parametrized finite element systems subjected to transient external forcing.

Chapter 7

Conclusion

7.1 Summary of contributions made

A detailed analysis of efficient uncertainty propagation methods within the framework of stochastic finite element framework has been presented in the previous chapters. The methods utilized to obtain the response statistics of the randomly parameterized systems have been compared in terms of their accuracy and computational efficiency with benchmark solutions and have been demonstrated with numerical examples. A summary of the principal contributions of this dissertation is categorically listed here under the following subheadings :

- **Stochastic structural dynamics using reduced order spectral functions**
  The frequency response of a stochastic structural dynamic system has been investigated by projecting the solution on a reduced subspace of eigenvectors of the deterministic operator weighted by a set of frequency dependent stochastic spectral functions. These spectral functions are rational functions of the underlying random variables and a study of the different orders of spectral functions are presented. A set of undetermined Galerkin coefficients are utilized to orthogonalize the residual to the reduced eigenvector space in the mean sense. The complex system response is represented explicitly with these Galerkin coefficients in conjunction with the modal basis and the associated stochastic spectral functions. This is a computationally efficient stochastic solution technique which gives good approximation of the statistics of the response (verified by the values of the relative error norm) even at resonance frequencies where finite order PCE or the classical Neumann expansion becomes quite expensive and/or fails to perform satisfactorily. Two examples involving a beam and a plate with stochastic parameters subjected to harmonic excitations have been studied. The results are compared with the direct Monte-Carlo simulation, the classical Neumann expansion technique and the polynomial chaos method for different orders stochastic functions and varying degrees of variability of input randomness.

- **Hybridization of the spectral function approach with metamodeling technique**
  The spectral function approach developed in the context of determining the frequency response statistics of randomly parameterized system has been combined with Gaussian process emulation to produce a computationally efficient solution algorithm. It is motivated by the fact that higher order spectral functions improves solution accuracy but has an added computational cost associated with it. This cost is mitigated by using a metamodeling technique where the samples drawn from the posterior distribution can be used to perform uncertainty analysis of the response. The proposed hybrid approach is used to the analyze the stochastic vibration response of a corrugated panel with random elastic parameters. Here the direct MCS is considered to provide a benchmark solution. The response curves obtained with the spectral function and the direct MCS method are in good agreement even near the resonance frequencies. The analysis of computational complexity demonstrates that spectral function approach in conjunction with the Gaussian process emulation is computationally favorable when compared to direct MCS or spectral method alone. Also, the relative error plots show an increase in the accuracy of the approximated solution when using higher order spectral functions.

- **Transient response with stochastic time adaptive spectral functions**
  The time domain response of randomly parameterized structural dynamic system was investigated with polynomial chaos expansion approach and a stochastic spectral function approach in conjunction with an unconditionally stable single-step implicit Newmark scheme using a stochastic integration operator. The spectral function approach uses time adaptive stochastic spectral functions as weighting functions of the deterministic orthogonal basis onto which the solution is projected. The simulations have been performed for different degrees of variability of the input randomness and different dimensions of the input stochastic space for structural dynamic systems and the results have been compared with the finite order PCE and the direct MCS in terms of accuracy and computational cost. It is seen that accurate estimation of the statistics of the stochastic system response is obtained even with the low order spectral functions which is computationally advantageous. Additionally, the spectral functions utilized here depends on the time-step size and the integration constants chosen for the problem. This results in the convergence being a function of the integration parameters. Hence these parameters can be fine tuned to obtain optimal convergence.

- **Discrete representation of the random field on complicated domains**
  The problem of representing random fields describing the material and boundary properties of the physical system at discrete points of the spatial domain is studied in the context of linear stochastic finite element method. The random field has been approximated on the nodes of an unstructured finite element mesh using a discrete Karhunen-Loève

(KL) expansion. The approximated random field exhibits good level of accuracy with respect to various synthesized error indicators. The approximated random field has been interpolated at the quadrature points using the multidimensional Lagrange polynomials (FE finite element shape functions). The parametric uncertainty has been modeled with random variables within the probabilistic framework and has been integrated with the isoparametric finite element formulation using stochastic mapping of the perturbed elements to the corresponding master element. Additionally, the explicit expressions for the coefficients of the lognormal random field have been derived in the Appendix A.1. This enables rapid evaluation of the coefficients of the lognormal field with Hermite polynomials of independent identically distributed Gaussian random variables.

- **Stochastic problems on domain with random boundary fluctuations**
  The discretized random field representation has been utilized to express the random fluctuations of the domain boundary with nodal position coordinates and a set of iid random variables. The description of the boundary perturbation has been incorporated into the weak stochastic finite element formulation using a stochastic isoparametric mapping of the random domain to a deterministic master domain. A method for obtaining the linear system of equations under the proposed mapping using generic high order finite elements and the stochastic spectral Galerkin framework is studied in detail. The mapping of the differential operators and the associated Jacobian matrices and the determinant of a matrix series have been expressed explicitly with random polynomials in order facilitate prior computation of the expectations of stochastic polynomials. The treatment presents a unified way of handling the parametric uncertainty and random boundary fluctuations for dynamic systems. The convergence behavior of the proposed methodologies has been demonstrated with numerical examples where the accuracy of the response statistics obtained with the proposed method has been compared with respect to brute force MCS (which serves as the benchmark solution) for various order of chaos expansions, number of quadrature integration points and the corresponding computational cost.

- **Model order reduction based on balanced truncation**
  A model order reduction scheme of the transient response of large-scale randomly parametrized linear finite element system in state space form has been studied. An a-priori model reduction strategy based on the balanced truncation method has been proposed in conjunction with the stochastic spectral Galerkin finite element method. Approximation of the dominant modes of the observable Gram matrix has been performed with iterative Arnoldi scheme applied to Lyapunov equations. The reduced order representation of the randomly parametrized dynamical system has been obtained with Arnoldi-Lyapunov vector basis using an implicit time stepping algorithm. An im-

plicit scheme of restarting the determination of the Arnoldi-Lyapunov vector basis has been proposed with theoretical justifications which can further enhance the computational efficacy for long time integration problems. The accuracy of the minimal realization of the dynamic characteristics of the randomly parametrized system has been illustrated with two stochastic finite element problems using relative error estimates which demonstrates their applicability in large computational mechanics problems.

7.2 Future research

The work carried out in this dissertation can be used to pursue further research in the following directions.

- The underlying idea of stochastic spectral functions can potentially be extended to analyze the response statistics of a class of non-linear stochastic dynamic problems. For example, the proposed spectral approach can be used for every linearization step or every time step. The choice of the optimum order of spectral functions and the number of the reduced vector basis is not obvious from the error analysis results obtained with the spectral function approach and there is a scope for making it adaptive, based on some optimization criterion, which would be interesting to investigate.

- The random field has been represented by the KL expansion or expansions that exploits the covariance structure of the input random field. This can be expanded to the case where such a description is not available. For example there are cases when complete information about the variability of an input random field is not available. Hence it is possible to to address general random fields without resorting to the KL expansion (such as the hierarchal matrix based approaches Allaix and Carbone [2013]). The applicability of the proposed random field discretization technique and its integration with the SFEM method would be interesting.

- Also, comparison of the computational efficacy of high dimensional stochastic problems where the stochastic integration is performed with dimension adaptive sparse grid algorithms would be another important aspect of future study for. Lastly, the applicability of various emulation methods, such as the Gaussian process emulator, can be investigated for their potential application in the study of stochastic partial differential equations on random domains. Future work in this domain would look at extending the proposed stochastic isoparametric mapping to study non-linear problems on random domains where arbitrarily small perturbation of the domain boundary may result in a significant modification of the response field. In such cases, the modification and dependence of the non-linear parameters and/or the element geometry on the stochastic

boundary at each step of the iterative non-linear solver, within the proposed stochastic isoparametric mapping framework would be a challenging problem.

- The reduced order modeling approach with Arnoldi-Lyapunov vectors can be extended to study the transient response of structural dynamic systems with input parametric uncertainty in state-space form. Additionally, the theoretical development which can provide an a-priori knowledge of the accuracy of the transient response of the randomly parametrized system as a function of the number of Arnoldi-Lyapunov basis would be quite useful for the computational scheme presented here. This might lead to a unique global error indicator combining the residuals of the Lyapunov equation and the stochastic LTI system which can be used to decide the implicit restart points of the Arnoldi-Lyapunov basis evaluation algorithm. Lastly, investigation into the possibility of using efficient preconditioners for the Arnoldi-Lyapunov algorithm, which can give better convergence of the solution with fewer number of basis functions, would be important in context of this study.

7.3 Published works

7.3.1 Journal papers

1. A. Kundu and S. Adhikari. Transient Response of Structural Dynamic Systems with Parametric Uncertainty. *Journal of Engineering Mechanics*, 140(2):315–331, 2014.

2. A Kundu, F. A. DiazDelaO, S. Adhikari, and M. I. Friswell. A hybrid spectral and metamodeling approach for the stochastic finite element analysis of structural dynamic systems. *Computer Methods in Applied Mechanics and Engineering*, 270(0):201–219, 2014.

7.3.2 Conference papers

1. A Kundu, F. A. DiazDelaO, M. I. Friswell, and S. Adhikari. Uncertainty analysis of corrugated skin with random elastic parameters and surface topology. SciTech 2014 (16^{th} AIAA Non-Deterministic Approaches Conference), January 2014, National Harbor, Maryland, USA.

2. A. Kundu. Stochastic Finite Element Method for dynamical systems with random boundary topology. 25th Biennial Conference on Numerical Analysis, 25-28 June, 2013, University of Strathclyde, Glasgow, UK.

3. A. Kundu and S. Adhikari. Transient Dynamics of Stochastic Systems using a Reduced Order Spectral Function Approach. 53rd AIAA/ASME/ASCE/AHS/ASC Structures,

Structural Dynamics and Materials Conference, April 2012, Honolulu, Hawaii, USA.

4. A. Kundu and S. Adhikari. Finite Element Analysis of Stochastic Structural Dynamic Systems using a Reduced Order Spectral Function Approach. 6th International ASRANet Conference for Integrating Structural Analysis, Risk and Reliability. July 2012, London, Croydon, UK.

5. A. Kundu and S. Adhikari. Novel Reduced Galerkin Projection Schemes for Stochastic Dynamical Systems. Proceedings of the 1st International Symposium on Uncertainty Quantification and Stochastic Modeling. February 2012, Maresias, Sao Sebastiao(SP), Brazil.

6. A. Kundu and S. Adhikari. Stochastic Structural Dynamics using Frequency Adaptive Basis Functions. International Symposium on Engineering under Uncertainty: Safety Assessment and Management. January 2012, Calcutta (WB), India.

7. A. Kundu and S. Adhikari. A Novel Galerkin Projection Approach for Damped Stochastic Dynamic Systems. COMPDYN 2011, 3rd ECCOMAS Thematic Conference on Computational Methods in Structural Dynamics and Earthquake Engineering, May 2011, Corfu, Greece.

8. A. Kundu and S. Adhikari. A Reduced Spectral Projection Method for Stochastic Finite Element Analysis, 52nd AIAA/ASME/ASCE/AHS/ASC Structures, Structural Dynamics & Materials Conference, April 2011, Denver, Colorado.

7.3.3 Book chapters

1. A. Kundu and S. Adhikari. A novel reduced spectral function approach for finite element analysis of stochastic dynamical systems Computational Methods in Stochastic Dynamics: Volume 2 , Edited by Manolis Papadrakakis, George Stefanou, Vissarion Papadopoulos, published by Springer, 2012.

Appendix A

Mathematical derivations

A.1 Derivation of closed form expressions for the finite order chaos representation of lognormal random fields

The derivation of the analytical expressions for the undetermined coefficients associated with the stochastic polynomial expansion of the lognormal field is presented here. We assume a lognormal random field $\mathbf{a}_l(\theta) = \exp\left(\bar{\mathbf{a}}_0 + \sum_{i=1}^{M} \xi_i(\theta)\widetilde{\mathbf{a}}_i\right)$ in a discretized spatial domain such that $\mathbf{a}_l(\theta) \in \mathbb{R}^n$. For the sake of computational convenience we express this random field as a series expansion of finite order multivariate Hermite polynomials $\mathscr{H}_i(\xi(\theta))$ spanning the M-dimensional stochastic hyperspace $\Theta^{(M)}$ as

$$\mathbf{a}_l = \sum_{i=0}^{m} \mathbf{a}_i^l \mathscr{H}_i(\boldsymbol{\xi}(\boldsymbol{\theta})) \quad \text{where} \quad \mathbf{a}_i^l = \frac{\langle \mathbf{a}_l(\boldsymbol{\theta}), \mathscr{H}_i(\boldsymbol{\xi}(\boldsymbol{\theta}))\rangle_{L^2(\Theta^{(M)}, dP_\xi)}}{\langle \mathscr{H}_i(\boldsymbol{\xi}(\boldsymbol{\theta}))\rangle^2_{L^2(\Theta^{(M)}, dP_\xi)}} \tag{A.1}$$

The aim is to express the undetermined coefficients as a closed form analytical expression in terms of the Gaussian iid random variables $\xi = \{\xi_1, \ldots, \xi_M\}$.

Theorem 1. *If a lognormal random field $\mathbf{a}_l(\theta)$ is expanded as a series of multivariate orthogonal Hermite polynomials spanning the stochastic Hilbert space of the input Gaussian random variables, then the undetermined coefficients associated with the individual polynomial terms are given by*

$$\mathbf{a}_i^l = \exp(\bar{\mathbf{a}}_0) \prod_{i=1}^{M} \exp\left(\frac{1}{2}\widetilde{\mathbf{a}}_i^2\right) \frac{\mathscr{H}_i^{hd}(\widetilde{\mathbf{a}}_1, \ldots, \widetilde{\mathbf{a}}_M)}{\langle \mathscr{H}_i(\xi(\theta))\rangle^2_{L^2(\Theta^{(M)}, dP_\xi)}} \tag{A.2}$$

where $\mathscr{H}_i^{hd}(\widetilde{\mathbf{a}}_1, \ldots, \widetilde{\mathbf{a}}_M)$ is the vector of the highest order term associated with the i-th Hermite polynomial and $(\widetilde{\mathbf{a}}_1, \ldots, \widetilde{\mathbf{a}}_M)$ being the M discrete eigenvectors of the spectral decomposition of the covariance kernel of the input random field.

Proof. We begin by noting that the p^{th} order multivariate Hermite polynomials are obtained

using the generating function

$$\mathscr{H}_i(\xi_1^{p_1},\ldots,\xi_M^{p_M}) = (-1)^{p_1+\ldots+p_M}\exp\left(\frac{1}{2}\sum_{j=1}^{M}\xi_i^2\right)\frac{\partial^{p_1}}{\partial\xi^{p_1}}\cdots\frac{\partial^{p_M}}{\partial\xi^{p_M}}\exp\left(-\frac{1}{2}\sum_{j=1}^{M}\xi_i^2\right)$$

$$\text{where} \quad p = p_1+\ldots+p_M \tag{A.3}$$

where $p_1,\ldots,p_M$ are the degree of the random variables $\xi_1,\ldots,\xi_M$ respectively. Hence the expression for $\mathbf{a}_i^l$ from Eqn. (A.1) can be written after some simplification as the integration in stochastic space as

$$\begin{aligned}\mathbf{a}_i^l &= \frac{(-1)^p(2\pi)^{-\frac{M}{2}}}{\langle\mathscr{H}_i(\xi(\theta))\rangle^2_{L^2(\Theta^{(M)},dP_\xi)}}\int_{-\infty}^{+\infty}\cdots\int_{-\infty}^{+\infty}\exp\left(\bar{\mathbf{a}}_0+\sum_{i=1}^{M}\xi_i\tilde{\mathbf{a}}_i\right)\cdot \\ &\qquad\left\{\frac{\partial^{p_1}}{\partial\xi_1^{p_1}}\cdots\frac{\partial^{p_M}}{\partial\xi_M^{p_M}}\exp\left(-\frac{1}{2}\sum_{j=1}^{M}\xi_i^2\right)\right\}d\xi_1\ldots d\xi_M \\ &= \mathscr{C}\int_{-\infty}^{+\infty}\cdots\int_{-\infty}^{+\infty}\prod_{i=1}^{M}\exp(\xi_i\tilde{\mathbf{a}}_i)\frac{\partial^{p_1}}{\partial\xi_1^{p_1}}\cdots\frac{\partial^{p_M}}{\partial\xi^{p_M}}M\left\{\exp\left(-\frac{1}{2}\sum_{j=1}^{M}\xi_i^2\right)\right\}d\xi_1\ldots d\xi_M\end{aligned} \tag{A.4}$$

$$\text{where,} \quad \mathscr{C} = \frac{(-1)^p(2\pi)^{-\frac{M}{2}}}{\langle\mathscr{H}_i(\xi(\theta))\rangle^2_{L^2(\Theta^{(M)},dP_\xi)}}\exp(\bar{\mathbf{a}}_0)$$

For the evaluation of the integral in Eqn. (A.4) we apply integration by parts with variable ξ_1 (whose order is p_1) and consider only a portion of the above integral as

$$\begin{aligned}\left(\mathbf{a}_i^l\right)_1 &= \int_{-\infty}^{+\infty}\exp(\xi_1\tilde{\mathbf{a}}_1)\frac{\partial^{p_1}}{\partial\xi_1^{p_1}}\left\{\exp\left(-\frac{1}{2}\xi_1^2\right)\right\}d\xi_1 \\ &= \left(\exp(\xi_1\tilde{\mathbf{a}}_1)\frac{\partial^{p_1-1}}{\partial\xi_1^{p_1-1}}\left\{\exp\left(-\frac{1}{2}\xi_1^2\right)\right\}\right)\Bigg|_{-\infty}^{+\infty} - \\ &\qquad\int_{-\infty}^{+\infty}\frac{\partial}{\partial\xi_1}\left\{\exp(\xi_1\tilde{\mathbf{a}}_1)\right\}\frac{\partial^{p_1-1}}{\partial\xi_1^{p_1-1}}\left\{\exp\left(-\frac{1}{2}\xi_1^2\right)\right\}d\xi_1\end{aligned} \tag{A.5}$$

It is easy to see for the first term that

$$\exp(\xi_1\tilde{\mathbf{a}}_1)\frac{\partial^{p_1-1}}{\partial\xi_1^{p_1-1}}\left\{\exp\left(-\frac{1}{2}\xi_1^2\right)\right\}\to 0 \quad \text{as} \quad \xi_1\to+\infty \quad \text{or,} \quad \xi_1\to-\infty$$

since the exponential function is C^∞ continuous and all the terms appearing in its successive derivatives would involve $\exp\left(-\frac{1}{2}\xi_1^2\right)$. Hence the terms tend to 0 identically as $\xi_1\to-\infty,+\infty$. Thus applying this procedure of integration by parts p_1 times and putting

the leading terms to 0 (as in Eqn. (A.5)) we have

$$\begin{aligned}\left(\mathbf{a}_i^l\right)_1 &= (-1)^{p_1}\int_{-\infty}^{+\infty}\frac{\partial^{p_1}}{\partial\xi_1^{p_1}}\left\{\exp\left(\xi_1\widetilde{\mathbf{a}}_1\right)\right\}\left\{\exp\left(-\frac{1}{2}\xi_1^2\right)\right\}d\xi_1 \\ &= (-1)^{p_1}\widetilde{\mathbf{a}}_1^{p_1}\int_{-\infty}^{+\infty}\exp\left(-\frac{1}{2}\xi_1^2+\xi_1\widetilde{\mathbf{a}}_1\right)d\xi_1 \end{aligned} \tag{A.6}$$

The Gaussian functions integral identity gives $\int_{-\infty}^{+\infty} a_0\exp\left(-a_1x^2+a_2x+a_3\right) = a_0\sqrt{\pi/a_1}\exp\left(\frac{a_2^2}{4a_1}+a_3\right)$ for $a_1>0$ following which we write Eqn. (A.6) as

$$\left(\mathbf{a}_i^l\right)_1 = (-1)^{p_1}\widetilde{\mathbf{a}}_1^{p_1}\sqrt{2\pi}\exp\left(\frac{1}{2}\widetilde{\mathbf{a}}_1^2\right) \tag{A.7}$$

The above equation can be combined with Eqn. (A.4) to obtain

$$\mathbf{a}_i^l = \mathscr{C}\int_{-\infty}^{+\infty}\cdots\int_{-\infty}^{+\infty}\left(\mathbf{a}_i^l\right)_1\prod_{i=2}^{M}\exp\left(\xi_i\widetilde{\mathbf{a}}_i\right)\frac{\partial^{p_2}}{\partial\xi_2^{p_2}}\cdots\frac{\partial^{p_M}}{\partial\xi_M^{p_M}}\left\{\exp\left(-\frac{1}{2}\sum_{j=2}^{M}\xi_i^2\right)\right\}d\xi_2\ldots d\xi_M \tag{A.8}$$

Applying the same procedure as in Eqns. (A.5)–(A.7) to the successive random variables from ξ_2 to ξ_M we would have the integral evaluated as

$$\mathbf{a}_i^l = \mathscr{C}\left(\mathbf{a}_i^l\right)_1\ldots\left(\mathbf{a}_M^l\right)_M \tag{A.9}$$

$$\begin{aligned}\text{or,}\quad \mathbf{a}_i^l &= \frac{(-1)^p(2\pi)^{-\frac{M}{2}}}{\left\langle\mathscr{H}_i(\xi(\theta))\right\rangle^2_{L^2(\Theta^{(M)},dP_\xi)}}\exp\left(\bar{\mathbf{a}}_0\right)\left((-1)^{p_1}\widetilde{\mathbf{a}}_1^{p_1}\sqrt{2\pi}\exp\left(\frac{1}{2}\widetilde{\mathbf{a}}_1^2\right)\right)\ldots \\ &\qquad\qquad\ldots\left((-1)^{p_M}\widetilde{\mathbf{a}}_M^{p_M}\sqrt{2\pi}\exp\left(\frac{1}{2}\widetilde{\mathbf{a}}_M^2\right)\right) \\ &= \frac{(-1)^p(2\pi)^{-\frac{M}{2}}}{\left\langle\mathscr{H}_i(\xi(\theta))\right\rangle^2_{L^2(\Theta^{(M)},dP_\xi)}}\exp\left(\bar{\mathbf{a}}_0\right)\left((-1)^p(2\pi)^{\frac{M}{2}}\widetilde{\mathbf{a}}_1^{p_1}\ldots\widetilde{\mathbf{a}}_M^{p_M}\prod_{i=1}^{M}\exp\left(\frac{1}{2}\widetilde{\mathbf{a}}_i^2\right)\right)\end{aligned} \tag{A.10}$$

where in the last step we have substituted back the value of $\mathscr{C}$ from Eqn. (A.4) and used the relation $p = p_1+\ldots+p_M$. Hence the i^{th} coefficient of the lognormal field is expressed in closed form as

$$\begin{aligned}\mathbf{a}_i^l &= \exp\left(\bar{\mathbf{a}}_0\right)\prod_{i=1}^{m}\exp\left(\frac{1}{2}\widetilde{\mathbf{a}}_i^2\right)\frac{\widetilde{\mathbf{a}}_1^{p_1}\ldots\widetilde{\mathbf{a}}_M^{p_M}}{\left\langle\mathscr{H}_i(\xi(\theta))\right\rangle^2_{L^2(\Theta^{(M)},dP_\xi)}} \\ &= \exp\left(\bar{\mathbf{a}}_0\right)\prod_{i=1}^{m}\exp\left(\frac{1}{2}\widetilde{\mathbf{a}}_i^2\right)\frac{\mathscr{H}_i^{hd}\left(\widetilde{\mathbf{a}}_1,\ldots,\widetilde{\mathbf{a}}_M\right)}{\left\langle\mathscr{H}_i(\xi(\theta))\right\rangle^2_{L^2(\Theta^{(M)},dP_\xi)}} \\ &\qquad\text{where}\quad \mathscr{H}_i^{hd}\left(\widetilde{\mathbf{a}}_1,\ldots,\widetilde{\mathbf{a}}_M\right) = \widetilde{\mathbf{a}}_1^{p_1}\ldots\widetilde{\mathbf{a}}_M^{p_M}\end{aligned} \tag{A.11}$$

i.e. $\mathscr{H}_i^{hd}\left(\widetilde{\mathbf{a}}_1,\ldots,\widetilde{\mathbf{a}}_M\right)$ denotes the term of highest degree (i.e. the term of degree $p_1,\ldots,p_M$

in random variables $\xi_1, \ldots, \xi_M$ respectively) of the i^{th} multivariate Hermite polynomial of degree p associated with the M Gaussian iid random variables. □

A.2 Expression for the determinant of a matrix series with stochastic coefficients

We derive the determinant of a matrix series with scalar coefficients of the form

$$\mathbf{A} = \sum_{i=1}^{m} \alpha_i \mathbf{A}_i \quad \text{where} \quad \mathbf{A}, \mathbf{A}_1, \ldots \mathbf{A}_m \in \mathbb{R}^{n \times n}; \quad \alpha_i \in \mathbb{R} \; \forall i \tag{A.12}$$

$$\text{with} \quad \det|\mathbf{A}| = \det|\sum_{\mathrm{i=1}}^{\mathrm{m}} \alpha_{\mathrm{i}} \mathbf{A}_{\mathrm{i}}| = \mathrm{f}\left(\alpha_1, \ldots, \alpha_{\mathrm{m}}\right)$$

where m can be greater than, equal to or less than n, the dimension of the square matrices in the series. It is can be deduced from observation that the determinant in the above equation would be a degree n homogeneous function of the coefficients α_i. Let us define a set $\mathscr{M}$ which consists of all powers (from 1 to n) of the scalars α_i as

$$\mathscr{M} = \{\alpha_1, \alpha_1^2, \ldots, \alpha_1^n, \ldots, \alpha_m, \alpha_m^2, \ldots, \alpha_m^n\} \tag{A.13}$$

and M is the set of all the elements derived from $\mathscr{M}$ which satisfies the following condition

$$M = \{\widetilde{\alpha}_i \; : \; \widetilde{\alpha}_i = \prod_{j=1}^{r} \alpha_j^{p_j} \;\; \text{with} \;\; \sum_{j=1}^{r} p_j = n, \;\; \text{for all} \;\; 1 \leq r \leq m\} \tag{A.14}$$

and let $\mathscr{I}_M$ be the cardinality of this set. In other words, the elements of M are such that the total sum of their powers is always equal to n. The determinant of $\mathbf{A}$ can be expressed as

$$\det|\mathbf{A}| = \sum_{i \in M_m} \widetilde{\alpha}_i \left(\sum_{j \in \mathscr{I}_n} \det|\widetilde{\mathbf{A}}_j| \right) \tag{A.15}$$

where the $\widetilde{\mathbf{A}}_j$ matrices are generated from combining the rows of the matrices $\mathbf{A}_i$ (from Eqn. (A.13)) associated with the scalar α_i-s (in the coefficient $\widetilde{\alpha}_i$) according to their powers in $\widetilde{\alpha}_i$. For example, if the coefficient associated with the scalar term $\widetilde{\alpha}_i = \alpha_1^{p_1} \ldots \alpha_m^{p_m}$ is sought then we define

$$\begin{aligned} S &= \{x : x = \text{Permutation of } \mathrm{p_1} \text{ number of } \mathrm{j_1}, \mathrm{p_2} \text{ number of } \mathrm{j_2}, \ldots, \mathrm{p_m} \text{ number of } \mathrm{j_m}\} \\ c_i &= \sum_j \det|\widetilde{\mathbf{A}}_x| \quad \forall \, x \in S \end{aligned} \tag{A.16}$$

where $\widetilde{\mathbf{A}}_x$ denotes matrix constructed from taking all permutations of p_1 rows taken from $\mathbf{A}_{j_1}$ matrix, p_2 rows taken from $\mathbf{A}_{j_2}$ matrix and so on up to p_m rows taken from $\mathbf{A}_{j_m}$ matrix. It should be noted that the dimension of $\widetilde{\mathbf{A}}_x$ is $n \times n$ so that $p_1 + \ldots + p_m = n$. To illustrate the point we provide a numerical example of a matrix series of 3×3 matrix $\widetilde{\mathbf{A}}$ expressed as $\widetilde{\mathbf{A}} = \alpha_1\widetilde{\mathbf{A}}_1 + \alpha_2\widetilde{\mathbf{A}}_2 + \alpha_3\widetilde{\mathbf{A}}_3$. The determinant of $\widetilde{\mathbf{A}}$ is expressed with polynomials of $\alpha_i,\ i = 1, 2, 3$ as

$$\begin{aligned}\det|\widetilde{\mathbf{A}}| = \alpha_1^3\det|\widetilde{\mathbf{A}}_{j_1j_1j_1}| + \alpha_2^3\det|\widetilde{\mathbf{A}}_{j_2j_2j_2}| + \alpha_3^3\det|\widetilde{\mathbf{A}}_{j_3j_3j_3}| + \alpha_1^2\alpha_2\det|\widetilde{\mathbf{A}}_{j_1j_1j_2}| + \\ \alpha_1^2\alpha_3\det|\widetilde{\mathbf{A}}_{j_1j_1j_3}| + \alpha_2^2\alpha_1\det|\widetilde{\mathbf{A}}_{j_2j_2j_1}| + \alpha_2^2\alpha_3\det|\widetilde{\mathbf{A}}_{j_2j_2j_3}| + \alpha_3^2\alpha_1\det|\widetilde{\mathbf{A}}_{j_3j_3j_1}| + \\ \alpha_3^2\alpha_2\det|\widetilde{\mathbf{A}}_{j_3j_3j_2}| + \alpha_1\alpha_2\alpha_3\det|\widetilde{\mathbf{A}}_{j_1j_2j_3}| \qquad \text{(A.17)}\end{aligned}$$

where $\det|\widetilde{\mathbf{A}}_{j_1j_1j_1}| = \det|\mathbf{A}_1|$;

$$\det|\widetilde{\mathbf{A}}_{j_1j_1j_2}| = \left[\det\begin{vmatrix} - & (\mathbf{A}_1)_1 & - \\ - & (\mathbf{A}_1)_2 & - \\ - & (\mathbf{A}_2)_3 & - \end{vmatrix} + \det\begin{vmatrix} - & (\mathbf{A}_1)_1 & - \\ - & (\mathbf{A}_2)_2 & - \\ - & (\mathbf{A}_1)_3 & - \end{vmatrix} + \det\begin{vmatrix} - & (\mathbf{A}_2)_1 & - \\ - & (\mathbf{A}_1)_2 & - \\ - & (\mathbf{A}_1)_3 & - \end{vmatrix}\right];$$

and,

$$\begin{aligned}\det|\widetilde{\mathbf{A}}_{j_1j_2j_3}| = \Bigg[\det\begin{vmatrix} - & (\mathbf{A}_1)_1 & - \\ - & (\mathbf{A}_2)_2 & - \\ - & (\mathbf{A}_3)_3 & - \end{vmatrix} + \det\begin{vmatrix} - & (\mathbf{A}_1)_1 & - \\ - & (\mathbf{A}_3)_2 & - \\ - & (\mathbf{A}_2)_3 & - \end{vmatrix} + \det\begin{vmatrix} - & (\mathbf{A}_2)_1 & - \\ - & (\mathbf{A}_1)_2 & - \\ - & (\mathbf{A}_3)_3 & - \end{vmatrix} \\ + \det\begin{vmatrix} - & (\mathbf{A}_2)_1 & - \\ - & (\mathbf{A}_3)_2 & - \\ - & (\mathbf{A}_1)_3 & - \end{vmatrix} + \det\begin{vmatrix} - & (\mathbf{A}_3)_1 & - \\ - & (\mathbf{A}_1)_2 & - \\ - & (\mathbf{A}_2)_3 & - \end{vmatrix} + \det\begin{vmatrix} - & (\mathbf{A}_3)_1 & - \\ - & (\mathbf{A}_2)_2 & - \\ - & (\mathbf{A}_1)_3 & - \end{vmatrix}\Bigg]\end{aligned}$$

In the above expressions $(\mathbf{A}_i)_j$ denotes the j^{th} row of the $\mathbf{A}_i$ matrix from the series representation in Eqn. (A.12). Hence, while forming the combination of matrix rows to evaluate the determinant associated with a particular scalar term (say $\prod_i \alpha_i^{p_i}$), the number of rows chosen from each coefficient matrix (say $\mathbf{A}_i$) is equal to the power of the scalar term (i.e. p_i) present in that coefficient. The chosen columns are permuted to give all possible combination of the coefficient matrices. Since $\sum_i p_i = n$, the resulting individual matrices would always be square matrices.

Bibliography

Adhikari, S. (2011), "A reduced spectral function approach for the stochastic finite element analysis", *Computer Methods in Applied Mechanics and Engineering*, **200** (21-22), pp. 1804 – 1821.

Adhikari, S. and Manohar, C. S. (2000), "Transient dynamics of stochastically parametered beams", *ASCE Journal of Engineering Mechanics*, **126** (11), pp. 1131–1140.

Adler, R. J. (1981), *The geometry of random fields*, Wiley, London, reprinted by Siam, 2010.

Allaix, D. L. and Carbone, V. I. (2013), "Karhunen-Loève decomposition of random fields based on a hierarchical matrix approach", *International Journal for Numerical Methods in Engineering*, **94** (11), pp. 1015–1036.

Antoulas, A., Sorensen, D., and Gugercin, S. (2001), "A survey of model reduction methods for large-scale systems", *Contemporary mathematics*, **280**, pp. 193–220.

Au, S. K. and Beck, J. L. (1999), "A new adaptive importance sampling scheme for reliability calculations", *Structural Safety*, **21** (2), pp. 135 – 158.

Babuška, I. and Chleboun, J. (2002), "Effects of uncertainties in the domain on the solution of Neumann boundary value problems in two spatial dimensions", *Mathematics of Computation*, **71** (240), pp. 1339–1370.

Babuška, I. and Chleboun, J. (2003), "Effects of uncertainties in the domain on the solution of Dirichlet boundary value problems", *Numerische Mathematik*, **93** (4), pp. 583–610.

Babuška, I., Liu, K., and Tempone, R. (2003), "Solving stochastic partial differential equations based on the experimental data", *Mathematical Models and Methods in Applied Sciences*, **13** (3), pp. 415–444.

Babuška, I., Nobile, F., and Tempone, R. (2005a), "Worst case scenario analysis for elliptic problems with uncertainty", *Numerische Mathematik*, **101** (2), pp. 185–219.

Babuška, I., Nobile, F., and Tempone, R. (2010), "A stochastic collocation method for elliptic partial differential equations with random input data", *SIAM Review*, **52** (2), pp. 317–355.

Babuška, I., Tempone, R., and Zouraris, G. E. (2004), "Galerkin finite element approximations of stochastic elliptic partial differential equations", *Siam Journal on Numerical Analysis*, **42** (2), pp. 800–825.

Babuška, I., Tempone, R., and Zouraris, G. E. (2005b), "Solving elliptic boundary value problems with uncertain coefficients by the finite element method: the stochastic formulation", *Computer Methods in Applied Mechanics and Engineering*, **194** (12-16), pp. 1251 – 1294.

Bai, Z. (2002), "Krylov subspace techniques for reduced-order modeling of large-scale dynamical systems", *Applied Numerical Mathematics*, **43** (1), pp. 9–44.

Bartels, R. H. and Stewart, G. W. (1972), "Solution of the matrix equation AX + XB = C [F4]", *Communications of the ACM*, **15** (9), pp. 820–826.

Barthelmann, V., Novak, E., and Ritter, K. (2000), "High dimensional polynomial interpolation on sparse grids", *Advances in Computational Mathematics*, **12** (4), pp. 273–288.

Bathe, K. J. (1996), *Finite Element Procedures*, Prentice Hall, New Jersey, USA.

Beck, C., Doyle, J., and Glover, K. (1996), "Model reduction of multidimensional and uncertain systems", *Automatic Control, IEEE Transactions on*, **41** (10), pp. 1466–1477.

Benner, P. and Damm, T. (2011), "Lyapunov equations, energy functionals, and model order reduction of bilinear and stochastic systems", *SIAM Journal on Control and Optimization*, **49** (2), pp. 686–711.

Blatman, G. and Sudret, B. (2008), "Sparse polynomial chaos expansions and adaptive stochastic finite elements using a regression approach", *C. R. Mecanique*, **336**, pp. 518–523.

Blatman, G. and Sudret, B. (2010), "An adaptive algorithm to build up sparse polynomial chaos expansions for stochastic finite element analysis", *Probabilistic Engineering Mechanics*, **25** (2), pp. 183 – 197.

Blyth, M. G. and Pozrikidis, C. (2003), "Heat conduction across irregular and fractal-like surfaces", *International Journal of Heat and Mass Transfer*, **46** (8), pp. 1329–1339.

Bobrowski, A. (2005), *Functional analysis for probability and stochastic processes: an introduction*, Cambridge University Press.

Boyaval, S., Bris, C., Maday, Y., Nguyen, N., and Patera, A. (2009), "A reduced basis approach for variational problems with stochastic parameters: Application to heat conduction with variable Robin coefficient", *Computer Methods in Applied Mechanics and Engineering*, **198** (41-44), pp. 3187–3206.

Caflisch, R. E. (1998), "Monte Carlo and Quasi-Monte Carlo methods", *Acta Numerica*, **7**, pp. 1–49.

Charmpis, D. C., Schuëller, G. I., and Pellissetti, M. F. (2007), "The need for linking micromechanics of materials with stochastic finite elements: A challenge for materials science", *Computational Materials Science*, **41** (1), pp. 27–37.

Chen, L. and Rao, S. (1997), "Fuzzy finite-element approach for the vibration analysis of imprecisely-defined systems", *Finite elements in analysis and design*, **27** (1), pp. 69–83.

Chen, W., Baghdasaryan, L., Buranathiti, T., and Cao, J. (2004), "Model validation via uncertainty propagation and data transformations", *AIAA Journal*, **42** (7), pp. 1406–1415.

Cheng, H. and Sandu, A. (2009), "Efficient uncertainty quantification with the polynomial chaos method for stiff systems", *Mathematics and Computers in Simulation*, **79** (11), pp. 3278–3295.

Ching, J. and Beck, J. (2004), "Bayesian analysis of the phase II IASC-ASCE structural health monitoring experimental benchmark data", *Journal of Engineering Mechanics*, **130** (10), pp. 1233–1244.

Choudhury, A., P.B. Nair, and A.J. Keane (2002), "A data parallel approach for large-scale Gaussian process modeling", in "Second SIAM International Conference on Data mining", SIAM, Arlington, VA.

Christakos, G. (1992), *Random field models in earth sciences*, Academic Press, San Diego, CA.

Dayyani, I., Ziaei-Rad, S., and Salehi, H. (2012), "Numerical and experimental investigations on mechanical behavior of composite corrugated core", *Applied Composite Materials*, **19**, pp. 705–721.

Deb, M. K., Babuška, I. M., and Oden, J. T. (2001), "Solution of stochastic partial differential equations using galerkin finite element techniques", *Computer Methods in Applied Mechanics and Engineering*, **190** (48), pp. 6359 – 6372.

Debusschere, B., Najm, H., Pebay, P., Knio, O., Ghanem, R., and Le Maître, O. (2005), "Numerical challenges in the use of polynomial chaos representations for stochastic processes", *SIAM Journal on Scientific Computing*, **22** (2), pp. 698–719.

den Nieuwenhof, B. V. and Coyette, J.-P. (2003), "Modal approaches for the stochastic finite element analysis of structures with material and geometric uncertainties", *Computer Methods in Applied Mechanics and Engineering*, **192** (33-34), pp. 3705–3729.

DiazDelaO, F. A. and Adhikari, S. (2010), "Structural dynamic analysis using Gaussian process emulators", *Engineering Computations*, **27** (5), pp. 580 – 605.

DiazDelaO, F. A. and Adhikari, S. (2011), "Gaussian process emulators for the stochastic finite element method", *International Journal for Numerical Methods in Engineering*, **87** (6), pp. 521–540.

DiazDelaO, F. A. and Adhikari, S. (2012), "Bayesian assimilation of multi-fidelity finite element models", *Computers and Structures*, **92-93** (0), pp. 206 – 215.

Dimarogonas, A. (1995), "Interval analysis of vibrating systems", *Journal of Sound and Vibration*, **183** (4), pp. 739 – 749.

Doostan, A., Ghanem, R. G., and Red-Horse, J. (2007), "Stochastic model reduction for chaos representations", *Computer Methods in Applied Mechanics and Engineering*, **196** (37-40), pp. 3951 – 3966.

Eldred, M. (1992), "Higher order eigenpair perturbations", *AIAA Journal*, **30** (7), pp. 1870–1876.

Falsone, G. and Ferro, G. (2007), "An exact solution for the static and dynamic analysis of FE discretized uncertain structures", *Computer Methods in Applied Mechanics and Engineering*, **196** (21-24), pp. 2390 – 2400.

Feldmann, P. and Freund, R. W. (1995), "Efficient linear circuit analysis by Padé approximation via the Lanczos process", *Computer-Aided Design of Integrated Circuits and Systems, IEEE Transactions on*, **14** (5), pp. 639–649.

Ferson, S., Kreinovich, V., Ginzburg, L., Myers, D. S., and Sentz, K. (2003), *Constructing probability boxes and Dempster-Shafer structures*, volume Sandia Report SAND 2002-4015, Sandia National Laboratories.

Flores, E. I. S., DiazDelaO, F. A., Friswell, M. I., and Sienz, J. (2012), "A computational multiscale approach for the stochastic mechanical response of foam-filled honeycomb cores", *Composite Structures*, **94** (5), pp. 1861 – 1870.

Foo, J. and Karniadakis, G. E. (2010), "Multi-element probabilistic collocation method in high dimensions", *Journal of Computational Physics*, **229** (5), pp. 1536–1557.

Freund, R. W. (1999), "Reduced-order modeling techniques based on Krylov subspaces and their use in circuit simulation", in "Applied and computational control, signals, and circuits", Springer, (pp. 435–498).

Freund, R. W. (2000), "Krylov-subspace methods for reduced-order modeling in circuit simulation", *Journal of Computational and Applied Mathematics*, **123** (1), pp. 395–421.

Fricker, T. E., Oakley, J. E., Sims, N. D., and Worden, K. (2011), "Probabilistic uncertainty analysis of an FRF of a structure using a Gaussian process emulator", *Mechanical Systems and Signal Processing*, **25** (8), pp. 2962 – 2975.

Ganapathysubramanian, B. and Zabaras, N. (2007), "Sparse grid collocation schemes for stochastic natural convection problems", *Journal of Computational Physics*, **225** (1), pp. 652–685.

Gerritsma, M., van der Steen, J.-B., Vos, P., and Karniadakis, G. (2010), "Time-dependent generalized polynomial chaos", *Journal of Computational Physics*, **229** (22), pp. 8333–8363.

Gersem, H. D., Moens, D., Desmet, W., and Vandepitte, D. (2005), "A fuzzy finite element procedure for the calculation of uncertain frequency response functions of damped structures: Part 2 - Numerical case studies", *Journal of Sound and Vibration*, **288** (3), pp. 463–486.

Ghanem, R. (1989), "The nonlinear Gaussian spectrum of log-normal stochastic processes and variables", *Journal of Applied Mechanics*, **66**, pp. 964–973.

Ghanem, R. and Ghosh, D. (2007), "Efficient characterization of the random eigenvalue problem in a polynomial chaos decomposition", *International Journal for Numerical Methods in Engineering*, **72**, pp. 486–504.

Ghanem, R. and Spanos, P. D. (1991), *Stochastic Finite Elements: A Spectral Approach*, Springer-Verlag, New York, USA.

Ghanem, R. G. and Kruger, R. M. (1996), "Numerical solution of spectral stochastic finite element systems", *Computer Methods in Applied Mechanics and Engineering*, **129** (3), pp. 289 – 303.

Goller, B., Pradlwarter, H., and Schuëller, G. (2011), "An interpolation scheme for the approximation of dynamical systems", *Computer Methods in Applied Mechanics and Engineering*, **200** (1-4), pp. 414 – 423.

Gosselet, P., Rey, C., *et al.* (2003), "On a selective reuse of Krylov subspaces in Newton-Krylov approaches for nonlinear elasticity", in "Domain Decomposition Methods in Science and Engineering, edited by I. Herrera, D. Keyes, O. Widlund and R. Yates. Proceedings of the fourteenth international conference on domain decomposition methods", Mexico City, Mexico, (pp. 419–426).

Graham, I. G., Kuo, F. Y., Nuyens, D., Scheichl, R., and Sloan, I. H. (2011), "Quasi-Monte Carlo methods for elliptic PDEs with random coefficients and applications", *Journal of Computational Physics*, **230** (10), pp. 3668–3694.

Grigoriu, M. (2000), "Non-gaussian models for stochastic mechanics", *Probabilistic engineering mechanics*, **15** (1), pp. 15–23.

Grimme, E. J. (1997), *Krylov projection methods for model reduction*, Ph.D. thesis, University of Illinois at Urbana-Champaign.

Gugercin, S. and Antoulas, A. C. (2004), "A survey of model reduction by balanced truncation and some new results", *International Journal of Control*, **77** (8), pp. 748–766.

Hahn, G. D. (1991), "A modified euler method for dynamic analyses", *International Journal for Numerical Methods in Engineering*, **32** (5), pp. 943–955.

Hammarling, S. J. (1982), "Numerical solution of the stable, non-negative definite Lyapunov equation", *IMA Journal of Numerical Analysis*, **2**, pp. 303–323.

Haylock, R. and O'Hagan, A. (1996), *Bayesian Statistics 5*, Oxford University Press, Oxford, UK, chapter On inference for outputs of computationally expensive algorithms with uncertainty on the inputs.

Hlaváček, I. (2007), "Uncertain input data problems and the worst scenario method", *Applications of Mathematics*, **52** (3), pp. 187–196.

Hou, T. Y., Luo, W., Rozovskii, B., and Zhou, H.-M. (2006), "Wiener chaos expansions and numerical solutions of randomly forced equations of fluid mechanics", *Journal of Computational Physics*, **216** (2), pp. 687 – 706.

Ipsen, I. C. F. and Meyer, C. D. (1998), "The idea behind Krylov methods", *The American Mathematical Monthly*, **105** (10), pp. 889–899.

Ishihara, J. and Terra, M. (2003), "A new Lyapunov equation for discrete-time descriptor systems", in "Proceedings of American Control Conference", volume 6, (pp. 5078–5082).

Jaimoukha, I. and Kasenally, E. (1994), "Krylov subspace methods for solving large Lyapunov equations", *SIAM Journal on Numerical Analysis*, **31** (1), pp. 227–251.

Jakeman, J., Eldred, M., and Xiu, D. (2010), "Numerical approach for quantification of epistemic uncertainty", *Journal of Computational Physics*, **229** (12), pp. 4648 – 4663.

Jakeman, J. D. and Roberts, S. G. (2013), "Local and dimension adaptive stochastic collocation for uncertainty quantification", in "Sparse Grids and Applications", Springer, (pp. 181–203).

Karatzas, I. and Shreve, S. E. (1988), *Brownian motion and stochastic calculus*, Springer-Verlag, New York.

Keese, A. (2003), "A review of recent developments in the numerical solution of stochastic partial differential equations (stochastic finite elements)", *Report No. Informatikbericht 2003*, **6**.

Keese, A. and Matthies, H. G. (2005), "Hierarchical parallelisation for the solution of stochastic finite element equations", *Computers and Structures*, **83** (14), pp. 1033 – 1047.

Kerfriden, P., Gosselet, P., Adhikari, S., and Bordas, S. (2011), "Bridging the proper orthogonal decomposition methods and augmented newton-krylov algorithms: An adaptive model order reduction for highly nonlinear mechanical problems", *Computer Methods in Applied Mechanics and Engineering*, **200** (5-8), pp. 850–866.

Khalil, M., Adhikari, S., and Sarkar, A. (2007), "Linear system identification using proper orthogonal decomposition", *Mechanical System and Signal Processing*, **21** (8), pp. 3123–3145.

Kiureghian, A. and Ditlevsen, O. (2009), "Aleatory or epistemic? Does it matter?", *Structural Safety*, **31** (2), pp. 105–112.

Kleiber, M. and Hien, T. D. (1992), *The stochastic finite element method*, Wiley, New York, USA.

Kloeden, P. E. and Pearson, R. A. (1977), "The numerical solution of stochastic differential equations", *The Journal of the Australian Mathematical Society. Series B. Applied Mathematics*, **20**, pp. 8–12.

Knio, O. M. and Maître, O. P. L. (2006), "Uncertainty propagation in cfd using polynomial chaos decomposition", *Fluid Dynamics Research*, **38** (9), p. 616.

Kokotovic, P., Jr., R. O., and Sannuti, P. (1976), "Singular perturbations and order reduction in control theory - an overview", *Automatica*, **12** (2), pp. 123 – 132.

Kokotovic, P., Khali, H. K., and O'reilly, J. (1987), *Singular perturbation methods in control: analysis and design*, volume 25, Siam, Philadelphia, USA.

Kolachalama, V., Bressloff, N., and Nair, P. (2007), "Mining data from hemodynamic simulations via Bayesian emulation", *BioMedical Engineering OnLine*, **6** (47).

Kolovos, A., Christakos, G., Hristopulos, D., and Serre, M. (2004), "Methods for generating non-separable spatiotemporal covariance models with potential environmental applications", *Advances in Water Resources*, **27** (8), pp. 815–830.

Kozyakin, V. (2009), "On accuracy of approximation of the spectral radius by the gelfand formula", *Linear Algebra and its Applications*, **431** (11), pp. 2134 – 2141.

Kreinin, A., Merkoulovitch, L., Rosen, D., and Zerbs, M. (1998), "Principal component analysis in Quasi Monte Carlo simulation", *Algo Research Quarterly*, **2** (2), pp. 21–29.

Kuo, F., Schwab, C., and Sloan, I. (2012), "Quasi-Monte Carlo finite element methods for a class of elliptic partial differential equations with random coefficients", *SIAM Journal on Numerical Analysis*, **50** (6), pp. 3351–3374.

Laub, A., Heath, M., Paige, C., and Ward, R. (1987), "Computation of system balancing transformations and other applications of simultaneous diagonalization algorithms", *Automatic Control, IEEE Transactions on*, **32** (2), pp. 115–122.

Lazarov, B. S., Schevenels, M., and Sigmund, O. (2012), "Topology optimization with geometric uncertainties by perturbation techniques", *International Journal for Numerical Methods in Engineering*, **90** (11), pp. 1321–1336.

Lehoucq, R. B., Sorensen, D. C., and Yang, C. (1998), *ARPACK users' guide: solution of large-scale eigenvalue problems with implicitly restarted Arnoldi methods*, volume 6, Siam.

Lei, Z. and Qiu, C. (2000), "Neumann dynamic stochastic finite element method of vibration for structures with stochastic parameters to random excitation", *Computers and Structures*, **77** (6), pp. 651–657.

Li, C.-C. and Kiureghian, A. D. (1993), "Optimal discretization of random fields", *Journal of Engineering Mechanics*, **119** (6), pp. 1136–1154.

Li, H. and Zhang, D. (2007), "Probabilistic collocation method for flow in porous media: Comparisons with other stochastic methods", *Water Resources Research*, **43** (9).

Li, J. and White, J. (2002), "Low rank solution of Lyapunov equations", *SIAM Journal on Matrix Analysis and Applications*, **24** (1), pp. 260–280.

Li, R. and Ghanem, R. (1998), "Adaptive polynomial chaos expansions applied to statistics of extremes in nonlinear random vibration", *Probabilistic Engineering Mechanics*, **13** (2), pp. 125–136.

Lin, Y. K. (1967), *Probabilistic Thoery of Strcutural Dynamics*, McGraw-Hill Inc, Ny, USA.

Liu, W. K., Belytschko, T., and Mani, A. (1986), "Random field finite-elements", *International Journal for Numerical Methods in Engineering*, **23** (10), pp. 1831–1845.

Liu, Y. and Anderson, B. D. (1989), "Singular perturbation approximation of balanced systems", *International Journal of Control*, **50** (4), pp. 1379–1405.

Loeppky, J., Sacks, J., and Welch, W. (2009), "Choosing the sample of a computer experiment: a practical guide", *Technometrics*, **51**, pp. 366–376.

Lucor, D., Su, C.-H., and Karniadakis, G. E. (2004), "Generalized polynomial chaos and random oscillators", *International Journal for Numerical Methods in Engineering*, **60** (3), pp. 571–596.

Ma, X. and Zabaras, N. (2009), "An adaptive hierarchical sparse grid collocation algorithm for the solution of stochastic differential equations", *Journal of Computational Physics*, **228** (8), pp. 3084–3113.

Maître, O. L., Knio, O., Najm, H., and Ghanem, R. (2004a), "Uncertainty propagation using Wiener-Haar expansions", *Journal of Computational Physics*, **197** (1), pp. 28 – 57.

Maître, O. L., Najm, H., Ghanem, R., and Knio, O. (2004b), "Multi-resolution analysis of Wiener-type uncertainty propagation schemes", *Journal of Computational Physics*, **197** (2), pp. 502 – 531.

Manohar, C. S. and Adhikari, S. (1998), "Statistical analysis of vibration energy flow in randomly parametered trusses", *Journal of Sound and Vibration*, **217** (1), pp. 43–74.

Mathelin, L., Hussaini, M., and Zang, T. (2005), "Stochastic approaches to uncertainty quantification in cfd simulations", *Numerical Algorithms*, **38** (1-3), pp. 209–236.

Matthies, H. (2007), "Uncertainty quantification with stochastic finite elements", *Encyclopedia of computational mechanics*.

Matthies, H. G., Brenner, C. E., Bucher, C. G., and Soares, C. G. (1997), "Uncertainties in probabilistic numerical analysis of structures and solids - stochastic finite elements", *Structural Safety*, **19** (3), pp. 283–336.

Matthies, H. G. and Keese, A. (2005), "Galerkin methods for linear and nonlinear elliptic stochastic partial differential equations", *Computer Methods in Applied Mechanics and Engineering*, **194** (12-16), pp. 1295–1331.

Maute, K., Weickum, G., and Eldred, M. (2009), "A reduced-order stochastic finite element approach for design optimization under uncertainty", *Structural Safety*, **31** (6), pp. 450 – 459.

McKay, M., Conover, W., and Beckman, R. (1979), "A comparison of three methods for selecting values of input variables in the analysis of output from a computer code", *Technometrics*, **21** (2), pp. 239–245.

Moens, D. and Vandepitte, D. (2002), "Fuzzy finite element method for frequency response function analysis of uncertain structures", *AIAA Journal*, **40** (1), pp. 126–136.

Moens, D. and Vandepitte, D. (2005), "A fuzzy finite element procedure for the calculation of uncertain frequency-response functions of damped structures: Part 1-procedure", *Journal of Sound and Vibration*, **288** (3), pp. 431 – 462.

Moore, B. (1981), "Principal component analysis in linear systems: Controllability, observability, and model reduction", *Automatic Control, IEEE Transactions on*, **26** (1), pp. 17–32.

Nair, P. B. and Keane, A. J. (2002), "Stochastic reduced basis methods", *AIAA Journal*, **40** (8), pp. 1653–1664.

Najm, H. N. (2009), "Uncertainty quantification and polynomial chaos techniques in computational fluid dynamics", *Annual Review of Fluid Mechanics*, **41** (1), pp. 35–52.

Newmark, N. M. (1959), "A method of computation for structural dynamics", *Journal of the Engineering Mechanics Division*, **85** (7), pp. 67–94.

Nicholls, D. P. and Shen, J. (2006), "A stable, high-order method for two-dimensional bounded-obstacle scattering", *SIAM Journal on Scientific Computing*, **28** (4), pp. 1398–1419.

Nickel, R. E. (1971), "On the stability of approximation operators in problems of structural dynamics", *International Journal of Solids and Structures*, **7** (3), pp. 301–319.

Nobile, F., Tempone, R., and Webster, C. (2008a), "An anisotropic sparse grid stochastic collocation method for partial differential equations with random input data", *SIAM Journal on Numerical Analysis*, **46** (5), pp. 2411–2442.

Nobile, F., Tempone, R., and Webster, C. G. (2008b), "A sparse grid stochastic collocation method for partial differential equations with random input data", *SIAM Journal on Numerical Analysis*, **46** (5), pp. 2309–2345.

Nouy, A. (2007), "A generalized spectral decomposition technique to solve a class of linear stochastic partial differential equations", *Computer Methods in Applied Mechanics and Engineering*, **196** (45-48), pp. 4521–4537.

Nouy, A. (2008), "Generalized spectral decomposition method for solving stochastic finite element equations: Invariant subspace problem and dedicated algorithms", *Computer Methods in Applied Mechanics and Engineering*, **197** (51-52), pp. 4718–4736.

Nouy, A. (2009), "Recent developments in spectral stochastic methods for the numerical solution of stochastic partial differential equations", *Archives of Computational Methods in Engineering*, **16** (3), pp. 251–285.

Nouy, A. and Clément, A. (2010), "Extended stochastic finite element method for the numerical simulation of heterogeneous materials with random material interfaces", *International Journal for Numerical Methods in Engineering*, **83** (10), pp. 1312–1344.

Nouy, A., Clément, A., Schoefs, F., and Moës, N. (2008), "An extended stochastic finite element method for solving stochastic partial differential equations on random domains", *Computer Methods in Applied Mechanics and Engineering*, **197** (51-52), pp. 4663–4682.

Oakley, J. (2002), "Eliciting Gaussian process priors for complex computer codes", *The Statistician*, **51** (1), pp. 81–97.

Oakley, J. E. and O'Hagan, A. (2002), "Bayesian inference for the uncertainty distribution of computer model outputs", *Biometrika*, **89**, pp. 769–784.

Oakley, J. E. and O'Hagan, A. (2004), "Probabilistic sensitivity analysis of complex models: a Bayesian approach", *Journal of the Royal Statistical Society B*, **66** (3), pp. 751–769.

Ogorodnikov, V. and Prigarin, S. (1996), *Numerical modelling of random processes and fields: algorithms and applications*, VSP, Utrecht.

O'Hagan, A. (1992), *Bayesian Statistics 4*, Oxford University Press, Cambridge, UK, chapter Some Bayesian numerical analysis, (pp. 345–363).

O'Hagan, A. (2006), "Bayesian analysis of computer code outputs: a tutorial", *Reliability Engineering & System Safety*, **91** (10-11), pp. 1290–1300.

Oksendal, B. (1995), *Stochastic differential equations: An introduction with applications*, Springer New York.

Papadrakakis, M. and Papadopoulos, V. (1996), "Robust and efficient methods for stochastic finite element analysis using Monte Carlo simulation", *Computer Methods in Applied Mechanics and Engineering*, **134** (3-4), pp. 325–340.

Parés, N., Díez, P., and Huerta, A. (2008), "Bounds of functional outputs for parabolic problems. part i: Exact bounds of the discontinuous galerkin time discretization", *Computer Methods in Applied Mechanics and Engineering*, **197** (19-20), pp. 1641 – 1660.

Pascual, B. and Adhikari, S. (2012), "Hybrid perturbation-polynomial chaos approaches to the random algebraic eigenvalue problem", *Computer Methods in Applied Mechanics and Engineering*, **217-220** (1), pp. 153–167.

Paté-Cornell, M. (1996), "Uncertainties in risk analysis: Six levels of treatment", *Reliability Engineering and System Safety*, **54** (2-3), pp. 95–111.

Pellissetti, M. and Ghanem, R. (2000), "Iterative solution of systems of linear equations arising in the context of stochastic finite elements", *Advances in Engineering Software*, **31** (8-9), pp. 607 – 616.

Penzl, T. (1998), "Numerical solution of generalized Lyapunov equations", *Advances in Computational Mathematics*, **8** (1-2), pp. 33–48.

Pettit, C. L. and Beran, P. S. (2004), "Polynomial chaos expansion applied to airfoil limit cycle oscillations", in "Proceedings of the 45th AIAA/ASME/ASCE/AHS/ASC Structures, Structural Dynamics and Materials Conference", volume 3, (pp. 1975–1985).

Pettit, C. L. and Beran, P. S. (2006), "Spectral and multiresolution Wiener expansions of oscillatory stochastic processes", *Journal of Sound and Vibration*, **294** (4), pp. 752–779.

Pettit, C. L., Canfield, R. A., and Ghanem, R. (2002), "Stochastic analysis of an aeroelastic system", in "15th ASCE Engineering Mechanics Conference", (pp. 2–5).

Petyt, M. (1998), *Introduction to Finite Element Vibration Analysis*, Cambridge University Press, Cambridge, UK.

Pichler, L., Pradlwarter, H., and Schuëller, G. (2009), "A mode-based meta-model for the frequency response functions of uncertain structural systems", *Computers and Structures*, **87** (5-6), pp. 332 – 341.

Pillage, L. T. and Rohrer, R. A. (1990), "Asymptotic waveform evaluation for timing analysis", *Computer-Aided Design of Integrated Circuits and Systems, IEEE Transactions on*, **9** (4), pp. 352–366.

Porter, D. and Stirling, D. (1990), *Integral Equations: A Practical Treatment, from Spectral Theory to Applications*, Cambridge Texts in Applied Mathematics, Cambridge University Press.

Powell, C. and Elman, H. (2009), "Block-diagonal preconditioning for spectral stochastic finite-element systems", *IMA Journal of Numerical Analysis*, **29** (2), pp. 350–375.

Pradlwarter, H. J. and Schuëller, G. I. (1997), "On advanced Monte Carlo simulation procedures in stochastic structural dynamics", *International Journal of Non-Linear Mechanics*, **32** (4), pp. 735 – 744, Third International Stochastic Structural Dynamics Conference.

Puig, B., Poirion, F., and Soize, C. (2002), "Non-Gaussian simulation using Hermite polynomial expansion: convergences and algorithms", *Probabilistic Engineering Mechanics*, **17** (3), pp. 253 – 264.

Reddy, J. N. (1993), *An introduction to the finite element method*, McGraw-Hill New York.

Richardson, S. (1971), "A model for the boundary condition of a porous material. part 2", *Journal of Fluid Mechanics*, **49** (2), pp. 327–336.

Roache, P. J. (1998), *Verification and validation in computational science and engineering*, Hermosa Publishers.

Rougier, J. (2007), "Probabilistic inference for future climate using an ensemble of climate model evaluations", *Climatic Change*, **81** (3), pp. 247–264.

Roy, C. J. and Oberkampf, W. L. (2011), "A comprehensive framework for verification, validation, and uncertainty quantification in scientific computing", *Computer Methods in Applied Mechanics and Engineering*, **200** (25-28), pp. 2131 – 2144.

Saad, Y. (2003), *Iterative methods for sparse linear systems*, Society for Industrial and Applied Mathematics.

Sachdeva, S. K., Nair, P. B., and Keane, A. J. (2006a), "Comparative study of projection schemes for stochastic finite element analysis", *Computer Methods in Applied Mechanics and Engineering*, **195** (19-22), pp. 2371–2392.

Sachdeva, S. K., Nair, P. B., and Keane, A. J. (2006b), "Hybridization of stochastic reduced basis methods with polynomial chaos expansions", *Probabilistic Engineering Mechanics*, **21** (2), pp. 182–192.

Sacks, J., Welch, W., Mitchell, T., and Wynn, H. (1989), "Design and analysis of computer experiments", *Statistical Science*, **4** (4), pp. 409–435.

Sakamoto, S. and Ghanem, R. (2002), "Simulation of multi-dimensional non-Gaussian non-stationary random fields", *Probabilistic Engineering Mechanics*, **17** (2), pp. 167–176.

Santner, T., Williams, B., and Notz, W. (2003), *The Design and Analysis of Computer Experiments*, Springer Series in Statistics, London, UK.

Sarkar, A. and Ghanem, R. (2002), "Mid-frequency structural dynamics with parameter uncertainty", *Computer Methods in Applied Mechanics and Engineering*, **191** (47-48), pp. 5499–5513.

Sarkar, A. and Ghanem, R. (2003), "A substructure approach for the midfrequency vibration of stochastic systems", *Journal of the Acoustical Society of America*, **113** (4), pp. 1922–1934, part 1.

Scheidt, J. V. and Purkert, W. (1983), *Random Eigenvalue Problems*, North Holland, New York.

Schuëller, G. I. (2001), "Computational stochastic mechanics - recent advances", *Computers and Structures*, **79**, pp. 2225–2234.

Schuëller, G. I. (2006), "Developments in stochastic structural mechanics", *Archive of Applied Mechanics*, **75**, pp. 755–773.

Shinozuka, M. (1972), "Monte Carlo solution of structural dynamics", *Computers and Structures*, **2** (5-6), pp. 855–874.

Sloan, I., Kuo, F., and Joe, S. (2002), "Constructing randomly shifted lattice rules in weighted Sobolev spaces", *SIAM Journal on Numerical Analysis*, **40** (5), pp. 1650–1665.

Sobol, I. M. (1998), "On quasi-monte carlo integrations", *Mathematics and Computers in Simulation*, **47** (2), pp. 103–112.

Stefanou, G. (2009), "The stochastic finite element method: Past, present and future", *Computer Methods in Applied Mechanics and Engineering*, **198** (9-12), pp. 1031 – 1051.

Stein, M. (1987), "Large sample properties of simulations using latin hypercube sampling", *Technometrics*, **29** (2), pp. 143–151.

Sudret, B. and Der-Kiureghian, A. (2000), "Stochastic finite element methods and reliability", *Technical Report UCB/SEMM-2000/08*, Department of Civil & Environmental Engineering, University Of California, Berkeley.

Swiler, L. P., Paez, T. L., Mayes, R. L., and Eldred, M. S. (2009), "Epistemic uncertainty in the calculation of margins", in "50th AIAA Structures, Structural Dynamics, and Materials Conference, Palm Springs, CA, USA", .

Takaba, K., Morihira, N., and Katayama, T. (1995), "A generalized Lyapunov theorem for descriptor system", *Systems and Control Letters*, **24** (1), pp. 49 – 51.

Tartakovsky, D. M. and Xiu, D. (2006), "Stochastic analysis of transport in tubes with rough walls", *Journal of Computational Physics*, **217** (1), pp. 248–259.

Taylor, G. (1971), "A model for the boundary condition of a porous material. part 1", *Journal of Fluid Mechanics*, **49** (02), pp. 319–326.

Thompson, J. F., Warsi, Z. U., and Mastin, C. W. (1985), *Numerical grid generation: foundations and applications*, volume 38, North-Holland Amsterdam.

van der Veen, A., Deprettere, E., and Swindlehurst, A. (1993), "Subspace-based signal analysis using singular value decomposition", *Proceedings of the IEEE*, **81** (9), pp. 1277–1308.

Vanmarcke, E. H. (1983), *Random fields*, MIT press, Cambridge, USA.

Vernon, I., Goldstein, M., and R.G. Bower (2010), "Galaxy formation: a Bayesian uncertainty analysis", *Bayesian Analysis*, **5** (4), pp. 619–670.

Wall, F. and Bucher, C. (1987), "Sensitivity of expected exceedance rate of sdof-system response to statistical uncertainties of loading and system parameters", *Probabilistic engineering mechanics*, **2** (3), pp. 138–146.

Wan, X. and Karniadakis, G. E. (2005), "An adaptive multi-element generalized polynomial chaos method for stochastic differential equations", *Journal of Computational Physics*, **209** (2), pp. 617–642.

Wan, X. and Karniadakis, G. E. (2006), "Beyond wiener-askey expansions: Handling arbitrary pdfs", *Journal of Scientific Computing*, **27** (1-3), pp. 455–464.

Wang, J. and Zabaras, N. (2005), "Hierarchical bayesian models for inverse problems in heat conduction", *Inverse Problems*, **21** (1), p. 183.

Wilkinson, J. H. (1988), *The Algebraic Eigenvalue Problem*, Oxford University Press, Oxford, UK.

Williams, M. (2010), "A probabilistic study of the influence of parameter uncertainty on thermal radiation heat transfer", *International Journal of Heat and Mass Transfer*, **53** (7-8), pp. 1461 – 1472.

Xiu, D. and Karniadakis, G. E. (2003a), "A new stochastic approach to transient heat conduction modeling with uncertainty", *International Journal of Heat and Mass Transfer*, **46** (24), pp. 4681–4693.

Xiu, D., Shen, J., *et al.* (2007), "An efficient spectral method for acoustic scattering from rough surfaces", *Communications in Computational Physics*, **2** (1), pp. 54–72.

Xiu, D. and Tartakovsky, D. M. (2006), "Numerical methods for differential equations in random domains", *SIAM Journal on Scientific Computing*, **28** (3), pp. 1167–1185.

Xiu, D. B. and Karniadakis, G. E. (2002), "The wiener-askey polynomial chaos for stochastic differential equations", *Siam Journal on Scientific Computing*, **24** (2), pp. 619–644.

Xiu, D. B. and Karniadakis, G. E. (2003b), "Modeling uncertainty in flow simulations via generalized polynomial chaos", *Journal of Computational Physics*, **187** (1), pp. 137–167.

Yamazaki, F. and Shinozuka, M. (1988), "Digital generation of non-Gaussian stochastic fields", *Journal of Engineering Mechanics*, **114** (7), pp. 1183–1197.

Yamazaki, F., Shinozuka, M., and Dasgupta, G. (1988), "Neumann expansion for stochastic finite element analysis", *Journal of Engineering Mechanics-ASCE*, **114** (8), pp. 1335–1354.

Yimin, Z., Chen, S., Liu, Q., and Liu, T. (1996), "Stochastic perturbation finite elements", *Computers and Structures*, **59** (3), pp. 425 – 429.

Zalewski, B. F., Mullen, R. L., and Muhanna, R. L. (2009), "Fuzzy boundary element method for geometric uncertainty in elasticity problem", *SAE International Journal of Materials and Manufacturing*, **2** (1), pp. 310–316.

Zhang, J. and Ellingwood, B. (1994), "Orthogonal series expansions of random fields in reliability analysis", *Journal of Engineering Mechanics*, **120** (12), pp. 2660–2677.

Zhu, W. Q., Ren, Y. J., and Wu, W. Q. (1992), "Stochastic FEM based on local averages of random vector fields", *Journal of Engineering Mechanics*, **118** (3), pp. 496–511.

Zienkiewicz, O. C. and Taylor, R. L. (1991), *The Finite Element Method*, McGraw-Hill, London, fourth edition.